Flying Doctor

DSE Final Report

Group 23

by

C.C.A. Bekkers	4371364
S.K. Birjmohan	4307488
M.J.G. van der Drift	4384180
E. Hernandez Moore	4363833
D.H.P.L. Koppes	4392698
A.J.J. Meegdes	4375521
H.W. Njo	4347943
P. Scheenloop	4099915
Ž. Vinskas	4353242

Tuesday July 4, 2017

Project duration:
April 24, 2017 - July 7, 2017

Supervisors:

Dr. R.M. Groves	TU Delft, tutor
J. Carvajal Godinez	TU Delft, coach
K. Jovanov	TU Delft, coach

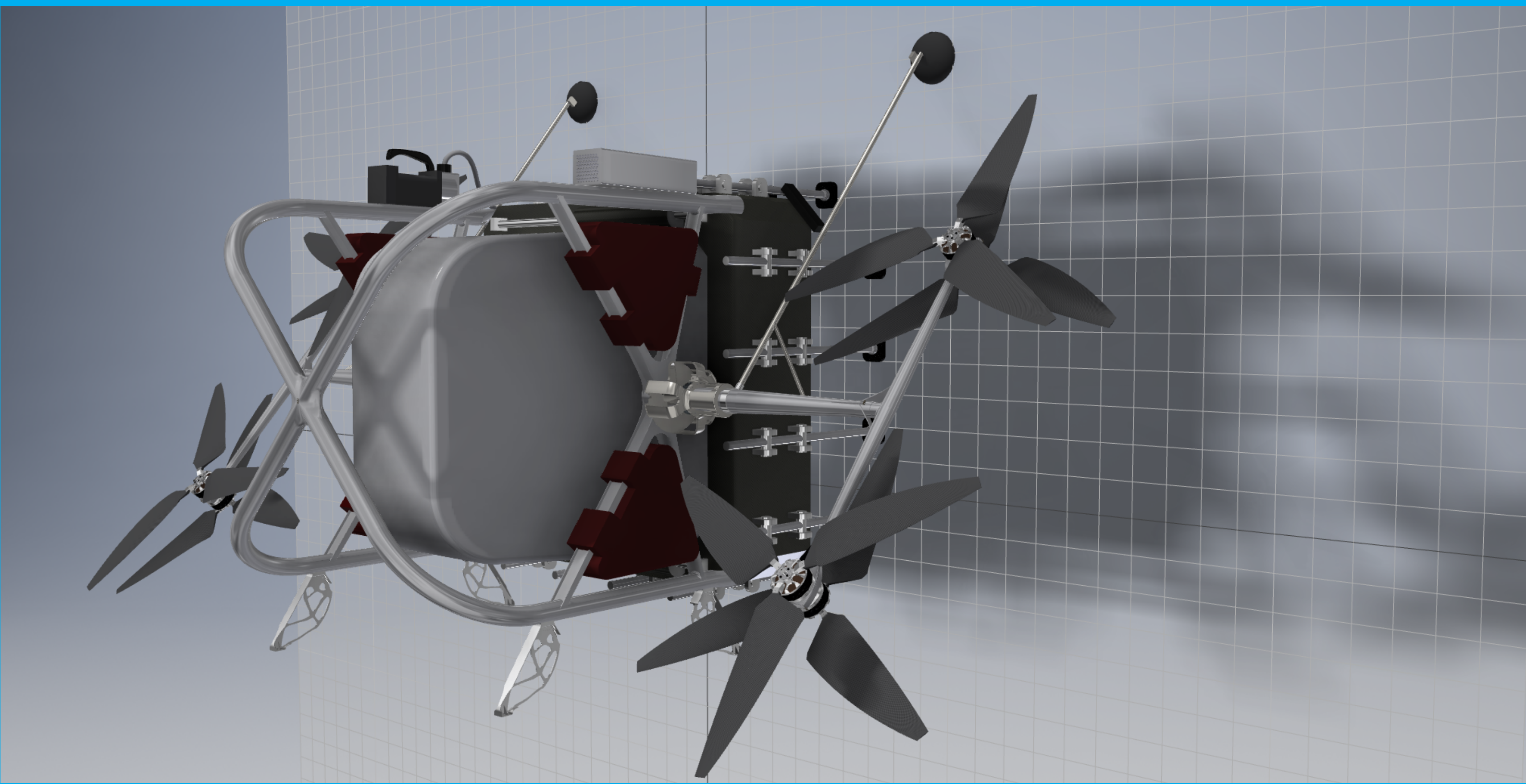

TU Delft

Preface

As part of the Aerospace Engineering bachelor programme at Delft University of Technology, we have to show our competence in the design process of aerospace related subjects. In order to assess this, a Design Synthesis Exercise (DSE) has been set up. The Flying Doctor group consists of Casper Bekkers, Sanjay Birjmohan, Maarten van der Drift, Emma Hernandez Moore, Daan Koppes, Jordan Meegdes, Hardi Njo, Paula Scheenloop and Žilvinas Vinskas. The group has to hand in a report presenting their final design and progress of the last nine weeks for to show their before mentioned competence. Previously a Project Plan, a Baseline Report and a Mid-Term Report have been handed about the preliminary design stages of the Flying Doctor. The Flying Doctor is an unmanned aerial vehicle (UAV), which mission is to carry a payload. The report lying before you is the Final Report, it is a continuation of the design that uses the previous reports as a base for a more detailed design.

We are very grateful to Dr. R.M. Groves for giving the opportunity to design the Flying Doctor and his guidance and support. We also want to thank J. Carvajal Godínez and K. Jovanov for the help, support and advice. Also, the help of ir. V.S. Viswanath Dhanisetty, ir. P.P.R.M.L. Harks, Dr.ir. W.J.C. Verhagen and ir. T. de Boer is very much appreciated.

We hope you enjoy reading the Final Report of the Flying Doctor.

Group 23
Delft, 22th of June 2017

Summary

The objective of Team 23 is to design an Unmanned Aerial Vehicle (UAV), which is capable of carrying a payload of 85kg and orientating it to the desired surface, in order for the payload to conduct its operation. Airline Maintenance Repair and Overhaul (MRO) is one of the cases that the UAV design can be utilised. This report will focus on the market analysis, design process and technical results of the design of the 'Flying Doctor' and its implementation in the MRO industry.

Situation

In one of the enduring wisdom of commerce, the airline industry is hard-pressed to make healthy profits. Intense competition, susceptibility to volatile oil prices and natural disasters, such as an Icelandic volcano eruption in 2010, are some of the main reasons why the airline industry has a very small profit margin.

One of the sectors of airlines operation that has the potential to increase cost-savings is the MRO industry. The key is to reduce the time that an aircraft spends undergoing inspection and repair. The longer an aircraft is on the ground, the more the airline loses its revenue.

The current solution requires the use of cherry pickers or scaffolding to serve as a platform for maintenance technicians to access any damaged surface location. This method is inefficient, not to mention that human error may create workplace hazards. In addition, the technician needs to perform the manual repair, which means the quality of the repair is highly dependent on the experience of the individual. Such time-consuming tasks renders the repair process expensive.

Analysis has shown that the Flying Doctor is able to save up to 20,000 € in the case of an unscheduled check up for a Boeing 737 aircraft. The Flying Doctor's benefit to the operation is two-fold. Firstly, it eliminates the need for scaffolding/cherry picker as it will be able to fly autonomously to the damage location, effectively saving time. Secondly, the payload chosen is capable of repairing composite damage repair. The automation will ensure that the work will immensely reduce the repair time, and enhance the quality of the repair.

Requirement

The design process started off with a set of requirements which drive the eventual design of the Flying Doctor. The main requirements are highlighted as follows:

- UAV weight requirement to be greater than 20kg.
- UAV shall be able to fit in 1.0m x 1.0m x 1.0m.
- UAV shall have a flight time of 30 minutes.
- UAV shall have a flight speed no greater than 5km/h.
- UAV shall autonomously navigate to the target and place the payload on the target.
- UAV shall be electrically powered.
- UAV shall be at least 95% recyclable.
- UAV shall be available for indoor (hangar) operation at least 95% of the time.
- UAV shall be available for outdoor operation at least 80% of the time.
- UAV shall provide a positive return on investment after at most 10 systems sold or leased to aircraft operators.

The following requirements highlighted the important ones, the more extensive mission and system requirements can be found in Chapter 17.

Selected Design

The report built on the concepts selected in the Midterm report. The four concepts considered are different in their adoption of the propulsion system, payload rotation, and integrated/modular frame. Figure 1 shows Concept 1 whose design choices were multiple rotary fans, active suction cups/lift support and an orbital payload mount with battery as the counterweight. For Concept 2, the design choices were multiple stacked rotary fans, with a power cable, active suction cups and a rotating payload mount, which is shown in Figure 2. For Concept 3, the design choices were large rotary blades, a power cable, and a detachable payload mount, which is shown in Figure 3. Figure 4 shows Concept 4, which relies on coaxial rotary fans, with a battery, extending suction cups, and a rotating payload mount.

From the propulsion system analysis, it is clear that the UAV has to use multirotors to provide the thrust to weight ratio of two. As the result, Concept 2 and Concept 3 are virtually the same. Both have the payload located below the UAV, and its payload rotation is provided by the motor and propulsion respectively.Table 1 shows the trade-off for every concept based on different criterion. Among them is ergonomics, which grades the user-friendliness of the system as the Flying Doctor is envisaged to be assembled by technicians. This is important as higher score means it will be less complex to assemble and result in time-savings. In addition, a sensitivity analysis is performed on placing different weight on the criterion. Mass-oriented and complexity-oriented trade-off were performed, and the result had proved that Concept 4 is the winning candidate for the Flying Doctor's design.

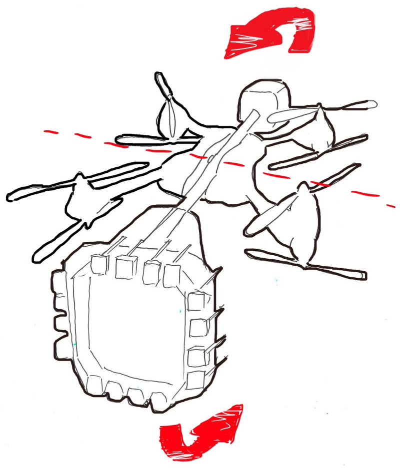

Figure 1: Visualisation of concept 1. The red arrow denotes the direction of rotation of the extending beam.

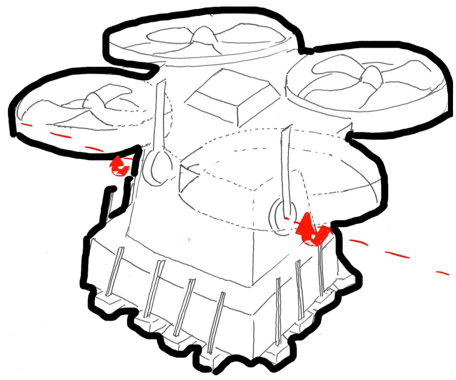

Figure 2: Visualisation of concept 2. The red arrow denotes the direction of rotation of the payload for orientation.

Figure 3: Visualisation of concept 3. The yellow arrow denotes the location of attachment to the grounded payload.

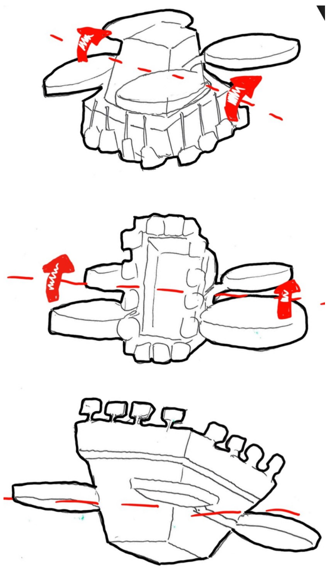

Figure 4: Visualisation of concept 4 rotation in three stages. The red arrow denotes the direction of rotation of the payload with respect to its frame.

Table 1: Trade-off table for each concept

Concept	**Mass (0.3)**	**Reach (0.3)**	**Ergo-nomic (0.1)**	**Size (0.1)**	**Complexity (0.2)**	**Weighted average**
1	4	4	2	1	3	3.3
2 & 3	4	5	4	5	1	3.8
4	5	5	3	3	2	4.0

The chosen concept has several features that do not present in other three concepts, and more importantly, it is a concept that met with most of the driving requirements, such as the weight and dimensions restrictions. The concept advantageous features are widely available multirotors technology in terms of software and hardware, redundant propulsion, minimal payload interference, small storage space and better reaching capability than other concepts. It does have some drawbacks nevertheless. They are complex rotor arm design, payload rotation imbalance and large operational space.

Subsystem design

The subsystem designs are divided into several subsystems. They are payload, propulsion, structural, perching, navigation and the ground stations.

The referenced **payload** was never intended for off-grid purpose and therefore, additional implementations are needed

Table 2: Midterm vs Final weight estimation for the Flying Doctor

Subsystems	Preliminary Estimation [kg]	Final Weight [kg]	Δ [kg]
Power& Propulsion	10.9	8.096	-2.804
Payload	3.00	4.644	1.644
Perching	1.00	0.973	-0.027
Arm	2.8	2.024	-0.776
Landing Gear	1.27	0.392	-0.878
Navigation	1.00	0.786	-0.214
Electronics	1.00	1.459	0.459
Total weight [kg]	20.97	18.37	-2.6

for the seamless operation for both the UAV and the payload. The required components for the Flying Doctor implementations are vacuum pump for the suction cups and inverter for the payload. Additional features for the Flying Doctor, such as the inspection by Non-Destructive Testing (NDT) and the painting of the repaired surface are taken into account. The choice of the NDT has yet to be decided, however, their mass and power budgets have been considered in the final weight of The Flying Doctor. The latter's mechanism will not be further discussed as it will be taken as a part of the Post-DSE.

The **propulsion** serves as the starting point of the design of the Flying Doctor as it dictates the power requirements of the flight as well as the battery mass. The system is comprised of eight independent rotors sourced from off the shelves products. It has coaxial multirotor in X8 configuration with 36" diameter rotor. The tri-blade rotors are with 12.3cm root chord, 1cm tip chord, non linear-taper and twist distribution. NACA 63-206 was chosen as the propeller airfoil for its relatively thick rear section making it easier for manufacturing.

The structural system consists of **rotor arms**, **payload frame**, **housing mechanism** and **landing gears**. The theory behind the loading subjected to each component is addressed with the help of a free-body diagram. The analysis is carried on with the use of CAD program, Autodesk Inventor, where iterative analysis through corresponding changes to the model can be performed. All components were assembled, and then subjected to final verification, where the simulation results are consistent with the individual simulation. The structural system has a minimum safety factor of 1.22. In addition, vibration analysis has been taken into account as well.

Perching refers to the action of the UAV attaching to the desired surface. With the aid of the perching arm, the Flying Doctor can rotate itself with respect to the payload and reach roughly 80% of the aircraft surfaces. However, as most damage occurs near the cargo door, the Flying Doctor covers almost 90% of the damage location.

Navigation system is one of the most important aspects of the flying doctor to enable autonomous navigation. It gives feedback to the main controller, which will control the navigation of the flying doctor. The elements that are used for navigation are WiFi, GPS, IMU, 2x sonar sensors, 12x proximity sensors, and 4x 3D cameras. The 3D sensors are used to map the nearby surroundings. The proximity sensors are placed in strategic positions to provide collision avoidance capability. The sonar sensors are implemented at the crucial location to aid the proximity sensors, for better range detection.

The **control simulation** yields important results regarding the performance of the Flying Doctor. Firstly, the UAV must maintain a minimum safe distance of 40cm to any nearby objects when navigating. Secondly, The gust input of 42km/h is used to simulate the UAV's gust resillence. The result is that the UAV must maintain a safe distance of 10cm. Lastly,0.8m recovery height is needed to recover from the failure of perching mechanism at 90-degree position.

The **storage** for the UAV has been designed to fit at the back of the truck. It takes approximately six minutes from the moment the operator arrives at the location till the UAV takes off. Three batteries are needed for three operations per day to ensure availability of the UAV. An industrial purpose laptop is chosen as the **ground station**.

Final Design

The hardware **architecture** consists of three main nodes. The Main Control Unit supports the interface between the payload and the Flying Doctor and provides the command for the navigation in terms of 3D cameras. The Flight Controller is responsible for the UAV's flight and stability and has enough processing power to handle the proximity sensors. The ground station provides the interface between the maintenance engineer and the Flying Doctor. The information flow and high-level software flow diagram are considered as well.

The final design of the Flying Doctor possesses several unique features. It contains large auxiliary components for the payload necessity. The system is meant for easy transportability and storage. As the results, the rotor arms are detachable, propellers rotors are foldable and perching arms are collapsible. These feature specifically heed the dimension requirement. The final design allows safe perching with adequate clearance without damaging the asset.

The Flying Doctor will fly at 146.4kg with its dry mass of 18.37kg, the Li-S battery of 22.88kg, payload and its miscellaneous mass of 105.15kg. Preliminary design estimated the larger dry weight of 20.97kg, roughly 2.6kg heavier than the one of the final design. This is reflected in Table 2. This mainly due to the better sizing of the propulsion which provides contingency mass to the other subsystems. Other structural elements have provided the weight savings due to structural optimisation. The budget reserved for the payload grew by 1.6kg due to the simplification made in the preliminary esti-

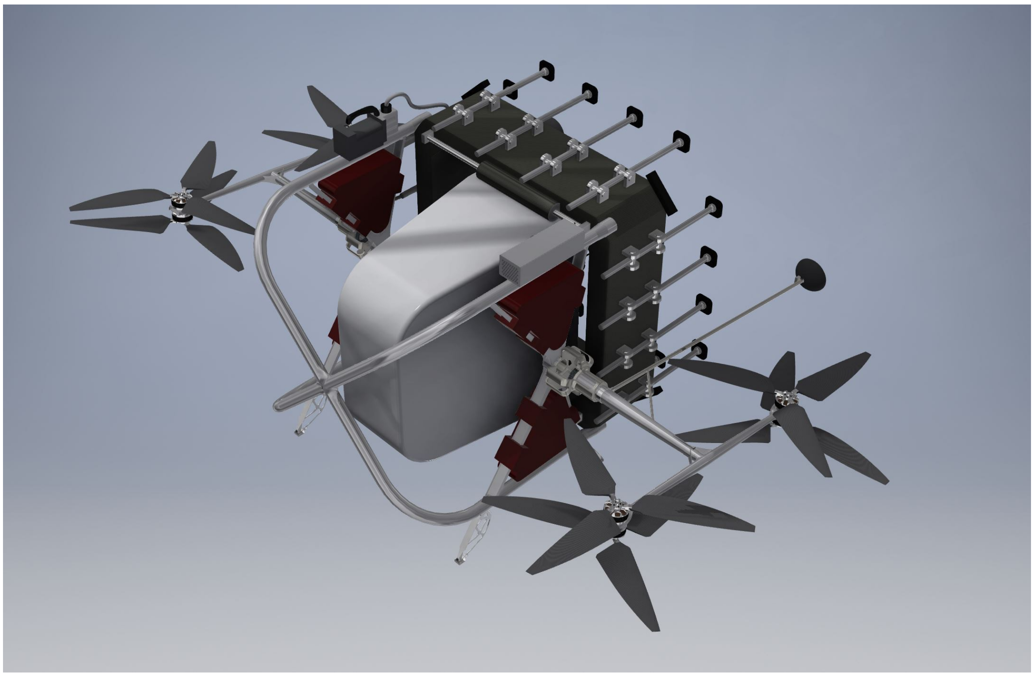

Figure 5: CAD model of the complete vehicle assembly in its typical landed or cruise flight configuration

Table 3: Mass budget of the Flying Doctor for the final design

Components	Weight [kg]
Flying Doctor dry mass	18.37
Li-S battery mass	22.88
ULTRASONIC mobileBLOCK	85
Payload miscelleanous	20.15
Complete Flying Doctor mass	**146.4**

mate. The tabulation of power consumption of different subsystems shows the total specified power, total available power and budget surplus power across the different stage of the Flying Doctor's mission. The battery is connected in parallel, and divided into to two, one for each side of the UAV. The Flying Doctor has three voltage rails of 24V, 12V and 5V, that are dedicated to various electronics used by different subsystems.

Non-technical design

Most of the components required will be either purchased off-the-shelves or fabricated by a conventional method by the company. Additive manufacturing will be used to produce the complex geometry, in particular, the rotation mechanism housing. This will cost 3,230 € Just In Time (JIT) manufacturing philosophy will be implemented with the production plan.

The cost of the Flying Doctor can be divided into five segments. The development cost, which is based on five years, totalled up at 3,040,000 €. It includes salaries, facility, prototype, production tools and certification. The production cost of the entire UAV is 16,098.7 €, taking into account extra volume cost for additive and conventional manufacturing at 10% and 30% respectively. The maintenance and operational cost are predicted to be 61,000 € and 6,000 € respectively. Three business models are considered. The sell, lease and service model. The sell model gives the quickest Return on Investment (ROI) within two years compared to the rest. But it will not yield larger ROI after several years. The opposite is true for the lease model which will have slow growth, and be more profitable at the end of the year. At the end of the five years, the service model has larger ROI potential than the lease model. The service model, hence, is chosen for the Flying Doctor.

Sensitivity analysis has been performed for two main features of the Flying Doctor. Should there be a case where the chosen Li-S battery proved to be infeasible, more robust Li-Po battery shall replace it. Its analysis, which is performed using the remaining contingency mass, shows that the flight time will be reduced to 1564s instead of minimum 1800s. Another feature that underwent sensitivity analysis is perching. The coefficient of friction has been changed to cater wet conditions, and the degree of the surface that the Flying Doctor can attach is reduced to 58% from 80%.

The reliability of the Flying Doctor's components is ensured by including extensive analysis such as the fatigue life and vibrations. In addition safety factors of at least 1.22 is present in the UAV's structure. The availability of the UAV depends mostly on weather conditions and charging time of the batteries. Due to the selected service business model, maintenance of the UAV has to be included to ensure its availability. Safety is highly related to risk and will be incorporated to risk assessment. Four aspects of risk are reviewed. They are pre-flight, mid-flight, post-flight and feasibility risks.Out of the three phases of flight, the mid-flight risk poses the largest threat. One of them is orientation mechanism malfunction, which can sourced to flight controller malfunctioning, and miscalculation perching manoeuvre. In another aspect, the entire feasibility of the Flying Doctor is highly restricted by regulations, and in some extent the Technology Readiness Level of the Li-S battery. All the risks identified has been mitigated by some measures. The technical risk such as collision avoidance, or propellers' failure have been rectified by installation of redundant sensors and the inherent of the multi-rotor configuration respectively. Most of the feasibility analysis will be treated during the post DSE period.

The Flying Doctor is electrically powered. The power source from renewable energy has been considered, however its practicality made it unfeasible. The power charging, hence, will be conventional from the conventional electrical source available in the hangar. Most of the structural materials and electrical components selected can be reused or recycled. Hence, 95% of the UAV is recyclable.

Future

With such limited time of 10 weeks, the design detail can be only achieved to certain extent. More detailed work can be performed on the individual subsystems to produce more efficient and robust design. For example, fatigue analysis can be performed on the perching and rotation mechanism to verify its life cycle. Structural elements can benefit from extra analysis such as the landing gear to consider torsional load. Noise emission has not been analysed, but could be performed to assess the sustainability aspect of the design. NDT solution has been conceptualised and could be further assessed on the integration of the ground station and the referenced payload.

The objective of the Design Synthesis Exercise is to highlight the technical feasibility of the design, while the feasibility and validation are beyond its scope. Plan for further of developments are considered. The plan is divided into funding process, further design, creating of prototype, validation, creating the final product and finally the selling process. These plannings were estimated to keep the team's hand full till mid-2019.

Contents

List of Figures

List of Tables

List of Symbols

Symbol	Definition	Units
A	Cross-sectional area or Force	[m^2] or [N]
c	Chord	[m]
C	Coefficient	[-]
C_p	Volumetric thermal capacity	[J/(m^{3}K)]
d	Distance or Diameter	[m]
E	Young's modulus	[Pa]
e	Error	[-]
ef	Thermal effusivity	[-]
F	Force	[N]
$F1$	Force 1	[N]
$F2$	Force 2	[N]
f	Frequency	[Hz]
g	Gravitational acceleration (≈ 9.81)	[m/s^2]
I	Area moment of inertia	[m^4]
K	Coefficient	[-]
k	Boltzmann constant ($\approx 1.3806 \cdot 10^{-23}$)	[m^{2}kg/(s^2 K)]
l	Axial length of the cylinder	[m]
L	Length	[m]
M	Moment	[Nm]
m	Mass	[kg]
N	Number	[-]
P	Power	[W]
p	Pressure	[Pa]
Q	Input energy	[J]
q	Volume rate	[m^3/s]
S	Surface area or Shear force	[m^2] or [N]
s	distance	[m]
T	Temperature	[K]
t	Thickness or Time	[m] or [s]
KV	Constant motor speed	[RPM/V]
V	Volume or Velocity	[m^3] or [m/s]
W	Weight	[N]
w	Distributed load	[N/m]
y	Distance to neutral axis	[m]
α	Thermal diffusivity	[-]
η	Efficiency	[°]
θ	Pitch angle or Orientation of the bar	[°]
μ	Friction coefficient	[-]
ρ	Air density	[kg/m^3]
σ	stress	[Pa]
τ	Torque	[Nm]
ϕ	Angle of surface onto which the passive suction caps are attached	[°]

List of Subscripts

Subscript	Definition
$assistingUAV$	Second assisting UAV
$back$	Back rotors
c	Cylinder
cup	Suction cup
$coax$	Coaxial
D	Drag or Derivative
d	Rotor disk
$elec$	Electrical
eq	Vacuum equation
$front$	Front rotors
h	Horizontal
I	Integral
max	Maximal
n	Normal
nat	Natural
P	Proportional
p	Pulse
$prop$	Between propellers
res	Resultant
s	Suction
sc	Suction cup
$section$	Cross section
t	Tangential
ts	Total of suction cup
v	Vertical
x	(Direction of) x-axis
y	(Direction of) y-axis
yy	Around the y-axis
z	(Direction of) z-axis
0	Initial or Enclosed
1	Final

List of Abbreviations

Abbreviation	Definition	Abbreviation	Definition
AC	Alternating current	*MID*	Mid-flight risk
AF	Air France	*Manuf*	manufacturing
Al	Aluminium	*MCU*	Main control unit
AM	Additive manufacturing	*MRO*	Maintenance, repair and overhaul
ATC	Air traffic control	*MWIR*	Medium wavelength infrared
AWG	American wire gauge	*NDT*	Non-destructive testing
CAD	Computer-aided design	*O*	Outdoor
CAM	Computer-aided manufacturing	*OLM*	Outsourced Line Maintenance
CFD	Computational fluid dynamics	*OP*	Operational
CFRP	Carbon fibre reinforced plastic	*Orient.*	Orientation
CM	Conventional manufacturing	*PID*	Proportional–integral–derivative
CNC	Computer numerical control	*POF*	Post-flight action
DC	Direct current	*POS*	Post-flight risk
DLF	Development, Legal and Financial	*PRF*	Pre-flight action
DoD	Depth of discharge	*PRE*	Pre-flight risk
Detach.	Detachment	*PV*	Present value
DSE	Design Synthesis Exercise	*RAMS*	Reliability, availability, maintainability and safety
ESC	Electronic speed controller		
FBS	Functional breakdown structure	*RGB*	Red-green-blue
FFD	Functional flow diagram	*RoI*	Return on Investment
FEM	Finite element method	*SAAR*	Side arm aided rotation
GEN	General	*Ti*	Titanium
GPS	Global positioning system	*TM*	Trademark
IR	Infrared	*Tot.*	Total
IC	Integrated circuit	*TRL*	Technology readiness level
IMU	Inertial measurement unit	*UAV*	Unmanned aerial vehicle
JIT	Just in time	*UML*	Unified Modeling Language
KLM	Koninklijke Luchtvaart Maatschappij	*USD*	United States Dollar
LIDAR	Light detection and ranging	*UT*	Ultrasonic thermography
Li-ion	Lithium ion	*V*	Vanadium
Li-Po	Lithium polymer	*X8*	X-shaped, eight propellers configuration
Li-S	Lithium-sulfur		
LWIR	Long wavelength infrared	*3D*	Three dimensional

1
Introduction

In the next decade the global fleet of aircraft is expected to grow from approximately 25,000 to 36,000 aircraft by 2025[1]. However, this growth may be restricted by the lack of Maintenance, Repair and Overhaul (MRO) industry capacity. Specifically, there are not enough fully qualified maintenance personnel to cover the needs in the growing market[1]. One solution to alleviate this problem is to integrate an autonomous drone in the maintenance procedure. At this point in time an inspection drone prototype for lightning strike damage has been tested by KLM-AF[2] and Easyjet[3]. Implementing drones to perform inspection allows reducing the man hours invested in this assignment in addition to decreasing the grounded time of the aircraft. Another advantage is that it enables a more dynamic maintenance scheduling and it provides continuous feedback that can be used to tailor maintenance.

DSE Group 23 - Flying Doctor seeks to design an UAV for inspection and repair of composite aircraft. Currently no UAV exists in the MRO industry that is capable of performing inspection and repair. The UAV is designed around a repair payload from DMG MORI called the ULTRASONIC mobileBLOCK, of which specifications can be found in the Baseline Report[2]. After that a Mid-Term Report[3] was made where a concept was provided for this drone. This report aims to elaborate on that concept to provide a more detailed view of the UAV and to support its feasibility.

Before elaborating the design, the functions of the UAV are analysed in depth in Chapter 2 to provide a base for required system capabilities. After the functionality, the mission will be elaborated upon through the use of a concept of operations visualisation in Chapter 3. After the mission is described, the market analysis is performed in Chapter 4 to emphasise the effect of the UAV on the profit of airliners. To provide a base for the design, the design starting point and the payload are described in Section 5. Then for a more in depth view of the DMG MORI payload[4], its functions and supplements are described in detail in Chapter 6. After the mission profile, the functionality of the UAV, the market analysis and the description of the DMG MORI, the design choices are explained. This is done by first showing the design process of the propulsion system in Chapter 7 as this will provide high forces which dictate further structural design. They provide a base for the design of the rotor arms, the frame of the payload, the rotation mechanism inbetween these two structural components and the landing gear. All of these structural components are described in Chapter 8. When these structural components are established, the perching to the aircraft is considered in Chapter 9 where the design of the perching mechanism is described together with all areas that can be reached by the UAV. When all of these structural components have been established, the vibrations that can occur are described in Chapter 10. With this, all structural components are designed, leading the way towards providing depth on the operations of the UAV by designing the navigation system in Chapter 11. For this navigation to be successful, control software is necessary. This control software is described in Chapter 12. In order for this control to be issued and for data to be transferred to the operator a ground station is required. The design of this ground station is described in Chapter 13. With all of these components present. The design is finalised and the layout is provided in Chapter 14. This considers the layout of the UAV, software and hardware as well as an electrical flow and data flow. Finally, a production plan is presented in Chapter 15.

When every aspect of the design so far has been described, a cost breakdown structure is provided to ensure the financial feasibility of the design in Chapter 16. Then, an overview of the requirements and whether they have been met is provided in the form of a compliance matrix in Chapter 17. Furthermore, the reliability, availability, maintainability and safety (RAMS) analysis is performed which indicates issues that the product could cause and issues that have been prevented in Chapter 18. After this in Chapter 19 special attention is paid towards how the UAV aids in sustainability due to the increasing direness of how sustainability is neglected in many aspects in the world. Following this, in Chapter 20, further progress that can be made in post-DSE stages are described. Finally Chapters 21 and 22 provide the conclusion of the report and recommendations for further design respectively.

[1] http://www.aviationtoday.com/2017/01/17/three-mro-trends-set-to-revolutionize-civil-aviation-in-2017/ [Accessed 4 May 2017]
[2] http://www.afiklmem.com/AFIKLMEM/en/g_page_standard/MRO_lab_Innovations/DRONE.html/ [Accessed 4 May 2017]
[3] http://aviationweek.com/mro-enterprise-software/more-airlines-turn-uavs-aircraft-inspection [Accessed 4 May 2017]

2
Functionality

Before providing the design of the UAV, the functions that the system performs are provided. This is to give an insight into the design criteria and to give an idea of how the UAV operates. This is done firstly in a chronological manner in Section 2.1 through the means of a Functional Flow Diagram (FFD). After the chronological visualisation, a constituent visualisation is provided in Section 2.2 by means of a Functional Breakdown Structure (FBS).

2.1. Chronological Functionality

To relay the mission in an operational manner, a chronological overview is provided of the mission. This overview is provided through the means of a FFD. This FFD establishes the top-level functions that the system performs and elaborates them in a more in depth fashion. The diagram can be seen in Figure 2.1. This diagram shows only a single layer of depth, more depth on certain system related functions is provided in their respective chapters. For this FFD an emergency abort mission is incorporated in the top level indicated by a red connection.

The foundation of this flow diagram is the mission profile. The top-level functions have been the driving force for the concept analysis before a final concept was chosen. This functional flow is an updated version of the previous functional flow seen in the Baseline Report[2]. It is more specified on this concept rather than on the mission in general.

2.2. Constituent Functionality

The chronological functions are useful for establishing the mission profile and some of the design criteria that are required to be met. They, however, do not envelop the entire design of the UAV. For example it does not specify anything about communicating with the ground station or about the power it needs to provide to the systems. To get an overview of these more generic functions that the system requires to have, functions are visualised in a constituent manner through the use of a FBS. This FBS can be seen in Figure 2.2.

The functions that have been differentiated are navigating, perching, controlling the payload, moving towards the target, providing power and communicating with the ground station. In this diagram, blue indicates the fist separation, yellow indicates the functions that fall under the top level functions and purple indicates a further level of depth.

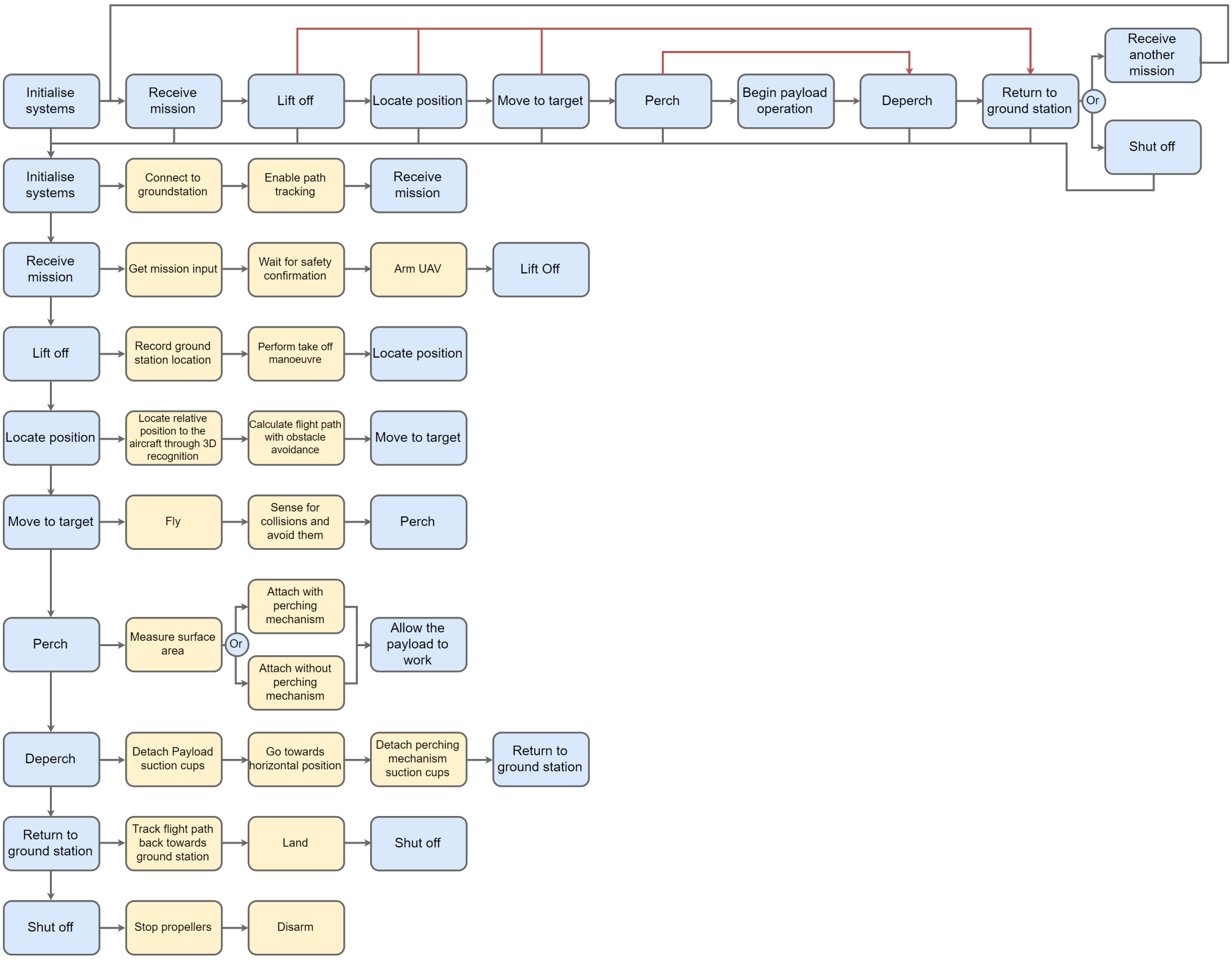

Figure 2.1: Functional flow diagram of the mission where the red lines indicate the flow in case of an emergency

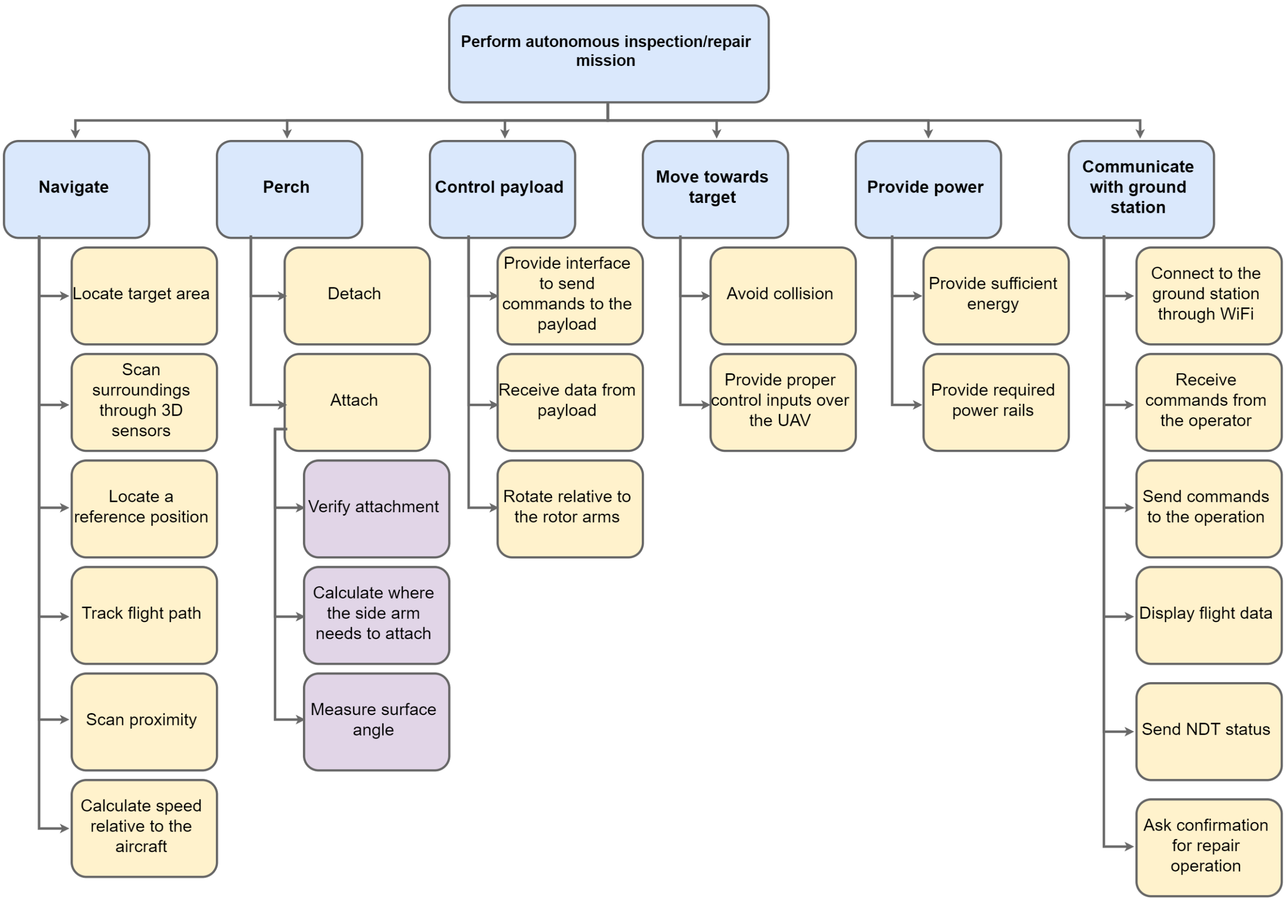

Figure 2.2: Functional breakdown structure of the mission. NDT stands for non-destructive testing.

3 Mission Profile & Logistics

In this chapter the mission profile and logistics are presented. It starts with Section 3.1, where the mission profile is given. hen, the use case diagram and the logistics are shown in Section 3.2. Finally, the inputs and outputs of the reparation mission are given in Section 3.3.

3.1. Mission Profile

The repair mission of the UAV can be split up in four stages as illustrated in Figure 3.1. Note that the functional machine is not designed by the team, and will be further discussed in Chapter 5. This machine is the payload of the system. The UAV is only required to lift the payload, attach the payload to the aircraft, perform pre- and post-inspection by means of NDT, perform communications (send data and receive user input) and finally return to the ground station.

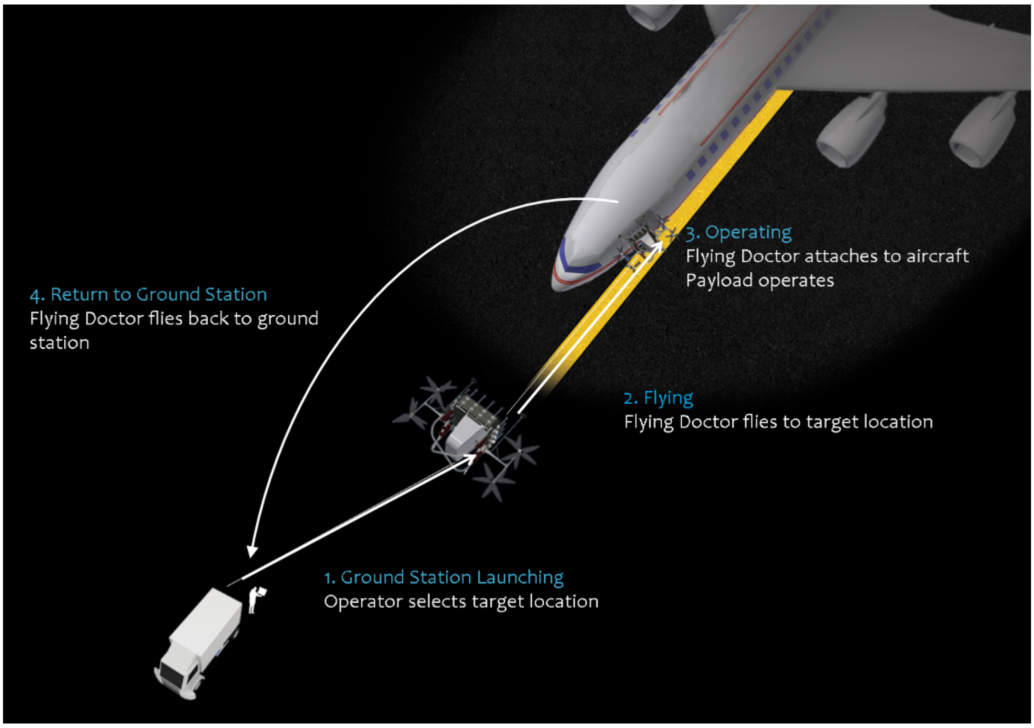

Figure 3.1: Visualisation of the mission profile

Now that it is known how the system should function, a broader overview needs to be provided. This overview is created by the use of a FFD which can be found in Figure 3.2. It shows the actions that need to be undertaken and which user performs this action. There are three users: the company (that designs and utilises the UAV), the customer (an airline in this case) and the system (the UAV). The colours indicate which action is done by which user. The blue coloured actions are performed by the customer, the yellow ones by the system and the purple actions are performed by the company and its operator.

The communications in "Perform communications" include all the data that need to be sent between the operator and the UAV. This includes sending and receiving the status update, information on the damage and granting and receiving permission. The communications are considered to be performed in the pre-inspection, payload operation and post-inspection stage.

"Perform after sales" is often forgotten, but to sustain a company it is important to perform. After sales means keeping the customer satisfied even after the initial sale of the product. The customer is entitled to give feedback by phone, email and personal meetings. The company may implement the feedback in the design for future UAVs or it may immediately solve the remarks on the particular UAV of the customer.

3.2. Use Case & Logistics

A use case diagram is a behavioural UML (Unified Modelling Language) diagram[1]. Typically, a use case diagram shows all actors involved with a system and what functions they require of the system. These functions are called use cases. Also the interaction between different use cases is displayed in a use case diagram. The use case diagram of the UAV is shown in Figure 3.3. To get an encompassing overview the logistics are displayed in a diagram that also includes the interactions between the different actors. For the logistics the actions and functions are more generalised compared to the functional flow diagram. The logistics are displayed in Figure 3.4. Again: the blue coloured actions are performed by the customer, the yellow ones by the UAV and the purple actions are performed by the company. The actions are arranged in boxes connected with lines to both the user(s) that performs the actions and the user(s) that is/are affected by these actions. For example, the box in the bottom right corner indicates that either the customer or the UAV performs the action and either the UAV or customer gets impacted by it. "Register and view data" and "Send and receive order" is performed by both the customer and the company and is therefore indicated in grey.

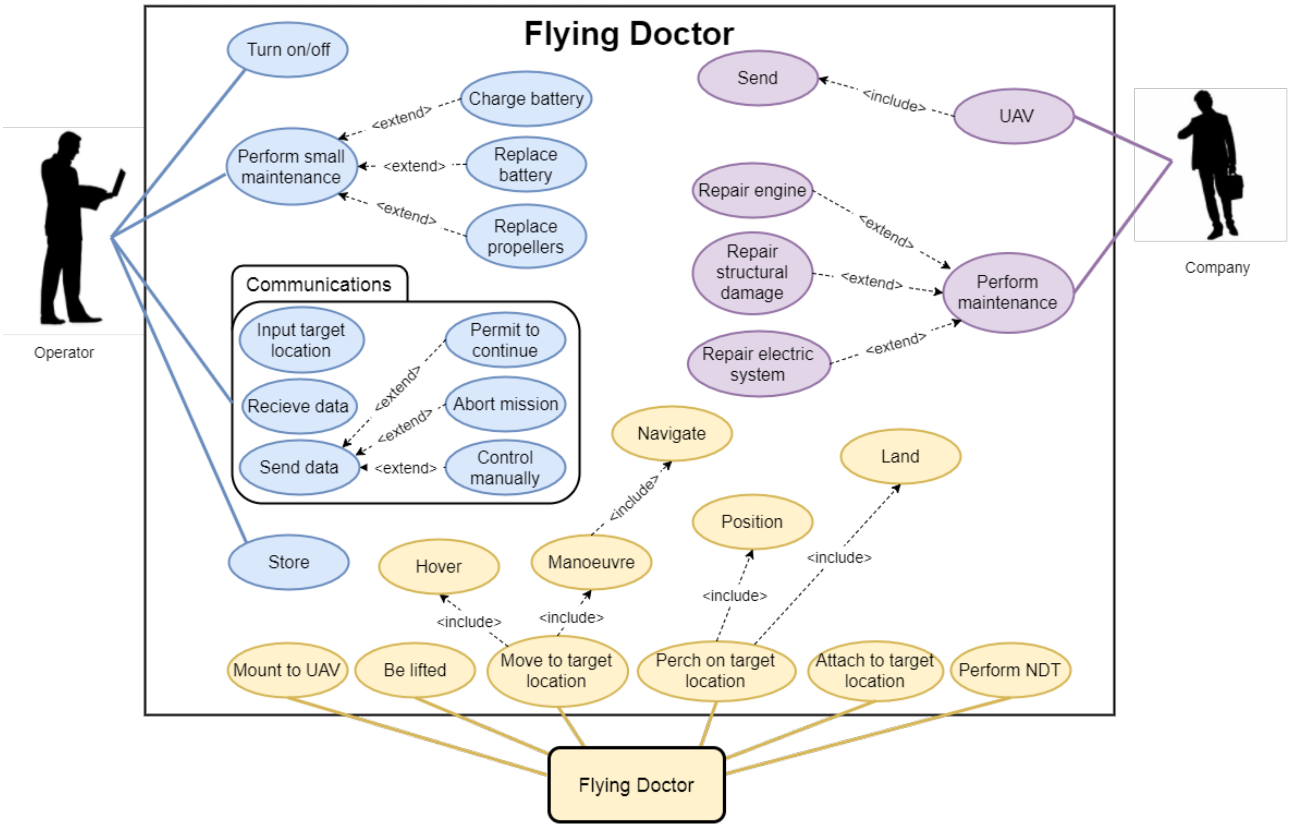

Figure 3.3: Use case diagram of the system

[1] http://creately.com/blog/diagrams/uml-diagram-types-examples/#UseCaseDiagram [Accessed on 2 June 2017]

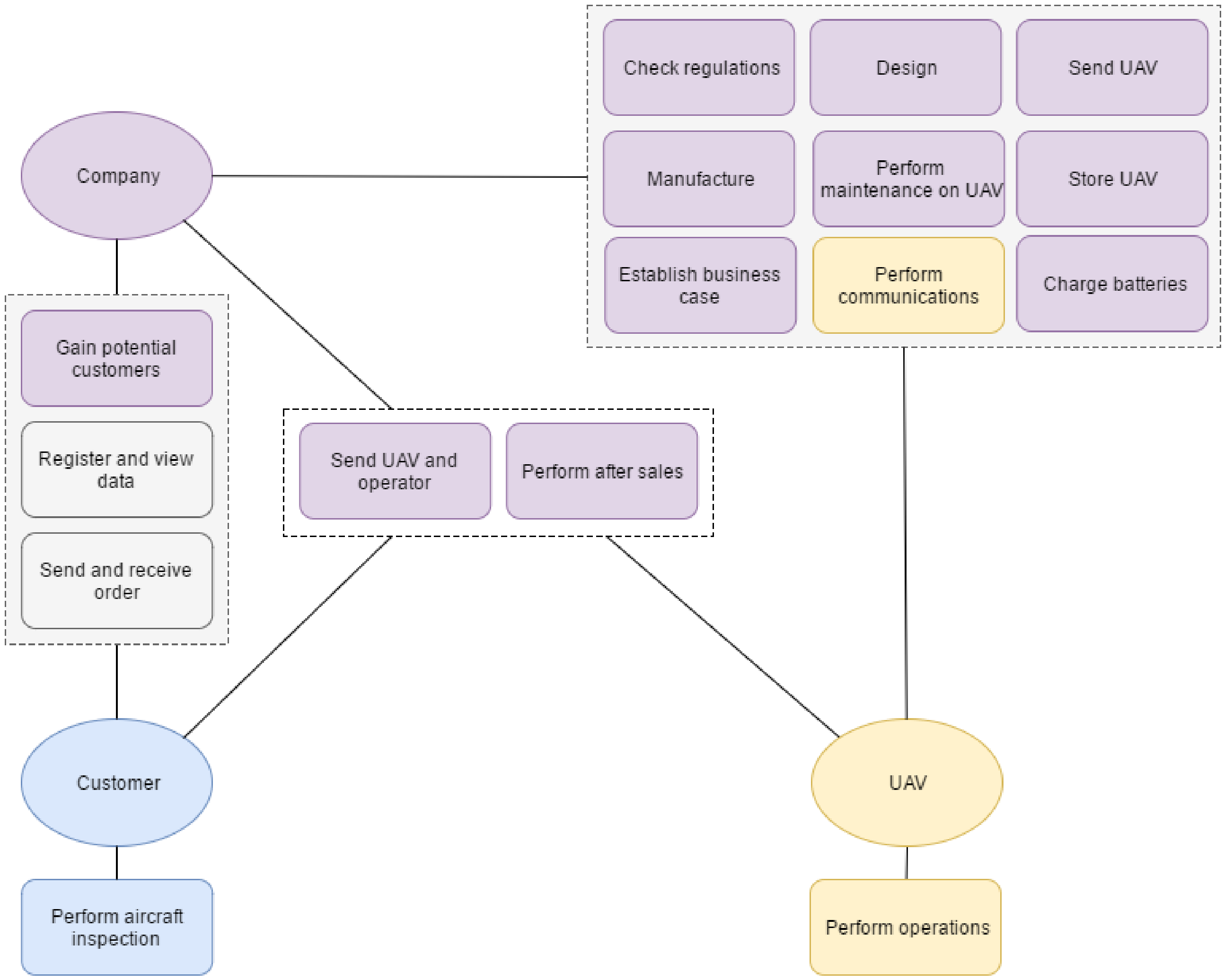

Figure 3.4: Logistics of the system

3.3. Inputs & Outputs

In order to perform the action "Operate system", displayed in Figure 3.2, inputs are required. These inputs are processed and outputs are provided by the UAV. These inputs and outputs are analysed for the main states and are visualised in Figure 3.5.

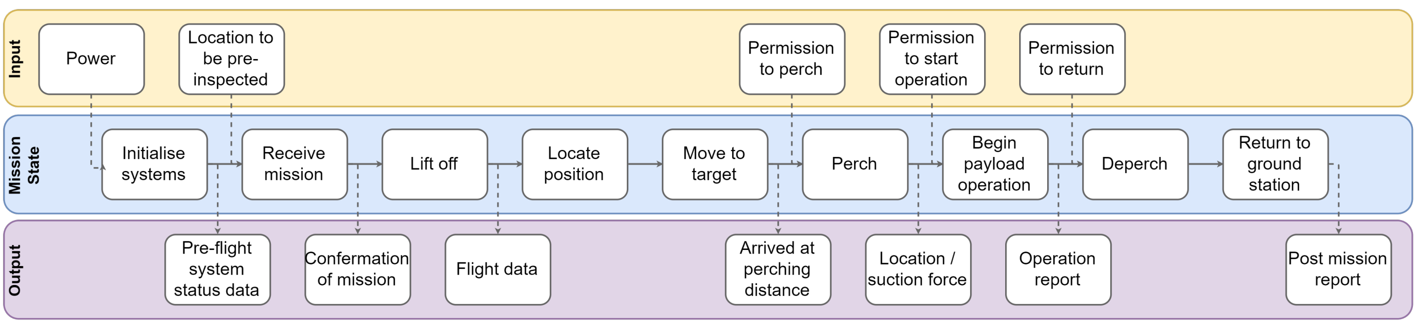

Figure 3.5: Inputs and outputs for each function

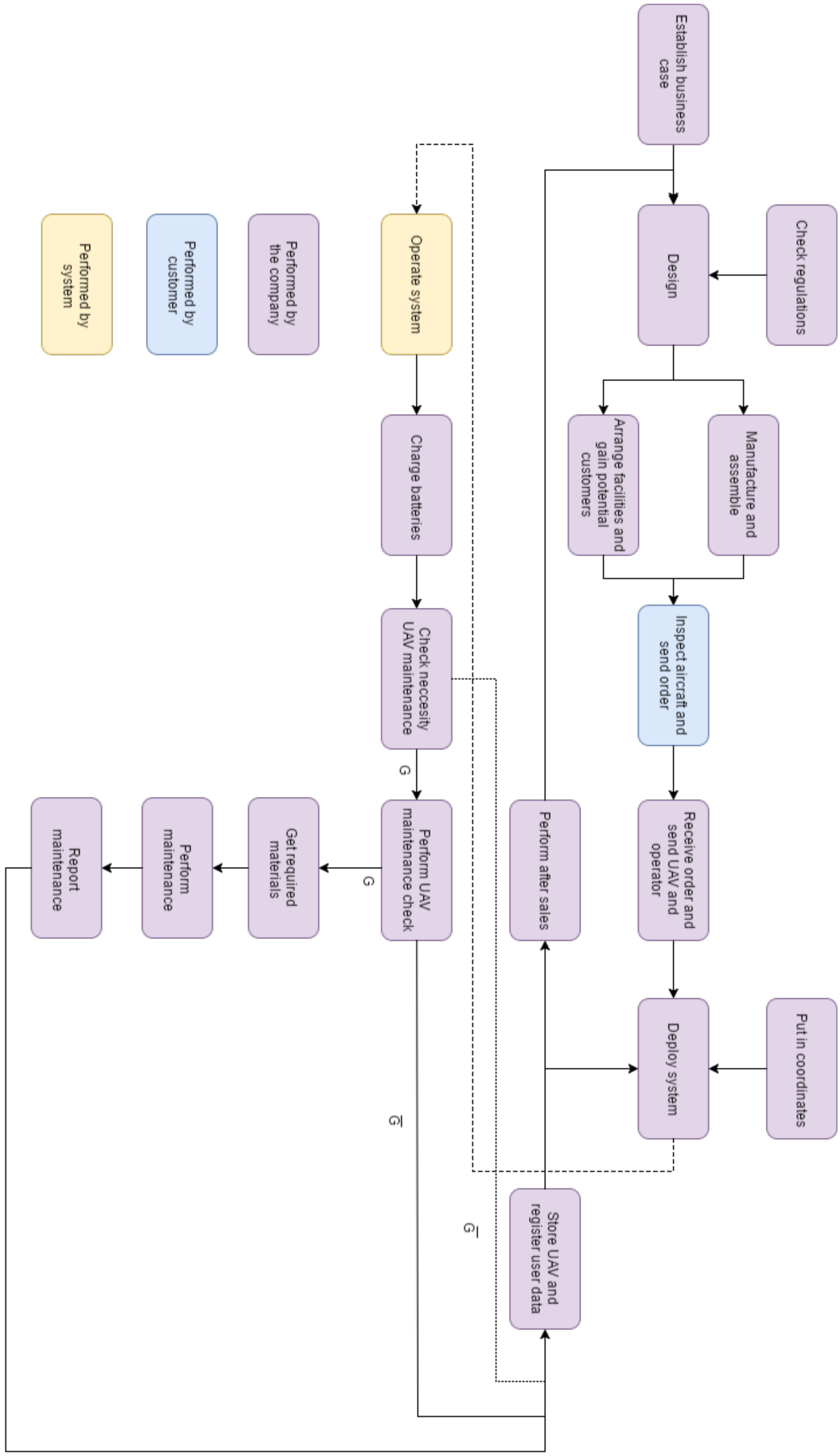

Figure 3.2: Functional flow diagram for logistics and operations. The blue coloured actions are performed by the customer (and its maintenance engineer), the yellow ones by the UAV and the purple actions are performed by the company.

4
Market Analysis

This chapter goes into detail about the market analysis performed for the Flying Doctor UAV. First, the opportunity and advantages of the UAV in the airline MRO industry are discussed combined with representative case studies. The current solutions are analysed and compared with the use of the UAV in Section 4.1.1 and Section 4.2 respectively. For the cost breakdown analysis, the business model trade off and the market share estimation refer to Section 16.3

4.1. Reducing Aircraft Downtime

Since the 2008 financial crisis airlines have had an increasing amount of difficulty in making profits. Figure 4.1 visualises the profits of airlines worldwide between 2004 and 2017. As can be seen from the graph, airlines are getting back to making higher profits, with a significant increase from 2015. This increase is caused by the fact that oil prices drastically fell in that year reducing operational costs for airlines. However, even with the low oil prices currently, airlines are aiming to increase profit margins.

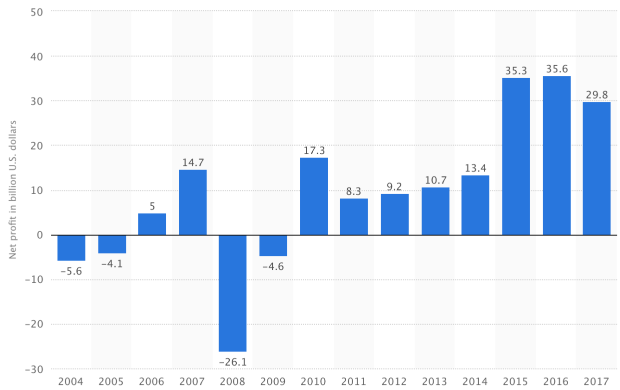

Figure 4.1: Profit of airlines worldwide in USD (2004-2017)[1]

It is a fact that aircraft can only make money for an airline while they are up in the air carrying passengers and/or cargo. Hence as an airline it is crucial to limit the time on the ground, referred to as "downtime", as much as possible. Downtime reduction can be approached in several ways. The Flying Doctor UAV is aiming and reducing downtime caused by incident damage by providing mobile inspection solutions and faster overall maintenance performance.

4.1.1. Current Solutions

Current airline *maintenance* operations are not performed using UAVs. Solutions have been developed for visual inspection, but there are no existing products capable of lifting NDT/repair units of significant size. The current solution to reach hard to access locations and perform repairs is to use cherry pickers (or scaffolding for more extensive repairs). This procedure consists of setting up the cherry picker as close as possible to the repair location, which may be complicated due to space constraints in hangars and manoeuvring the arm towards the damage location. This process is often time consuming resulting in both direct and indirect costs.

1. Longer maintenance procedures results in increased labour costs (direct).
2. Longer maintenance will cause the aircraft to be grounded longer, decreasing the amount of time it can generate income for the airline (indirect).

4.1.2. Flying Doctor Advantages

The time required to repair certain damage on aircraft depends on the type of damage, manpower (amount and skill level), equipment and spare parts available for repair. Improving any of these parameters will result in faster maintenance pro-

[1] https://www.iata.org/events/Documents/MCC2016/Program_MCC.pdf [Accessed on 21 June 2017]

cedures resulting in downtime reduction and cost savings. The main advantages of using the UAV over current solutions are listed below.

1. The UAV can perform on apron inspections, preventing the aircraft having to be towed away to a hangar.
2. The UAV can manoeuvre around the hangar without having the need to move obstacles on the ground.
3. The UAV requires less manpower for maintenance since it operates autonomously (only an operator is required).
4. The UAV is not constrained by reach, as opposed to cherry pickers which are which are limited by the arm length.

Summarising, making use of the UAV will provide time and consequential cost advantages. In order to quantify these advantages and determine the operational profit of the chosen business model, two representative case studies are performed in Section 4.2. The case studies represent two distinct cases: on apron operations and hangar operations. Both case studies make a comparison between the conventional solutions and the use of a UAV.

4.2. Case Study

The following two case studies are made in order to provide a quantitative example on the advantages of the UAV. Case study 1 assumes the possibility of on apron inspection/repairs, which will yield a large time advantage for airlines with gate delays. Note that cost assumptions are based on estimates since airlines keep detailed numbers classified.

4.2.1. Case 1 - Inspection at Gate

The aircraft in consideration is a Boeing 737, being currently on of the most used aircraft by airlines. It is assumed the aircraft is at the gate to perform a flight within a 1500 km radius. However, it is suspected there might be lightning damage from the previous flight on top of the front part the fuselage. In order for the airline to verify whether it is safe to continue the flight, a NDT inspection has to be performed.

The conventional solution would be to tow away the aircraft to the hangar and perform an inspection there. In order to continue the flight a replacement aircraft has to be arranged. The costs for compensating passengers delay should also be included.

Next to the costs mentioned above, additional costs such as ATC (Air Traffic Control) rerouting costs, exceeding of slot times and potential replacement of the crew should be taken into account as well. Eurocontrol developed a mathematical model to estimate "at gate" delays and is used for this case study. It was concluded that for delays longer than 15 minutes the cost is €72/minute in European airspace using twelve reference airports [2]. Note that this number varies under different circumstances and that this is an average value. However, for comparison purposes this number is deemed to be sufficiently accurate.

Using the €72/minute cost, a rough comparison can now be made between the case that the Flying Doctor UAV is available or not. For the conventional case, it is assumed the whole procedure of towing away the aircraft and setting up a replacement aircraft with crew will take on average 1.5 hours, assuming a replacement aircraft is available. This will yield a cost of 90 minutes $\cdot$ €72 = €6,480. Furthermore, the cost of the replacement aircraft should be added to this as well. Estimates of these costs are typically classified by airliners. However, from contact with KLM Engineering and Maintenance it was found that replacing a Boeing 737 flight will cost between €20,000-€30,000, depending on availability of standby aircraft. The average of this range is used in the remainder of the comparison.

In the case a Flying Doctor UAV is available, there is no need for towing away the aircraft. Assuming the UAV is available on a service model basis (See Chapter 16), the inspection can be started at the gate within (at most) 20 minutes, taking into account the response time of the UAV operator. The inspection and quick fix repair can be performed in 30 minutes if the damage is suitable for repair by the DMG MORI. This will yield a maximum delay time of 50 minutes resulting in 50 minutes $\cdot$ €72 = €3,600. Furthermore, the cost of a repair has to be added to this to come to the complete UAV repair and inspection price. This price depends on the following aspects:

- Operator costs
- Material costs
- Transport
- Service fee

A cost estimate per repair is presented in Table 4.1

Table 4.1: Repair cost breakdown

Cost element	Cost €	Assumptions
Operator cost	42	Hourly wage of €50
Material cost	30	Price of Al-6061 patch
Transport	30	Transportation of UAV to apron
Service fee	500	Expert damage inspection assessment

[2] https://www.eurocontrol.int/sites/default/files/field_tabs/content/documents/single-sky/pru/publications/other/cost-of-delay.pdf

This will yield the total cost of a UAV inspection and repair procedure of €4,202. Comparing this to the replacement of aircraft solution, this will save the airline €25,000 - €4,202 = €20,7980. Naturally, this cost saving is based on average numbers and assumptions as stated in the above analysis. However, this comparison is aimed at estimating the order of magnitude of cost savings. Concluding, making use of the Flying Doctor UAV in this particular case will take 17% of the conventional maintenance and repair cost. This cost advantage is primarily coming from the fact that the inspection is now performed at the apron instead of in a hangar, resulting in large time savings and consequential cost savings.

4.2.2. Case 2 - Hangar Repair

For the second case study again a Boeing 737 is considered. It is assumed that the aircraft is inside the hanger with lightning damage located on the top of the fuselage at the wing section. This is a particularly hard to reach location for cherry pickers due to the obstruction by the wings resulting in an increased maintenance time required for positioning.

Since the maintenance cost per hour on an aircraft depends on a large amount of parameters, this analysis will focus on the time savings specifically. From this, depending on the flight hours of the aircraft, the type of damage and amount of personnel required the cost savings can be determined.

Regarding the conventional solution, the time required for this procedure is estimated to be around 15 minutes for the setup of the cherry picker. Furthermore, it is assumed at least two maintenance technicians are required for this operation. Regarding the UAV setup time, only 7 minutes roughly are required. Furthermore, only one operator is required. This will have a time saving of, on average, 8 minutes per repair/inspection procedure in a hangar. Finally, to make a fair comparison the repair time is assumed to be the same. However, in most cases the DMG MORI payload will be faster and more accurate in most repairs with respect to those performed manually.

4.3. Opportunity in New Markets

Apart from airline maintenance the UAV can be applied in more industries. Effectively it is capable of carrying and positioning heavy payloads of around 85kg. Several other applications of this could be:

1. Delivery of Search and Rescue equipment to remote and/or hard to reach locations.
2. Lifting of construction material replacing the use of conventional cranes.
3. NDT inspection and repair of land based (oil) pipelines.
4. Ship inspection and repair (above water level).
5. Wind mill inspection and repair.

Applications 1 and 2 make use of the high lifting capabilities of the UAV which is a market with high opportunity due to the lack of competition and relatively expensive alternatives (e.g. use of cranes vs a UAV). Applications 3-5 are almost identical to the inspection and repair of aircraft, however different repair units might have to be used and certification requirements are different for aircraft.

5
Detailed Design Starting Point & Designated Payload

This chapter summarises the design state transitioning to detailed design. It builds on the Section 5.1, which covers the selected concept vehicle. The aim is to inform the reader about the payload prior to elaborating on the subsystem designs in the preceding chapters. Section 5.2 describes briefly the payload that the Flying Doctor intends to carry and Section 5.3 explains how the more detailed dimensions of the payload were estimated.

5.1. Selected Concept

Prior to the detailed design, several concepts were explored and based on different criteria their defined parameters are traded-off and analysed on their sensitivity [3]. At the end, scores were graded each concept,and the concept with highest grade is selected. The section will further develop on the selected concept's unique operation, advantages and disadvantages.

The concept of a multirotor vehicle built around the payload was selected for detailed design. It is fully electrically powered using on-board lithium-sulpur batteries. It has rotating arms that can reorient the payload to any required angle while keeping the propulsion system in a constant plane, allowing slow and precise manoeuvring during perching. The rotor arms can be disconnected for compact storage and transportation layout, reducing the total volume of the vehicle to nearly that of the payload itself. The vehicle has eight rotors, mounted in coaxial pairs in four corners of the frame. The most significant dimensions such as of the rotors, arms and the major component clearances in the layout are known and covered in the sections detailing respective systems' design.

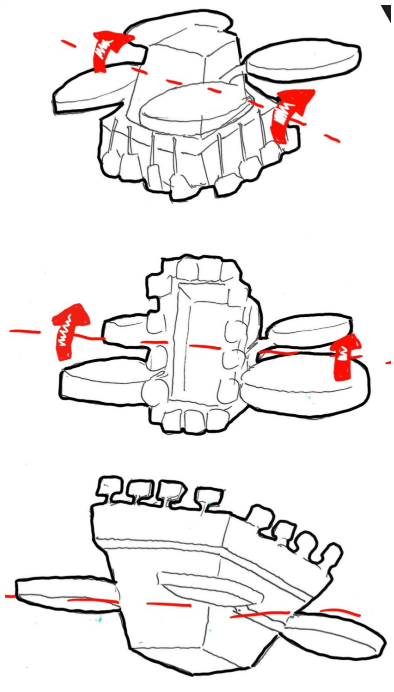

Figure 5.1: Sketch of selected concept vehicle, showing the most distinctive layout features. The line indicates the rotation axis of the payload.

The selected concept has the following advantages:

- **Mature flight hardware and software** - Multirotor vehicles have seen great development in the past decade. Highly capable flight controllers, sensors and compact compute boards are readily available. Multiple projects are open-source, providing a functional base and reducing development costs.
- **Stable and easily controllable** - Multirotor vehicles are stable, relatively insensitive to shifting centre of gravity and capable of precise flight.
- **Redundant propulsion** - The eight rotor configuration is fully redundant for one lost rotor, increasing reliability.
- **Minimal interference with payload** - The vehicle is built around the payload's hoisting frame. Because the attachment uses already present connections on the payload, it does not require any structural modification. Vehicles or even payloads could be easily swapped by the operator, if necessary.
- **Low weight** - Because the vehicle is built around the payload's hoist frame, significant weight is saved by eliminating the need for most of the centre structure.
- **Small storage footprint** - The removable rotor arms allow the whole vehicle to be stored in a volume not much larger than the payload.
- **Easily accessible horizontal surfaces** - The vehicle can safely and directly perch on surfaces which are relatively horizontal, either from the top and bottom.

However this design also has drawbacks, of which the main ones are:

- **Additional measures to access vertical surfaces** - Due to propeller clearance, the vehicle cannot directly land on relatively vertical surfaces as it is able to on more horizontal ones. Additional support mechanism and special landing manoeuvres are required to safely perch on these surfaces.
- **Complex rotor arm design** - The rotational mechanism for the arms has to withstand large bending and torsional loads and still allow easy detachment. Additionally, the design has to also account for any electrical connections

present.
- **Large operational footprint** - Although the vehicle is small in storage, once deployed and ready for flight it is approximately twice as wide. This introduces additional considerations about operation. In this sate, it cannot be handled without additional equipment due to weight and will require additional attention for mobile deployment strategy.
- **Balance** - The vehicle has to be well balanced to allow rotating the payload. Although the multirotor configuration is capable of handling large shifts in centre of gravity, unbalanced weight degrades flight performance and should be avoided within reason.

5.2. ULTRASONIC mobileBLOCK

The Flying Doctor's payload is an ULTRASONIC machining system of DMG MORI for MRO and production purposes[1]. It is an automated and mobile repair solution for damaged composite surfaces. Its lightweight construction, makes it adaptable and flexible to be carried by the Flying Doctor.

The main highlights of the ULTRASONIC mobileBLOCK are as following:
- Powerful, mobile milling unit
- Lightweight construction with carbon fibre reinforced plastic (CFRP)
- Universal operation: scarfings and edge trimming for production and MRO
- All composites, aluminium- and magnesium alloys machinable
- Highest precision and reproducibility
- Enormous time benefit
- Computer-aided manufacturing (CAM) fully integrated
- Easy and user-friendly, computer-based control

Figure 5.2: ULTRASONIC mobileBLOCK attached to an aircraft fuselage[1]

[1] http://en.dmgmori.com/blob/172070/5439d5778a35de4a332cd668a5ddb973/pu0uk15-ultrasonic-composite-pdf-data.pdf/ [Accessed on 10 May 2017]

Table 5.1: ULTRASONIC mobileBLOCK specifications

Description	Value
Rapid transverse	14m/min
Dimensions	1.3x1.3x1m
Weight	85kg
Suction power	256N (per foot)
Adaption system	SAUER 16 Vacuum feet

5.3. Mock Payload

Only the outer dimensions of the DMG Mori's ULTRASONIC mobile-BLOCK are openly stated by the manufacturer[2]. The design, however, requires much more detailed information about the payload for integration and determining clearances. Using the limited set of dimensions available and various images from manufacturer's catalogues, brochures and other advertising, a more detailed approximation of the payload was produced in CAD and is shown in Section 5.3. The vehicle's design will be built around this model during the detailed design.

The estimated geometry provides key information about the size of major structural features and areas traversed by the moving components of the payload. For example, the clearance between the moving centre structure and the outer edge of the frame determines maximum depth of the root connection of the rotor arms as explained in Section 8.1.1.

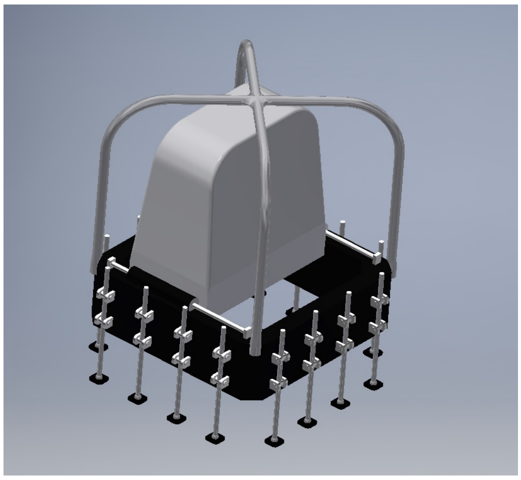

Figure 5.3: Mock payload and its hoist frame. This is the estimated payload geometry used as a reference for design of the vehicle.

[2] http://en.dmgmori.com/blob/172070/5439d5778a35de4a332cd668a5ddb973/pu0uk15-ultrasonic-composite-pdf-data.pdf/ [Accessed on 19 June 2017]

6
DMG MORI ULTRASONIC mobileBLOCK's Supplements

This chapter introduces the miscellaneous subsystems that will be added to the DMG MORI ULTRASONIC mobileBLOCK. These modifications are included to satisfy the stakeholders' requirement and meet the Flying Doctor stringent requirements. The adjustments are deemed critical to the main design of the payload, such as software integration in terms of data processing from various functions, including, for example, the NDT. Hence, consulting the representative from DMG MORI on the proposed design is inevitable. The changes could be regarded as recommendations in order to fulfil the Flying Doctor's fullest potential. Section 6.1 describes the merit of the additions to the payload and presents the components necessary in a weight table. Section 6.2 highlights how to tackle the external vacuum hose of the DMG MORI ULTRASONIC mobileBLOCK. One of the important aspects of the entire operation is to be able to confirm the maintenance engineer's previous visual inspection that the damage exists and is repairable with the mobileBLOCK. Its design aspect will be treated in Section 6.3. The payload power consumption's information cannot be obtained therefore a mock milling machine with similar capability is compared to assess its power consumption, which will be in Section 6.4. Finally, the chapter ends in Section 6.5 with a discussion of how to paint the surface after the repair is completed.

6.1. Necessity of Externalities to the Payload

The DMG MORI ULTRASONIC mobileBLOCK relies on an external power supply for running the machine, and an external vacuum pump for operating its suction cups. This implementation in the Flying Doctor will be unfeasible as the weight requirement will be violated by the enormous weight of the electrical cables for given flight envelope requirement **[OP-2.5]**[3]. In addition, the Flying Doctor strives to offer a packaged service of inspection, repair, and painting in order to effectively reduce downtime as described in Chapter 4. As the payload focuses solely on repair technology, retrofitting it for the Flying Doctor is eventually required. Hence in the following sections the vacuum pump, NDT and painting are described. Their individual components are summarised in Table 6.1.

Table 6.1: Overview of the payload's supplementary components in terms of weight and power consumption

Components	**Weight [kg]**	**Power Consumption [W]**
Vacuum Pump	3.00	Own Supply
Spindle	mobileBLOCK	1000
Inventer	3.60	200
IR-Camera	2.37	60
Halogen bulbs	0.10	500
Shearography Camera	5.80	60

6.2. Attachment via Vacuum System

In order to select a vacuum pump for the payload, several criteria have to be taken into account: the pressure to be removed to ensure the optimal suction force, the air suction rate which is dependent on the suction cup dimensions, and finally the weight and power consumption in regards to the requirements.

6.2.1. Pressure Supply

A suction cup is a device that utilises the pressure difference between the enclosed cavity and the surroundings to exert a holding force, which is responsible for adhering to the desired object. Its usage in mobile machines has gradually been gaining popularity. For the Flying Doctor's payload, DMG MORI's mobileBLOCK, the assumption is that it uses sixteen rectangular suction cups, whose dimensions are shown in Figure 6.1. The dimensions of the suction cups are inaccessible to the public and are therefore measured from the picture in the catalogue 5.2.

It was estimated that sixteen suction cups of DMG MORI are capable of holding the Flying Doctor's weight[3]. Each suction cup has a holding force of 256N. Two cases will be studied. They are the holding force against vertical and

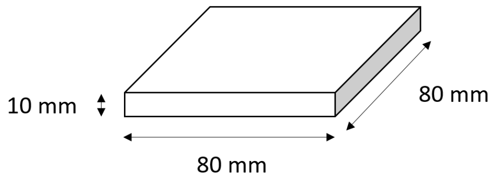

Figure 6.1: Dimensions of DMG Mori's ULTRASONIC mobileBLOCK's suction cup

horizontal forces which are reflected in Equations 6.1 and 6.2 respectively. They are to simulate the pressure needed to perch at a different location around the aircraft. The ambient pressure is assumed to be the pressure at sea level, which is 1 bar.

$$\Delta p_v = \frac{F}{A_{sc}} \tag{6.1}$$

$$\Delta p_h = \frac{F\mu}{A_{sc}} \tag{6.2}$$

With a suction cup area, A_{sc}, of $64cm^2$, and a coefficient of friction, μ, of 0.5, the pressure differences required to counteract the vertical and horizontal forces are 40,000Pa and 80,000Pa. The effective suction cup area refers to the area that is subjected to the vacuum. For the purpose of simplification, the suction cup skins are not taken into account. The coefficient of friction is normally obtained by the process of trial and error, in this case, however, the metal skin surface is assumed.

The computation of pressure difference is important in choosing the vacuum pump as the result will help to determine the specifications of the vacuum pump. The vacuum pump should be able to supply rough vacuum of 40,000 Pa against the ambient pressure.

6.2.2. Vacuum Pump

A vacuum pump is a device that removes air from an enclosed space in order to create vacuum space.

Suction Rate

Flow rate or suction rate is one of the driving parameters for vacuum pump selection. Flow rate dictates the volume rate of air being released to create the desired vacuum. In addition, the right amount of flow is needed to supply the holding force. The Suction rate is highly dependent on the suction cup dimensions. The relation between suction cup diameter and the suction rate is shown in Figure 6.2.

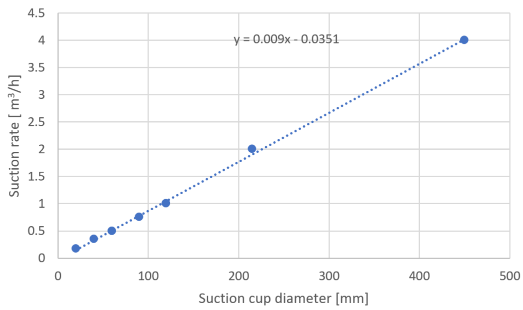

Figure 6.2: Linear regression between suction cup diameter and suction rate

Information based on rectangular suction cups are not available as the convention for the suction cup is a circle. Therefore for $64cm^2$ rectangular suction cup area, it has to be converted to the diameter of a circular suction cup. The corresponding diameter is 9.02cm.

From the linear regression equation from the collected data[1 2], with a diameter of 9.02cm, the required suction rate is $0.777m^3/h$ or 12.96L/min.

[1] https://www.schmalz.com/en/vacuum-knowledge/the-vacuum-system-and-its-components/vacuum-suction-cups/design-of-the-suction-cup/[Accessed 13 June 2017]

[2] http://www.avs-yhtiot.fi/sites/default/files/pdf/7.01.05_alipaine_ohje.pdf/[Accessed 13 June 2017]

Table 6.2: Vacuum pump specifications

Model	**Makita DVP-180**
Dimensions [hxlw] [cm]	26.5x9.3x17.5
Weight [kg]	2.9
Power [W]	Self supply
Flow rate [L/min]	50

Weight & Power Consumption

With the interest of the limiting the power consumption to the battery, a cordless vacuum pump has been selected. The vacuum pump has its own internal battery, which is able to run for 55 min[3]. Its addition will add a weight of 2.9kg. Its specification is shown Table 6.2.

As it has been mentioned previously, the suction cup engagement was selected based on the flow rate required and the pressure supplied. The imposed suction rate of 12.96L/min is fulfilled by the selected vacuum pump, which provides 50L/min.

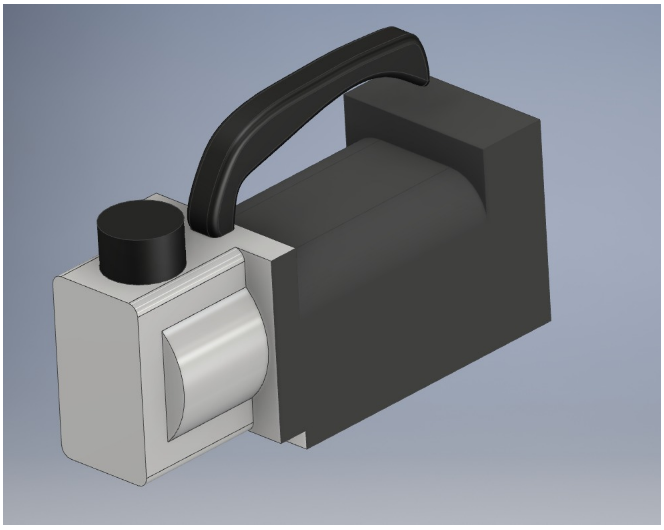

Figure 6.3: Vacuum pump Makita DVP-180 in CAD

Safety

The vacuum pump plays a vital role in the vigilance of the Flying Doctor system. One aspect is vacuum evacuation time. It refers to the time required for the suction cup to be fully engaged/disengaged to/from the surface. It is an important parameter in regards to emergency detachment, in a case of any mission aborts.

$$V_{ts} = N_{sc} \cdot V_{sc} \tag{6.3}$$

$$t_{sc} = \frac{V_{ts}}{q \cdot \ln \frac{p_0}{p_1}} \tag{6.4}$$

Using Equation 6.3, the total volume of the 16 suction cups, V_{ts} are 1.024L. With volume rate from Makita DVP-180 of 50L/min, the time required to release, t_{sc} can be calculated using Equation 6.4. Consequently, the time taken to attach or release the suction cups is 1.34s.

6.2.3. Connection

The mobileBLOCK houses a vacuum inlet at the side of its frame. The vacuum pump will be placed at the side of the payload frame as shown Figure 6.10. A relay has to be connected between the Main Control Unit (MCU) and the vacuum pump in order to remotely control the switching of the vacuum pump. Based on the specification, Makita DVP-180 vacuum pump inlet uses 8mm hose[4]. The signal line and vacuum hose weight and connection have been addressed in Appendix C.

[3]http://www.makita.my/products/dvp180-cordless-vacuum-pump/ [Accessed on 20 June 2017]
[4]http://www.makita.my/products/dvp180-cordless-vacuum-pump/ [Accessed on 20 June 2017]

6.3. Non-destructive Testing

One of the operational requirements stipulated is providing pre and post- inspection of the damaged area with a standard NDT tool. NDT has to be automated with least human interference, and implementable with the current design of the Flying Doctor. The ultrasonic testing method is effective in detecting surface, however with some disadvantages, including the need for couplant to introduce acoustic waves and lack of sensitivity to shallow surface breaking defects[5]. The dye-penetrant technique seemingly needs post cleaning which is unfeasible, considering the operation of the UAV. Many of the contact methods are unfeasible, as they require complex arm mechanism to be implemented to the already crowded mobileBLOCK. In addition, automating them are more challenging relative to the non-contact counterpart. Therefore, two non-contact NDT technique, namely thermography and shearography will be discussed. Since there are several types of composite damages, this section only focuses on surface cracks.

6.3.1. Thermographic Camera

Thermographic inspection can be divided into two. They are passive, which mainly used to observe the difference temperature of the environment, and active which utilises an energy source to produce thermal contrast between the feature of interest, in the case of the Flying Doctor is the surface crack. Different techniques for active thermography can be viewed in Figure 6.4. For instance, composite surface cracks can be inspected by the pulsed thermographic eddy current. However as this technique is very expensive, it will not be considered[6]. Mechanical excitation is not considered as its non-contactless nature, made it incompatible with the Flying Doctor.

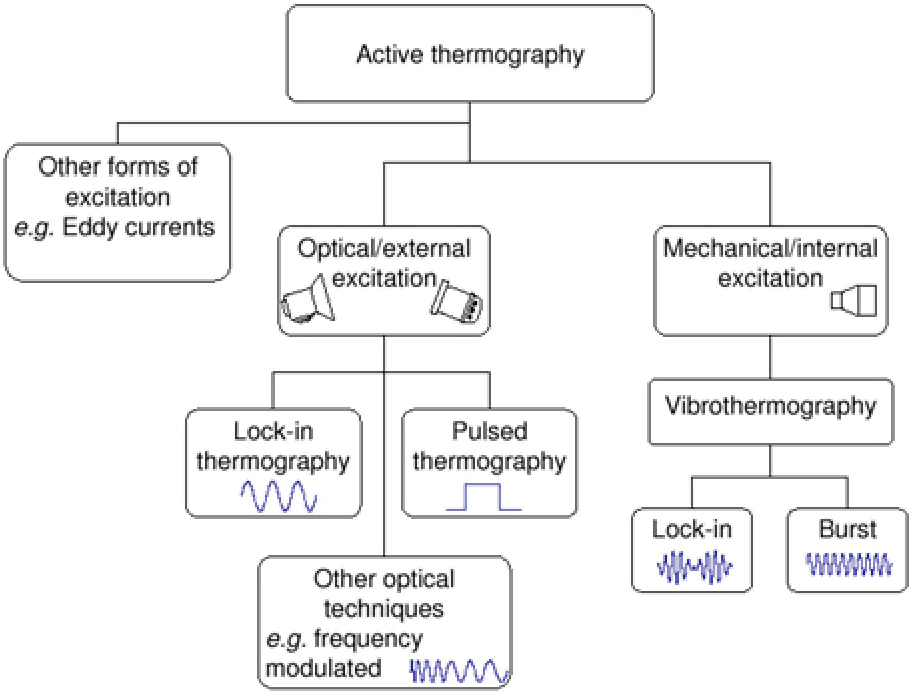

Figure 6.4: Different techniques for active thermography
[7]

The optical excitation aspect of the thermographic inspection can be divided into two types: Lock-in and pulsed thermography. They differ on the method of heating the specimen. The former heats by periodically modulated lamps and thermograms are captured under the periodic sinusoidal heating. The term lock-in points to the fact that images used for the thermograms are extracted at the same frequency as the excitation[8]. Its simpler counterpart, makes use of an optical flash to achieve instantaneous heating. Pulse thermography is suitable for thin structures such as fuselage of an aircraft as the method becomes less accurate as the depth of the defect grows[9]. Its simplicity, as in not requiring any additional component for modulating the excitation, makes it more attractive, and therefore, and it is preferred to the lock-in thermography.

Theory

the theory of thermography NDT is briefly introduced. Its aim is to understand that the basic principle of thermography for evaluation of damage detection. When a material is subjected to heated during a predetermined period of time and with a specific power profile, the response is dependent on several parameters[10].

- **Thermal properties:** conductivity, diffusivity, effusivity, specific heat.
- **Spectral properties:** emissivity, absorption, reflection, transmission.

Table 6.3: Commonly used excitation sources for active thermography[10]

Stimulus Source	**Flash lamp**	**Pulsed laser**	**Ultrasonic transducer**
Power Approximation	1kW	100J	2kW
Pulse duration	1-50ms	1-10ps	few ms

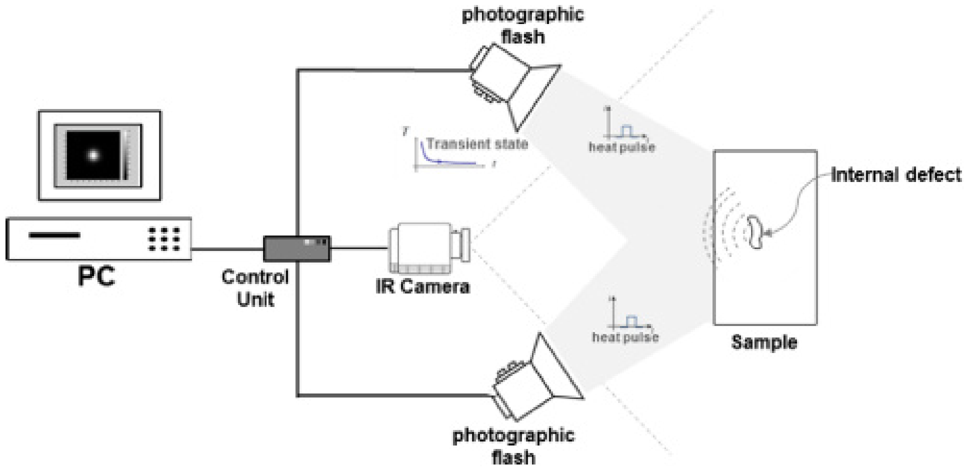

Figure 6.5: Schematic of active heat thermography[12]

To contain the scope of the report, only the important parameters are treated in this section.

When a material is excited by an external heat source, the temperature of the material will rise. For given input energy, Q and pulse duration, t as shown in table 6.3, the expected temperature could be predicted through Equation 6.5. This behaviour is highly related to its effusivity values, ef which can be obtained with volumetric heat capacity, ρC_p using Equation 6.6.

$$T = \frac{Q}{ef\sqrt{\pi t_p}} \tag{6.5}$$

$$ef = \sqrt{k\rho C_p} \tag{6.6}$$

Thermal diffusivity is altered when there is a presence of surface damage in the material. This means that the conduction of heat transfer within material will be affected.

$$\alpha = \frac{k}{\rho C_p} \tag{6.7}$$

Application

The external heat sources are used to apply heating to the material. The heat flow will travel within the material leading to change in its surface temperature will be reflected in temperature gradient as a function of time. A thermographic camera will register the surface thermal radiations and represent them as thermograms, where temperature gradients along the surface are shown as image bright contrast.

NDT thermographic procedure consists of an Infrared (IR) camera and external heat sources which are connected to a computer as shown in Figure 6.5. The choice of the IR camera is limited to its spectral range and weight. Essentially the IR camera ought to be able to provide sufficient performance to detect cracks. The selected spectral band is highly related to the material thermal and spectral properties, though they are difficult to quantify. Medium wavelength infrared (MWIR) with a wavelength of 2 μm to 5 μm are better suited for NDT inspection compared to long wavelength (LWIR) whose wavelength is between 8μm and 14μm due to latter's susceptibility to noise and the reflective surface of the material. Furthermore, MWIR technology has enjoyed a significant technological advancement that it made it more attractive solution for NDT inspection[11]. With the limited scope of this report, other criteria are not discussed. Therefore MWIR camera, FLIR A6750sc[5] is chosen. The IR-camera is envisaged to be synchronised with DMG MORI mobileBLOCK's current operation, which means the data link also will be integrated to the payload. The flow of Flying Doctor function can be referred at Figure 2.1.

Utilising external excitation to simulate heat change is the main principle of active thermography. Referring to Table 6.3 different type of excitation are available. One of the traditional methods, which is not listed, is by using a heat gun. Its application for the Flying Doctor, however, is not feasible as its mechanical mechanism requires more space. The

[5] http://www.flir.com/science/display/?id=67022/ [Accessed on 18 June 2017]

Table 6.4: Different type of excitation source for active thermography

Function	**Excitation source**	**IR camera**
Model	2x Halogen lamp	FLIR A6750sc
Spectral range [μm]	-	3-5
Power consumption [W]	2 x 250	50
Weight [kg]	0.1	2.27

discussion will proceed with the three excitation methods. For Ultrasonic Thermography (UT), the material of interest have to be subjected to vibration as the heat production is captured by an IR-camera. This configuration requires a horn which injects the ultrasound waves as the stimulus. This contact method is unfeasible for the complex mechanism, not to mention its extensive set-up. In addition, a laser as a heat source consumes large power which is unaffordable for the power budget. Halogen lamps are the simplest configuration and therefore selected for the heat source.

Literature review has shown that the rated power of halogen power varies from 500W to 1kW. However there are several considerations for choosing the proper halogen bulb. They are as follow:

- **Amount of light bulbs:** Multiple halogen bulbs will allow different variation of heating and cooling down the specimen which ensures it redundancy and more importantly allows the possibility of repeatable analysis.

- **Lumination Angle:** Different type of bulbs have a different housing which is responsible for their lumination angle. A small angle is preferred as this will reduce the heat loss, and focus on the desired area where heat is needed.

- **Input Voltage:** to prevent unnecessary weight addition and complexity, the bulb has to rely on existing voltage rails, or the inverter nominal voltage output which will be discussed in Section 6.4.2. The bulb input voltage should be one of $5V_{DC}$, $12V_{DC}$, $24V_{DC}$, $60V_{DC}$ or $240V_{AC}$.

- **Size restrictions:**The halogen lamp location has to correspond to the location of the IR-camera at the mobile-BLOCK's spindle as seen Figure 6.7.

The multiple requirements given previously, have limited the option to one option as far as the market availability is concerned. Two 250W halogen bulbs are chosen with a swivel head which allows location flexibility. It has 50 degrees of beam angle and uses 24 V rail[6].

The thermographic NDT is concluded with simplified specifications are presented in Table 6.4.

6.3.2. Shearography Camera

Shearography is an optical method that gives information about surface deformation of a loaded structure[7]. . Similar to active thermography, this load has to be provided by an external stimulus, in this case, laser. The area with damage will deform differently which will be captured by the shearography camera in a form of interferometric footprint. Two images which will be taken with and without laser load, are subtracted to create a shearogram as shown in Figure 6.6

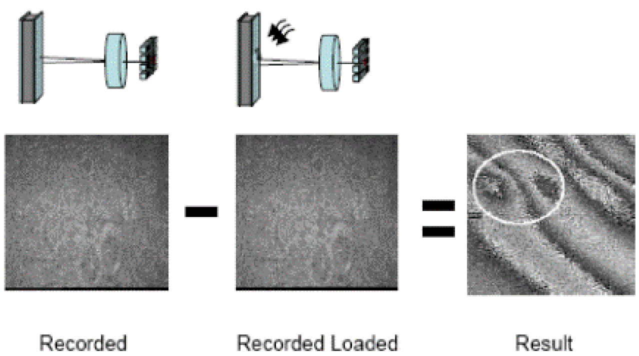

Figure 6.6: Subtraction of two images that yields a topology that shows defects as hills[7]

The theory of the shearography is relatively more advanced than the one of the thermography, and it was decided to be omitted as it does not bring value to the report.

[6]http://www.lighting.philips.com/main/prof/conventional-lamps/special-lamps/optical-medical-equipment/halogen/halogen-reflector/924010520594_EU/product/ [Accessed on 20 June 2017]

[7]https://www.dantecdynamics.com/measurement-principles-of-shearography/ [Accessed on 20 June 2017]

Application

Tripod mounted shearography cameras, are used frequently with thermal stress shearography techniques. Halogen lamps are normally used for this purpose [13].

Due to the limited knowledge on shearography, two commercial off the shelf products have been selected based on their compatibility with the Flying Doctor. The two models as shown in Table 6.5 are compared by their dimensions, weight, and power.

Table 6.5: Two shearography cameras of interest

Model	**Laser Technology Inc. LTI-2100M**	**Dantec Dynamics FlawExplorer**
Dimensions [h x l x w] [cm]	30.5 x 10.2 x 14.0	25.0 x 22.0 x 22.0
Weight [kg]	2.8	5.7
Power [W]	60	60

6.3.3. Conclusion

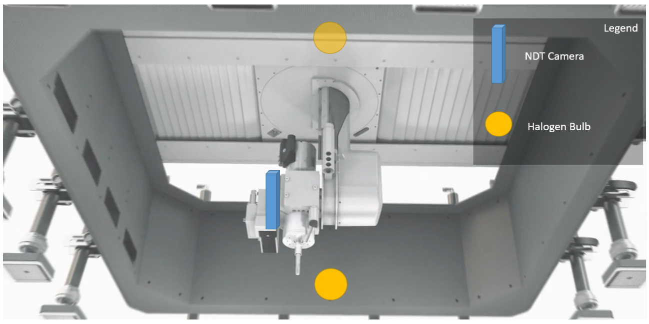

Figure 6.7: Proposed configuration of the non-destructive testing with the excitation source in a form of two halogen bulbs[8]

Thermography has some disadvantage as it is sensitive to thermal variations from the environments. Furthermore, it is susceptible to errors in a non-controlled environment. On the other hand, shearography is more sensitive to mechanic vibrations, which pose a challenge for the Flying Doctor. Both techniques hold their advantages and disadvantages that complement each other, and if implemented they will tremendously improve the performance in the detection of defects [13].

Its implementation of the NDT in the Flying Doctor is shown in Figure 6.7, using a captured footage of the underside of the mobileBLOCK [8]. It should be noted that the feasibility of the addition is determined based on the manufacturer's discretion. The decision to include both NDT cameras, at this point, is not made, however for the mass and power budget both of them are taken into account.

6.4. Machining

Machining is a process of material removal to the desired shape. DMG MORI utilises state of the art ultrasonic milling which allows cutting a hard material such as composite in an economical fashion. Ultrasonic milling is an operation that involves a vibrating tool fluctuating in ultrasonic frequencies in order to remove the material from the workpiece. The advantage includes a better-finished product and less wear of the cutting tool. Although the degree of designing of the Flying Doctor interface does not extend to the one of the payloads, its power consumption has to be taken into account to ensure adequate power supply as demonstrated in Table 14.5. In this section, a similar spindle with similar capability is sourced to find its power estimation. Furthermore, a corresponding inverter will be described to account for the alternating current voltage input for the spindle.

6.4.1. Spindle

One of the hallmarks of the mobileBLOCK is its capability to automate bonded repair for composite surface damage. This will eradicate human errors, eliminate waste and enhance the efficiency of the repair process. The elaborate description of automated scarfing is beyond the scope of this report. However, the main functions of the process is highlighted in Section 5.2.

The mobileBLOCK uses ultrasonic machining, which machines a workpiece with vibration of ultrasonic frequency (19 25 kHz) and an amplitude of around 15 – 50 μm over the workpiece[9]. Generally the tool is pressed downward with

[8] https://vimeo.com/123335786/ [Accessed on 20 June 2017]
[9] http://nptel.ac.in/courses/112105127/pdf/LM-36.pdf/ [Accessed on 20 June 2017]

a feed force, F.

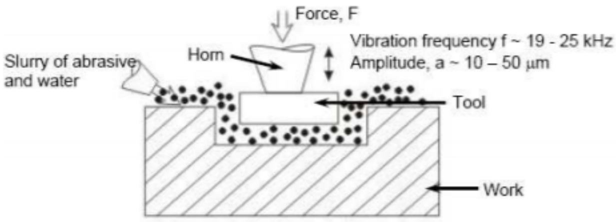

Figure 6.8: Theory of ultrasonic milling[9]

Since the power consumption of the payload is not readily available, assumptions have to be made. It is assumed that out of all the automated repair stages, machining consumes the largest power. In addition, a reference milling machine with similar capability has been sourced for the comparison.

The parameters considered are as follow:

- Ultrasonic machining
- Spindle power of 35,000 rpm[10]

Altrasonic HS-M2011 is one of the ultrasonic milling sourced that has similar specifications to the mobile block. The parameter of interest is the power consumption, which is taken as a reference for the inverter[11].

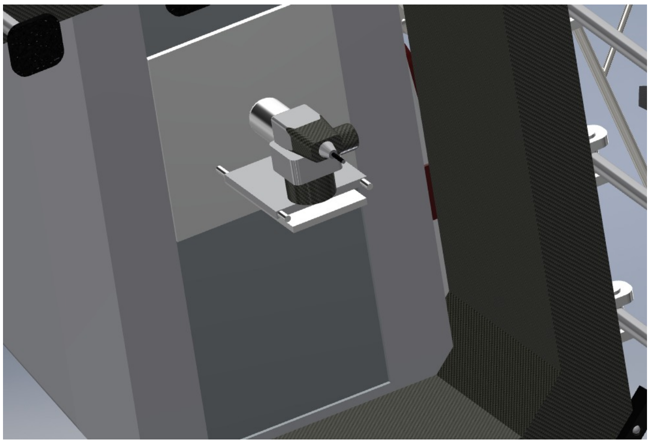

Figure 6.9: CAD version of the spindle on the Flying Doctor

6.4.2. Inverter

An inverter is an electronic device that changes Direct Current (DC) to Alternating Current (AC). For the purpose of the Flying Doctor, it is supposed to convert the $60V_{DC}$ to $240V_{AC}$ for appliances such as the ultrasonic milling, IR-camera and the halogen bulbs such as reflected in Figure 14.7.

Initially, two voltage input has been considered: $12V_{DC}$ and $60V_{DC}$. The former is considered due to their wide availability. However as reflected in Table 6.6, for the inverter nominal voltage of 2000W, its weight is not very attractive for the Flying Doctor application. In addition, the power is larger than needed as the spindle, the IR-Camera and the halogen bulbs are only require 1kW, 60W and 500W respectively.

It is, therefore, Eltek Valere INV222 is chosen to be the inverter that supplies AC to IR-Camera and the spindle. The surplus power allows for omitted operation required for the full functionality of the DMG MORI ULTRASONIC mobileBLOCK.

6.5. Painting, Aesthetics & Erosion Protection

Painting is one of the most important functionalities of the UAV. In addition to aesthetics, painting affects the weight of the aircraft and protects the integrity of the air-frame by protecting the exposed surfaces from corrosion and deterioration.

[10]http://us.dmgmori.com/blob/269958/b23d8087fc832744d806746a7d7bcae4/pu0us-ultrasonic-pdf-data.pdf/ [Accessed on 18 June 2017]

[11]http://ultrasonicweldingtransducer.sell.everychina.com/p-103998504-high-power-vibration-ultrasonic-assisted-machining-tool-with-special-steel-cutting-blade.html/ [Accessed on 18 June 2017]

Table 6.6: Inverter comparison for the Flying Doctor

Model	**Eltek Valere INV222**	**KickAss KA2000WPNR**
Dimensions [hxlw] [cm]	8.8x10.7x33.5	10.8x37.2x230
Weight [kg]	3.5	5.8
Nominal Output Power [W]	1800	2000
Nominal Input Voltage [V]	60	12
Nominal Output Voltage [V]	230	230

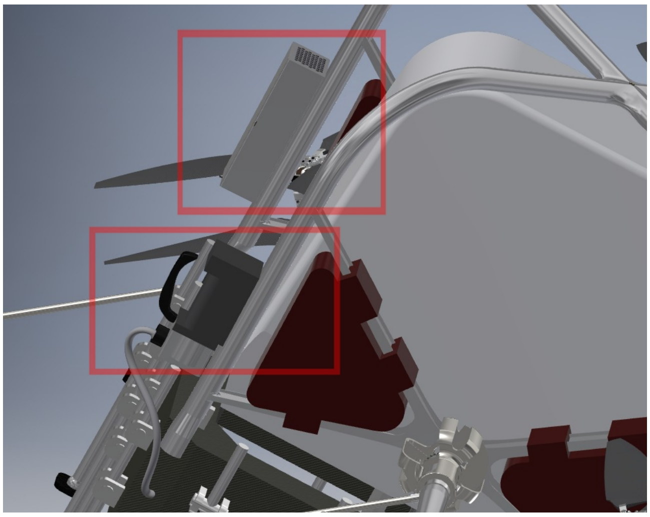

Figure 6.10: The location of the vacuum pump with its hose (bottom) and the inverter(top)

The paint is composed of a resin that acts as a coating material, colour pigment, and solvents to reduce the viscosity. Paint has three components: resin as the coating material, pigment for colour, and solvents to reduce the mix to a workable viscosity. There are several methods of applying paint to the aircraft. The most common ones are dipping, brushing, and spraying. Spraying is the most cost effective technique and consists of applying a uniform layer coat of paint over the surface. Furthermore, spraying provides the best quality finish. To be able to perform this function three main components are necessary: a source of compressed air, a reservoir to supply the paint and a device that can control the combination of the air and the paint[12]. There are three main alternatives that can be considered to protect the exposed surface from corrosion and deterioration:

1. **Spray guns** - They have an integral spray container and they are fit to coat with paint both big and small surfaces. Moreover, they are flexible to spray in any direction, but they require large equipment[13]. Spray guns also need to be serviced regularly to avoid blockage of the air supply to the gun. Compressed air 5x5cm.
2. **Pressurised spray can** - They can be used to coat small surfaces with paint and can be used with the help of a light dispenser mechanism[14]. However the aviation coating materials that can be obtained in these cans are restricted and having a dispenser with a spray can mechanism hanging under the UAV could constrain its performance, as illustrated in Figure 6.11.
3. **Tape** - It can be used for anti-corrosion protection[15]. For example, 3M^{TM} Polyurethane Protective Tapes provide excellent surface protection by preventing damage caused by fluids, foreign object damage impact, abrasion and erosion caused by airborne particles. These tapes are made of an elastic thermoplastic coasted with a high-performance pressure sensitive acrylic adhesive. 3M^{TM} Polyurethane Protective Tapes are used in military, commercial and civilian aerospace applications due to its resistance to degradation from ultra violet light and most aerospace fluids. It can be applied easily and fast and can be easily handled without tearing. Moreover, they do not contain hazardous chemicals[16].

Given the additional complexity of painting the repair patch on the air by the UAV, it has been determined that placing a tape coverage will be the most efficient solution. The tape shall have to be available, for example for KLM's fleet in white and KLM blue colour. The reference codes of the colours required for the patch are provided by their manuals. Once the DMG Mori has performed repair by applying the patch and flatten it with a roller, the transparent 3M^{TM} Polyurethane

[12]https://www.faa.gov/regulations_policies/handbooks_manuals/aircraft/amt_airframe_handbook/media/ama_Ch08.pdf[Accessed on June 15, 2017]
[13]http://www.binks.com/products/spray-guns [Accessed on the 16 June 2017]
[14]https://learn.adafruit.com/quadcopter-spray-can-mod/ [Accessed on the 16 June 2017]
[15]http://www.adhetec.com/en/aerospace/speciality-tapes-and-masking-solutions [Accessed on the 16 June 2017]
[16]http://solutions.3m.com/wps/portal/3M/en_EU/AerospaceSolutions/Home/Applications/RainAndSand/ [Accessed on the 16 June 2017]

Figure 6.11: Spray can mechanism[14]

Protective Tape 8672 will be applied on top of the patch to provide protection against erosion and impact damage of the repair-patch itself and the contour around the repair patch where it has contact with the original fuselage surface.

6.5.1. Tape Application

Tape adhesion of the 3M^{TM} Polyurethane Protective Tape 8672 can be performed on top of paint, bare composite or aluminium surfaces. Before adhesion, the surface should be in a smooth and clean condition. If the tape is applied over a painted surface, the paint must be fully cured beforehand. The tape comes in a roll and its thickness is 0.2 mm[17]. The process for tape application should be conducted as following [18]:

1. Define the area to which the 3M^{TM} Polyurethane Protective Tape will be applied. If the repair patch is 5x5cm, then the respective tape area should be 6x6cm.
2. Apply 3M^{TM} Adhesion Promoter 86A wipes to a 5.1cm wide area around the outside edge of the surface to be taped.
3. Allow drying for 10 minutes before applying the 3M Polyurethane Protective Tape.
4. Cut a piece of the tape 1.3cm less than needed length to allow for edge sealing.
5. Allow the adhesive to cure a minimum of 8 hours at 22°C before the flight. The cure is complete after 24 hours at 22°C.

Note that the minimum curing time of all 3M^{TM} Polyurethane Protective Tapes is 8 hours according to their application regulations. During future development of this project, the aim will be to minimise the curing time of the tape employed to further reduce down time of the aircraft.

[17]http://www.3m.com/3M/en_US/company-us/all-3m-products/ /3M-Polyurethane-Protective-Tape-8672?N=5002385+3292668424&rt=rud [Accessed on 16 June 2017]

[18]http://multimedia.3m.com/mws/media/131107O/polyurethane-protective-tape-application-instructions.pdf [Accessed on the 16 June 2017]

7
Design of the Propulsion System

This chapter details the design of and component choice for rotors of the vehicle.

7.1. Introduction

The propulsion system allows the vehicle to fly. In previous sizing it was decided that the vehicle would be a coaxial multirotor in X8 configuration with 36" diameter rotors. The propulsion system is then comprised of eight independent rotors, mounted in vertically stacked pairs of two. The stacked rotors rotate in opposite directions of each other and opposite to other adjacent rotors. A sketch of the rotor positioning and their direction is show in figure Figure 7.1. In this section the design of the propeller and selection of a fitting motor and motor controller combination is explained. The same components would then be used in all eight rotors, with half of the propellers having a mirrored design for the opposite rotation direction. This arrangement also provides sufficient redundancy, as the vehicle retains full control and the ability to fly upon loss of a single rotor. In this state, it is still capable of safely performing failsafe manoeuvres and returning to land at the ground station.

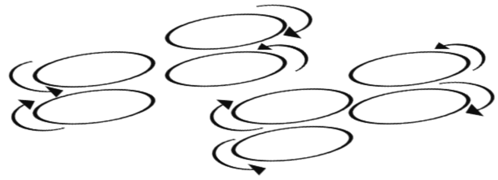

Figure 7.1: Layout of the X8 multirotor configuration

7.2. Propulsion Architecture

The electromechanical components of the propulsion system are not complex due to the vehicle being a multirotor. It consists of eight mutually independent rotors which are controlled by the flight controller presenting eight individual digital signals. Each motor-propeller assembly is driven by a separate speed controller. The speed controllers are connected in parallel across the main flight battery and their signal wires are connected to individual pins of the flight controller. A nominal operation voltage of around 50V was selected due to being the typical limit for high-power motors designed for multirotor use. Further following typical motor specifications, a typical speed constant of the motor is around 100KV, which stands for 100 revolutions per minute per volt. The architecture is visualised in Figure 7.2.

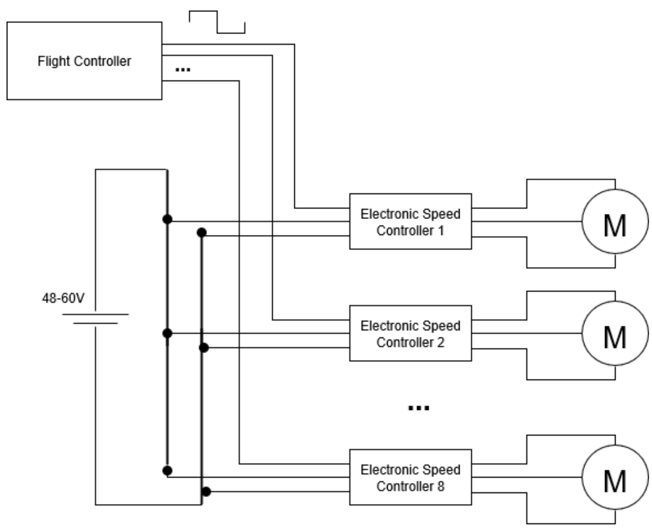

Figure 7.2: Propulsion system architecture.

7.3. Designed Rotor

The resultant rotor design uses a tri-blade 36" diameter foldable propeller, a modified KDE8218XF motor and off-the-shelf KDEXF-UAS95HVC speed controllers. Total assembly weight is 1.056kg per rotor. The propeller design is a candidate and could be replaced by an equivalent 36" off-the-shelf unit if they were to become available. As of now, largest units available are around 31". The motor is consequently also designed for these smaller propellers and although having sufficient power ratings, would have to be rewound from 120KV to around 80KV to make it compatible with the larger propeller. The unmodified motor using the largest readily available propeller would be sufficient for the vehicle to fly, although it would only provide thrust to weight ratio of approximately 1.2 rather than the target of 2, greatly limiting controllability.

The designed rotor is expected to produce 18.8kg of lift at 2500RPM, requiring 1.96kW of power from the flight battery at hover. The maximum short period thrust is 37.6kg at 3500RPM, drawing 5.6kW of power. The expected efficiency at hover is $9.6\frac{g}{W}$ which is realistic, as low KV motors swinging large propellers often provide over $12\frac{g}{W}$. This

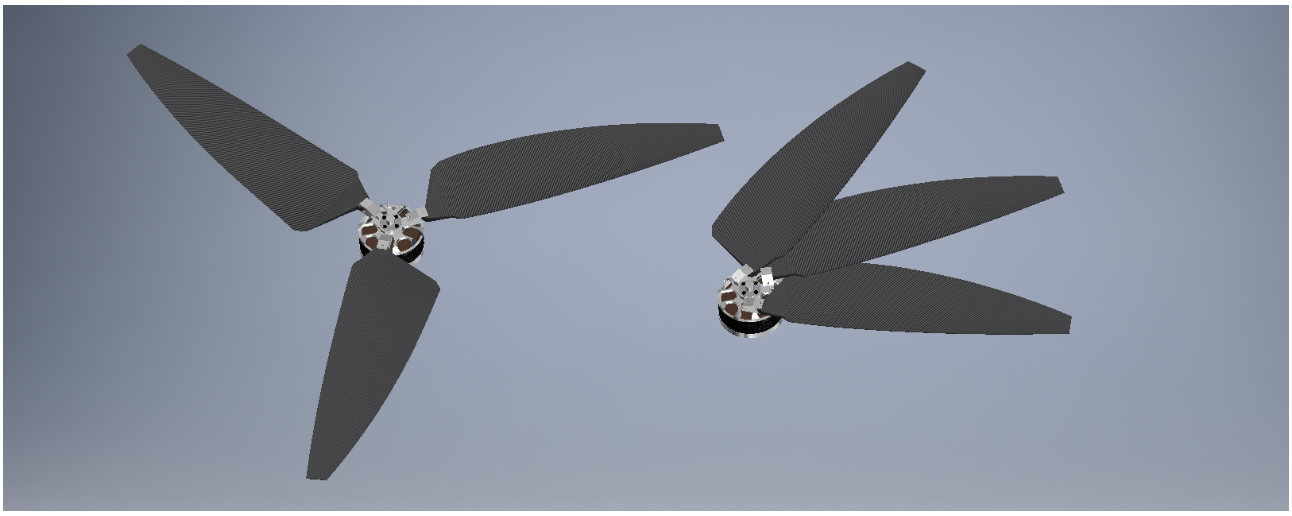

Figure 7.3: Rotor in its deployed and folded configurations

brings typical total power use of the propulsion system to 15.7kW at hover or slow steady flight and up to 44.8kW during short bursts of full throttle. The CAD model of the motor-propeller assembly is shown in Figure 7.3.

7.4. Rotor Design

To further explore feasibility of the propulsion system and to provide reasonable estimations of rotor properties for use in flight simulations, a candidate propeller was designed and matched with an adequate motor and electronic speed controller combination. Although, due to the coaxial configuration, the upper and lower rotors operate in slightly different conditions, a single design will be used for both. An efficiency penalty is included, but could be avoided given a much more in-depth optimisation which the current time constraints do not allow.

7.4.1. Correction of Previous Sizing

During earlier phases of development, the power requirements for flight as well as battery mass were estimated using an iterative solver based on statistical relationships found in available rotor test data. It was estimated that hover would require around 36kW of power while bursts of full thrust would require around 123kW. It is now apparent that the values were overestimated due to an incorrect exponent of the leading term. The data used to create the model was fitted using polynomial functions, where the second degree provided the best fit. It was later discovered that the leading term actually is of lower exponent of form $x^{1.5}$ rather than x^2.

The less aggressive power scaling was noticed during search for possible optimisation rules for the propellers. It can be shown that $P \propto L^{1.5}$ and not L^2 as indirectly assumed during initial sizing. The result is greatly reduced power requirements, especially at high thrust settings. Although the design should be fully reiterated to optimise for the new power requirement relationships, due to time constraints this will not be done currently. The available headroom will be used mainly to relax the originally extremely strict requirements on the power system and to reduce the flying weight by removing some of the battery mass.

Alarmingly, the statistics-based sizing model has been previously successfully validated with flight tests of two personal vehicles. This false positive can be explained by the small data size, a concern already expressed at the time, and the low disk loading at which both vehicles operate. In both comparisons the model was showing a small, but consistent error of 6% under-prediction in power required. At the low disk loading of the validation vehicles (around $0.006\frac{g}{mm^2}$) the power predicted by a function of type $P = A_d\left(\left(\frac{L}{A_d}\right)^2 + \frac{L}{A_d}\right)$ predicts 6% lower power requirement than a function of type $P = A_d\left(\left(\frac{L}{A_d}\right)^{1.5} + \frac{L}{A_d}\right)$. Although by coincidence this closely matches the observed error, it does not fully explain it as the fit functions involved more terms. This difference still holds as a partial explanation for the error, however.

The results from earlier power sizing will not be discarded, but will be adapted with a rough correction formula and further used as reference value for sanity checking. A simple correction of $P_{new} = P_{old}^{\frac{3}{4}}$ reveals that expected hover power is around 14kW and expected maximum thrust power is around 37kW, or 1.75kW and 4.64kW per single rotor.

7.4.2. Typical Operational Conditions and Selected Airfoil

The typical mission consists of mostly hovering or very slow, steady flight at low altitudes. Initially, a throttle setting of 50% is assumed at hovering. Given the typical operational voltage of 50V and typical motor speed constant of 100KV, rotors should be designed for operation at 2500RPM. Given the 36" diameter of the rotors, the blades will be typically operating in low Reynolds number conditions with magnitude of 10^5. Research suggests that at such Reynolds numbers thin airfoils at low angles of attack perform best [14]. NACA 63-206 was chosen as the propeller airfoil due to having a relatively thick rear section making it easier to manufacture the design. This feature is uncommon among thin airfoils aimed at low Reynolds numbers for which geometry data is openly available. This is likely due to multirotor-specific airfoils with thicker trailing edges being a recent development focus and not yet released to public. All airfoil data used comes from Airfoil Tools database[1]. The airfoil profile is shown in Figure 7.4.

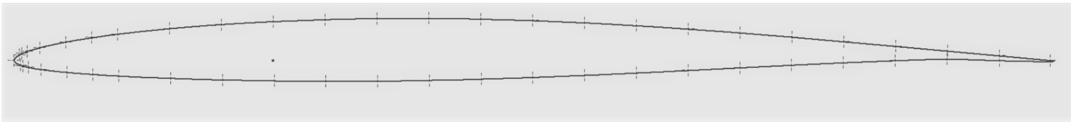

Figure 7.4: NACA 63-206 airfoil used for the propeller

7.4.3. Propeller Model

Propeller performance was modelled using an own implementation of blade element and momentum theory. The propeller blade is approximated by splitting it into smaller elements which are then evaluated as individual lifting sections under constant angle of attack and velocity. Because the theory is commonly used, further details of it are not explained here. The governing equation of the model is given below:

$$\sum L = \sum \Delta p_{air}$$

Here L is the lifting force and p_{air} is the change in momentum of the air flow through the propeller disk area. The model was verified by sanity checking and by comparing output blade properties to values expected from theory and efficiency observed in real world designs. This is mentioned more along with the output of the blade optimisation in Section 7.4.6 and the complete rotor in Section 7.3.

The following assumptions were made:

- **Stationary air** - Vertical velocity of the airflow before capture is assumed to be 0.
- **Constant inflow velocity** - Vertical airflow velocity is constant along the span of the blade.
- **Approximate tip loss** - Tip loss was not corrected for within the model. 15% loss of thrust was applied to the converged solution as an approximation.
- **No radial flow or other rotational effects** - Non-vertical momentum induced in airflow and tip vortex drag were not modelled. 15% increase in torque required was added as an approximate correction.
- **Small blade twist angle** - Lift is assumed normal to the rotation plane.
- **Constant, independent sections** - Blade and airflow properties are assumed constant along a single element. Elements are assumed to not be interacting with adjacent ones.
- **Independent blades** - Separate blades of the propeller are assume to not affect each other.

7.4.4. Other Losses

Additional losses are also present in the propulsion system. Some aerodynamic losses regarding the propeller were already mentioned in the previous section and this section will focus on additional losses which result from the system as a whole. This is done to provide the expected power of the propulsion system required at the source for use in design of the power system.

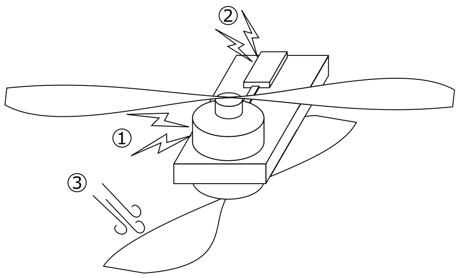

Figure 7.5: Losses in a rotor. 1 - motor losses, 2 - electrical losses, 3- rotor configuration losses.

Three main losses were considered: losses in the electrical system, mechanical losses in the motor and increased power use due to coaxial rotor interaction. The electrical losses arise from wiring, imperfect motor drivers and batteries. These are difficult to evaluate without modelling the entire circuit and the total electrical efficiency was assumed at 85%. The efficiency of brushless motors which are typically used is very high, often reaching close to 98% for high quality ones. However, in actual operation the rotor might become overloaded at higher torques, reducing efficiency. Because propellers are direct-driven, no gearbox is present to keep the motor at optimal conditions. Motors for multirotor use are designed with this in mind and have lower maximum efficiency but at a wide range of speeds and torques. Therefore, the motor efficiency is assumed as 90% overall. Finally, the coaxial configuration of the rotors typically reduces the efficiency. Research into coaxial multirotors [15][16] shows that this is typically around 15% in total when viewing both the upper and the lower rotors combined. All of these losses are combined into a single factor which is then added to the mechanical power requirements of the propeller. The correction factor used is given below:

[1]http://airfoiltools.com/airfoil/details?airfoil=naca63206-il [Accessed on 31st May 2017]

$$\eta_{total} = \eta_{prop} \cdot \eta_{elec} \cdot \eta_{motor} \cdot \eta_{coax}$$

$$\eta_{total} = \eta_{prop} \cdot 0.85 \cdot 0.9 \cdot 0.85 = 0.65\eta_{prop}$$

7.4.5. Optimisation Method and Constraints

The shape of the propeller was optimised by varying the chord length and twist of individual sections. For optimum efficiency, the angle of attack of the blade sections should be kept at 4° to 6°. To reduce the average chord length and number of blades, it was decided to keep the blade at 6° at hover conditions, this also results in more efficient operation at higher thrust as angle of attack is not pushed outside optimal range when it decreases at higher rotational speeds.

Because optimisation targeted only at the minimum weight and maximum efficiency results in a propeller with a disproportionally large centre part of the blade, additional rules on chord length distribution were introduced based on structural considerations. It was assumed that $I \propto c^4$, based on the fact that an airfoil's profile is fixed and simply scaled according to chord length. It was also assumed that the bending moment due to lift generated is the limiting load on the blade. Combining the previously mentioned proportionality of I with the standard equation for normal stress due to bending results in an equation for indirect evaluation of stress in top and bottom surfaces: $\sigma \propto \frac{M}{c^3}$ where M is the moment load on the section. Most even stress distribution was chosen as the target of the optimisation with the assumption that most evenly stressed structure also represents optimal weight.

Limiting values for optimisation script were given. First, the required thrust after loss correction was $185N$, or, the 151kg hover weight evenly distributed over eight rotors. Second, the maximum allowed twist angle was limited to 20° because lift is assumed normal to the rotor plane. Finally, the chord length was limited between 1 and 15cm. Here, the limits on chord length were chosen arbitrarily, but should be tailored to specific manufacturing constraints, if applicable.

The optimisation logic is summarised below:

- Generated propeller blade is evaluated using the method described in Section 7.4.3
- If a section is not within 1% of 6° angle of attack and twist angle is less than 20°, change the twist angle of the section slightly towards the required value.
- If the generated lift is not within 1% of the required, scale the chord of all sections by a uniform factor required to achieve correct thrust.
- If stress on a section is not within 2% of the average along the blade and chord length is 1-15cm, change it slightly towards the required value.
- Iterate until conditions are satisfied.

7.4.6. Resultant Propeller

The resultant propeller is a 36" diameter tri-blade with 12.3cm root chord, 1cm tip chord and non-linear taper and twist distributions. It is expected to produce 18.8kg of thrust at 2500RPM and 37.6kg at 3500RPM. The expected power required to spin it when including approximations for typical losses of the X8 configuration and other components is 1.96kW at hover and 5.6kW at max thrust. This agrees with the statistics based sanity check values of 1.75kW and 4.64kW, respectively. The latter values were not direct predictions, but a rough target, as explained in Section 7.4.1.

After around 400 iterations, the resultant optimisation manages to keep most of the blade at the target 6° angle of attack and constant surface stress as seen in Figure 7.7. The twist angle and chord length distributions are shown in Figure 7.6. The resultant twist distribution is hyperbolic and agrees with the ideal solution from blade element theory. The lift distribution seen in Figure 7.7 is also typical. The output being consistent with the theory is used as the basis to verify the model. The inner 15% of the span which is not producing lift due to negative angles of attack with respect to the airflow was replaced by a centre hub for motor attachment, the folding mechanism and the gradual transition into the airfoil profile.

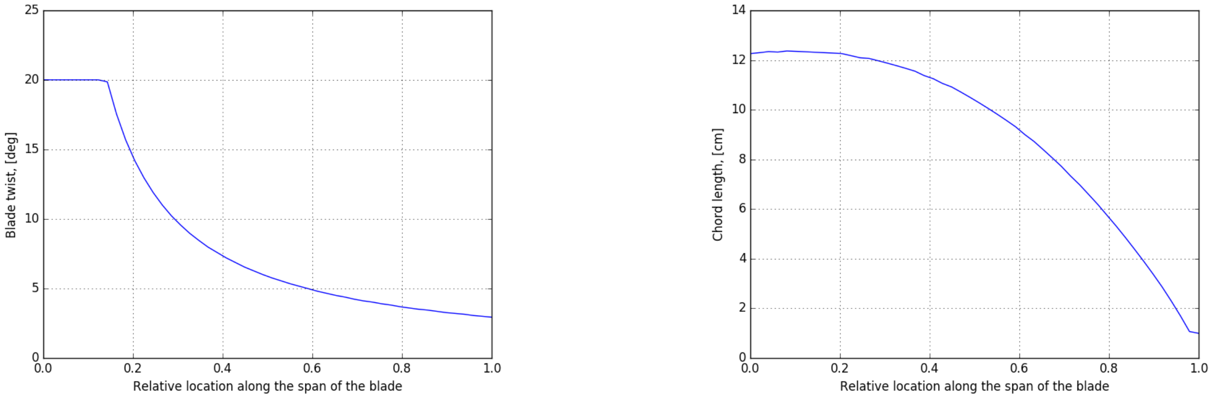

Figure 7.6: The twist (left) and the chord length (right) distributions along the blades of the propeller

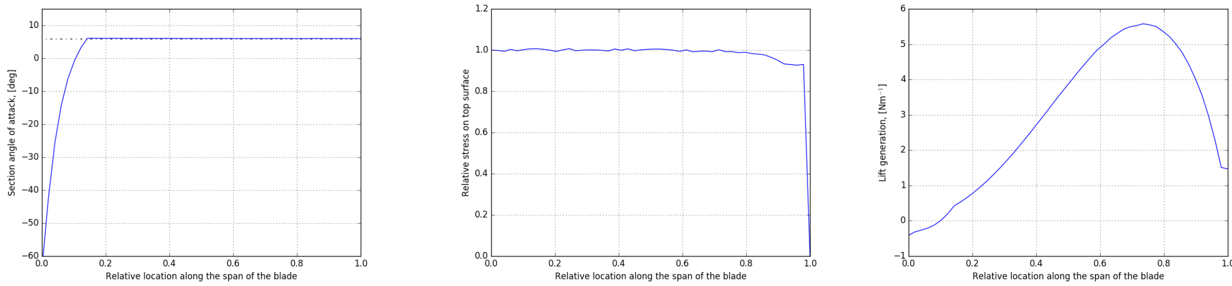

Figure 7.7: Various properties of the blade along the span.

7.4.7. Motor and Speed Controller

During the final moments of the design, a larger version of the motor was announced, which potentially would not need any modifications. Because the propulsion system's design had already been frozen and other components such as frame arms designed around the chosen motors' dimensions, this upgrade was not incorporated or further investigated.

After the propeller was designed and the expected power draw was known, the motor and a speed controller for it were selected. The chosen components were the KDE8218X[2] motor and KDEXF-UAS95HVC[3] speed controller. They are designed for high-power heavy lifting aerial vehicles and have large thrust and power capacities at relatively low weight. The motor has a maximum continuous power rating of 5.7kW and the speed controller has a continuous power rating of 4.2kW with 7.6kW short period bursts. Therefore they are capable of handling both the 1.96kW typical continuous load and 5.6kW short period bursts. Neither component requires additional cooling. Unfortunately, the available configuration of the motor itself is targeted at faster rotating, smaller propellers up to 30.5" in diameter as these are the largest typically available. Accounting for the typical slow-down at high loads observed in the motor's test data available [4], the motor would have to be modified by rewinding from its current 120KV to a lower, 80KV speed constant. This increases torque, reduces maximum speed closer to the required 3500RPM and increases maximum size of the propeller it can spin without overloading. The modification does not require to redesign the motor and can either be done after purchase or ordered as a custom version from the manufacturer. The speed controller would not require any modification.

[2] https://www.kdedirect.com/collections/uas-multi-rotor-brushless-motors/products/kde8218xf-120

[3] https://www.kdedirect.com/collections/uas-multi-rotor-electronics/products/kdexf-uas95hvc

[4] https://cdn.shopify.com/s/files/1/0496/8205/files/KDE_Direct_XF_CF_Brushless_Performance_Testing_-_KDE8218XF-120.pdf?7734511287488513374

8
Structures

With the propulsion system designed, and the payload known, a structural frame must be designed to maintain the correct propeller spacing, and transfer the loads between propulsion system and payload. In this chapter, the arms to which the propellers are attached, the structural frame supporting load transfer into and around the payload, and the landing gear will be designed.

8.1. Rotor Arms

8.1.1. Introduction

The rotor arms act as the attachment point to the rotors and carry large vertical and torsional loads to the centre of the structure. From previous sizing it is already known that the minimum achievable weight of a single arm without a safety factor is around 850g. An 'H' shaped frame with two 'T' shaped arms proved to be the lightest and was be used as the starting reference. Additionally, it is known that rotors must be at least 91cm apart and at least 50cm from the centre structure. Some other qualities of the part are also known. First, by the nature of the vehicle's design, it will only be subjected to well defined loads in a constant direction during normal operation. Second, the arms must support a rotational mechanism at the root and be relatively low profile to prevent interference with the rotors. Finally, due to their large size, it is preferable that the design is compatible with conventional manufacturing to avoid a great increase in its cost.

8.1.2. Support Geometry and Load Cases

The rotor arms have two limiting load cases: bending due to vertical force and torsion combined with a lower vertical force. The two load cases correspond to all four mounted rotors producing maximum thrust or only one side's rotors set to full thrust, generating torque on the arm. Even considering the perching manoeuvres, these are still the ultimate loads.

The arms were originally intended to be mounted close to the payload, with clearance to the payload's moving parts limiting connection depth to around 12cm. This limited maximum spacing between bearings to 10cm. The arms were designed before the connection mechanism was relocated to outside the frame and thus have retained the 10cm spaced bearings without having anything directly imposing the value anymore.

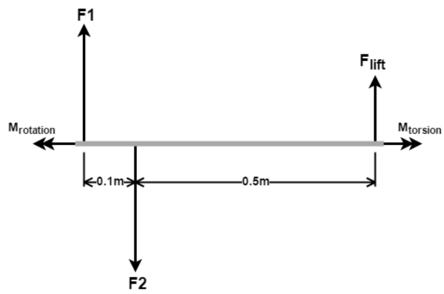

Figure 8.1: Free body diagram of the general loads on an arm

Given the known outer arm length of 50cm and the 10cm spacing of support bearings, a general free body diagram can be constructed for the arm as seen shown Figure 8.1. Here, F1 and F2 are forces generated by the support bearings. The forces on each of the bearings can be calculated assuming stating equilibrium:

$$\sum F_y = 0 = F1 - F2 + F_{lift}$$
$$\sum M = 0 = F_{lift} \cdot (50cm + 10cm) - F2 \cdot 10cm$$

Given that at max thrust F_{lift} would be equal to 1481N, the bearing reaction forces can be solved for: $F1 = 7405N$ and $F2 = 6F_{lift} = 8886N$. In this case, the large bending loads in the outer arm result in large shear loads between the bearings. In Section 8.3.4 bearings were selected to hold the arm, setting the diameter of the root of the arm to 60mm. Under torsional load, only half of the rotors present on the arm would be active, halving the vertical load but introducing torque.

FEM analysis tool used requires at least some of the part's geometry to be fixed. To achieve this, the most in-board bearing is considered to be the point of fixture. The front bearing's reaction force is applied to the arm as a bearing load $F2$ equal to $6F_{lift}$. This setup can is shown in Figure 8.2. This approximation will be used during during most of the design to allow quick simulations without including rest of the structure.

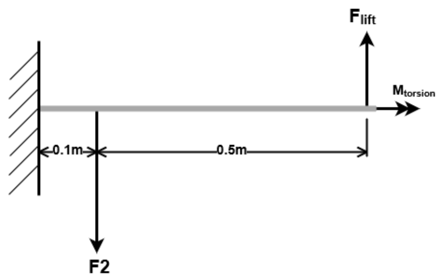

Figure 8.2: Free body diagram of the loading used in the FEM analysis

8.1.3. Designed Arm

The designed arm seen in Figure 8.3 is from from Aluminium 6061-T6 , weighs 1.012kg, and is welded together from tapered tubing and small machined flanges. The achieved safety factor is 1.55 under maximum torsional load and 1.9 in pure bending. It has a ticker, untapered extension at the root which provides attachment room for the bearings and the perching arms. The main structure is made from tapered tubing. The connection between the main and the side arms is reinforced by thin flanges and a short aluminium sleeve. Press-formed motor mounts are welded to the ends of the side arms. The tubes are hollow with the inside cavity usable for pathing of wiring and holding electronic components. The root diameter is limited by the smallest size of the bearing capable of withstanding the loads to 60mm. The centre arm is 50cm long and tapers down to 35mm at the connection. Each minor arm is 45cm long to keep the total width below the required 1m when the motors are mounted. Smaller arms taper from 40mm to 20mm diameter.

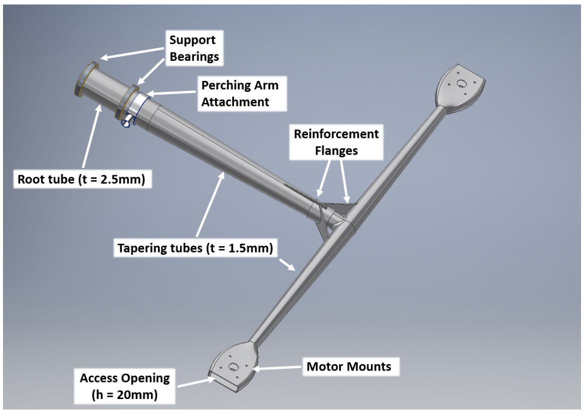

Figure 8.3: Rotor arm

Initially, a few different designs were experimented with such as beams of various cross-section and various taper ratios. Due to large torsional loads, a circular cross-section was performing the best for a given weight. Various linear and nonlinear taper profiles were experimented with to reduce the weight without compromising strength. In the end, the linear taper was selected as it is compatible with conventional manufacturing, although limited to aluminium. More complex geometries do save weight and the best observed was a 15% weight reduction. However, the complex geometry and reliance on additive manufacturing greatly increases the cost to the point where the small weight savings are simply not worth while, as the whole component only makes up less than 2% of the total flying weight.

After it was settled that the arms would be linearly tapered tubes made from aluminium, numerous minor iterations and modifications to tube radii, thicknesses and connection bracing were done to eliminate stress concentrations around the joints and reduce the weight. Over a span of a few days around 30 iterations of simulation and modification were completed, resulting in the final design. The FEM stress simulation results of the final design can be seen in Figure 8.4. Loads applied to structure are explained in Section 8.1.2.

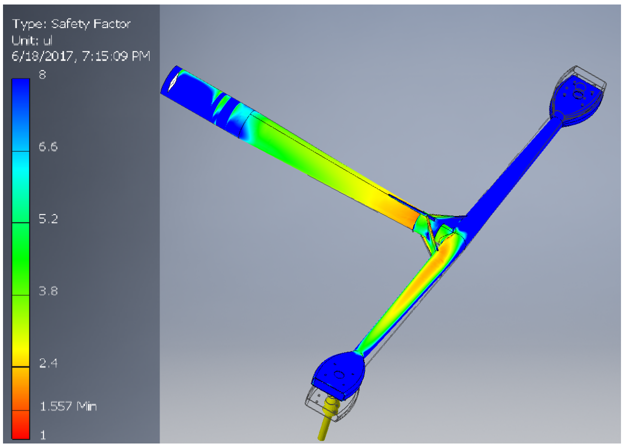

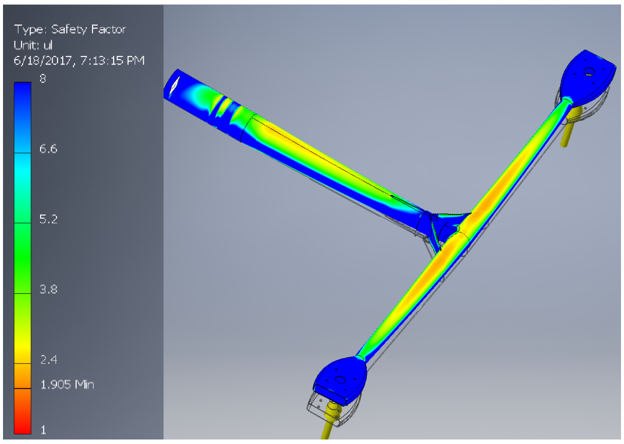

Figure 8.4: FEM stress simulation results of the arm under maximum torsional (left) and maximum bending (right) loads, showing the safety factor. The torsional loads affect the main arm and the connection differently from bending and require additional bracing on the connection.

The simulation shows minimum safety factor of 1.55 at the maximum torsional load, which is when only one side's rotors are producing full thrust. The safety factor for the pure vertical bending load is higher, at 1.9, indicating that the structure can be further optimised. However, further optimisation is time consuming and yields small weight savings. Given this component corresponds to less than 2% of the total flying weight, the design was frozen to work on the rest of the structure. At this point, most of the stress concentrations around the main-side arm connection have been eliminated by bracing it with 1.5mm thick flanges, prolonging the fatigue life of the component. The Goodman method was used to estimate fatigue life of the component as approximately 5500 flights, or five years of service at the expected three flights a day.

8.2. Payload Frame

To connect the propeller arms to the computer numerical control (CNC) machining payload, a connecting frame is necessary. The propeller arms must be aligned through the center of gravity to maintain moment balance around the propeller arm axis, and ensure that the propellers will not need to generate large control moments to maintain a constant pitch angle. The position of this axis is above the DMG Mori's surrounding frame, which means that the propellers cannot be directly connected to it. Furthermore, the propeller arms will generate large moments and forces at the point where they connect to the frame, which the CNC machine's frame may not be capable of carrying alone. For these reasons, it was decided to create a frame capable of transferring the loads into the CNC machine while relieving some of the stress itself.

8.2.1. Frame Design Starting Point

To carry the loads around the frame, a construction around the frame is necessary. From the specification sheet of the DMG Mori CNC machine, it can be seen that an external frame exists which is capable of supporting the weight of the machine. This frame is chosen to be the starting point for the design of the frame, and modifications shall be made to allow the arms to connect to it.

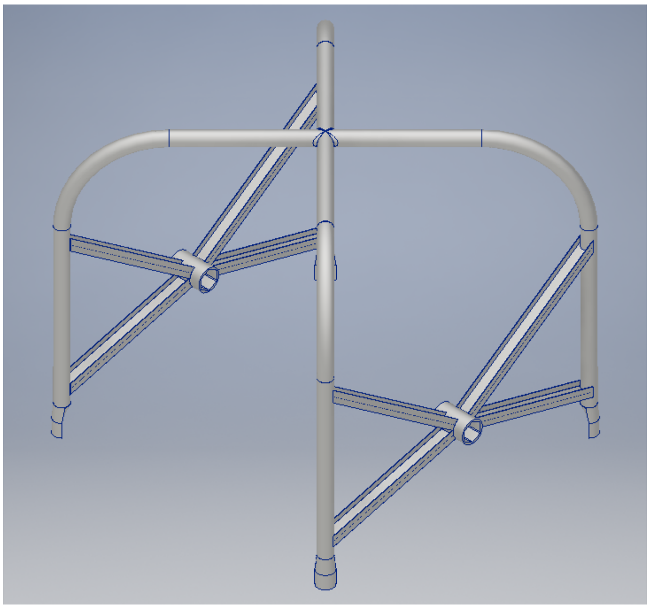

Figure 8.5: First iteration of the payload frame design

8.2.2. Cross Bar Structure

To connect the arms to the external frame, a cross bar structure is necessary. This structure was chosen over a direct connection to the CNC machine's frame, to facilitate load transfer around the CNC machine as opposed to into it.
The first design iteration resulted in a cross bar using I-beams connected to a circular centerpiece which the arm will be inserted to. The beams in the cross bar carry the loads very well, but using finite element analysis, stress concentrations were discovered near the intersections between beams and the intersections between beam and centerpiece. These can be seen in Figure 8.6.

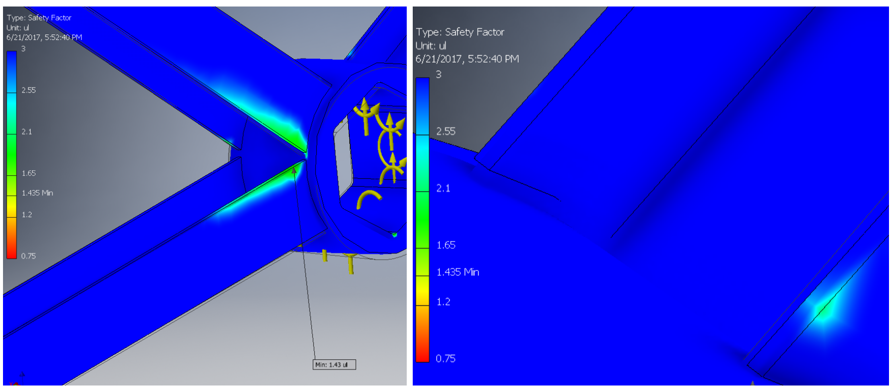

Figure 8.6: Stress concentrations in the first iteration of the payload frame

Rounding out these edges resulted in a design which greatly reduced these stress concentrations, as can be seen in

Figure 8.7. This adds a slight amount of mass.

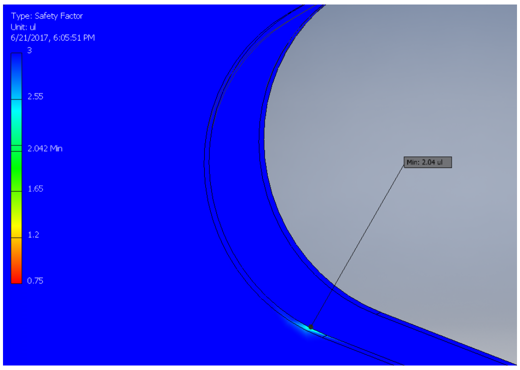

Figure 8.7: Rounded edges in the second iteration mitigate the stress concentrations in the design

The design now has a sufficiently high safety factor. However, further inspection shows that there are large areas where the flanges of the I-beams have a very large safety factor. Thus, weight can be saved in these areas by reducing the width of the flanges. The final design can be seen in Figure 8.8. The cross-bar structure now has a mass of 2.4 kg, which when combined with the estimated mass of the DMG Mori frame totals up to 5.5 kg. The final design can be seen in Figure 8.9. In this picture, it can be clearly seen that the cross bar arms get thinner as the distance to the centre increases.

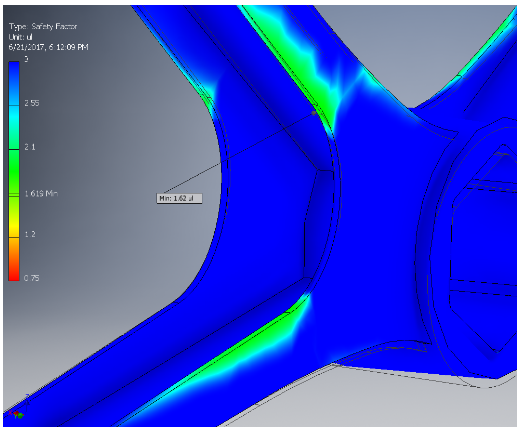

Figure 8.8: Stresses in the third iteration of the design

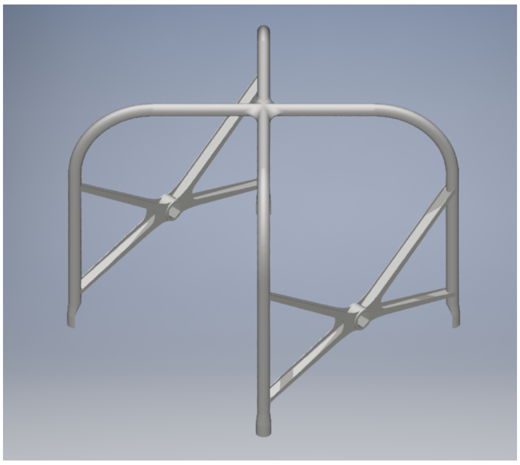

Figure 8.9: Finalized payload frame design

8.3. Rotation Mechanism

This section goes in detail about the the rotation mechanism to orientate the payload of the UAV to reach multiple surfaces on the aircraft. Section 8.3.1 discusses the necessity of the rotation mechanism. The components that are needed for the mechanism are discussed in Section 8.3.2. After the components, the torque that has to be provided and the loads that the frame has to withstand are analysed in Section 8.3.3. The design of the rotation mechanism is discussed in Section 8.3.4.

8.3.1. Necessity Rotation Mechanism

The uniqueness of the design is mainly achieved by the rotation to orientate the payload. The UAV is required to repair top, side and bottom surfaces. The rotation is important to meet this requirement, since the orientation will not be a problem and the payload can attach to each surface. Unfortunately, when the UAV uses the rotation to orientate the payload not all the surfaces can be reached due to the propellers that will not give enough clearance. If the surfaces have to be reached a perching mechanism is required as well. The perching mechanism is discussed in Chapter 9.

8.3.2. Component Analysis

In order to orientate the payload in the correct direction, multiple components are needed. The most obvious one for this mechanism is a motor, but also gearing is needed in order to obtain a high output torque which is required for the rotation. Besides enough torque to rotate the arms a frame is needed to integrate the rotation arms in the payload frame. This frame also works as the outer casing of the gearbox.

Stepper motor and driver

In order to rotate the UAV such that the payload is oriented in the correct direction a motor is needed to provide a torque. A stepper motor is an electric motor that is able to rotate continuously when it is powered. The stepper motor also needs a stepper driver. Stepper motors have multiple electromagnets around its central gear and these electromagnets are energised by the stepper driver. To make the shaft turn, an electromagnet is given power and after that the next electromagnet is given power such that the shaft makes rotational steps. The motors needs pulses current as input to rotate, these pulses are controlled by the stepper driver and will determine the rotational speed. By altering the frequency of the pulses, the motor is instructed to accelerate, decelerate and stop.

Gearing

Motors that have to provide a significant high torque are generally heavy. Therefore, gearing is needed to obtain a high output torque from a light motor that provides a small torque. To obtain this high torque, multiple gears can be used in the same mechanism. In a compound gear system, multiple gear pairs are used with shared axis to connect the pairs. Using the compound gear system the gear reduction ratio adds up quickly. Within the design multiple types of gearing are considered; worm gearing, spur gearing, planetary gearing and bevel gearing were all possibilities. In the design it is desired to keep the rotation mechanism as compact as possible. This is the main reason that two pairs of worm gearing and one pair of bevel gearing are used.

Worm gearing is a type of gearing in which a worm meshes with a worm gear. A worm gear can reduce rotational speed or highly increase torque. A big advantage is that they can transfer motion in 90 degrees. They also have a braking system, so when using worm gearing there is no locking system needed.
Bevel gearing is a type of gearing where the axis of the two gears are intersecting. Bevel gears can be designed to work at multiple angles, but in this case they will be mounted to transfer motion in 90 degrees.

Figure 8.10: Worm gear

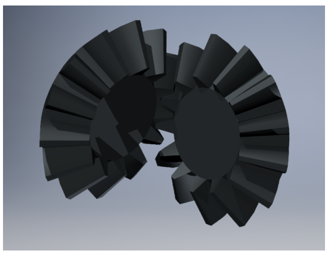

Figure 8.11: Bevel gear

Bearings

For the connection between the arm and the rotation mechanism, it is needed to have two bearings to hold the rotating components within the system in place on both sides of the UAV. As is explained in Section 8.1 the bearing has to withstand very high loads.

Rotation Mechanism Frame

The rotation mechanism frame is necessary to integrate the rotation arms in the payload frame. Moreover, it works as the outer casing of the gearbox. The rotation mechanism frame is fixed to the payload frame and will rotate with it. This frame has to carry all the loads introduced by the arms through the bearings and transfer them into the payload frame. For this reason the stiffness of the frame is crucial. Since one of the most constraining requirements is the mass constraint (Requirement **[OP-5]**) the performance and geometry of this structure requires an optimisation process to minimise its weight.

The rotation mechanism frame is one solid part composed of three different sections as illustrated in Figure 8.12. The first section is the attachment to the frame. This frame will be inserted into the socket of the payload frame by means of a hexagonal connector. Each face of the connector has a triangular tooth spring driven mechanism that connects and locks the insert into the socket of the payload frame. The second and middle section of the frame is the housing of the gear box, which only needs to surround the gear box but no additional loads are introduced by them directly in the structure. Thirdly, the last section is composed of two connecting rings to transfer the loads from the bearings into the payload frame.

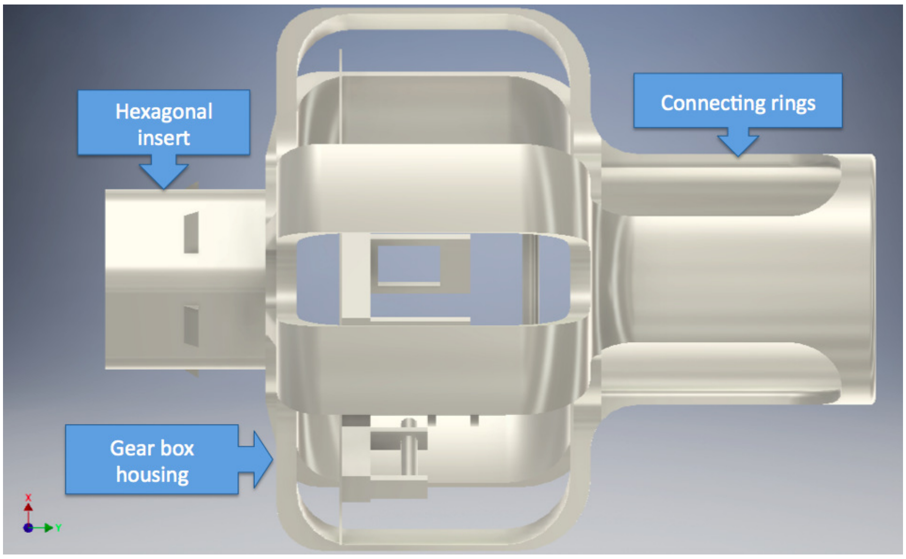

Figure 8.12: Components of the final rotation mechanism frame design

The gearing that is used to obtain the required torque from the motor has to be supported to stay at their locations, this is also the case for the motor. The shaft of the motor, the gears and the arm are on both side of the UAV the elements that will move to orientate the payload. The support of the gearing and motor is implemented in the rotation mechanism frame.

8.3.3. Torque and Load Analysis

This subsection describes the torque that is required for rotation and the load cases on the rotation mechanism frame.

Torque Analysis

For the rotation it is decided to rotate both arms to orientate the payload the right way. The determination of the torque τ that is required to rotate the arms is done using Equation 8.1. In this equation F is the magnitude of one of the forces of the couple shown in Figure 8.13 and d is the perpendicular distance between the two forces.

$$\tau = F \cdot d \tag{8.1}$$

In Figure 8.13 the force couple that is needed to create the rotation of the arms is shown in green. The pairs of forces due to the propulsion on the arms are shown in grey and red respectively. In flight the motors of the propulsion system provide within 0.8 and 1.2 times the hover thrust and that means that the force in Equation 8.1 needs to be multiplied with 0.2. Since there are two arms that take care for the lift and the perpendicular distance between the two forces is 1m, the total torque that is needed for the rotation assuming no rotation of the arms under more extreme conditions than hover is:

$$\tau = \frac{m \cdot g}{2} \cdot 0.2 \cdot d = \frac{151 \cdot 9.81}{2} \cdot 0.2 \cdot 1 = 148.13 Nm$$

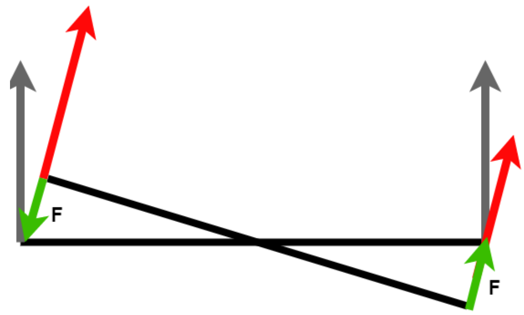

Figure 8.13: Visualisation of force couple that the rotation mechanism has to provide

Load Analysis of the Rotation Mechanism Frame

The two load cases experienced by the arm and transferred by the bearings into the rotation mechanism frame have been analysed. As mentioned in Section 8.1.1, the first load case corresponds to all four mounted rotors producing maximum thrust and the second load case to only one side's rotors set to full thrust. The spacing between both support bearings is 10cm. The critical loading case from these bearing is when the vertical force introduced is maximum which occurs at maximum thrust of all rotors. For this load case, the vertical forces that the inner bearing (closest to the payload) and the outer bearing (closest to the rotor) introduce in the rotation mechanism frame are 7405N and 8886N respectively, as depicted in the free body diagram of the arm loading in Figure 8.1. To use the FEM analysis tool, the inner surface of the hexagonal insertion was set to be fixed.

8.3.4. Design of the Rotation Mechanism

This subsection describes the design of the rotation mechanism, it is divided for the components that are discussed in Section 8.3.2.

Rotation Mechanism

Firstly research was done for a motor that could deliver the torque required for the rotational movement. It was observed that a motor for this amount of torque would be too heavy and critical to met the mass requirement **[OP-5]** for the entire design. After the findings for such a motor, it is clear that for the design a rotation mechanism with only a motor is not feasible. It is decided that gears are needed to adjust the mechanical advantage of the mechanism. This mechanical advantage implies that the high torque could be achieved by a motor that only provides a little bit of torque.

Gearing

Starting with the gearing, a preliminary design of the gearing was made consisting a big worm gear and two spur gears for a massive gear reduction. The preliminary design shown in Figure 8.14 would have the motor attached to the small spur gear in the front. The arms of the UAV would be attached within the worm gear, so the rotation of the arms would be equal on the rotation of the last gear. The problem with this preliminary design came when the rotation mechanism frame had size and position restrictions for the gearing and motor. The motor had to be located behind the gear on the arm and there had to be space for cables as well.

Adjusting the design so that it fitted within the section that was reserved for the gear box, a design is made that is composed by two pair of worm gearing and a pair of bevel gearing. Again the arms are attached within the worm gear and between the two pairs of worm gearing a pair of bevel gearing is placed for an extra transfer in motion of 90 degrees. As can be seen in Figure 8.15 the gearing is more compact and compared to the preliminary design it has a lower gear reduction. The reason for the lower gear reduction is the bevel gear that has no gear reduction since the number of teeth of both bevel gears is the same. Since the gear ratio and the efficiency of the gears were provided by Autodesk Inventor, the calculations of the gearing was easily done. Table 8.1 shows the gear ratio and the efficiency for the pairs of gearing and the total. The material Cast Iron is used for the gearing, it is a commonly used material for this application.

Table 8.1: Gear ratio and efficiency gearing

Part	**Gear ratio**	**Efficiency**
Worm gear arm	30	0.604
Bevel gear	1	0.98
Worm gear motor	28	0.579
Total	840	0.3427

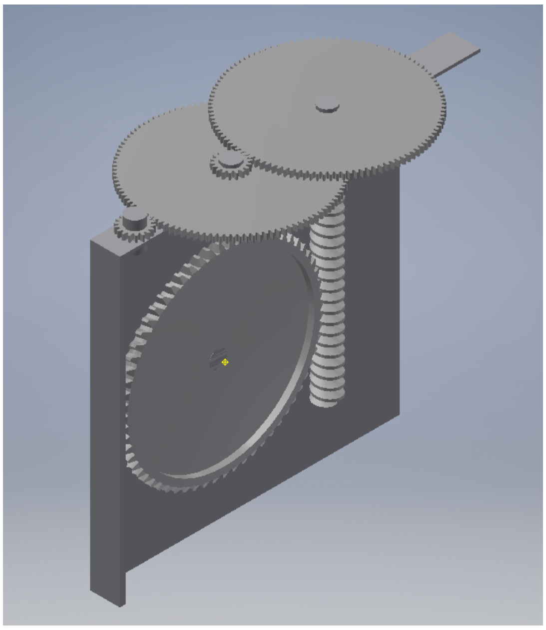

Figure 8.14: Preliminary design of gearing

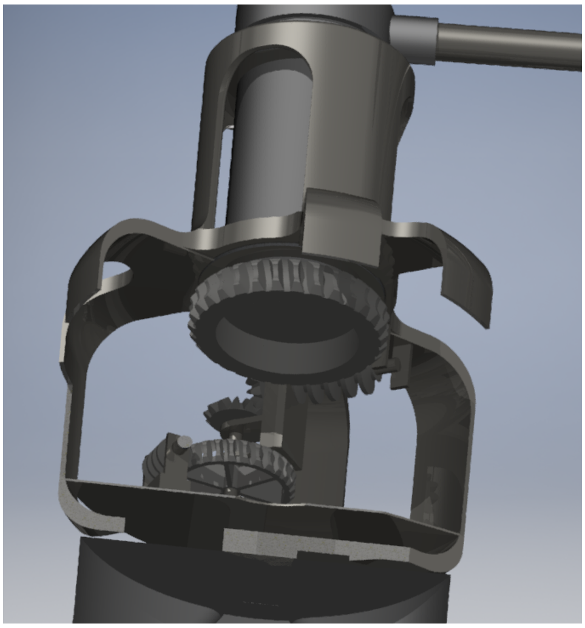

Figure 8.15: Design of gearing

Stepper motor and driver

The required torque the motor has to provide can be calculated from the gear ratio and the efficiency from the gearing. By Section 8.3.3 it is found that the torque the motor has to provide is 0.515Nm.

$$\text{Torque required motor} = \text{Torque required rotation} \cdot \frac{\text{Total efficiency}}{\text{Total gear ratio}} = 148.13 \cdot \frac{0.3427}{840} = 0.515Nm \tag{8.2}$$

The Nema 8 Stepper Motor with Planetary Gearbox [1] is a very light stepper motor with additional gearbox that can provide a torque of 0.9 Nm with an efficiency of 73%. The torque provided by the stepper motor and the gearing is sufficient for the rotation of the arms. Its weight is equal to 130 gram. Lastly, the stepper driver has to be considered that is compatible with the voltage of the stepper motor. It is decided to use the Big Easy Driver[2]. With this stepper driver the rotational speed of the mechanism can also be set such that the payload is orientated correctly within 30. The final design with the motor also attached in the mechanism can be seen in Figure 8.16.

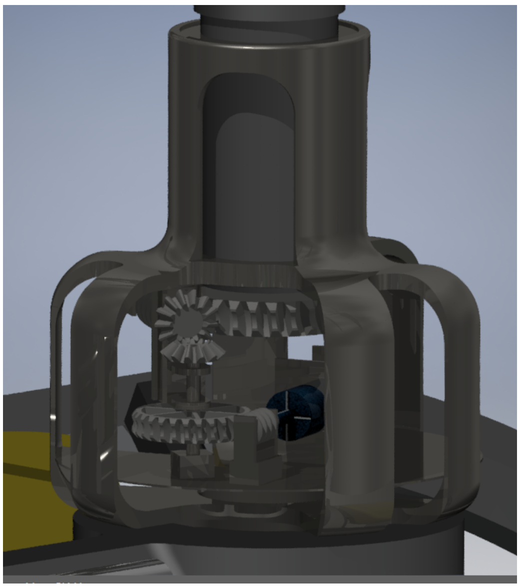

Figure 8.16: Rotation mechanism design

[1]http://www.omc-stepperonline.com/gear-ratio-641-planetary-gearbox-with-nema-8-stepper-motor-8hs150604spg64-p-310.html[Accessed on the 20 June 2017]

[2]http://www.robotshop.com/en/big-easy-driver.html [Accessed on the 20 June 2017]

Bearings

The bearings for the design are selected off-the-shelf. Based on the diameter of the arms and the loads that has to withstand described in Section 8.1 are deep groove ball bearings with a mass of 110 grams[3].

Rotation Mechanism Frame

The rotation mechanism frame has to be a very stiff structure. To provide housing for the gear box and transfer the loads from the bearings into the payload frame a complex structure is designed with the objective of reducing weight. Auto-desk Inventor will be the CAD tool used to design and analyse the critical stress concentrations of this frame. Moreover, this tool will provide critical information on the areas which are over designed and the information will be used to cut holes of the structure without endangering structural performance. This will allow for further weight reduction.

The rotation mechanism frame is made from Titanium 64. It will be produced by means of AM and it weighs 1.65 kg per unit including the brackets for supporting the gears. Since two rotation mechanism frames are required per UAV (one per arm) the total weight will be 3.3kg. AM will be the production method employed to produce this structure due to its high geometrical complexity. The final design has a safety factor of 1.3 and is illustrated in Figure 8.19.

Preliminary design

Firstly a preliminary sketch was made to determine the initial dimensions of this frame. The sketch was created taking into account the estimated dimensions of the gearbox and the location of the two arm bearings. This sketch was then used to make a preliminary design of the rotation mechanism frame in Auto-desk.

The rotation mechanism frame is one solid part composed of three different sections which are the following:

- **Hexagonal insert** - The frame will be connected into the socket of the payload frame by means of this hexagonal insert. Each face of the connector has a triangular tooth spring driven mechanism that connects and locks the insert into the socket of the payload frame. Note that the payload frame socket is also designed to accommodate this attachment by cutting small rectangular holes inside its inner face such that the triangular teeth can be securely fixed.
- **Gear box housing** - The rotation mechanism frame will be cylindrical shell which surrounds the gear box. The loads introduced by the gear box will be carried by the rotation mechanism frame.
- **Two connecting rings** - To more effectively transfer the load from the bearings into the payload frame, the rotation mechanism frame has two rings which are welded to the bearings. The advantage of using these rings is that the load introduced by the bearing will be more evenly distributed on the inner surface of the rings.

After completing the preliminary design of the rotation mechanism frame illustrated in Figure 8.17, the forces introduced by the bearing are added. The load carrying behaviour of the structure is analysed by inspecting the highest stress concentration areas of the structure, determining its safety factor and adjusting the frame geometry consequently.

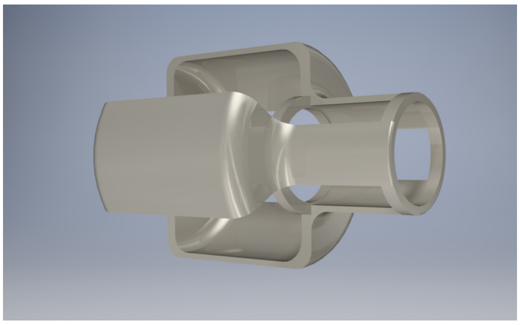

Figure 8.17: Preliminary rotation mechanism frame design

Optimization and integration

After completing the preliminary design and evaluating the critical stresses located in the structure, optimisation of the rotation mechanism frame was carried out. With the aim of reducing its weight to a minimum, the thicknesses of surfaces which presented unnecessarily high safety factors were decreased and several holes were cut out in the frame. The surface between the gearbox cylindrical housing and the payload mount is the most critical surface. For reinforcement purposes, a circular plate and twelve small flanges were added to the attachment surface of the rotation mechanism. After completion of the gear box design and determining that its final length is approximately half the size as the initial estimation, the cylindrical housing of the rotation mechanism frame was subsequently adapted and made shorter. Moreover, an additional plate was added inside the cylindrical housing to accommodate the electronics placement.

[3]http://www.skf.com/group/products/bearings-units-housings/ball-bearings/deep-groove-ball-bearings/deep-groove-ball-bearings/index.html?designation=61812&unit=metricUnit

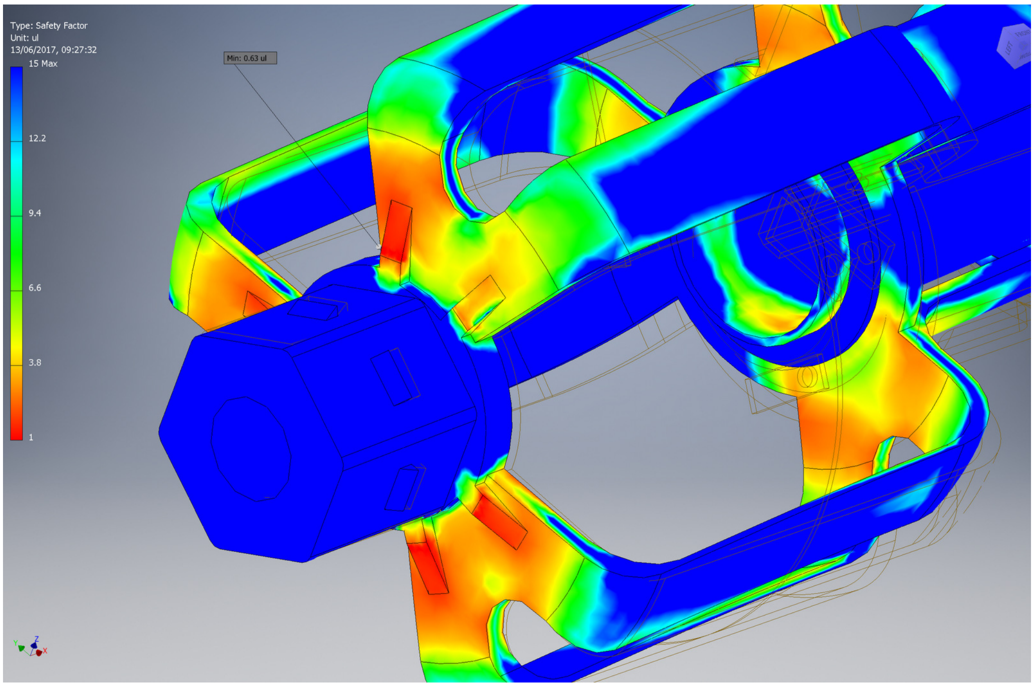

Figure 8.18: Critical stress concentrations after integration of the rotation mechanism frame in the payload frame, which were corrected during the final optimisation process.

Integrating the arms into the rotation mechanism frame and performing the stress analysis does not present any complications. This is due to the fact that the loads introduced by the bearings were one of the main design driving parameters which were considered early in the design phase. However, when the hexagonal insert is attached to the payload frame the surface facing directly to the payload frame fails is illustrated in Figure 8.18. The reason behind it is that the rotation mechanism frame adds more length to the complete arm structure, increasing the moments created at the connection between the payload frame and the rotation mechanism frame. This problem was corrected for by locally thickening surfaces and strategically using fillets and chamfers to reduce stress concentrations at the corners. After optimisation of the structure a safety factor of 1.3 was achieved. The final rotation frame design is illustrated in 8.19. Since the safety factor of the rotation mechanism frame at maximum thrust setting is 1.3, the safety factor for hovering will be 2.6. After analysing the ultimate static load and the oscillating loads, Goodman's diagram allowed to determine the fatigue life of this structure. Since the stress amplitude of the combined loading is below the fatigue strength, it has an extremely long operational life and should not fail in fatigue[4].

8.4. Landing Gear

In this chapter the design and configuration of the landing gear is described. Firstly, the final design is presented in Section 8.4.1 and then it is described where and how the landing gear is placed in Section 8.4.2. Finally, the load cases are analysed in Section 8.4.3.

8.4.1. Design

With the placement and load cases presented in Sections 8.4.2 and 8.4.3, respectively, the design options can be set up. Three configurations are considered: bird-like legs shown in Figure 8.20, two leg struts aligned depicted in Figure 8.21 and a sheet with a bar and two standards configuration displayed in Figure 8.22. These three configurations are meeting the stability requirement as stated in Section 8.4.2.

After setting up the initial configurations in Inventor, a load analysis is performed. The applied material is Aluminium-6061. It turned out that all three configurations can handle the load applied of 1481.31N and that even the configurations are a bit overdesigned.

After topology optimisation, it turned out that the design presented in Figure 8.22 is the most preferred. It is carrying the load the best and it is the most lightweight. A load analysis again is performed and it is found out that the structure is still able to carry the critical loads. The results are presented in Section 8.4.3.

For the final layout a rubber is attached to the part the landing gear is touching the ground. This is done to spread the load and reduce the impact force. Excluding the rubber the mass of one landing gear leg is 98g and including 100g. The final design is presented in Figure 8.23.

[4]http://www.faculty.fairfield.edu/wdornfeld/ME311/ME311MachineDesignNotes06.pdf [Accessed on 21 June 2017]

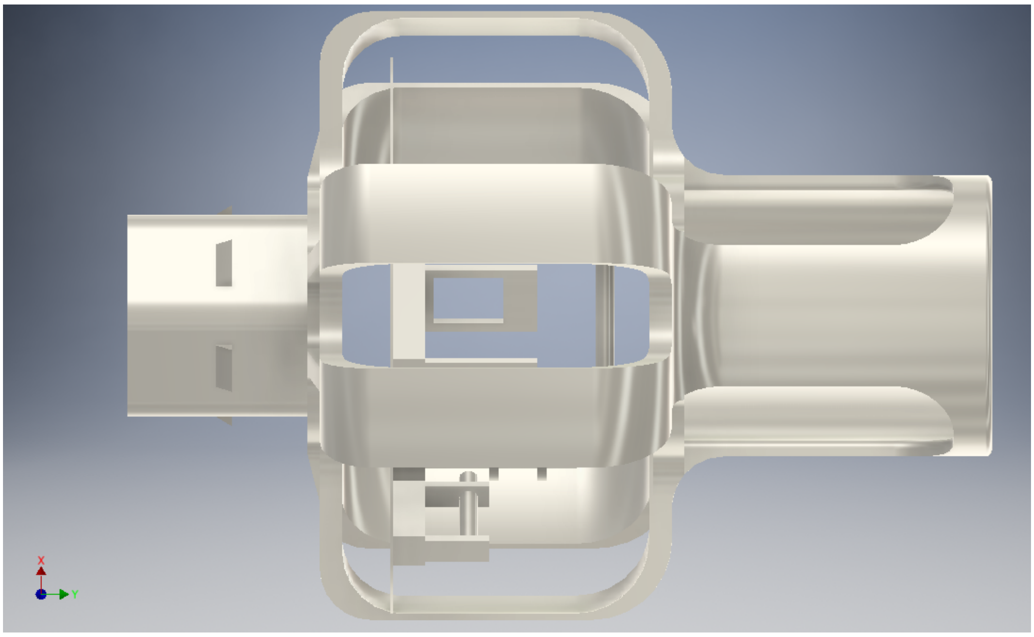

Figure 8.19: Final rotation mechanism frame design

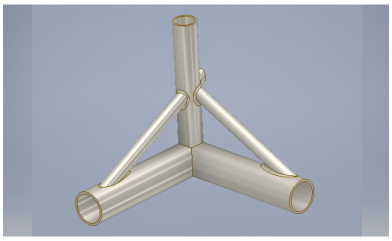

Figure 8.20: Bird-like leg

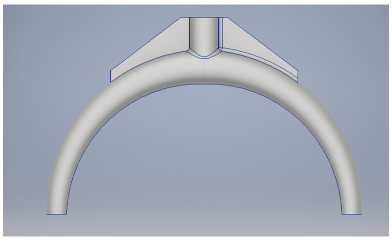

Figure 8.21: Two parts of the leg aligned

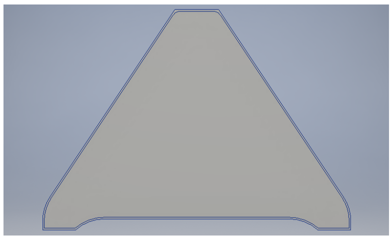

Figure 8.22: Sheet with a bar and two standards

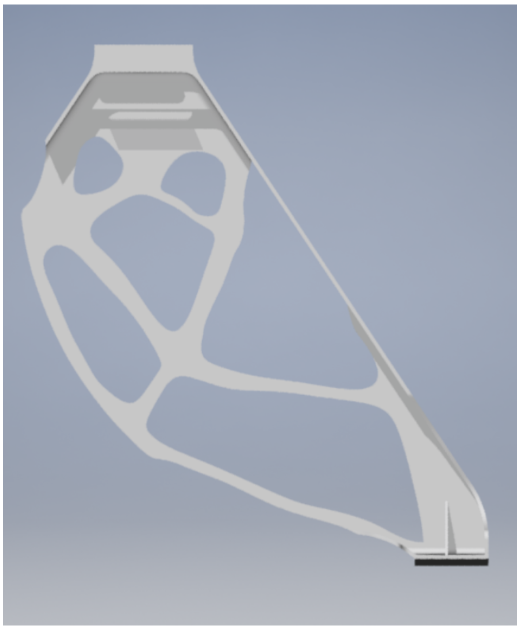

Figure 8.23: Optimized landing gear with rubber feet

8.4.2. Placement

Since there is not much space on the UAV left to fit the landing gear on, first the location is determined and then the landing gear is designed. Since attaching the landing gear to the arms results in a significant increase in mass, the landing gear is not attached there. Therefore the design presented in the Mid-Term Report[3] is not feasible and therefore new designs and a different placement should be considered. Several other locations on the frame and on the DMG Mori are considered, but it is expected that the DMG Mori can not carry the full weight of both itself and the UAV. Therefore the landing gear is placed on the side of the frame. For this placement, it is important that the landing gear provides clearance to the UAV. It is not expected to land symmetrically. Therefore also a landing angle is required. An angle of 10^o is considered to be sufficient. In order to cope with the centre of gravity, which is not located exactly in the middle of the system, the landing gear should be placed approximately 51cm from the end of the suction cup. Then a leg length of 20cm is sufficient and the UAV will then have a maximum landing angle of 11^o.

To ensure stability when landed, the motions in three directions (x,y,z) have to be blocked. Also, the UAV can tip over, therefore the rotation around the three axes (x,y,z-axes) need to be blocked as well. This can only be done with at least three landing gear legs. Therefore, three options for landing gear legs are analysed. This is already discussed in Section 8.4.1. The landing gear is placed in such a way that it is forming a cross.

8.4.3. Load Cases

In general two landing manoeuvres can be performed by the aircraft. Symmetrical landing, when the landing gear will simultaneously hit the ground, dividing the weight equally over the four landing gear legs. And asymmetrical landing where first one or two legs touch the ground. The last case is considered to be the critical one. A force of 1481.31N is then applied on the landing gear in different orientations. The analysis of the critical load cases are depicted for the final design and are analysed in Section 8.4.1.

The results of two load cases are shown in Figures 8.24 and 8.25. One load case with the full weight vertically placed on the rubber feet and the other case having the full weight diagonally (with an angle of 11^o) placed on the rubber feet. The structure does not fail and has a safety factor of at least 2 (which is indicated in green). There is only one load case, which is not depicted, for which the landing gear on the other side of the UAV already failed. Here the safety factor is low, however, when the landing gear fails in this load case unexpectedly the other landing gear should be replaced anyway.

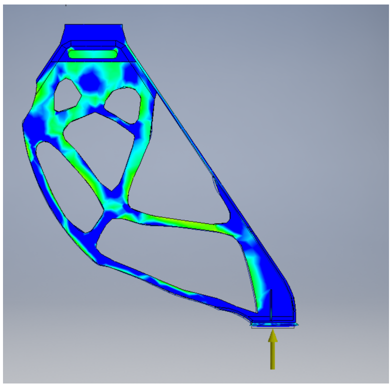

Figure 8.24: Full weight vertical load on landing gear

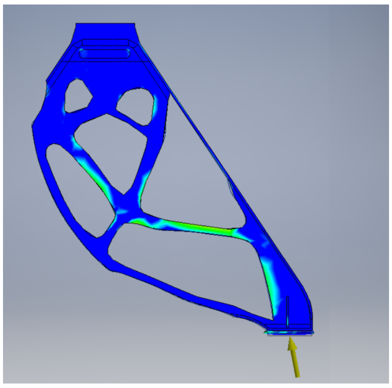

Figure 8.25: Full weight diagonal load with an angle of 11^o on landing gear

8.5. Final Verification of Core Structure

After the major load carrying structural components were designed in isolation with idealised loading conditions, the integrated structure was simulated once to verify correctness of these idealisations. Given the much larger structure, the meshes of individual components are coarser than ones used previously. Therefore, the quantitative results do not match the those of previous simulations' exactly. This is expected and the purpose of this final simulation was to confirm that interactions between components were correctly evaluated rather than to recreate identical results.

The chosen assembly consisted of the payload frame, the rotation mechanism housing, the rotor arm and the connecting bearings. The load applied was the maximum thrust generated by the rotors and the forces were applied to the rotor mounts. The structure was considered fixed at the points where the payload frame connects to the payload. The results of the simulation is shown in Figure 8.26

The simulation results are consistent with previously observed in isolated simulations and components show the same overall stress distributions. The minimum safety factor observed in this simulation was slightly lower than in individual ones, dropping from 1.3 to 1.22. The location of the minimum did not change and it is still at the root of the rotation mechanism housing. The difference can be attributed to the coarser mesh, as the geometry in that location is fairly complicated and the results are thus sensitive to meshing changes. Better results could be obtained by manually controlling the local mesh generation, but this simulation served its purpose as-is, verifying that the boundary conditions considered in component design were representative of the structure.

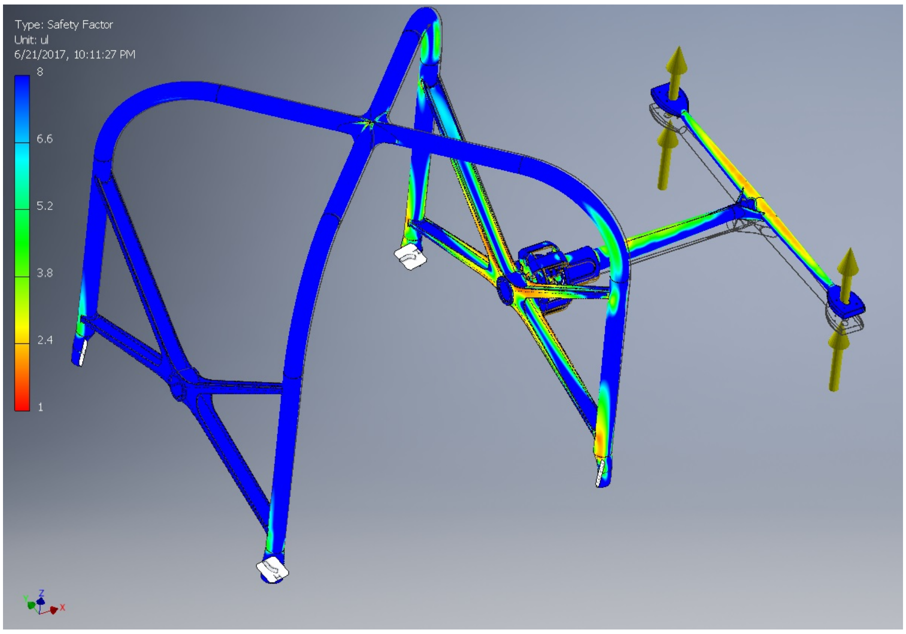

Figure 8.26: Simulation results of the integrated structural components showing safety factor. The minimum is 1.22 at the connector between the payload frame and the rotation mechanism housing.

9 Perching

This chapter goes into detail about the perching mechanism required to increase the reach of the UAV. Section 9.1 discusses why this mechanism is required. Following this is Section 9.2 which states all components that are involved in the perching mechanism as well as the specifications of these components. After this, Section 9.3 discusses the critical loads that act on the system. In Section 9.4 these loads are used to provide information as to why these components have their specifications and why they have been chosen.

9.1. Necessity Perching

The UAV is required to attach to top, side and bottom surfaces as defined in requirement **[OP-1.1]**. This is to increase the merit of the UAV by creating a large spectrum of cases where it can assist in reparation. The UAV has a rotating payload relative to the frame of the aircraft, which aids in attachment to angled surfaces. Due to the configuration of the UAV not all of these surfaces can be reached as the propellers will not grant clearance for the suction cups of the payload. This is due to the obstruction of the propellers with the attachment area. The visualisation of what areas can be accessed and which area's require a perching mechanism can be seen in Figure 9.1.

Here θ is equal to 37.5 degrees due to the geometry of the payload. For the remaining areas a mechanism is designed which will aid in the rotation of the frame through the use of reaction forces created by the aircraft. This is done by attaching with passive suction cups.

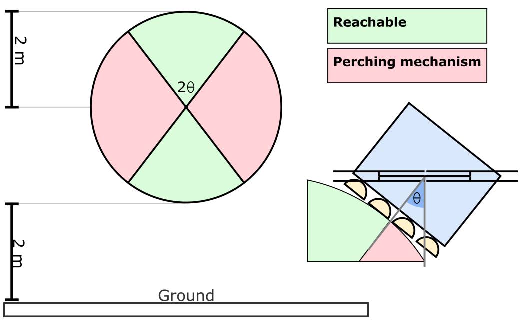

Figure 9.1: Visualisation of reachability of the UAV where θ equals 37.5 degrees

9.2. Component Analysis

For the design of the perching mechanism, the components are identified. This is done by first looking at the functions that the perching consists off. The functions are visualised in Figure 9.2.

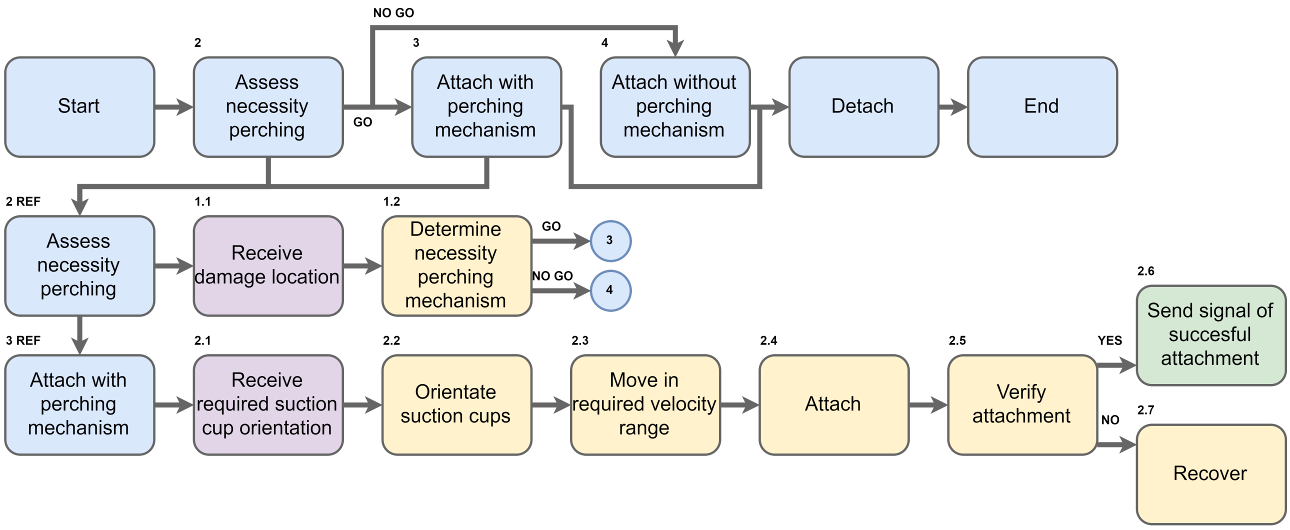

Figure 9.2: Functions that need to be performed to perch to the aircraft

These functions act as a way to identify additional required components. There are five structural components and three operational components. The structural components are two bars, a side bar, a hinge and a suction cup. The operational components are an orientation servo, a detachment servo, and a pressure sensor.

The two bars provide an arm for the reaction forces to allow for rotation. The arm consists of two bars instead of one to increase its storage ability. The hinge allows for rotation of the suction cup relative to the bar and the frame of the UAV and consists of a pin and facilitating bar ends. The suction cup is required to create reaction forces on the aircraft which will rotate the frame. The side bar adds stiffness to the bar which is required to ensure clearance with the propellers when wind is present.

The orientation servo rotates the suction cup relative to the frame before attachment to ensure that the suction cup can properly attach to a surface. The surface angle is measured to relay the required suction cup attitude to the orientation servo. The detachment servo allows for the suction cup to be detached by introducing a peel force on the suction cup. The pressure sensor ensures that attachment has been successful and that the suction cups will provide sufficient suction force. All of these structural and operational components can be seen in Figure 9.3.

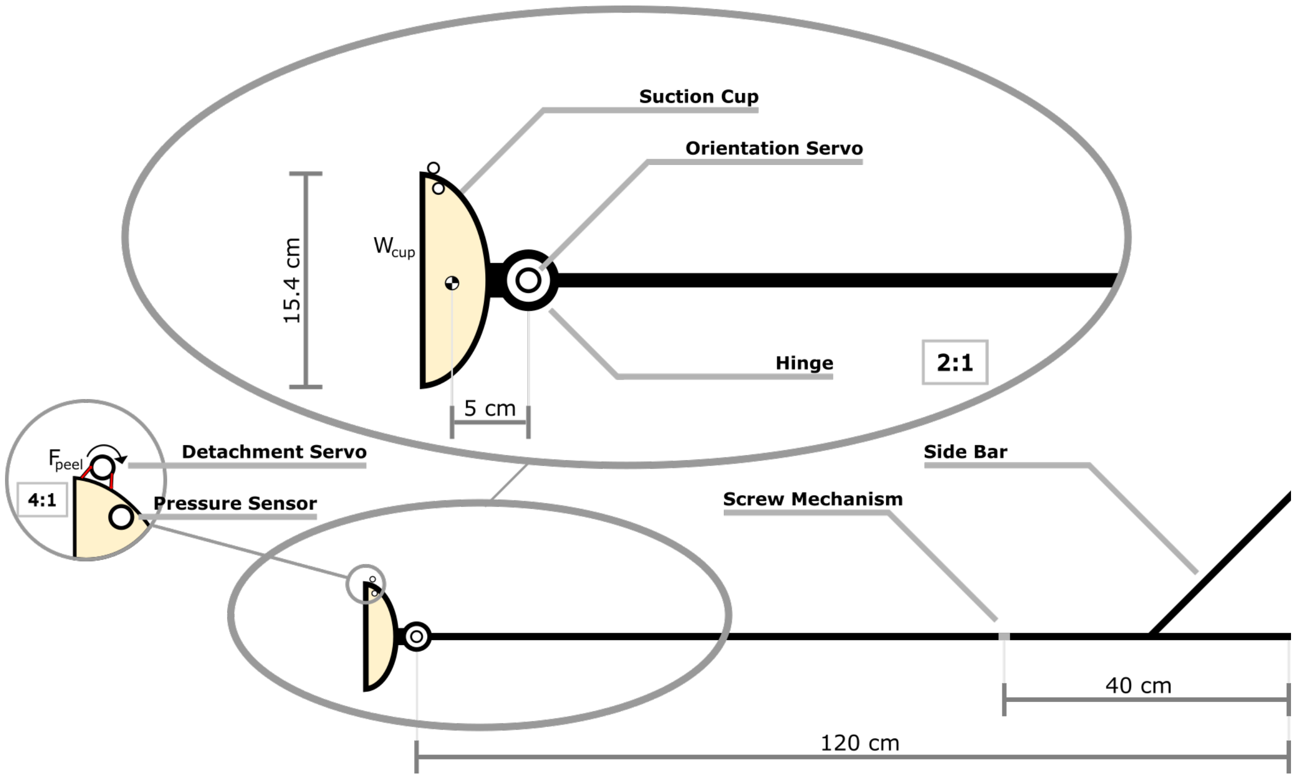

Figure 9.3: Visualisation of the perching mechanism components

The mechanism will consist of two bars in total for symmetry reasons meaning that all of these components are present twice. The perching mechanisms are fixed to the frame near the payload by means of fusion welding as this welding technique has a high compatibility with titanium. The dimensions of these components can be seen in Table 9.1 and the weights can be seen in Figure 9.4.

9.3. Load Analysis

This section describes the loads acting on the orientation mechanism. Every component of the perching mechanism will have to withstand different loads in every phase of the flight. Furthermore, a fatigue analysis is performed in the final part of Section 9.3.4. The following mission phases are used in the following load analysis.

- Flight phase
- Attachment & Rotation phase
- Repair & Inspection phase

9.3.1. Flight Phase

The flight phase starts from the moment the UAV lifts off the ground station and moves towards the designated target. During this phase no other significant loads are present but the weight of the system itself and the vibrations caused by the engines. The weight of the mechanism can be modelled as a distributed load, with an additional concentrated mass at the end of the bar accounting for the suction cups, servos and sensors as visualised in Figure 9.5. The vibrational loads are discussed in Section 9.4.1.

[1] https://www.reichelt.com/de/en/Pressure-Sensors-Force-Sensors/MPX-2100AP/3/index.html?ACTION=3&GROUPID=6676&ARTICLE=42064 [Accessed on 14 June 2017]

[2] http://www.active-robots.com/3205-0-towerpro-mg90-micro-servo [Accessed on 14 June 2017]

Dimension	Value	Unit
Suction cup		
Radius	77	mm
Type	Bevelled	-
Main bar		
Radius	8	mm
Thickness	1	mm
Material	Ti-6Al-4V	-
Side bar		
Radius	5	mm
Thickness	1	mm
Material	Ti-6Al-4V	-
Other components		
Hinge	Pin hinge	-
Pressure sensor	MPX 2100AP [1]	-
Orientation servo	3205_0 Towerpro MG90 [2]	-
Detachment servo	3205_0 Towerpro MG90 [2]	-

Table 9.1: Dimensions of the components of the perching mechanism

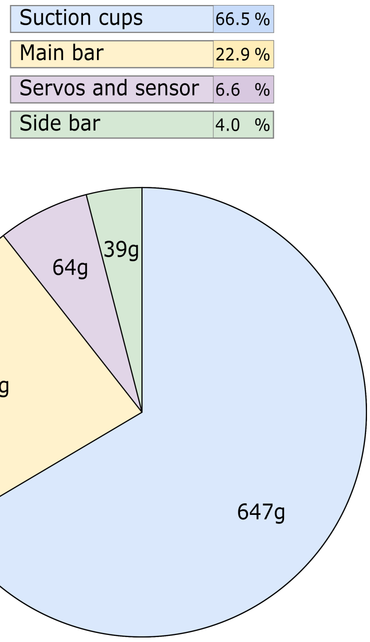

Figure 9.4: Percentile and absolute masses of the perching components

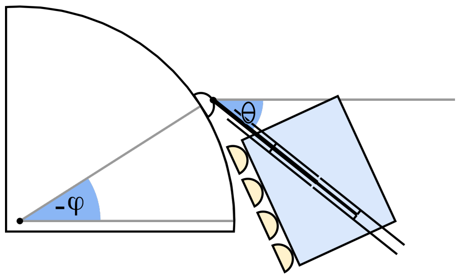

Figure 9.6: Visualisation of the angles ϕ and θ

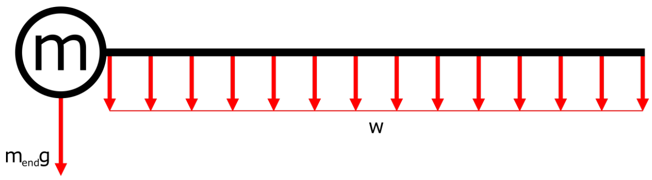

Figure 9.5: Simplification of the bar

9.3.2. Attachment & Rotation Phase

The attachment & rotation phase is defined as from the moment the passive suction cups of the perching mechanism attach until the moment the suction cups of the DMG MORI are attached to the aircraft. Due to the specific nature of suction cup loads, first the force required for safe attachment of the suction cups is described in detail, followed by the loads acting on the perching bar and hinge.

Passive Suction Cup Loads

Before analysing the required suction force, two angles are defined to aid in the description of the passive suction cup loads:

- The orientation of the surface onto which the passive suction cups are attached (ϕ)
- The orientation of the bar (θ)

These angles are visualised in Figure 9.6.

A round fuselage of an aircraft provides several angles to which the suction cups need to maintain attachment. Furthermore, when rotating the bar around the hinge at the suction cup, the loads on the suction cups change between normal and tangential loads. This situation is visualised in Figure 9.7.

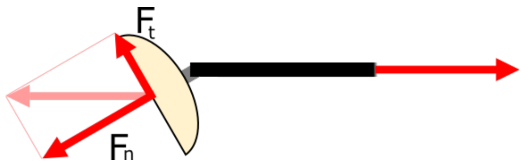

Figure 9.7: Transferral of the normal bar force into a normal suction force and a tangent suction force

The suction cup has to be sized based on the normal force and tangential force acting on it, which depend on ϕ and θ. In order to determine the required suction force F_s the following approach is used: In order to be able to handle both normal and tangential loads, the suction cup should provide more suction force than the normal force applied to it. This will result in a resultant force F_{res} as depicted in Equation 9.1

$$F_{res} = F_s - F_n \tag{9.1}$$

The tangential force depends on the resultant force and the friction coefficient as seen in Equation 9.2.

$$F_t = F_{res} \cdot \mu \tag{9.2}$$

By substituting Equation 9.2 into Equation 9.1 and rearranging terms, the relation between the required suction force and the applied normal and tangential forces, F_n and F_t, respectively is obtained in Equation 9.3.

$$F_s = F_n + \frac{F_t}{\mu} \tag{9.3}$$

The different combinations of ϕ and θ will result in different combinations of F_n and F_t. In order to determine the angle combinations at which the required suction force is maximum, a software tool has been developed to iterate through all possible angles. For each angle the corresponding required suction force is calculated. The results of this iteration are presented in Figure 9.8.

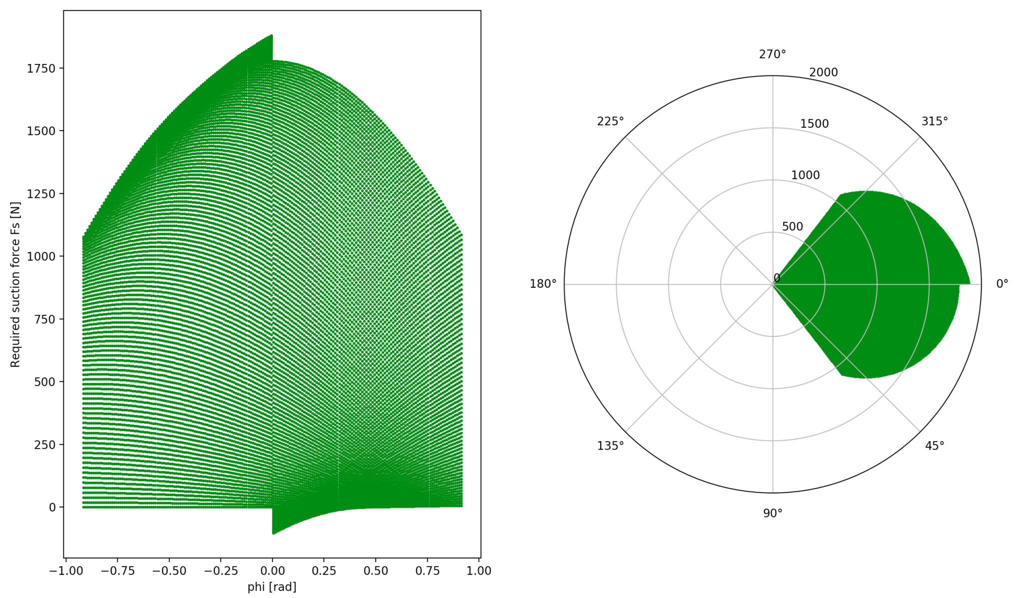

Figure 9.8: Required suction force for all combinations of θ and ϕ that can occur (left). Visualisation of required suction force projected on a fuselage (right)

From this analysis, the maximum suction force required is found to be $F_{s,max}$ =1880N. This occurs at the situation when $\phi = 0^o$ and $\theta = 76.8^o$ as depicted in Figure 9.8. At this combination of angles, Equation 9.3 is at the maximum, both a normal force and tangential force are present in this particular situation. Initially it was expected the maximum suction force is experienced at the angles $\phi = 0^o$ and $\theta = 90^o$. However, since the required suction force is a function of both tangential as well as normal forces (refer to Equation 9.3) this is not the case.

In order to obtain a suction force of 1880N, the suction cup needs to be attached with a certain pressing force to the aircraft. For passive suction cups, a pressing force of a tenth of the suction force is required to attach the suction cup[3].

[3]https://books.google.nl/books?id=kfJlc2wP_ssC&pg=PA108&lpg=PA108&dq=passive+suction+cup+weight&source=bl&ots=Iscql2f1mj&sig=-9Pv-7I2s5Jajdni9QA5XXwCEJc&hl=nl&sa=X&ved=0ahUKEwi706HbqurTAhUGaFAKHXv3BosQ6AEIIzAA#v=onepage&q=200&f=false

Hence for a suction force of 1880N the required pressing force is 188N. Now that the required suction forces are known for every angle combination, along with the required pressing force, the loads on the bar and hinge are analysed.

Bar & Hinge Loads

The bar will be experiencing both compression tensile loads and some bending. The presence and magnitude of these loads depends on the orientation angle required for the suction cup. For example, in the case that the suction cup needs to be attached to the bottom of the aircraft they need to be rotated by 90^o. In this case, the UAV will need to have an upwards velocity component to attach the suction cup with sufficient pressing force. However, attachment using the perching mechanism at the middle of the bottom of the aircraft will not be required since the DMG MORI can rotate upwards and there is no need for the perching mechanism, as visualised in Figure 9.1.

Making use of Equation 9.4 and the bar properties as indicated in Figure 9.4, the maximum load which can be applied perpendicular to the bar, resulting in a bending moment is equal to 151N . This corresponds to a maximum suction force of 1510N as can be obtained from Equation 9.5 (Using the same relation as before, where one newton of suction force requires one tenth of a newton of pressing force).

$$F = \frac{\sigma \cdot I}{y \cdot L} = \frac{1100 \cdot 10^6 \cdot 1.3 \cdot 10^-9}{0.008 \cdot 1.2} = 151N \tag{9.4}$$

$$F_{s,max} = \frac{151}{20/200} = 1510N \tag{9.5}$$

As was stated previously, the maximum required suction force is equal to 1880N. Now the above text argues that the maximum suction force which can be obtained is equal to 1510N. This appears to indicate that a redesign is required. However, the 1880N maximum required suction force is at an angle of $\phi = 0$, hence there will be no bending loads present in the bar. The 1510N suction force is only required at $\phi = 90^o$ and $\phi = -90^o$, the angles at which the bar will be loaded in bending. This will enable the bar to attach such that the higher required suction force of 1880N can be obtained, given that the buckling and compression modes are taken into account. These modes are highlighted next.

Regarding the buckling and compression loads, the critical failure mode needs to be determined making use of Equation 9.6 and 9.7 for buckling and compression respectively. Use is made of the thin walled assumption, hence the inertia is equal to $\pi t r^3$ and the surface area $A_{bar} = 2\pi t r$.

$$F_{buckling} = \frac{2n^2\pi^2 EI}{L^2} = \frac{2 \cdot 1^2 \cdot \pi^2 \cdot 114 \cdot 10^9 \cdot 1.32 \cdot 10^-9}{1^2} = 2982N \tag{9.6}$$

$$F_{compression} = \sigma_{yield} \cdot A_{bar} = 1100 \cdot 10^6 \pi \cdot 0.008 \cdot 0.001 = 27646N \tag{9.7}$$

Since the buckling load is the lowest, this will be used as the critical load for the design. Section 9.4 goes into detail about the final choices made for the dimension of the bar, taking into account additional vibrations and maximum deflections.

Finally, the pinned hinge is analysed. The hinge will experience shear loads as visualised in Figure 9.9. The shear stress τ can be determined, making use of Equation 9.8. The shear flow q is determined by using Equation 9.9.

$$\tau = \frac{q}{t} \tag{9.8}$$

$$q = \frac{V \cdot S_x}{I} \tag{9.9}$$

Making use of CAD software the optimal dimensions for the pinned hinge have been determined as explained in Section 9.4. The shear force acting on the pinned hinge in is visualised in Figure 9.9.

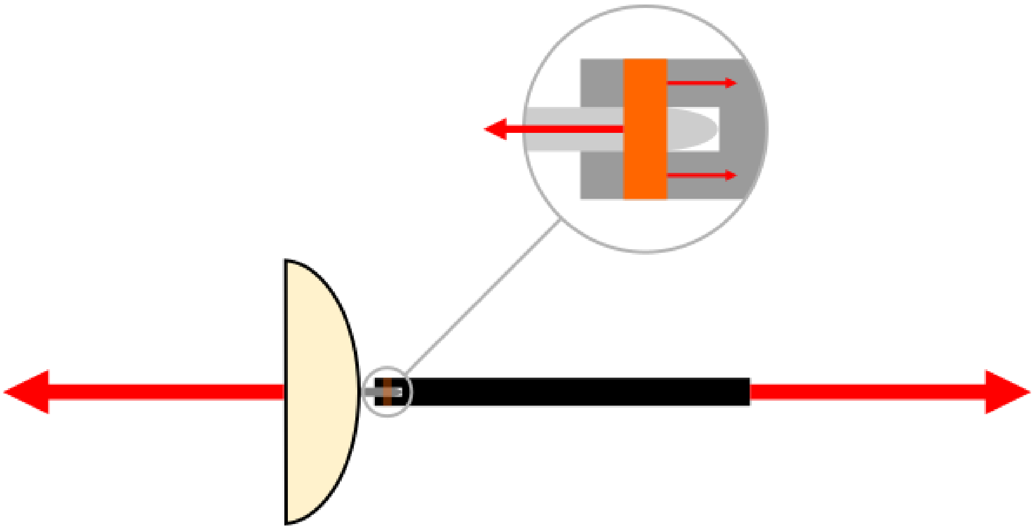

Figure 9.9: Free body diagram of the hinge

9.3.3. Repair & Inspection Phase

The repair and inspection phase starts from the moment the DMG MORI is attached to the aircraft and starts the NDT inspection up until the moment it detaches. The loads acting on the system during attachment are visualised in Figure 9.10.

The weight of the UAV and DMG MORI is supported by the suction cups of the DMG MORI.Wind is an important factor during outside operations, especially during the repair and inspection phase. For this analysis the wind is assumed to act in the plane of the propellers, perpendicular to the UAV. This will impose a horizontal bending moment on the bar. In order to account for the possible deflection this load causes, additional side bars are added to prevent the main bar from deflecting into the propeller area. This deflection under an 80N load is visualised in Figure 9.13.

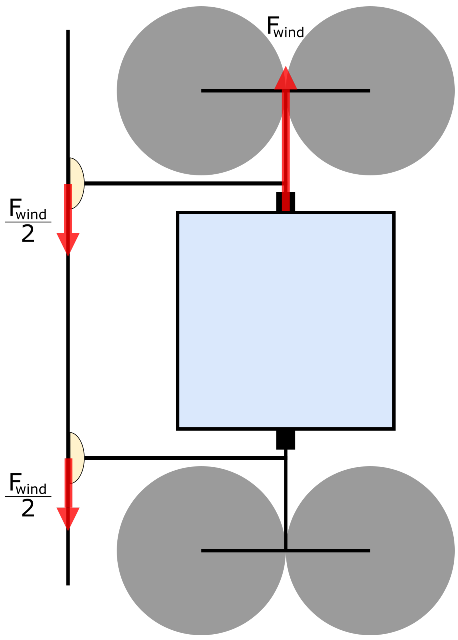

Figure 9.10: Free body diagram of the UAV during attachment

9.3.4. Fatigue Analysis

For the fatigue analysis of the perching mechanism, the emphasis will be on the bar and the suction cup, since these are the most critical structural components of the perching mechanism. The maximum load the titanium bar will experience is determined to be during the attachment phase when a wind force of 160N is acting on the UAV. This will yield a force of 80N to the bar. Considering the dimensions of the bar as depicted in Table 9.1 and the presence of the side bar, the maximum stresses in the bar can be determined. It is assumed the 80N will act on the frame as visualised in Figure 9.10. The normal stresses in the bar can then be determined through Equation 9.10. However, the influence of the side bar to the moment of inertia should also be taken into account. This is done by varying I over the length of the mechanism taking into account both the inertia of the main bar and side bar for the relevant parts. Finally, the y=0.008m is used since this will yield the highest normal stress.

$$\sigma = \frac{My}{I} = \frac{80 \cdot 0.008}{1.37 \cdot 10^{-}9} = 466\,\mathrm{MPa} \tag{9.10}$$

With the use of the S-N curve (indicated in red) of Ti-6Al-4V in Figure 9.11 and the corresponding maximum cyclic stress of S = 466 MPa, it can be determined that the maximum number of cycles the bar can withstand is at least 20000 cycles which corresponds to an equal number of flights (Assuming one perching manoeuvre per flight).

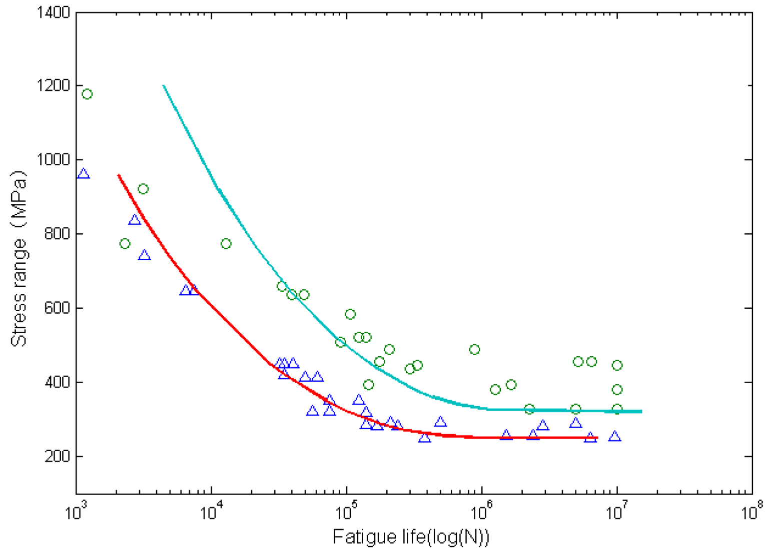

Figure 9.11: S-N curve of Ti-6Al-4V[4]

Regarding the suction cup fatigue cycles it is assumed the maximum stress amplitude on the suction cups is equal to 101325 Pa (1 bar). At this stress amplitude, the material of the suction cups (Nitrile rubber) can withstand over 100,000 cycles. However, it is recommended to replace the suction cups before this amount is reached.. This is because contaminations might occur on the suction cups, without being noticed. These contaminations will greatly reduce the suction force since the friction coefficient μ will decrease.

9.4. Design

The aim of this section is to describe the design process that was used in order to create the dimensions and weights of the components. This is done by first looking at the structural components in Section 9.4.1 followed by the operational components in Section 9.4.2. Finally the reachability with the perching mechanism is shown based on a generic aircraft in Section 9.4.3.

9.4.1. Structural Components

There are five components for the structural design as has been described in Section 9.2. Together with the critical forces, these components can be sized.

Suction Cup

The first component to be sized is the suction cup. The suction cup is designed according to a bevelled suction cup as described by Festo[5]. The bevelled suction cup design weight more for the same amount of suction power relative to simple suction cups, however it is more flexible with attaching to curved surfaces. Data is collected about bevelled suction cups to create a best fitting curve between the weight and the suction capabilities. This can be seen in Figure 9.12.

From this figure, it can be seen that for a suction force of 1880N, a suction cup weight of 0.324kg is required. The area of the suction cup is determined through the required suction force and the atmospheric pressure. This is seen in Equation 9.11.

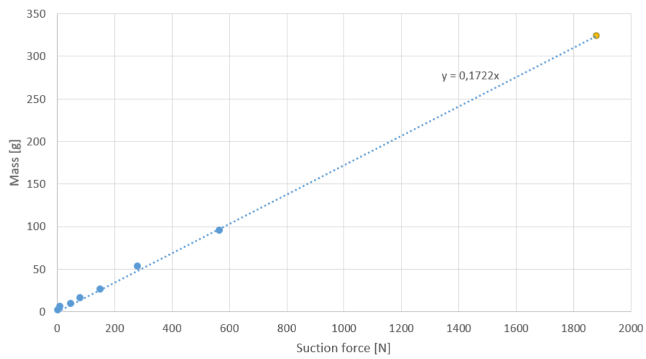

Figure 9.12: Best fitting curve for suction cup mass relative to suction force where the yellow dot is the design point

$$A = \frac{p}{F} \tag{9.11}$$

The area of the suction cups is 186cm^2 meaning that the radius is equal to 7.7cm. For these suction cups it should be noted that it can operate in temperatures ranging from -20^o to 200^o[5]. Therefore outside temperatures will not compromise the capabilities of the suction cups.

[4]http://www.mdpi.com/1996-1944/8/10/5367/htm [Accessed on 20 June 2017]

[5]https://www.festo.com/net/SupportPortal/Files/10595/VAS_ENUS.pdf [Accessed on 10 June 2017]

Bars

There are three considerations for the bar system, these are the main bar which is split in two parts due to its length and the side bar. The main bar is constant in radius and thickness and the side bar as its own separate thickness and radius. For all bars, a hollow tube is chosen as it has a high multi-directional inertia over weight ratio.

The dimensions of the main bar are dictated by two features it should have. The first is feature is that its natural frequency should be lower than the frequency produced by the propellers. The second feature is that it should allow for clearance with the propellers. The first feature dictates that the radius of the bar should not be higher than a certain value while the second feature dictates that the bar should be stiff enough. However, there is no radius that will allow for enough clearance while also providing a small enough structure to not resonate with the propellers. For this reason a side bar is added, to increase stiffness without increasing the frequency beyond an unacceptable value. The natural frequency of the bar is calculated through Equation 9.12.

$$f_{nat} = \sqrt{\frac{3EI}{(m_{head} + m_{bar} \cdot 0.23) \cdot L^3}} \tag{9.12}$$

For this frequency a length of 1m (measured from the suction cup) is used due to the supporting side bar adding rigidity. For m_{head} the mass of the two servo's and the suction cup is used. For m_{bar} the mass of the main bar up until the one meter mark is used. This results in a frequency of 34.7Hz. This is above the frequency range of frame arms (e.g. resonance will not happen).

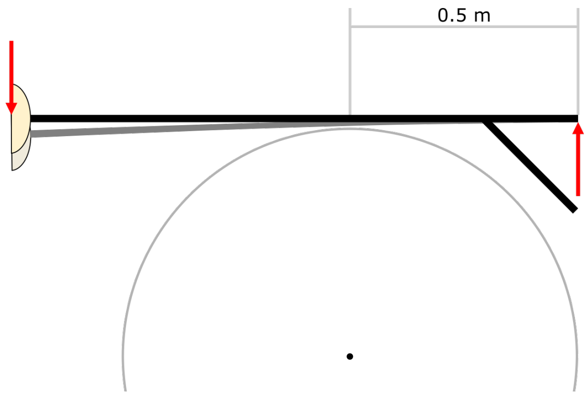

Figure 9.13: Required propeller clearance for the bar

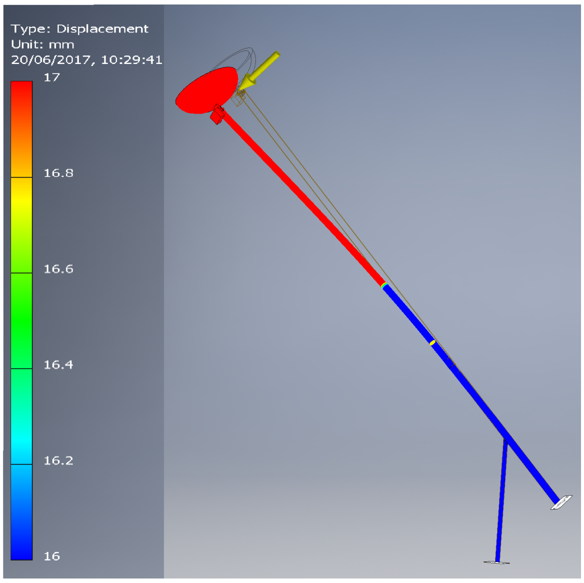

Figure 9.14: deflection of the perching arm for a force of 80N where the yellow dot indicates the 0.5m mark

The deflection of the side bar is simulated with FEM. For this deflection the point of interest is the bar at 50 centimetres from the frame as the propeller is closest to the bar at this point. This can be seen in Figure 9.13. The FEM analysis results in a deflection lower than 1.7cm which is the maximum allowed deflection at this point. For this deflection a force of 160N (80N per bar) is used as this is the maximum average wind force present for the UAV on Schiphol[6]. The dimensions that were chosen for the side bar were 5mm in radius and with a thickness of 1mm. The radius of the side bar is chosen to be 5mm as its attachment to the frame arm should remain in the areas where only low stress is present, which is near its neutral axis.

From the main bar and the suction cup a minimum and maximum impact speed is obtained. The minimum impact speed is determined by the required force to properly attach the suction cups. This force is determined in Section 9.3 and is used in Equation 9.13 to get the minimum impact speed.

$$V_{impact} = \sqrt{\frac{2F \cdot s}{m}} \tag{9.13}$$

From this a minimum impact speed of 0.158m/s is acquired. For the maximum impact speed the lowest critical force of the compression and buckling force is used to obtain the maximum impact speed. This results in a maximum impact speed of 0.629m/s.

[6]http://projects.knmi.nl/kbs/doc/windclimatology.pdf [Accessed on 14 June]

Hinge

The hinge in the arm is a pin hinge. This pin needs to be sufficiently thick to withstand a shear force equal to half the weight of the UAV. The hinge has a radius of 5mm which is verified with FEM analysis to be sufficient to withstand this load.

9.4.2. Operational Components

Besides the five structural components, there are three operational components which have been described in Section 9.2. The components require power which is provided through the use of a connector.

Orientation Servo

The orientation servo has to rotate the suction cup relative to the bar to make sure that attachment will be proper. To do this it needs to have a torque high enough to hold the weight of the suction cup and the detachment servo. This means that it requires a torque of at least 0.165Nm. As the 3205_0 Towerpro MG90 micro servo can create a torque of 0.196Nm and due to its light weight, this servo is used as the orientation servo. Its weight is equal to 14 grams[7].

Detachment Servo

The detachment servo needs to create a peel force that is sufficient to detach the suction cup from the surface. The force that is needed for this is 500 times as small as the suction force[17]. This force has to be transformed in a torque by determining the arm that this force will have. This arm is lower than 2cm, meaning that taking 2cm for calculation purposes will result in a torque that will be sufficient for smaller arms as well. This results in a required torque of 0.075Nm. For this servo the 3205_0 Towerpro MG90 micro servo is also used.

Pressure Sensor

The pressure sensor needs to verify proper attachment by measuring the pressure within the suction cup. This can be combined with a pressure sensor on the ground station that measures the outside pressure to provide the suction force that is present. This sensor needs to be able to measure pressure in the range of 0 to 1bar whilst still being as light as possible. The MPX 2100AP pressure sensor can measure this range and only weights 3g[8]. Therefore it is used as the pressure sensor for the design.

9.4.3. Reach

The final reachability of the aircraft is depicted in this section. This is done by creating a heatmap of a generic aircraft where green areas are reachable and red areas are not reachable. The heatmap is seen in Figure 9.15. The areas that can not be accessed are the engines, the control surfaces, the horizontal tail surfaces, areas with a curvature with a radius lower than 2m and the tips of the wings and vertical tail surface. Also surfaces that can be accessed by the drone have no room for the perching mechanism to attach (e.g. the fuselage slightly above and under the wing).

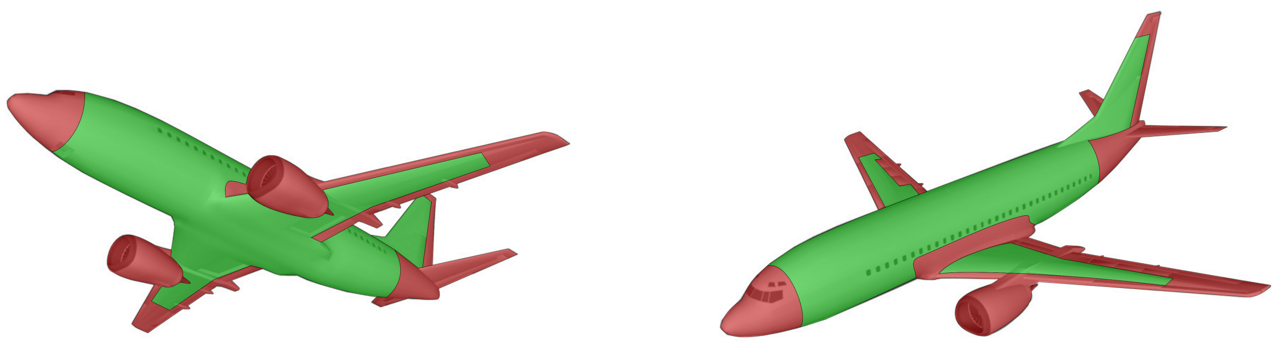

Figure 9.15: Heat map of the reachability of the UAV where green depicts areas that can be reached

From this figure it can be estimated that roughly 80% of aircraft locations can be reached (this is highly dependent on the aircraft model). However when this is combined with the consideration that most damages occur at the reachable cargo doors of the aircraft due to baggage cars and catering vehicles, it can be considered that roughly 90% of all damages to the outside of most aircraft can be reached by the UAV.

[7] http://www.active-robots.com/3205-0-towerpro-mg90-micro-servo [Accessed on 10 June 2017]

[8] https://www.reichelt.com/de/en/Pressure-Sensors-Force-Sensors/MPX-2100AP/3/index.html?ACTION=3&GROUPID=6676&ARTICLE=42064 [Accessed on 10 June 2017]

10
Vibrations

This chapter covers a short investigation into the vibration properties of the extremities of the structure using modal analysis. To avoid unnecessary in-flight oscillations, the perching and rotor arms were analysed for their resonant modes to verify that they do not coincide with flight loads. Section 10.1 aims to provide context while Section 10.2 and Section 10.3 focus on the analysis of the rotor and the perching arms, respectively.

10.1. Design Considerations

During flight, the vehicle experiences various cyclical loads. They arise from vibrations generated by moving parts as well as from the nature of how multirotors are controlled by temporarily changing the thrust of individual rotors. If they were to excite resonant modes of the structure, the resulting oscillations could affect performance of the vehicle. While unlikely to cause outright failure, the oscillating structure would experience unnecessary stress, reduce the stability and controllability of the vehicle or even prevent landing on the target if the perching arms are moving too excessively to be aligned with the surface.

Due to limited time and computational resources only the most susceptible parts of the structure were investigated during typical flights. Using the flight simulation described in Chapter 12 conditions during a typical mission flight were estimated. Firstly, the vehicle is unlikely to experience flight controller induced oscillations with frequency of over 10Hz due to its large size. Secondly, for more than 90% of the time, the rotors are operating between 37 and 49Hz. More sporadic disturbances such as gusts of wind or atypical momentary corrections are not considered at the moment, but should be included if the study is revisited in more detail later. The payload is inactive during flight and is thus also not considered.

10.2. Rotor Arms

This section explains how the rotor arms were investigated, the results of these investigations and their implications.

10.2.1. Design Goals

The main consideration regarding rotor arm oscillation is the resulting degradation of flight stability and controllability. The flight controller relies on an exact knowledge of rotor locations relative to vehicle's centre of mass. Therefore, rotor dislocation results in incorrect force balance calculations and degrades flight controller's capability to control the vehicle. This is especially concerning as the vibrations would be most prominent in critical situations such as when a rotor is damaged and the flight controller is already stressed. Change in a rotor's plane angle is especially unwanted as even small changes can significantly reorient the direction of lift, causing unexpected coupling between the different axis of control. In-plane displacements of the arm, while still unwelcome, are less impactful.

10.2.2. Simulation Setup

The sub-assembly of the load carrying structure of the rotor arms was simulated using FEM analysis tools available in **Autodesk Inventor**. Mock motor models with equivalent weight were attached to their respective locations. Although the propellers were not included themselves, their weight was migrated to the weights representing motors to achieve better approximation without introducing excessively complex geometry. Gyroscopic effects from the spinning rotors were not considered. The sub-assembly was considered fixed at the point where it attaches to the main frame of the vehicle. The structure was prestressed by applying vertical loads to the mock motors which are equivalent to the lift produced during hover. A screenshot of the model with boundary conditions present is shown in Figure 10.1.

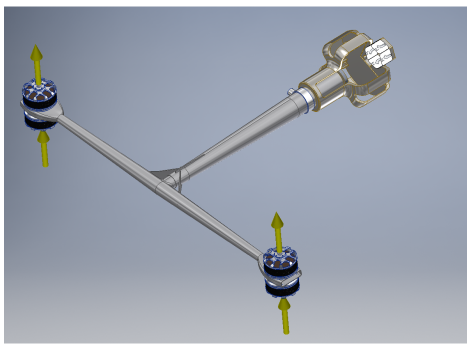

Figure 10.1: Screenshot from Autodesk Inventor showing the sub-assembly model and boundary conditions used for modal analysis

10.2.3. Review of the Simulation Results and the Recommendation

Six resonant modes were identified: three low frequency modes at approximately 18, 19 and 25Hz where mostly the side arms are displaced (Figure 10.2) and two higher frequency modes at 147 and 225 where the main arm and the root connection are displaced (Figure 10.3). The higher frequency modes are unlikely to be excited and result in low rotor displacements and thus are ignored. The low frequency modes result in much greater displacements of the rotors and are much closer to the frequencies of in-flight disturbances, making them more critical. The low frequency modes are all present around 20Hz and potentially could severely degrade control over yaw, roll and pitch axis of the vehicle. The torsional oscillation along pitch axis seen in the rightmost picture of Figure 10.2 is extremely unwanted as the sensors for navigation will rely on a steady pitch angle and the perching manoeuvres also require a high degree of pitch control.

Currently, none of the resonant frequencies are directly within the most dangerous <10Hz or 37-49Hz ranges, but the flight controller's code should still avoid repeated thrust corrections at around 20Hz, especially along pitch axis, to avoid exciting the low frequency modes. In case the effects on controllability were to prove too excessive during testing of a prototype, the arms should be redesigned for higher stiffness at the cost of increased weight.

ff
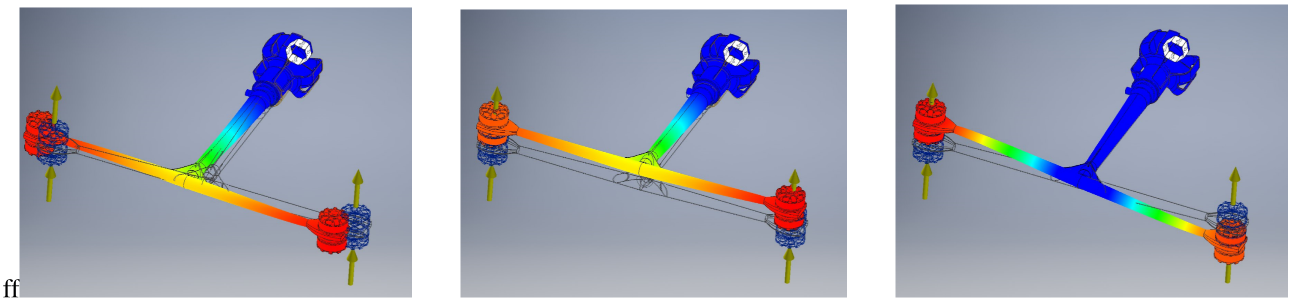

Figure 10.2: Low frequency modes. Left to right: horizontal oscillation at 18Hz, vertical oscillation at 19Hz and torsional oscillation at 25Hz. Colour represents relative displacement amplitude where red is high and blue is low.

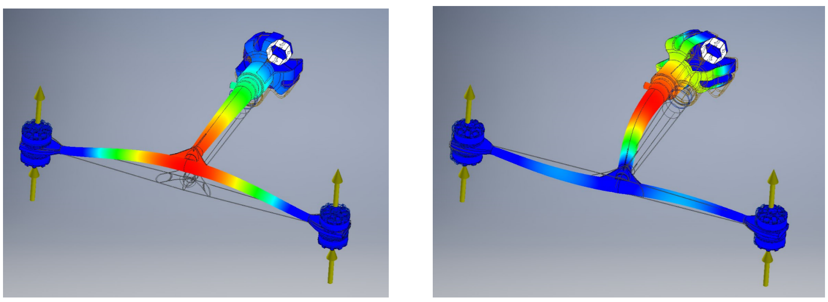

Figure 10.3: High frequency modes. Left to right: vertical oscillation around the connection at 147Hz and vertical oscillation around the root at 225Hz. Colour represents relative displacement amplitude where red is high and blue is low

10.3. Perching Arms

When analysing the vibrations of the perching arms, two risks are taken into account. The first being that the if the eigenfrequencies are in the same range as the frequency of the propellers resonance can occur. The second risk is that deflection from vibrations should not make the perching arm collide with the propellers.

Through the use of FEM analysis the frequencies of the bar have been examined. In Figure 10.5 two of the eigenfrequencies of the beam are displayed. On the left the frequency mode of the suction cup is shown, and on the right the horizontal frequency mode of the perching arm bar is shown. The frequency of the suction cup is 3.28Hz and the frequency of the bar is 8.15Hz. This means that the risk resonance is avoided. As can be seen on the right of Figure 10.5 the vibrations of the bar happen mostly at the tip of the bar and not at the 0.5m point where the bar is closest to the propeller. This means that the second risk is also avoided.

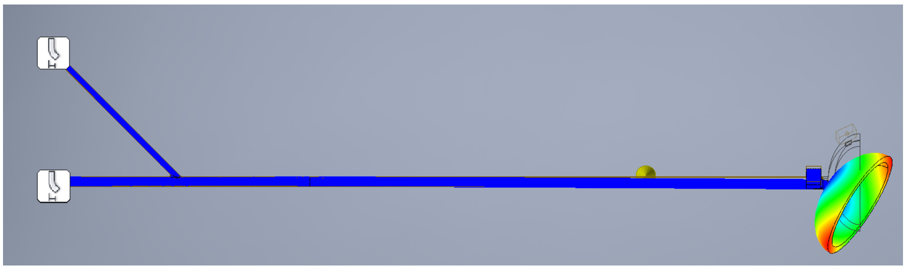

Figure 10.4: Frequency mode of the suction cup. Colour represents relative displacement amplitude where red is high and blue is low

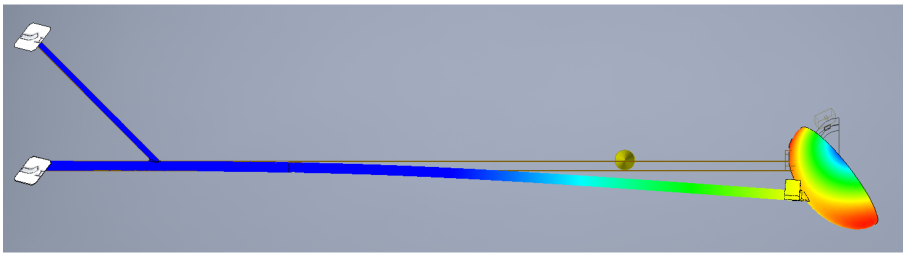

Figure 10.5: Frequency mode of the perching bar. Colour represents relative displacement amplitude where red is high and blue is low

11
Navigation

With the structural design complete, the electronics and software needed to make the UAV operational have to be designed. This chapter deals with the navigation. First, the mission profile will be discussed again in Section 11.1 to see what sensors the UAV will need to successfully complete each stage and to identify the challenges concerning navigation. Then the sensor requirements will be stated and the sensor selection is discussed in Section 11.2. Finally, the functional flow and the required software will be described in Section 11.3.

11.1. Mission Profile

The mission consists of different stages and each stage needs navigation in a different way. From Chapter 3 the rough mission profile is target location input, flying to the target, attachment to aircraft, inspection and repair, payload retraction and return to ground station. Each of these stages will be described more accurately and what kind of sensors could be used per stage is discussed.

Setup

The UAV will receive a reference location to fly towards. This can be either a GPS input, since the UAV already has a GPS on-board for the flight controller, or a Wi-Fi signal. Both can provided by a beacon placed at the aircraft by a technician. If GPS is used, also the transponder of the aircraft could be used. An alternative is to give the instruction that the UAV shall be set up with its direction of flight already towards the aircraft, so the simple 'forward' command will have it arrive at the aircraft. With this last option however, the UAV flies blindly and is not able to correct for disturbances induced during cruise.

The UAV will have a database with 3D maps of all the aircraft it may have to perform a repair on. This map could be provided by the manufacturer of the aircraft, which would induce extra workload on the airlines. However, the UAV would also be able to map the aircraft itself. This only needs to be done once per aircraft. The UAV will have to be controlled manually for this, though it could also be considered to provide an automated program for this.This would be a separate mission that is not considered any further at this stage, but might be looked into post DSE. This map would, most ideally be separated in different sections. The operator can then select the section in which the damage is located. Another option is that the exact location of the damage is received from, for example, an inspection drone.

Lastly, the UAV needs a database of signatures it can compare the damage it sees with in order to recognise it as the damage. Or, if an inspection drone is used, the signature can directly be copied from the data the inspection drone has on the damage.

Takeoff

After all inputs are given, the UAV takes off and ascends to a specific altitude. To know at what altitude the UAV is it will need a sensor to measure the distance between the UAV and the ground. The range of this sensor should have a range of at least a couple of metres. Most convenient for this is a sonar sensor pointing downward during take off.

Cruise

In the cruise stage, the UAV first flies to the reference location inserted in the setup. During cruise the UAV needs to detect objects and plan its trajectory around them. To do so the UAV should have a depth perception of its surroundings. There are multiple possibilities for 3D mapping the surroundings. The first option is 3D LIDAR (Light Detection and Ranging). Another possibility is a depth camera that works with an IR laser transmitter and two IR sensors working together with an RGB (red-green-blue) camera. Preferably the ground is visible by the depth sensors during cruise so it can map the ground. This way it has a better idea of its location, since it has the ground as a reference point.

For unexpected changes in the surrounding outside the field of view of the 3D sensors and cameras the UAV needs to have collision avoidance. For this, simple proximity sensors placed at tactical locations on the UAV would suffice. These proximity sensors would be a short range distance sensor with a sufficient sampling rate and range. The layout should be such that there are no dead angles in going forward, also when making a turn.

In order to fly steadily and in the correct direction, the UAV relies on its IMU and GPS, which are both part of the flight control unit. Another option is to have a normal camera for a view of reference.

Find & Lock
Once the UAV is close enough it will start mapping the aircraft. It will compare the map it creates with the map in its database to determine where it is located with respect to the aircraft. From there it can navigate itself to the location of the damage. All the while the UAV will keep comparing what it is mapping with the map in its database. The sensors needed for this are the 3D sensors and cameras and the proximity sensors for collision avoidance. Possibly a different range of the 3D sensors and cameras is needed for this stage. Also, a recognition software is required.

Perch, Attach & Land
When the UAV found the sector in which the damage is located, it has to place the payload over it such that the payload can successfully perform its repair sequence. This is where the signature of the damage, given to the UAV during the setup, comes in. First of all, the UAV needs to be able to 'see' the damage so it can compare what it sees with the signature in its database. This can be done with multiple different sensors. The depth cameras would suffice, or a normal RGB camera with high enough resolution to see the damage clearly such that it can recognise it from the provided signature.

Then it should lock on the damage and align with it while descending till touchdown and land. The alignment will mainly be software, but for the descending a distance sensor is needed in combination with the depth perception. For touchdown and attachment the surface the UAV is landing on needs to be mapped such that the suction cups can be positioned so that they will hold. With the 3D mapping and the right algorithm the UAV will know the angles and curvatures of the surface it will land on. With the information provided by the sonar the UAV can adjust its speed accordingly to make a soft landing. If the perching mechanism is needed, and extra calculation is needed to know where to perch so the payload will ultimately be placed in alignment with the damage.

Return to Ground Station
After the payload is done repairing, or if the repair mission is aborted, the UAV has to return to the ground station. To locate the ground station, the UAV could trace back the path it flew before. This way it does not have to process more data. However, the UAV may get lost if there is any disturbances in its flight path, straying it off the path it flew before. The collision avoidance would still be in place. Furthermore it is mainly software and memory at work.

Another option is the same procedure it has for finding the mission target. In this case the ground station would contain either a GPS beacon or a Wi-Fi beacon to guide the UAV back. Instead of a beacon the UAV could also already have saved its location in the take off stage. The UAV would use the saved location as its reference location. It would then recognise its landing platform and use the same procedure as for the landing at the mission target. For this option the UAV again needs its GPS, IMU, depth sensors and cameras, proximity sensors and sonar sensor.

11.2. Sensor Requirements & Selection

Which sensors are most optimal for navigation depends on the requirements for the sensors. The most constraining requirement is the accuracy. The requirements already imposed on the navigation from the Mid-Term Report are:

[FD-NAV-1]: The system shall be able to scan the nearby surroundings in 3D for navigation
[FD-NAV-2]: The system shall be able to detect imminent collisions
[FD-NAV-3]: The system shall be able to find and track a location in 3D space
[FD-NAV-4]: The system shall be able to keep tracking the target through obstructions
[FD-NAV-5]: The system shall provide the UAV with position knowledge of within 10mm along all axes

Besides these requirements there is some targets that would be convenient to reach, but do not necessarily kill the design if not reached. These targets are as follows:

- Comply with a weight budget of 1kg including cables
- Try to have all sensors connectable to a power rail of 5V
- Have a complete depth field view within 1.5m ahead
- Stay within the budget in terms of cost
- Map the ground while moving towards the target

With these requirements and targets in mind, sensors are selected. The first requirement asks for 3D scanning of the surroundings. In the previous section two options were discussed: LIDAR sensors and IR depth cameras. Two LIDAR sensors on opposite sides of the quality spectrum are the Scanse SWEEP[1] and 'the Scout' from Phoenix LiDAR systems[2]. Even the lower end LIDAR is expensive and provides more than needed. Also, they both weigh more than what would be ideal.

Clearly, a simpler system is required. Inspiration was found in the Kinect used by X-box. When looking into how the Kinect camera works it becomes clear that the system might suffice. The first Kinect uses a PrimeSense CARMINE sensor[3]. It uses an IR transmitter and two IR sensors, working together with an RGB camera to create a perception

[1] http://scanse.io/ [Accessed on 8 June 2017]
[2] https://www.phoenixlidar.com/scout-series/ [Accessed on 8 June 2017]
[3] http://www.i3du.gr/pdf/primesense.pdf [Accessed on 12 June 2017]

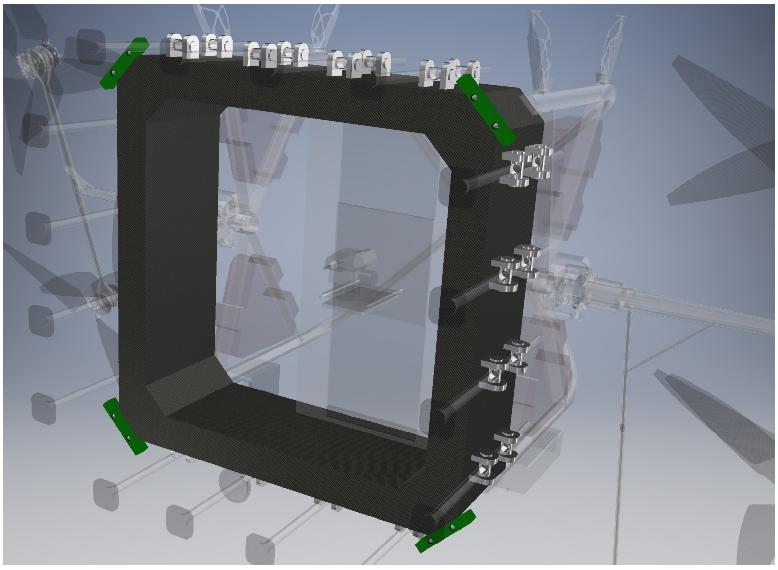

Figure 11.1: Layout 3D sensors (in green)

of depth. The specifications were worth looking into to see if the requirements and targets would be met. However, it turned out that after the acquisition of RealSense the production of the CARMINE sensors was discontinued[4]. Therefore, sensors with the same principle are found. As a reference, the RealSense R200 from Intel[5] is chosen. See Table 11.1 for an overview of the main specifications.

Table 11.1: Main specifications of 3D depth camera

Specification	Value
Price [€]	132.60
Weight [kg]	0.1[6]
Operating voltage [V]	5
Range of depth [m]	0.4-2.8
Field of view	59° H, 46° V, 70° D

Requirements **[FD-NAV-1]** and **[FD-NAV-3]** are met per definition with this camera. However, for Requirement **[FD-NAV-3]** additional software is needed to be met. With a maximum depth range of 2.8m Requirement **[FD-NAV-2]** is met also. Determining the precision would require testing, which can only be done once there is a working prototype. Research on the quality of this camera is already executed and proves that the camera meets Requirement **[FD-NAV-5]**[7]. The connection is with USB 3.0, meaning it can be connected to a 5V power rail. For the field of view overlapping within 1.5m some calculations and layout optimisation are done. In the specifications of the camera[5] the horizontal, vertical and diagonal field of view are given. Given these, it can be calculated at what distance the fields of view of the cameras overlap if they are positioned as can be seen in figure Figure 11.1. For calculations a distance of 1.3m between the sensors is used. The horizontal field of view overlaps at the shortest range, which is at a range of 1.13m. The longest distance for overlap is in the vertical field of view at 1.53m. Since the target specifies to have a complete depth field of view within 1.5m and an even smaller distance would be preferable, the layout is optimised with the horizontal distance between the sensors fixed. It then turns out that a complete field of view, without any blind spots, is reached at 1.15m distance if the vertical distance between the sensors is 1m. This implies that in the vertical direction the sensors need to be placed closer together. However, the 1.3m distance is actually the outer dimension from suction cup arm to suction cup arm. The distance between the cameras is in reality 1m when placed like in the figure. Since this complete field of view is reached at a distance of 1.15m away, the UAV will first have to map the surface it wants to approach, from a distance of at least 1.15m before approaching and attempting to land. Otherwise, details about the curvature of the surface may be missed which could result in a faulty perch.

When the UAV flies horizontally, the distance it can see below itself with the depth cameras is 1.96m. This is calculated with the maximum range of 2.8m and the angle for the diagonal field of view. For safety it is advised to have the UAV operate at an altitude that exceeds the length of a (tall) person. An altitude of 3m (to the centre of gravity of the UAV) is therefore advised for hover and cruise. (This results in an altitude of 2.5m till the lowest part of the UAV.)

[4] https://en.wikipedia.org/wiki/PrimeSense [Accessed on 13 June 2017]
[5] https://software.intel.com/sites/default/files/managed/d7/a9/realsense-camera-r200-product-datasheet.pdf [Accessed on 20 June 2017]
[6] https://software.intel.com/en-us/articles/introducing-the-intel-realsense-camera-sr300 [Accessed on 19 June 2017]
[7] https://arxiv.org/pdf/1705.05548.pdf [Accessed on 16 June 2017]

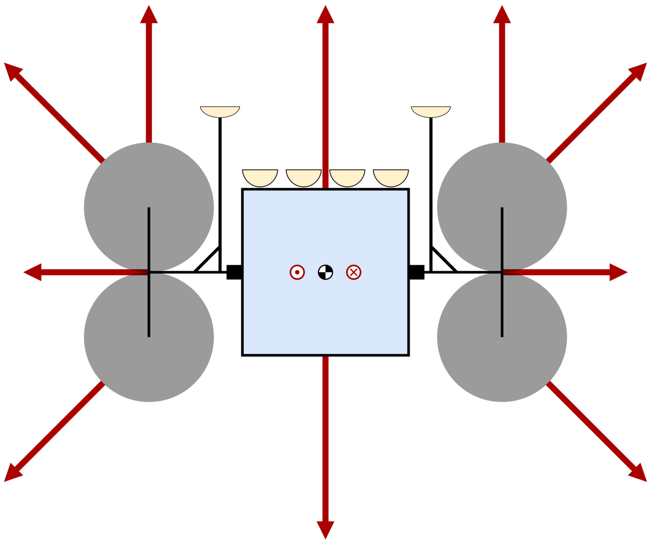

Figure 11.2: Layout proximity sensors

If the ground has to be mapped while cruising from this altitude, the UAV has to fly at a 7° pitch downwards minimum. Therefore a pitch of 10° is advised.

For the collision avoidance, simple proximity sensors are sufficient. The sensors should be close range, because it is an emergency measure if non-collision flight path calculated from the 3D sensors failed, or if the surroundings unexpectedly change outside the view of the 3D sensors. Also, the proximity sensors replace the shielding of the propellers. Since shielding the propellers would make the design too large, it had to be dropped. The proximity sensors will therefore take over most of the roles shielding would have.

The most common proximity sensors are sonar sensors. They generally have a larger range than needed for the purpose they would be serving in this case. Also, they cost more than alternatives. One of the alternatives is an IR laser sensor[8]. They have a shorter range, but weigh less and are cheaper. As a reference, the Sharp GP2Y0A60SZLF Analog Distance Sensor[9] is used. Its general specifications can be found in Table 11.2.

Table 11.2: Main specifications IR proximity sensor

Specification	Value
Price [€]	10.70
Weight [kg]	0.0025
Operating voltage [V]	5
Range [m]	0.1-1.5
Sampling rate [Hz]	60

The shorter range of 1.5m is still sufficient for collision avoidance and with the smaller weight and lower price, more of them can be placed so there will be sufficient redundancy. The disadvantage of this kind of sensor is that their field of view is just a straight line compared to an angle like sonar sensors have. Since the UAV will be moving, and multiple of them will be placed strategically, this will not impose a problem. Even if one of them would fail, the other sensors would still be able to detect the approaching object in time for the UAV to react to it. Only if two sensors next to each other were to fail the dead corner becomes too large to still guarantee safety. Therefore, if this is the case, it is advised to abort the mission immediately. The layout of the proximity sensors is portrayed in Figure 11.2. The sensors work on 5V input and can therefore be plugged into a 5V power rail, fulfilling the target on that matter. Also, they add to Requirement **[FD-NAV-2]**. The sensors are also a backup in case the 3D sensors fail or appear to give false readings. With just the proximity sensors and the IMU of the system, the UAV would still be able to land without colliding with anything.
With an advised hover and cruise altitude of 3m, the proximity sensors will not suffice to know at what altitude the UAV is located. This might contradict with safety regulations. Therefore, sonar sensors are considered. The sensor is needed when lifting off so the UAV will hover at the right altitude. That is why a sonar sensor is needed pointing downwards where the landing gears are located. The sensor is helpful again when perching onto the aircraft. So, another one is useful pointing in the direction of the suction cups of the payload. This will also provide for extra redundancy if the 3D sensors fail, or if the proximity sensors pointing forward fail. All sensors and their ranges can be seen in Figure 11.3. As

[8]https://www.pololu.com/product/2474/specs [Accessed on 21 June 2017]
[9]https://www.pololu.com/file/0J812/gp2y0a60szxf_e.pdf [Accessed on 21 June 1017]

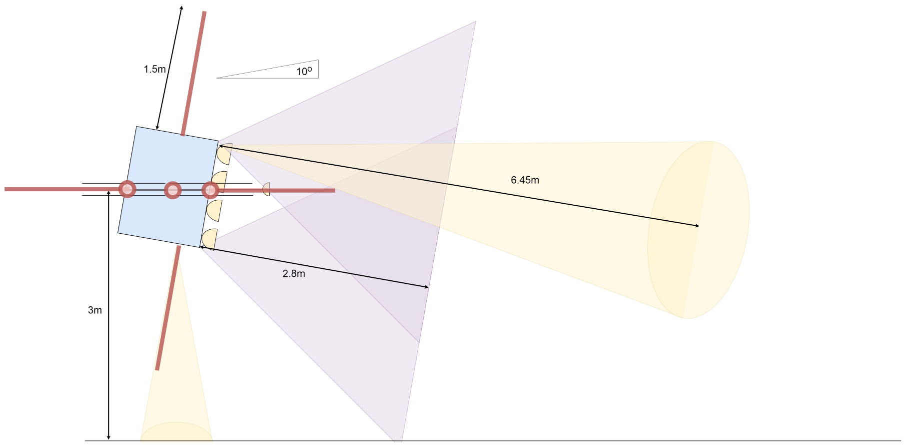

Figure 11.3: Layout sensors

a reference, the Maxbotix LV-MaxSonar-EZ2 Sonar Range Finder MB1020[10] is considered. The main specifications of this sonar sensor are given in Table 11.3.

Table 11.3: Main specifications sonar sensor

Specification	Value
Price [€]	30
Weight [kg]	0.0043
Operating voltage [V]	5
Range [m]	0.15-6.45
Sampling rate [Hz]	20

11.3. Functional Flow

With the sensors selected and the layout decided, the interaction between the navigation elements can be determined.

The elements that are used for navigation are:

- Wi-Fi
- GPS
- IMU
- 2 Sonar sensors
- 12 Proximity sensors
- 4 3D cameras

The Wi-Fi and GPS are used to get a general location determination. The Wi-Fi will be connected with the ground station. This way the UAV always has a reference to the ground station. The Wi-Fi connection will have to be secure against hackers. The Wi-Fi link will be used if the operator has to take over the control. Navigation will then be done by the operator. For the return to the ground station, the UAV will track back its flight path. The Wi-Fi connection can be used as backup in case the UAV stays from the flight path. This way it will have a reference location it can work with. The GPS gives the UAV its general location. Since the mission will generally be at an airport, any code containing no-fly zones should be avoided. Also the aircraft will be marked with a GPS beacon to give the UAV its general heading until the 3D cameras can map the aircraft. The Wi-Fi and GPS will exchange data with the IMU of the flight controller.

The sonar sensors will provide the flight controller with the mean distance to the surface it is pointing at so the UAV's velocity and direction can be adjusted accordingly.

The proximity sensors give input when an object gets within their range. If necessary, this triggers an evasive manoeuvre from the flight controller. An evasive manoeuvre can already be so much as coming to a full-stop and keep hovering until a collision-free flight path is calculated.

The 3D cameras will be used the most for navigational purposes. They will map their surroundings and accordingly have the flight controller calculate a flight path. This is a continuous process. Once the UAV starts mapping the aircraft, it will determine its location with respect to the aircraft from a 3D map it has of the aircraft in its database. A recognition software will be used to match what is sees with the map it has. The recognition software will also be used to recognise

[10]https://www.pololu.com/product/792 [Accessed on 19 June 2017]

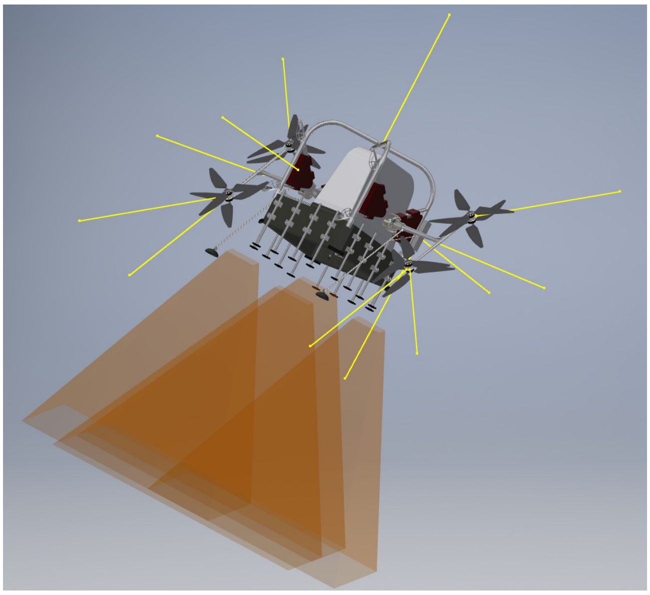

Figure 11.4: Rendering of sensor layout

the damage from the signature it has been provided with. The surface mapping will be used to calculate the angle of the surface it would be approaching. With from this calculation it is decided if the UAV can land on its own or needs the perching mechanism. If the perching mechanism is needed, it uses the angle of the surface to determine if the perching arm should be used to descend to the damage from, or to ascend to the damage from. If the surface angle is positive, the perching arm has to be placed above the damage, if the surface angle is negative it has to be placed below the damage.

Potentially, an autonomous health determination software will oversee if the sensor output makes sense. If sensor readings do not match with each other this software can manage which sensor readings are assumed to be true. More about this can be found in Section 14.1. A rendering with the sensors and their field of view is shown in Figure 11.4

12
Control & Simulation

To evaluate the flight performance of the UAV, a model describing the flight dynamics of the UAV will be used. In this chapter, the creation, usage and results of the model will be described. In 12.1, the simulation method will be described. In 12.2, the results will be detailed, and in 12.3

12.1. Simulation Setup

In this section, the simulation setup will be described. In Section 12.1.1, the model and the assumptions made will be described. In Section 12.1.2, the coordinate system and reference frame will be explained. In Section 12.1.3, the forces acting on the model will be described, in Section 12.1.4, the equations of motion will be derived, and in Section 12.1.5, the control system that will control the inputs to the system is described.

12.1.1. Model & Assumptions

To model the flight of the UAV, a three-dimensional model could be used. However, as time and computational resources are limited, a two-dimensional model will be used. The UAV will be assumed to be in symmetric flight. As the UAV will only be dealing with a one-directional drag force, using the axis with the largest ratio of moment of inertia to propeller moment axis will result in a worst case approximation of flight performance. Drag will be modelled by assuming a constant cross section for the UAV, and taking the average drag coefficient of the milling machine, calculated by means of CFD, as the UAV's drag coefficient. The milling machine will take up the largest part of the cross section anyway, so this C_D is a good assumption. Nevertheless, these assumptions make this a very coarse model; a more detailed analysis could be made by using directional drag coefficients. Finally, the rotors are modelled as simple thrusters, as it is assumed the response is fast enough to be assumed as direct thrust control. The Earth will be assumed to be locally flat, and gravitational acceleration will be assumed to be constant. The wind speed will be assumed to be constant, and gusts are assumed to be a sinusoidal increase and decrease in wind speed over a five second period.

12.1.2. Coordinate System and Reference Frame

The coordinate system used is the standard right-handed coordinate system, with the z-axis pointing up and the rotation angle θ being positive counterclockwise. The coordinate system can be seen as part of Figure 12.1. The model is evaluated in the inertial reference frame, relative to the ground.

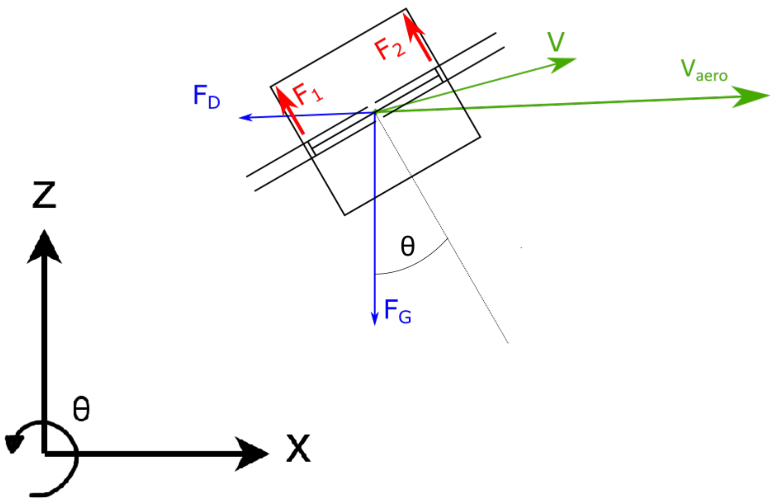

Figure 12.1: Force & moment free body diagrams of the UAV in flight

12.1.3. Forces

There are two main forces working on the UAV: drag and gravity. The gravitational acceleration is assumed to be constant at 9.81m/s^2. The drag force is assumed to act opposite to the airspeed velocity. The airspeed velocity is determined by adding the wind velocity to the velocity in the inertial reference frame relative to the ground. The drag force is then calculated using Equation 12.1, where $S_{section}$ is the cross sectional area facing the wind (assumed to be constant in this assignment), V_{air} is the UAV's airspeed velocity, ρ is the density of the air (assumed to be the standard sea-level condition of 1.225kg/m^3 here) and C_D is the drag coefficient, which is assumed to be constant here and determined by CFD, as seen in Figure 12.2 to be 2.5.

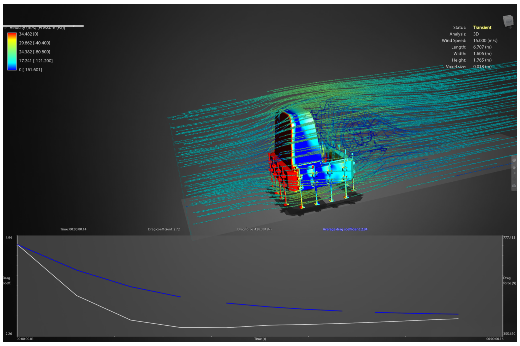

Figure 12.2: Low-speed windtunnel CFD simulation of the payload

$$F_D = \frac{1}{2} C_D \rho V_{air}^2 S_{section} \tag{12.1}$$

12.1.4. Equations of Motion

Using the forces described and placing them in the inertial reference frame, a diagram can be created from which the equations of motion can be derived. The diagram can be seen in Figure 12.1. The equations of motion for the system can then be described as the system of equations seen in Equation 12.2. These equations are nonlinear, and can therefore not be transformed into a state-space matrix form. However, linearizing the model would introduce large errors, due to the large angles required in some manoeuvres - most notably the perching emergency recovery manoeuvre. Therefore, the derivative vector is calculated by substituting the state vector's elements into each equation, as opposed to multiplying the state vector with a state space matrix. As no eigenvalue analysis will be performed, and the system is merely intended to give an indication of flight performance, this will not negatively affect the results.

$$\ddot{x} = -\frac{(F_{back} + F_{front})\sin(\theta)}{m} - \frac{F_{x_{drag}}}{m} \tag{12.2a}$$

$$\ddot{z} = -g + \frac{(F_{back} + F_{front})\cos(\theta)}{m} + \frac{F_{z_{drag}}}{m} \tag{12.2b}$$

$$\ddot{\theta} = (F_{front} - F_{back}) d_{prop} / I_{yy} \tag{12.2c}$$

12.1.5. Control Loop

To control the system, the use of PID controllers was decided upon. This is how many commercial flight controllers operate. PID controllers operate using one single error term per controller, with their behaviour relating to the error according to Equation 12.3. In this equation, K_P, K_I and K_D are the coefficients proportional to the error, its integral and its derivative. These coefficients are tuned by increasing K_P until the system becomes unstable, then adding enough K_D so that the system becomes stable again, and adding K_I to compensate for steady state error. The integral term is clamped to a minimum and a maximum value to reduce overshoot while allowing for correction of smaller steady state errors.

$$u(t) = K_P e(t) + K_I \int e(t) dt + K_D \frac{d}{dt} y(t) \tag{12.3}$$

To control the model, several of these controllers are layered: at the lower level, a PID controller controls the difference in thrust of the propellers based on the angular velocity of the UAV. A controller above that sets the target angular velocity based on the desired angle. A velocity controller sets the desired angle, based on the difference between current and target velocity relative to ground. At the top level, this target velocity is set by the position controller, making sure to limit it to the maximum velocity of 5km/h as defined in the system requirements. Seperately, a vertical velocity controller is used to control the combined thrust of the propellers, and a vertical position controller sets the target velocity for the velocity

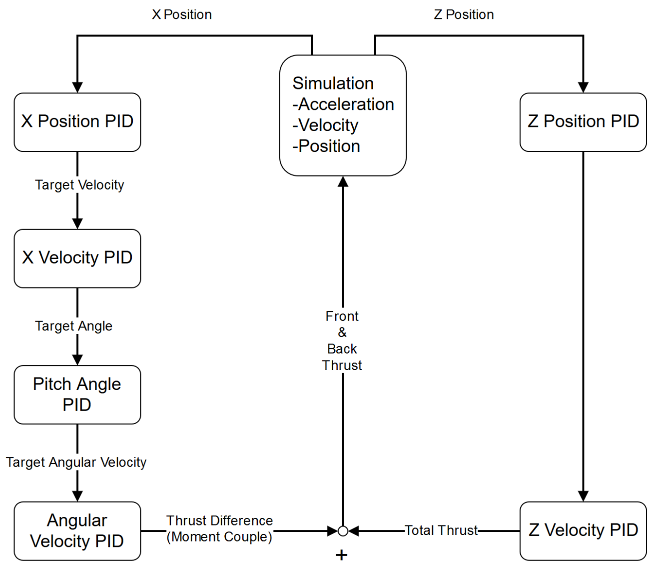

Figure 12.3: Architecture of the PID control loop

controller, which is also limited to the 5km/h speed limit requirement. The architecture of this control system is shown in Figure 12.3.

The parameters of the PID controllers are tuned from the bottom up, layer by layer. Each layer is given a step input for the tuning. First, K_P is increased until the system becomes unstable. Then, K_D is increased to make the system more stable while still ensuring a quick response. K_I is then increased to remove any steady-state error. The integral term is implemented as an accumulator. This integral term is clamped to a minimum and maximum value, to reduce overshoot when the error is less than or greater than zero for a prolonged period of time. After one layer is tuned, the layer controlling that layer is tuned, e.g. after the x-velocity controller is tuned, the x-position controller is tuned. This allows for greater control over the step response without destabilizing the system, as the layer being changed is never controlled by another layer.

Using these two control loops, the UAV can correct for any errors in horizontal and vertical positions. By adding the coordinates of a set target position, a waypoint, to the error term of the controller, the UAV can be instructed to fly to that waypoint. This way, the flight path can be defined by the navigation subsystem using a set of waypoints.

12.2. Results

In this section, the test scenarios that are simulated and their results will be described. In Section 12.2.1, the test scenarios will be described, and in Section 12.2.2, Section 12.2.3, Section 12.2.4 and Section 12.2.5, the data obtained by simulating these scenarios will be shown and explained.

12.2.1. Test Scenarios

Several scenarios will be simulated, differing in initial conditions and wind speeds. Firstly, a standard flight in which the UAV has to traverse a horizontal distance of 50m and a vertical distance of 20m with headwind will be simulated. This case provides a good approximation of the flight time during a standard mission, as the UAV will travel almost to the edge of its operational area. Secondly, the standard thrust response range will be determined by adding random noise to the position error to simulate frequent adjustments. Then, the response to wind gusts will be determined. Finally, a worst-case recovery manoeuvre for an aborted perching manoeuvre at 90° will be analysed. The wind speeds used in the simulations were 24km/h wind speed, and 42km/h gust speed, as determined by interpolating the results from a KNMI report on Schiphol wind conditions to find the 80th percentile wind statistics [18].

12.2.2. Standard Flight

The first case that will be analysed is the standard flight. In this case, the important values are the time to destination, as well as the overshoot upon arriving at that destination. From Figures 12.4 and 12.5, it can be seen that the time taken to reach the destination is approximately 40s. Furthermore, it can be seen that the curves are linear when flying to the destination. This is because the speed is limited to 1.3m/s by the velocity controller. Dividing the distance covered by the time taken does, indeed, result in a speed of 1.3m/s along each axis.

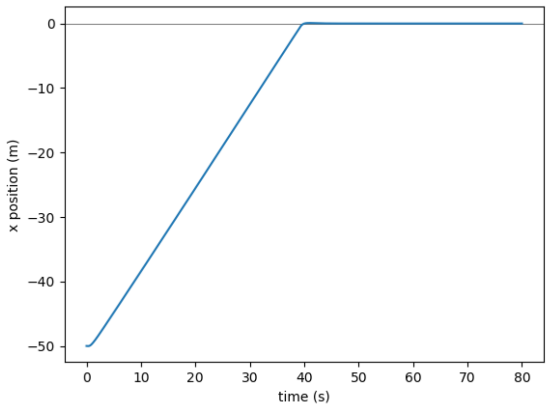

Figure 12.4: Standard flight, x position over time

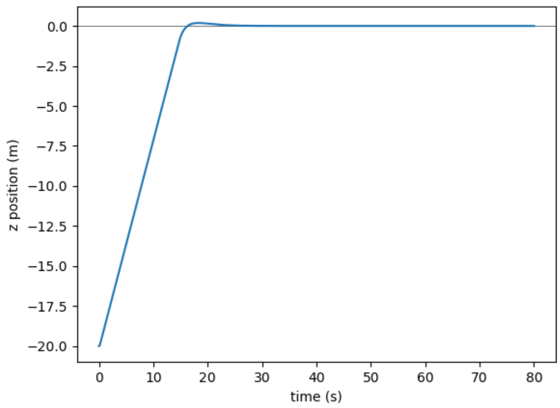

Figure 12.5: Standard flight, z position over time

To determine the overshoot, a closer look at the flight path is required. In Figures 12.6 and 12.7, the overshoot is clearly visible. There is 10cm of overshoot along the x-axis, and 20cm of overshoot along the z-axis. This means that the UAV must maintain a minimum safe distance of 20 cm to any nearby objects when navigating - to ensure safety, this will be doubled to 40cm. When moving in for attachment, the UAV will move more slowly, reducing the overshoot.

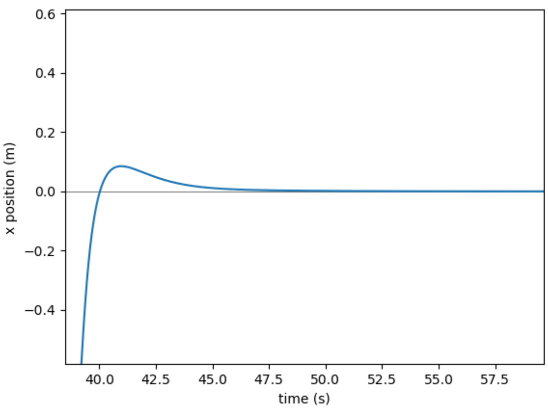

Figure 12.6: Standard flight, x position over time, zoomed in

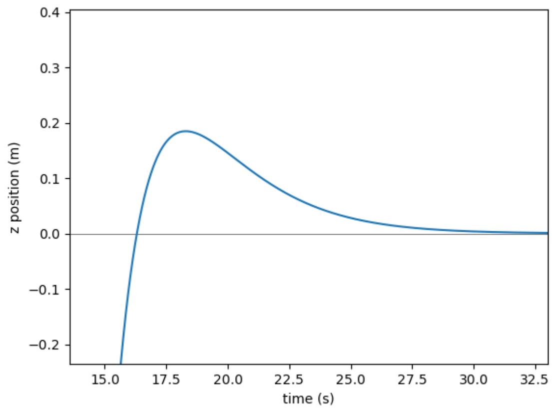

Figure 12.7: Standard flight, z position over time, zoomed in

In Figures 12.8 and 12.9, the distribution of thrust settings for a standard flight can be seen. From these histograms, it can be determined that virtually all of the time, the thrust is within 5% of the thrust in hover.

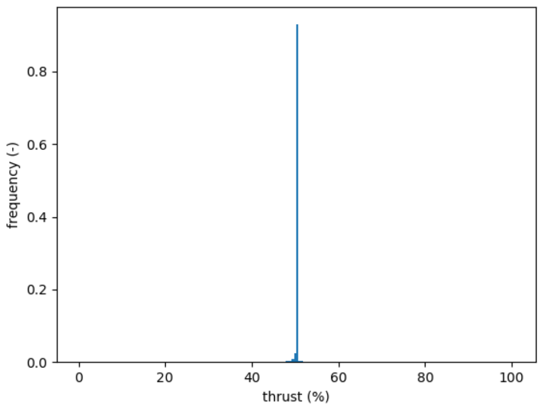

Figure 12.8: Standard flight, thrust distribution

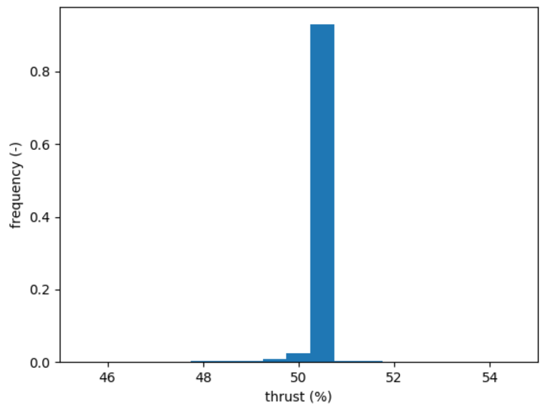

Figure 12.9: Standard flight, thrust distribution, zoomed in

12.2.3. Thrust Response

To determine the thrust response, noise is applied to the position error such that many frequent corrections are simulated. The thrusts per side are logged, and plotted in a histogram showing the frequency of occurence of thrust percentages. This plot can be seen in Figure 12.10. From this plot, it can be seen that nearly all of the thrust settings used during flight are between 40% or 60%. As the thrust required for hover is 50% of the total available thrust, this means the thrust per rotor is within a 20% range of the thrust in hover.

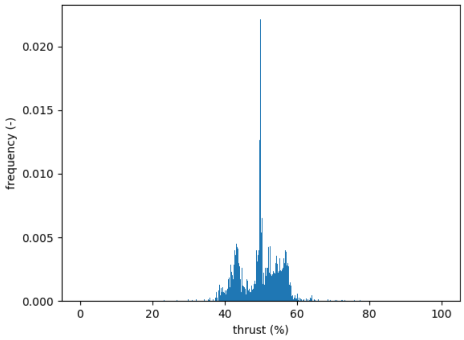

Figure 12.10: Noisy flight, thrust distribution

12.2.4. Gust Response

To determine the response to gusts, a five second gust is applied, starting at t = 10s. The UAV is in hover before the gust, with no wind, to maximise the effect. In Figure 12.11, the x-position response to the gust is displayed. There is no need to display the z-position response, as the control loop maintains a constant altitude during the gust. From the figure, it can be seen that the gust results in a deviation of 5cm, both away from the wind at first, and into the wind later. The later response is explained by the wind slowing down again as the UAV overshoots its target. This result means that the UAV must maintain at least 10cm of clearance at all times, which is acceptable.

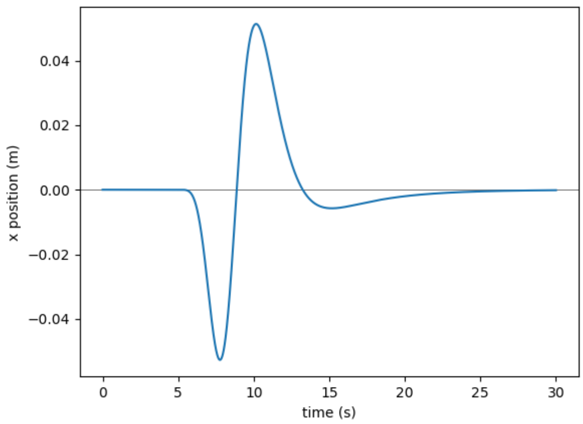

Figure 12.11: Gust response, x position

12.2.5. Perching Failure

In the event of the perching mechanism releasing, the UAV will start falling. The response to this situation is calculated by starting the UAV at 90°. Firstly, the minimum distance traversed along the x-axis is calculated. From Figure 12.12 it can be seen that the minimum distance is three meters.

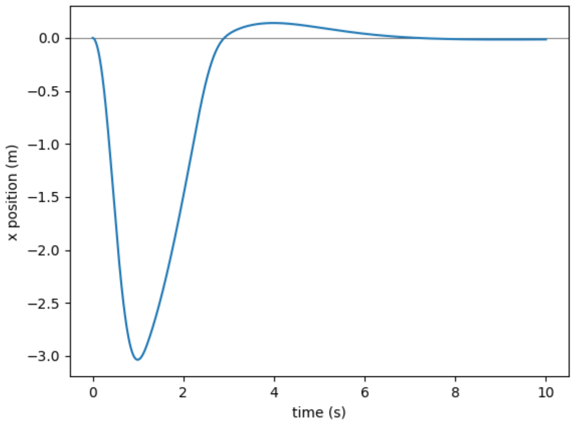

Figure 12.12: Perching release recovery swing-out along the x-axis

The minimum traversed distance is then used to set the waypoint the UAV will fly towards when perching fails. This point is set to be 3m away from the point at which the UAV is released from the surface it is perched on. The trajectory of this manoeuvre can be seen in Figures 12.13, 12.14 and 12.15. From Figure 12.14, the minimum height required to recover from the perching failure is determined to be 0.8m. This is much less than the height of the side of the aircraft; therefore, the UAV will have no problem recovering when not above the wing. When it is above the wing, care must be taken to maintain enough space for recovery.

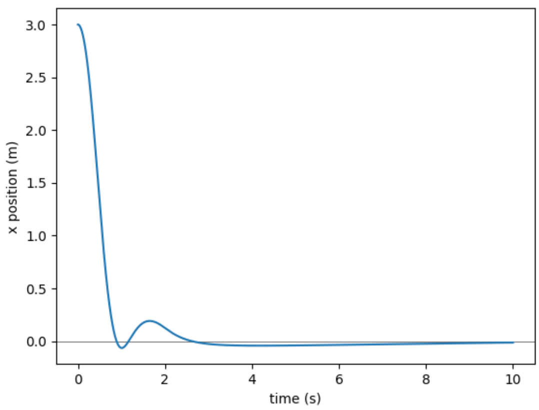

Figure 12.13: Perching release recovery movement, x-axis position over time

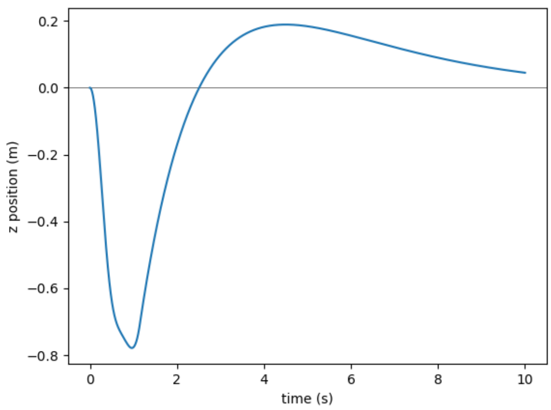

Figure 12.14: Perching release recovery movement, z-axis position over time

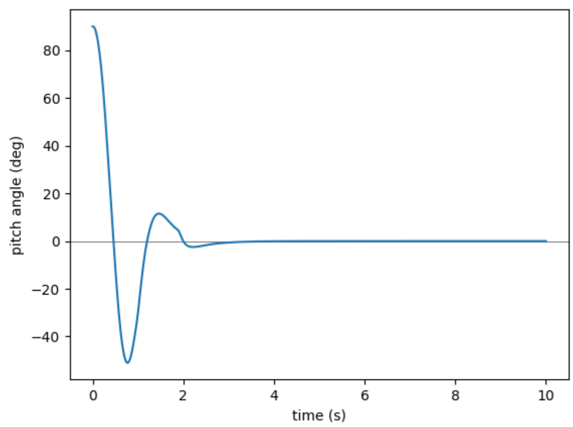

Figure 12.15: Perching release recovery movement, pitch angle over time

12.3. Control Hardware

From the results, it can be determined that even at a low update frequency of 100Hz, the UAV is capable of maintaining smooth, responsive control without oscillating too much. This means that most off-the-shelf flight controller hardware can be used to control this UAV, and it is just a matter of deciding which system will have the most functionality for operation. For this purpose, the PIXHAWK (PX4) autopilot[1] was chosen. This flight controller can be integrated easily with the Intel AeroCompute Board seen in Section 14.1 using the UART protocol. Furthermore, the controller provides enough Pulse Width Modulation (PWM) outputs to control the eight rotors, operates at a frequency of 168MHz which should be more than plenty to achieve a 100Hz update frequency, and contains a failsafe co-processor which can be used in case of main processor failure, contributing considerably to reliability. Propeller failure will be compensated for by the nature of the PID loops - if there is an error in the angle or altitude of the UAV, it will simply keep increasing the thrust to the other propellers to compensate.

[1] https://pixhawk.org/modules/pixhawk [Accessed on June 19, 2017]

13
Ground Station

In this chapter the design of the ground station is described. First, the design of the storage box is shown and the mobility is described in Section 13.1. Then, the battery charging is explained and battery chargers are picked in Section 13.2. Finally, in Section 13.3 the hardware and software needed for the ground station are described.

13.1. Storage & Mobility

It is required that the UAV is mobile and should fit in the back of a truck to transport it. Therefore a truck is first sorted out for the transport. The Mercedes-Benz Sprinter 411 CDI[1] is used as the reference truck. But of course the airliner can also use a truck they already have, as long as its dimensions are identical or higher then the reference truck. The dimensions of the truck are depicted in Figure 13.1. Using a truck makes sure that the Flying Doctor is arriving quickly at the destination.

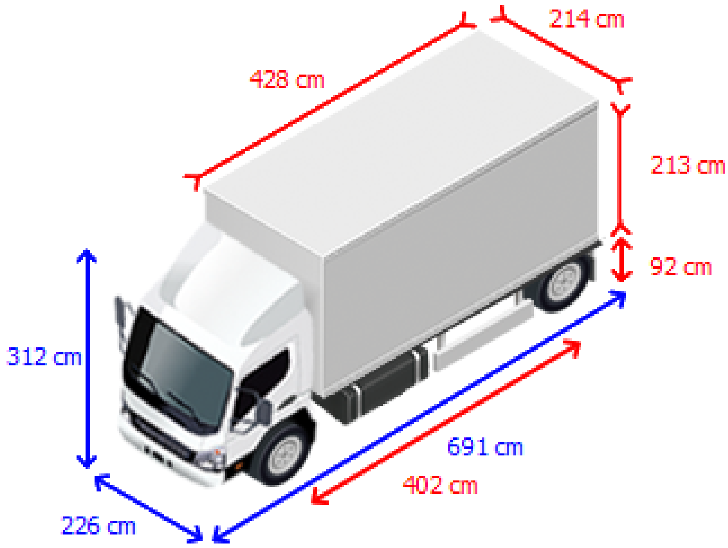

Figure 13.1: Dimensions of Mercedes-Benz Sprinter 411 CDI[1]

The design for the storage box is presented in Figure 13.2. The box consists of six sheets. There is a storage compartment considered for the arms and the perching arms. But the design should be space efficient and with the navigation system in mind, the storage compartment is unfeasible. The arms will be attached on the walls of the box. The dimensions are 275(width)x230(depth)x185(height)cm and the wheels are 19.5cm high. The total weight of the storage station is 81kg. The storage box is designed in such a way that it is easy to store and move the system. Four wheels are attached on the bottom to make it roll over flat surfaces. Also, the sheets are connected with two hinge locks per rib. In this way the sheets can be folded open. On the walls there are eight tube clamps for the arms attached, properly sized for the dimensions of these arms, are attached on the wall. This is for storing the arms. For storing and moving the UAV some clamping straps will be placed on the floor. For every leg to straps needs to be tightened. A representation of the system landed is shown in Figure 13.3. It is important that the navigation sensors are always pointing to a wall which is unfolded, since navigation requires a reference surface.

The truck (or hangar, when the airliner does not want to have the truck as a ground station) will be equipped with the battery charger with cooling system, a router, a desk, a chair, power plugs and a cupboard-like storage for batteries,

[1]https://kleynvans.nl/truck/detail/247291/mercedes-benz-sprinter-411-cdi/ [Accessed 13 June 2017]

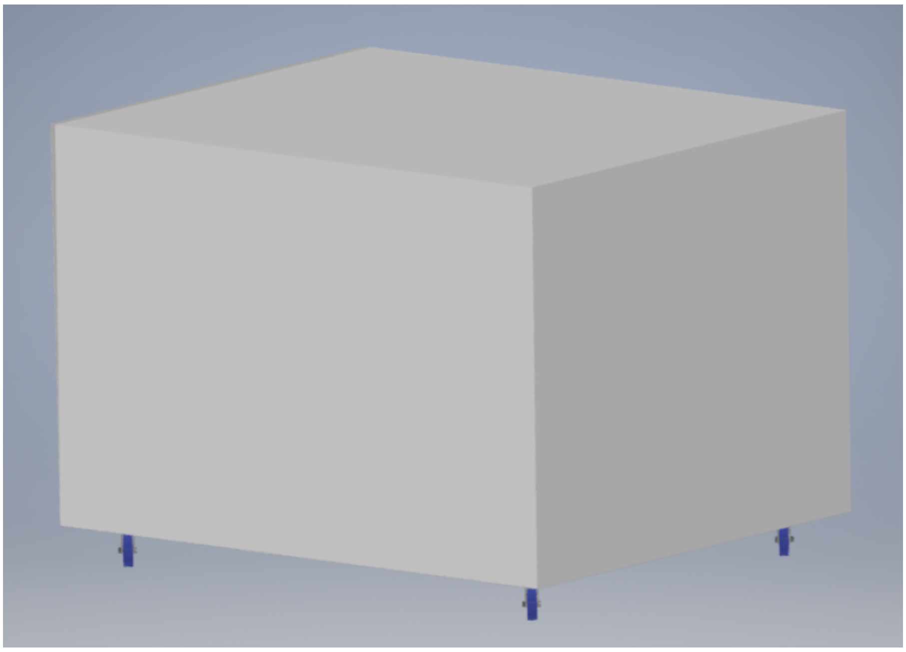

Figure 13.2: Design of the folded storage box

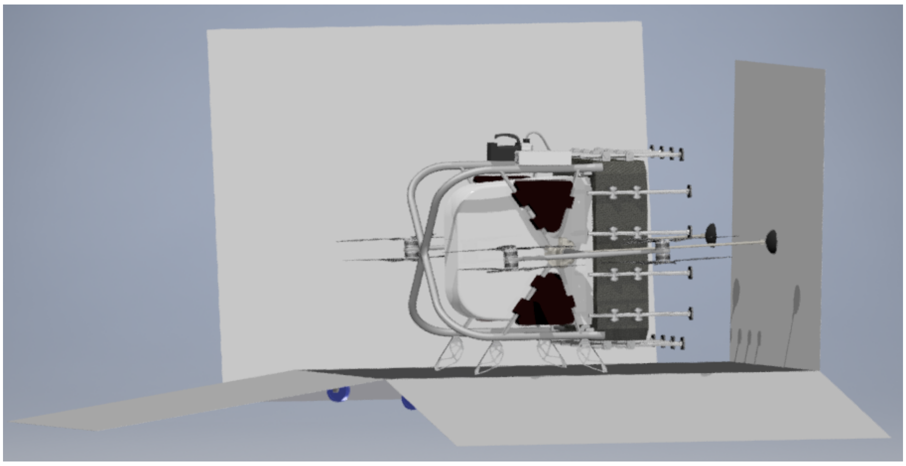

Figure 13.3: Representation of the grounded Flying Doctor on the storage box

communication hardware, a laptop and spare parts of the UAV. The furniture should be properly attached to the walls and floor of the truck and resist the movement of the truck. Therefore the furniture usually used for ships will be used. The power needed will be taken from power sources available on the airport. During transport it is not possible to charge the batteries, since charging the batteries requires too much power.

The actions which needs to be undertaken and the time required to perform the action is displayed in Table 13.1. It can be seen that the time required from the moment the truck arrives at the location till the UAV takes off is less than 6 minutes. Landing till departure also takes less than 6 minutes.

13.2. Battery Charging

Charging lithium batteries brings a lot of risks. Batteries can explode or catch fire. Also, batteries need to be monitored constantly in order to ensure their performance and reliability. Therefore a battery charger integrated circuit (IC) is needed. Because Li-S batteries are not yet commercially available, also no battery charger ICs are available for these kind of batteries. Therefore the specifications needed are described. As can be seen in Figure 13.4, the most efficient charging and discharging for Li-ion batteries (which is comparable to Li-S batteries, according to a Li-S battery specialist) is on 1C, which means that both charging and discharging should take one hour. However, charging is leading. A discharge rate of 2C (so discharging in half an hour) does not affect the battery that much. So charging should occur at 1C and all the 26 batteries should be simultaneously charged. Finally, in order to increase the life time of the battery first it needs to be charged on constant current and later on constant voltage. For Li-ion batteries this charging scheme is shown in Figure 13.5.

Table 13.1: Actions and its time duration. PRF stands for pre-flight action, POF for post-flight action and O for outdoor.

Action no.	Action	Time required [mm:ss]	Total time [mm:ss]
	Pre-flight		
PRF1-O	The operator arrives on location.	–	00:00
PRF2-O	The operator walks from the driver's cabin to the storage compartment of the truck.	00:45	00:45
PRF3-O	The operator moves the storage box from the truck to the lifting platform.	00:20	01:05
PRF4-O	The lifting platform moves down.	00:35	01:40
PRF5	The operator moves the box to the desired location.	00:35	02:15
PRF6	The operator opens the hinge locks and unfolds the box.	00:35	02:50
PRF7	The operator attaches the arms to the payload.	00:30	03:20
PRF8	The operator attaches the perching arms on the arms.	00:30	03:50
PRF9	The operator attaches the battery on the UAV.	00:15	04:05
PRF10	The system initialises.	01:00	05:05
PRF11	The UAV takes off from the ground station.	00:35	05:40
	Post-flight		
POF1	The UAV lands on the ground station.	00:45	00:45
POF2	The system shuts down.	00:30	01:15
POF3	The operator detaches the battery from the UAV.	00:15	01:30
POF4	The operator detaches the perching arm from the arm.	00:35	02:05
POF5	The operator detaches the arm from the payload.	00:30	02:35
POF6	The operator folds the box and closes the hinge locks.	00:45	03:20
POF7-O	The operator moves the box to the lifting platform.	00:35	03:55
POF8-O	The operator moves the lifting platform up.	00:35	04:30
POF9-O	The operator stores the box in the truck.	00:20	04:50
POF10-O	The operator moves from the storage compartment to the driver's cabin.	00:45	05:35
POF11-O	The operator departs from the location	–	05:35

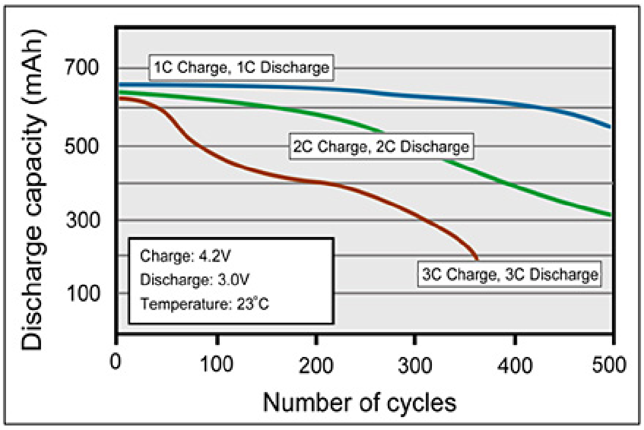

Figure 13.4: Cycle performance of Li-ion[2]

For charging the battery as quick as possible three phase power is used. The line voltage is calculated to be 398V using Equation 13.1[4], with a current supply of 32A per phase a 38.2kW power is supplied. The battery itself has a nominal voltage of 50.7V and it needs to be charged on 8237W, then the current needs to be stepped up to 162.5A. The cables have to be properly designed to handle this current.

Then the thermal control has to be taken into account. Li-ion batteries have a high charging efficiency of 99%[5]. However, assumed is that this is 95%, just to take some contingencies into account. Also, the switching regulator has an efficiency of 85%[6]. This means that the charging has an overall efficiency of 80.75%. And thus 1.6kW on heat is generated. There are coolers meant for this purpose. One of them has a thermal resistance of 16.1K/kW[7].

[2]http://batteryuniversity.com/learn/article/ultra_fast_chargers [Accessed on 15 June 2017]
[3]http://batteryuniversity.com/learn/article/charging_lithium_ion_batteries [Accessed on 15 June 2017]
[4]https://en.wikipedia.org/wiki/Three-phase_electric_power [Accessed on 16 June 2017]
[5]http://batteryuniversity.com/learn/article/comparing_the_battery_with_other_power_sources [Accessed on 16 June 2017]
[6]https://www.dimensionengineering.com/info/switching-regulators [Accessed on 16 May 2017]
[7]http://www.dau-at.com/module/downloads/download.aspx?key=DF1B51CFA9EE&LNG=en [Accessed on 16 June 2017]

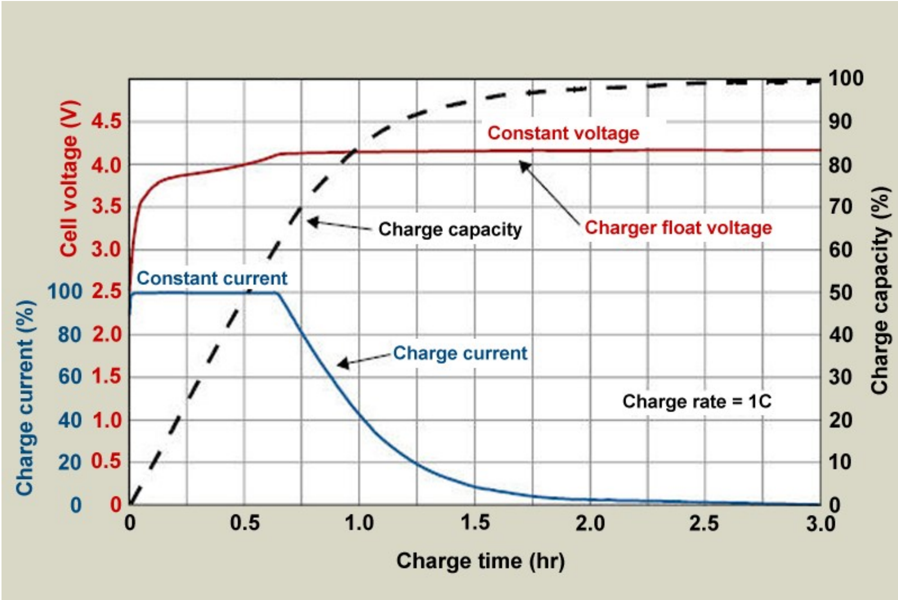

Figure 13.5: Scheme for battery charging[3]

Then the availability of the UAV is considered, as the battery charging takes one hour and the UAV's operation takes sometimes less, three batteries need to be provided. It is also sufficient for three operations per day for five years, taking battery degradation in mind.

$$V_{LL} = \sqrt{3}V_{NL} = \sqrt{3} \times 230 = 398V \tag{13.1}$$

13.3. Ground Station

The ground station is a device that bridge the data and communication link between the flying doctor and a ground-based computer. It should display real-time data on the UAV's performance.

13.3.1. Hardware

The hardware offers an interface between the maintenance engineer and the flying doctor. As the mobileBLOCK has its own dedicated ground station, the ground station is conceptualised such that it will have autonomy over the mobileBLOCK and the UAV. The ground station has to be a laptop with touch screen, running on common platform, equipped with Wifi 802.11ac such as windows with protection classification IP 52, according to MIL-STD-810G[8].

13.3.2. Software

Most of the commercially available ground stations are designed for outdoor operation with Google map API for navigation or surveillance. For the purpose of the Flying Doctor, with a flying envelope of 50x50x50m, a ground station with custom code will be created, the type of data relayed to the UAV is highlighted inFigure 14.3. The software architecture for the ground station is shown in Figure 13.6.

At the start-up of the ground station it will prompt for basic functions such as logging in to employee ID, and connecting the ground station to the flying doctor. The software are divided into four threads: log, UAV communication, UAV Flight Controller and Payload.

[8]http://everyspec.com/MIL-STD/MIL-STD-0800-0899/MIL-STD-810G_12306/ [Accessed on 20 June 2017]

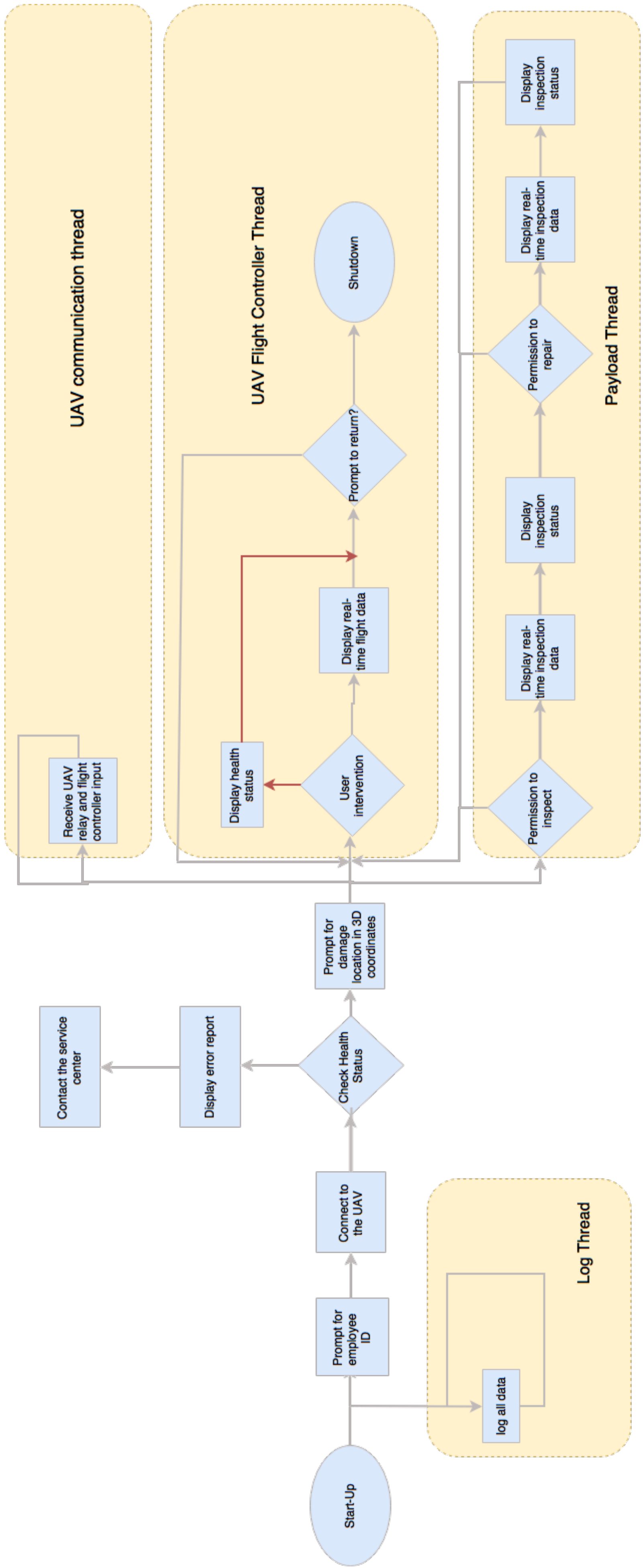

Figure 13.6: Ground station software

14 Final Design

This chapter concludes the detailed technical design of the flying doctor. The chapter starts with the system architecture of information flow, software and electrical and power electronics are described in Section 14.1. Furthermore, the general layout of the flying doctor is shown in Section 14.2. Lastly, the mass and power budget of the final design of the Flying Doctor will be addressed in Section 14.3.

14.1. Architecture

Electronics are the brain of the UAV which controls the other subsystems. Therefore understanding its architecture is key in ensuring success operation for the flying doctor.

14.1.1. Processing Hardware & Information Flow

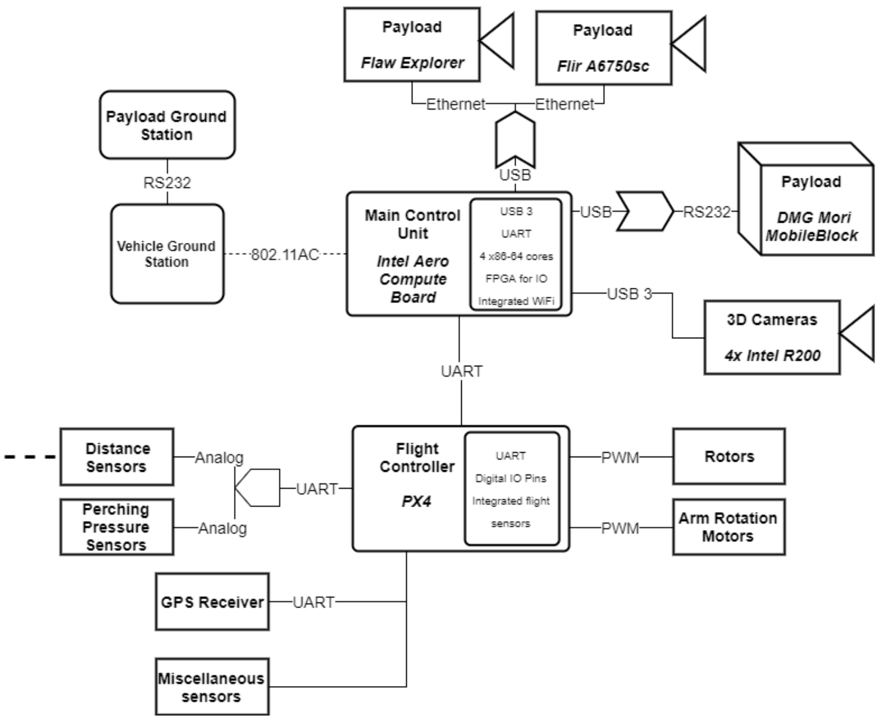

Figure 14.1: Architecture of the data collection and processing hardware. The connections between components show the communication method used to transfer data.

The processing hardware's architecture shown in Figure 14.1 has three main nodes. These are the groundstation, the main control unit (MCU) and the flight controller (FC). The aerial vehicle is physically unconnected to the groundstation, but retains a high bandwidth connection using WiFi or equivalent equipment. Onboard the UAV, there is a separation between computationally intensive tasks and the more immediate tasks related to flight and safety of the vehicle. The former are handled by the MCU while the latter is delegated to a dedicated flight controller.

The MCU has high bandwidth, easily reconfigurable interfaces that are capable of supporting the three major payloads as well as sufficient processing capacity for real-time 3D mapping which is used for navigation. It does not directly pilot the UAV, but rather provides the FC with accurate 3D position data and the required flight manoeuvres. These might be a series of waypoints or precalculated landing approaches.

The FC has simpler interfaces with lower-level protocols. It directly controls the mechanical components of the vehicle and is responsible for vehicle's stability and flight. While it does not have the processing power for advanced sensors such as the 3D cameras, it fully supports basic distance sensors for collision avoidance with response times within a few ms possible, given the main control loop operates at 1000Hz. It primarily relies on in-built sensors for flight and in case of the MCU failure, the vehicle fully retains flight and coarse navigation capabilities. This allows a fallback to safely and automatically return to the take-off area in case of an emergency. The FC itself has a high degree of redundancy built-in in terms of redundant flight sensors and co-processors. This makes FC hardware failure extremely unlikely compared to the rest of the system.

The core information transferred through the interfaces is shown in Figure 14.2. In this figure, the disparity in information complexity around the MCU and FC nodes is easier to notice. The Intel AERO compute board acting as the MCU handles a variety of different data types from various devices, more variable data rates and a combination of sequential and highly parallel processing tasks. The FC node is much more stable in terms of data flow with fewer and more constant data rate inputs.

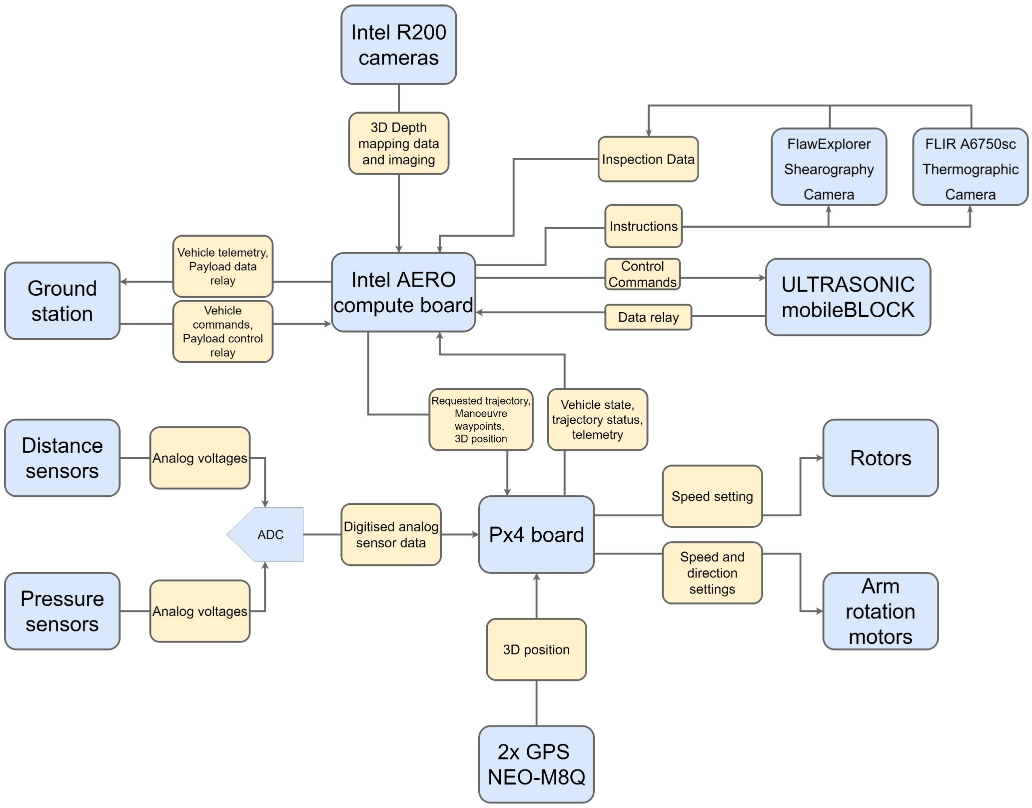

Figure 14.2: Information flow within the architecture

14.1.2. Software

A high level framework for the software of the UAV is shown in Figure 14.3. Initially, various startup and preparation routines are executed until the vehicle is ready for flight. This involves connecting to the groundstation and actions like the startup calibration of gyroscope drift or waiting for the GPS receiver to confirm sufficient signal. After the initial startup phase, the vehicle is ready for operation. Now five different main functional threads are in execution. Out of these, four of are running on the main control unit and one on the flight controller.

Two threads are simple, handling relatively basic 'housekeeping' tasks. One simply performs live logging of the sensors, vehicle location, power usage and other similar monitors. The logged data can later be used for diagnostics, health evaluation or debugging purposes. The vehicle control thread communicates with the groundstation, receiving mission parameters, updates or other commands for the vehicle which are later passed on to other processes.

The tunnelling thread also interacts with the groundstation, but for the purpose of controlling the payload rather than the vehicle. The payloads carried by the vehicle are typically used tethered to a computer which provides the user interface and is often required for functionality of the payload device. Because a physical tether to the flying vehicle is not practical, these connections would have to be to intercepted by the system and relayed over the wireless link. The aim is to provide complete transparency for the payload's communications to avoid any need for modifying the carried payload or its programming. Although represented very concisely in the diagram, the implementation of this functionality would vary greatly based on the specifics of the intercepted protocol. Protocol translation, data compression, hardware emulation, buffers, etc. may or may not be needed depending on the bandwidth, latency or other requirements imposed by the connected device. In case hardware emulation is required, the chosen MCU already has a user configurable FPGA integrated in its design.

The navigation thread focuses on 3D mapping and pathing. It reads the input from 3D cameras and processes it in order to build a map of the surrounding environment. It also performs object recognition, mostly aimed towards locating the repair target, such as the aircraft the vehicle is meant to repair. This process then generates a mission trajectory and converts it into a set of instructions for the flight controller to follow.

Finally, the flight controller thread is running essentially standard flight controller code. With only minor changes to adapt it for awareness of the rotating frame design, the Pixhawk flight controller is already capable of executing autonomous missions comprised of a scripted sequence of waypoints or actions. This sequence of instructions would be provided by the navigation thread on the MCU.

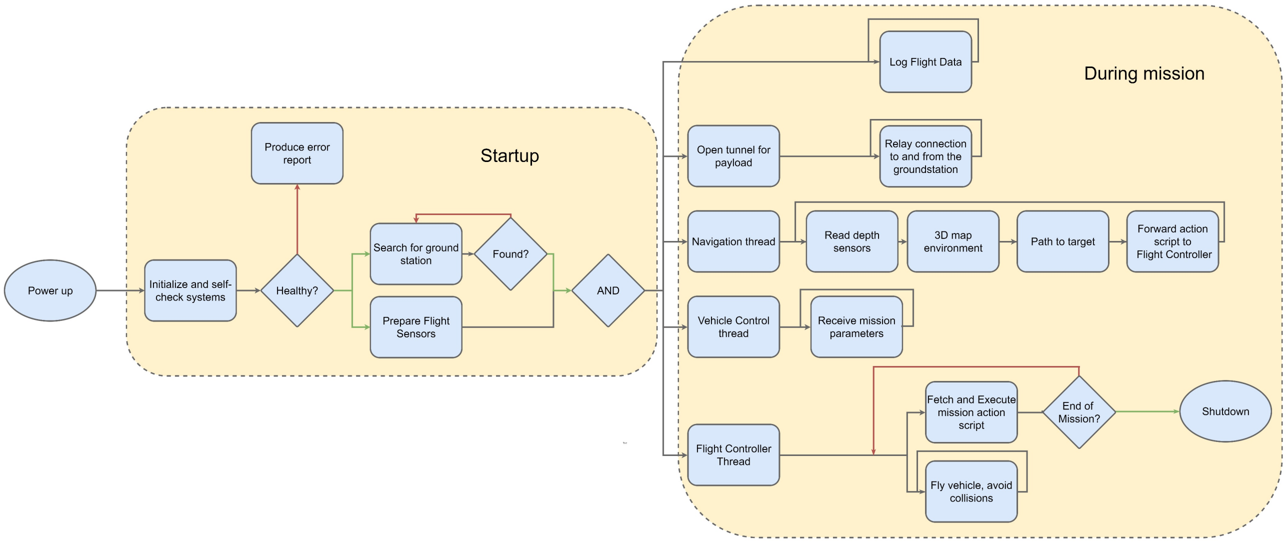

Figure 14.3: High level software flow diagram

14.2. General Layout

The previously designed structural components were assembled into the full model with mock models for mechanical and electrical components is shown in Figure 14.4. This model shows how the components are integrated. The rotors are mounted to the available mount plates on the arms, the whole rotation mechanism assembly is present and functional. The large triangular containers mounted within the payload frame are the the designated electronics boxes. Batteries and most of the electronic components are integrated into these units. Large auxiliary components such as the power supply of the payload and the vacuum pump and externally mounted to the payload frame on the upper side of the vehicle. The bottom side is dedicated for the landing gear and ground clearance. The vehicle flies 'mouth open', with the payload nominally tilted on its side as this allows navigation sensors to face in the flight direction.

The system was built for easy partial disassembly for storage and transportation. The removable rotor arms, foldable rotors and collapsible perching arms are shown in Figure 14.5. To keep storage simple and deploy times short, the structure can be quickly partially disassembled. While the maximum size requirement is not meant without further removing propellers from the rotors, this still greatly reduces the footprint of the vehicle.

Finally, Figure 14.6 shows vehicle perched on a vertical surface. The fully articulate model can be easily manipulated to verify correct clearances between the rotor, perching arms and the payload extremities. The rotor arms rotate together with the perching arms, allowing to tilt the rotors for clearance near steeply angles surfaces. The forward facing sensors are always kept pointed towards the target landing surface for optimal precision.

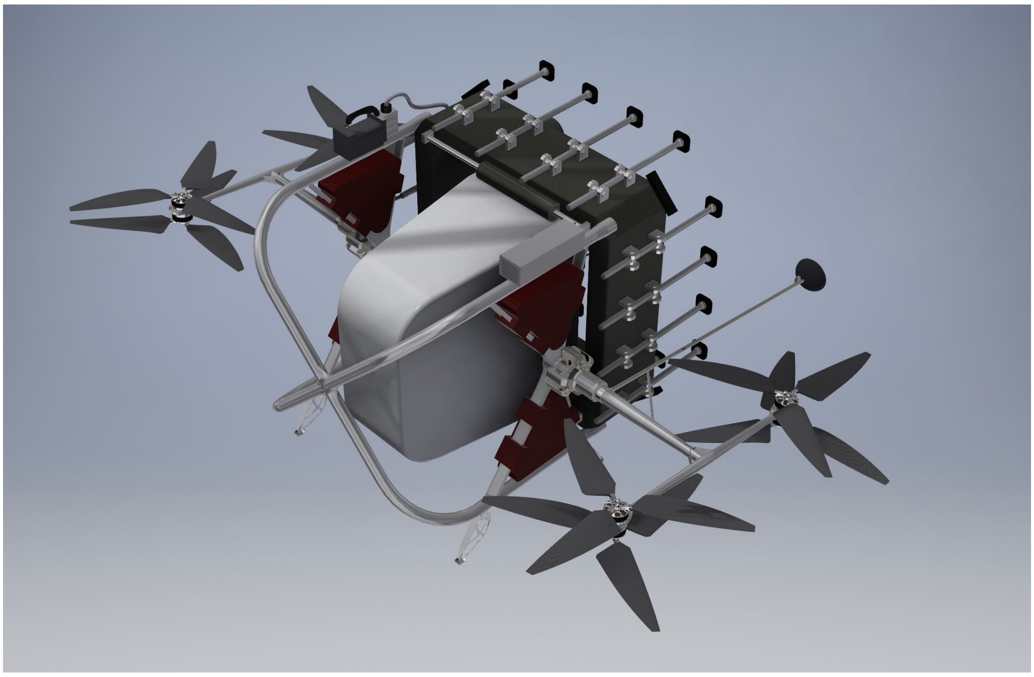

Figure 14.4: CAD model of the complete vehicle assembly in its typical landed or cruise flight configuration

14.3. Mass & Power Budget

The Flying Doctor's design point mass has been determined initially to be 151kg with contingency mass of 23kg. Table 14.1 shows the breakdown of the mass budget for the Flying Doctor's final design. The battery mass has been revised to 22.88kg, which includes its shell. The flying doctor's dry weight has met the requirement **OP-5**, to be under 20kg. The contingency mass, which is meant to cater for unforeseen subsystems, has been taken by the payload frame and payload miscellaneous of 20.15kg. In another word, it can be effectively said that the flying doctors flies at 146.4kg with 105.15kg payload. With comparison to the 151kg design point, the flying doctor is able to carry extra weight of 4.6kg.

Table 14.2 highlights the breakdown of the payload miscellaneous. On top of the masses contributed for the supplementary components for the flying doctor's application, payload frame, which has been specially designed for the mobileBLOCK, has been included. It can be observed that the half of the weight consists of the NDT. As it has been mentioned in Section 6.3.3

Table 14.1: Mass budget of the Flying Doctor for the final design

Components	Weight [kg]
Flying Doctor dry mass	18.37
Li-S battery mass	22.88
ULTRASONIC mobileBLOCK	85
Payload miscelleanous	20.15
Complete Flying Doctor mass	**146.4**

Table 14.2: Payload miscellaneous breakdown including its respective attachment

Components	Weight [kg]
Payload frame	5.28
Vacuum pump	3.00
Inverter	3.60
IR camera	2.37
Halogen bulbs	0.10
Shearography camera	5.80
Total	**20.15**

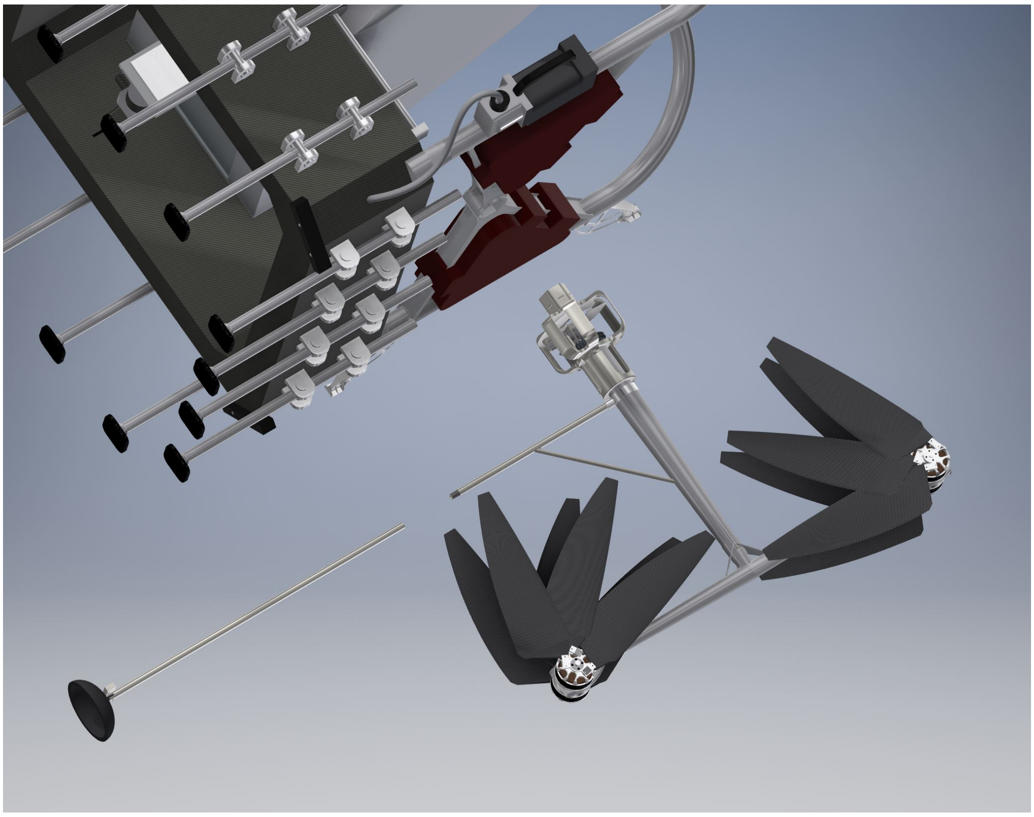

Figure 14.5: Model showing detachable arms along with collapsible rotors and perching arms. This greatly reduces the overall footprint of the vehicle, allowing much easier storage and transportation

14.3.1. Mass Budget

Table 14.3 shows the overview of the preliminary estimation performed initially [3] in comparison of the one of the finalised design. One can observe that the preliminary estimation have been performed based on the subsystem levels, while its advanced counterpart has mass estimation based on components level. Propulsion subsystem power requirements were corrected as highlighted in Section 7.4.1, which brings weight reduction from 10.9kg to 8.096kg. That reduction is compensated by payload subsystems, whose initial estimation did not consider the rotation mechanism housing. As this one of the unique feature of the flying doctor, the design received more attention in terms of its load bearing capability as well as its quick attach/detachment mechanism. In the final design, the perching subsystems explored numerous cases including high gust conditions of 40km/h in Section 9.3.2. The addition of the side bars to ensure robustness under that condition gives an excess of 0.713kg than the initial estimation. As described in Section 8.1.3, heavy optimisation of the rotor arm through tapering has reduce the estimated weight although the load analysis became more extensive. Furthermore the landing gear used topology optimisation as described in Section 8.4.1, helped in in the better weight performance than expected. In the initial design, both navigation and wiring received mass budget of 1kg each. For the former, sensors used are very lightweight and the most weight is taken by the 3D-sensors. It managed to save weight of approximately of 300g. The wiring consists of signal, electronics line and vacuum hose for the electronics and vacuum pumps respectively. The breakdown of the different type wire are shown in Table 14.4. More extensive breakdown of each wiring can be found at Appendix C.

14.3.2. Power Budget

The power budget is concocted such a way that each subsystems power consumption are taken into account in every mission stage. The mission is divided into six stages: Take Off, Flying, Perching, Inspection, Repair and Landing. The Total specified power, available power and budgeted power are given for all the six stages. The available powers were based on the maximum power consumption added with ten percent safety factor.

As it can be observed in Table 14.5, most power consumption occurs during perching, leaving

Propulsion ON State

One remark is that the propulsion's ON state is based on the average thrust used in the common manoeuvre from the thrust histogram obtained from control simulation in Chapter 12. That average thrust ranges from 20 percent more or less of the hovering value, which is converted to power consumption using Equation (14.1).

$$P = L^{1.5} \tag{14.1}$$

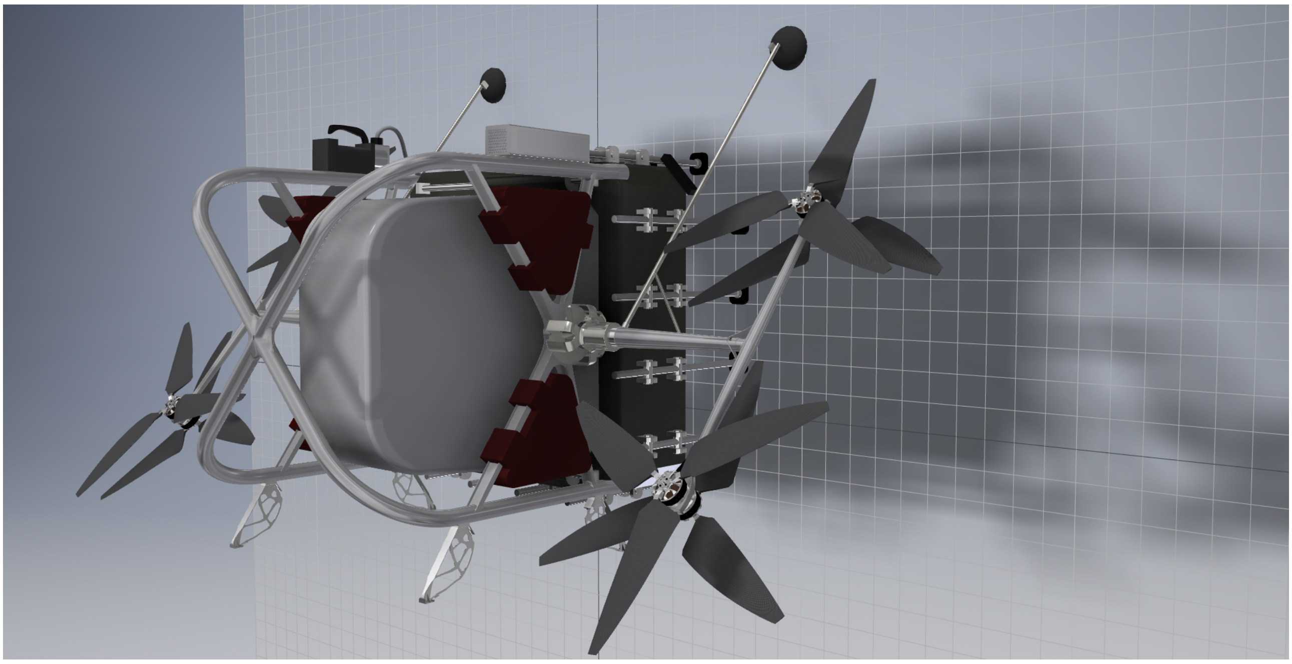

Figure 14.6: Model showing vehicle perched on a vertical surface. This shows clearances between components and the functional result of the integration.

With hovering power for 15.7kW for eight rotors, the resulting thrust that accounts for average thrust used based on the simulation is 15.9kW as shown in Table 14.5.

14.3.3. Electrical & Power Electronics

Figure 14.7 provides an overview of the electronics architecture which highlights the three voltage rails of 5V, 12V and 24V. The batteries are divided into two sides to power the components at each side, however contrary to what shown in Figure 14.7 the components block diagram constitute of the components of two sides. The voltage rails are bridged by switching regulators converting the main power supply of 60V to the respective voltages.

Dividing the batteries into two sides aids building a more efficient system and enables easier damage control if for instance, one of the batteries fails. To prevent a single point failure due to switching regulators, each rail will have two switching regulators connected in parallel.

14.3.4. Batteries

The batteries chosen for the system are lithium-sulfur (Li-S) batteries, since these batteries are lightweight, have a high specific energy of 500Wh/kg and have a sufficient power output. Li-S batteries are not commercially available yet, thus there is not much information available. Therefore lithium-ion (Li-ion) and lithium-polymer (Li-Po) batteries are used as a reference. They are assumed to have an almost equal behaviour as Li-S batteries.

Li-S batteries have a Depth of Discharge (DoD) of 100% DoD. However, 80% is the point to which the battery degrades at the battery's end-of-life. Therefore a DoD of 80% is chosen to have a lifetime of 2500 cycles in the near future[1]. Therefore for a required energy of 8237Wh, which is calculated in Table 14.5, a battery is needed with an energy capacity of 11325Wh, this is including a safety margin of 10%, since the required energy is an approximation. Now already Li-S batteries with a specific energy of 400Wh/kg are produced by OXIS Energy, a battery producer specialised in Li-S batteries. With a theoretical specific energy of 2700Wh/kg[1], it is assumed that in the near future batteries can be produced with a specific energy of 500Wh/kg. This is also confirmed by Peter-Paul Harks, specialist in Li-S batteries at Delft University of Technology. Also the volumetric energy of 450Wh/L is expected to be achievable by OXIS Energy. This gives a mass of 22.65kg and a volume of 25.17L. With a maximum output voltage of 2.33V, a nominal of 1.95V and a minimum of 1.5V[2], 4x26 cells are needed in series to provide a peak current of 60V. Each battery has then a capacity of 2060Wh. These batteries need to be divided in 26 cells. These 26 cells should have a volume of 0.24L each. This will easiliy fit in the triangulars, the room which is free is used for electronics. The weight of each battery excluding shell is 0.22kg.

Then, with a 2mm thickness for the shell and a density of 0.9g/cm^3 for acrylonitrile butadiene styrene[3], assuming cubes with ribs of 6.2cm each, the weight of the shell becomes 46.1g and thus the total weight becomes 4.8kg. This is,

[1] https://oxisenergy.com/technology/ [Accessed on 15 June 2017]
[2] http://newatlas.com/lithium-sulfur-battery-energy-density/29907/ [Accessed on 15 June 2017]
[3] https://en.wikipedia.org/wiki/Acrylonitrile_butadiene_styrene [Accessed on 15 June 2017]

Table 14.3: Mass budget of Mid-Term weight estimation against the final weight

Subsystems	Components	Preliminary Estimation [kg]	Final weight [kg]
Propulsion	Motors	10.9	5.712
	Propellers		1.76
	Speed Controllers		0.624
Payload Mount	Motor	3.0	0.26
	Gear		0.696
	Housing		3.248
	Bearing		0.44
Perching	Bar	1.0	0.233
	Side bar		0.039
	Suction cups		0.647
	Servos		0.064
Frame & Arm	Arm	2.8	2.024
Landing Gear	Landing gear	1.27	0.392
Electronics	Navigation and Flight	1.0	0.786
	Wiring	1.0	1.460
Total [kg]		20.97	18.37

Table 14.4: Different type of wire weight and distance

Type	Distance [m]	Weight [kg]
Power	35.65	0.653
Signal	33.45	0.406
Vacuum	1.5	0.3975
Total [kg]		1.460

however, worst case, when every cell is packed. But this is not necessary, only the outer sides of the battery should be shelled. It is considered that then the shell mass can be brought down to 230g using structure optimisation. The mass of the shells can still be optimized. The total weight of the batteries is then kg. The batteries will be stuffed in the bottom halves of the triangular boxes meant for electronics. It is checked and the batteries will fit in these boxes. On the top halves there will be enough room for the electronics. Inside the triangular boxes there will be a battery connector which is sufficiently strong to withstand all the battery switches the entire life time.

Finally, with the contingency mass of 3.5kg in mind, the specific energy can decrease to 315Wh/kg in order to still meet the mass requirement. This is still an energy capacity which only can be obtained by Li-S batteries. It is now considered that when Li-Po batteries are taken instead of the chosen Li-S ones, till what extent the flight time needs to be reduced. With a maximum energy density of 265Wh/kg[4] and a maximum total battery mass of 26.15kg, the flight time is reduced to 1506s. This is not meeting the requirement of 30 minutes flight time. The 500Wh/kg specific energy is according to OXIS and Peter-Paul Harks definitely possible to reach, but already 400Wh/kg Li-S batteries are made. The batteries can fall back on this specific energy.

[4]https://en.wikipedia.org/wiki/Lithium_polymer_battery [Accessed on 21 June 2017]

Table 14.5: Power budget for the Flying Doctor across the six stages

Subsystems	State	Value [W]	Take Off	Flying	Perching	Inspection	Repair	Landing
Propulsion	ON	15915	x	x	x			x
	OFF	0				x	x	
Main Control Unit	ON	10	x	x	x	x	x	x
	OFF	0						
Flight Controller	ON	5	x	x	x	x	x	x
	OFF	0						
3D sensors	ON	1.15	x	x	x	x	x	x
	OFF	0						
Collision avoidance	ON	1.98	x	x	x	x	x	x
	OFF	0						
Payload motor	ON	72			x			x
	OFF	0	x	x				
Pressure sensor	ON	0.072			x	x	x	
	OFF	0	x	x				x
Perching servo	ON	0.45			x	x	x	
	OFF	0	x	x				x
Rails	ON	0.60				x	x	
	OFF	0	x	x	x			x
60V Inverter	ON	200				x	x	
	OFF	0	x	x	x			x
Milling	ON	1000					x	
	OFF	0	x	x	x	x		x
IR-Camera	ON	50				x		
	OFF	0	x	x	x		x	x
Shearography Camera	ON	60				x		
	OFF	0	x	x	x		x	x
Halogen Bulb	ON	500				x		
	OFF	0	x	x	x		x	x
Total Specified Power [W]			15934	15934	16006	829	1219	15933
Total Available Power [W]			19598	19598	19598	19598	19598	19598
Budget Surplus Power [W]			3664	3664	3592	18769	18379	3664

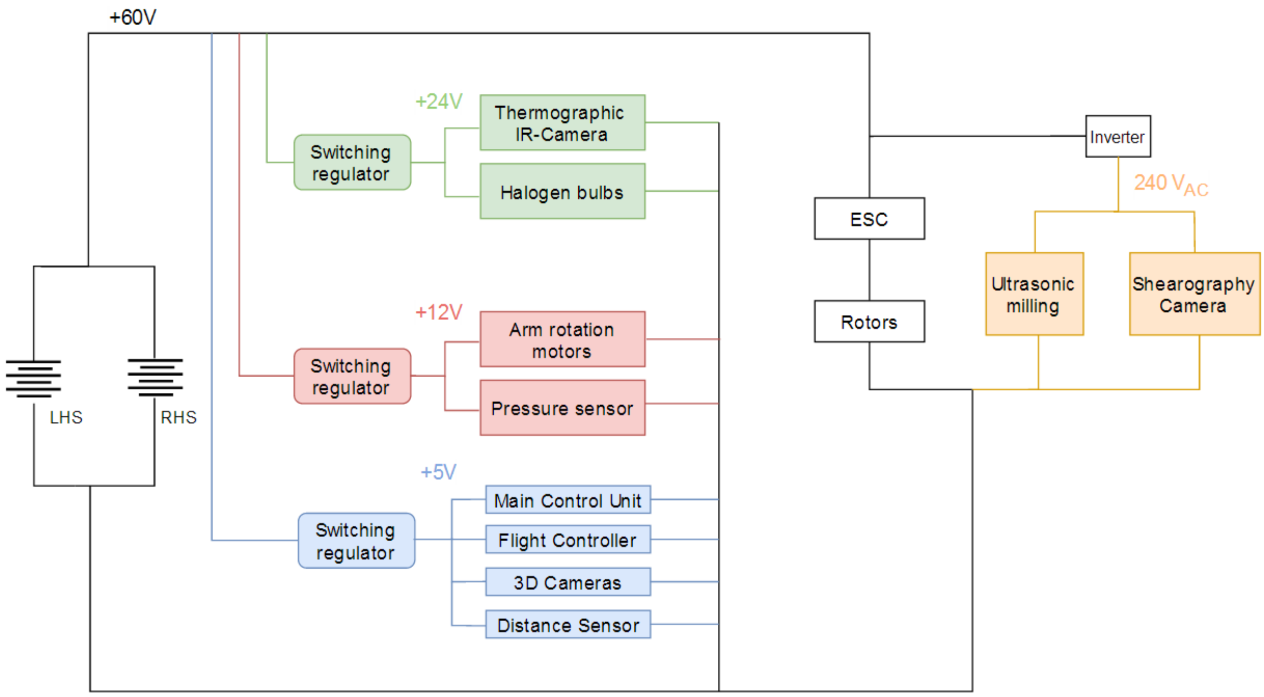

Figure 14.7: Voltage rail of the Flying Doctor

15 Manufacturing, Assembly & Integration

The UAV sector is one of the most progressive sectors in the aerospace industry at the moment. As UAVs become more attractive to the military sector and for inspection and maintenance purposes to commercial airlines, production volumes of UAVs keep growing every year. In this chapter, the capabilities of additive manufacturing (AM) technologies at this point in time are discussed in Section 15.1, followed by Section 15.2 where materials most suitable for manufacturing the UAV are presented. Furthermore, Section 15.3 determines the production method and the cost estimation of manufacturing each component of the UAV, followed by Section 15.4 which provides the manufacturing, assembly and integration plan for the UAV.

15.1. Additive Manufacturing

AM is a profitable tool for rapidly developing a new concept and testing its efficiency before it is manufactured in larger quantities. AM allows for customised production of lightweight parts and can be a cost effective manufacturing method for small batch sizes. Given requirement **[GEN-4]** which states that there shall be a positive RoI after at most ten systems sold or leased to aircraft operators, the batch size is indeed small. With this objective, a first batch of five units will be manufactured and after six months a second batch of another five will be produced. Because mass production is not the aim of this project, AM could be more cost-effective than a more conventional manufacturing technique requiring moulds.

Additive manufacturing joins materials to create 3D models and it is compatible with a large variety of materials such as plastics, metals, ceramics, glass and composites. First of all, a computer generated 3D model is created with a CAD drawing. The model is then constructed by adding material layer by layer, contrary to subtractive methods, which remove the undesired material from an initial block of material. This reduces the amount of raw material required for manufacturing. Oppositely to AM, conventional manufacturing such as computer numerical control (CNC) milling does not allow for the production of complex hollow structures, which are desirable for producing a light weight UAV structure. Moreover, conventional manufacturing would lead to a higher waste of material, making the production process less sustainable.

In the past, AM was usually not designed for strength or durability, but to test the shape or size of the design. Nonetheless, nowadays AM technologies have developed and are able to create fully functional parts. One of the main advantages of using AM is that it allows for combining complex internal structures with other geometric features such as outer shells, one of the most common structures in the aerospace field[1]. These shapes cannot be manufactured by more conventional techniques such as milling or welding. Moreover, AM reduces the necessity of stock, since the parts can be manufactured on demand.

15.1.1. Additive Manufacturing Today

AM technologies are in development, improving the quality of the parts produced and increasing the building space for the manufacturing of large structural elements[2]. At this point in time, the quality of the production of polymers by AM technology, such as stereolithography apparatus and powder bed sintering of plastic, is high. Moreover, these technologies enable the production of large sized parts. However, AM of metallic parts is currently not as developed as AM of polymers, presenting some disadvantages such as the size restriction on the parts it can produce.

15.1.2. Costs

The costs of production can be divided in "well-structured" costs and "ill-structured" costs. "Well-structured" costs include labour, material and machine costs and are the most commonly analysed. However, it is necessary to also consider "ill-structured" costs, which are related to build failure, machine setup and inventory of the parts. The advantages of AM mainly result in "ill-structured" cost savings and present key benefits for lean production. [3]

---

[1] http://www.metal-am.com/introduction-to-metal-additive-manufacturing-and-3d-printing/design-advantages-of-metal-additive-manufacturing/ [Accessed on 4 May 2017]

[2] http://www.computerweekly.com/feature/How-3D-printing-impacts-manufacturing [Accessed on 2 May 2017].

[3] http://nvlpubs.nist.gov/nistpubs/SpecialPublications/NIST.SP.1176.pdf [Accessed on 2 June 2017]

Analysing the "well-structured" costs, the two main cost drivers of AM are the build time and the energy consumption of the AM machines. AM machines are usually rented per hour and the price per hour of operation is extremely high. Given the slow printing speed of AM systems and considering the large size of the UAV, approximately one week of continuous operation of the machine would be necessary to manufacture one UAV. For at least nine more units, the cost would therefore multiply. Compared to the machine operational cost, the material and the machine operator costs are much lower. Taking into account the advantages and disadvantages of AM, a combination of conventional and non-conventional manufacturing technologies have been chosen for production of the UAVs main structure. Conventional manufacturing will be used to produce the larger volume parts with simple geometries, while AM will be used for complicated and detailed parts. By adopting these complementary technologies, the benefits will be greater than if only one of them were to be adopted. An example of the complicated and detailed parts which will be AM are the rotation mechanism frames for both arms.

15.1.3. Lean Manufacturing

Lean manufacturing aims at minimising waste. Waste not only stands for physical waste, like rework of defective parts, but also for other categories that do not add value to the product, such as transportation and inventory. For example, 14% of the annual revenue in 2011 were directed to inventory costs on average for medium and high technology manufacturing[4]. AM enables producing various parts simultaneously at the same location, which is a big advantage compared to conventional manufacturing where parts are produced at multiple locations. Using AM technologies would therefore reduce the necessity for inventory and transportation, which will further reduce expenses and increase the sustainability of both the manufacturing and logistics processes[3].

15.2. Materials

The Trinity concept shown in Figure 15.1 illustrates the interrelation between the design concept, the material of the product and the manufacturing process suitable for building the product. The production technique chosen will limit the material choice. Moreover, the strength of the structure needed for transportation of the payload and the overall UAV operation will determine the properties of the material needed, and therefore will also limit the material choice. The design concept, material and manufacturing process are linked and the outcome of one field will affect the others. Special attention will be payed to sustainability, aiming at manufacturing the UAV with a recyclable and reusable material. The

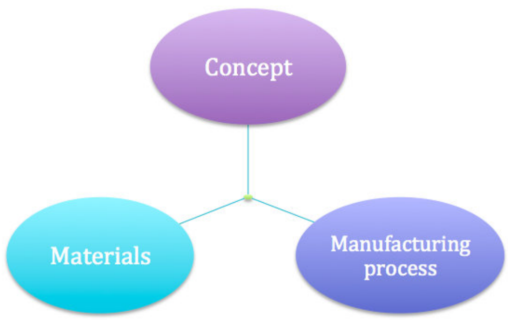

Figure 15.1: Trinity concept

scope of manufacturing technologies evaluated should first be limited by the material desired for the UAV. Requirement **[OP-5]** restricts the maximum weight of the UAV to 20kg. Moreover, requirement **[OP-4A]** states that the UAV shall be operable at least 80% of time at Schiphol airport. This operating time includes weather with wind and rain. To fulfil these requirements, the UAV shall be lightweight and durable, limiting the selected materials for its components to be resistant to the environment in and outside a hangar. With this aim, oxidation of the metallic structure of the UAV should be avoided and resistance to corrosion should be considered when selecting the material. The materials that present the qualities mentioned above are Aluminium, Titanium and Stainless steel [5]. Titanium has a high strength-to-weight ratio and is also a refractory metal, making it remarkably resistant to heat and wear, however, it has a relatively high cost. Aluminium is lighter than titanium but it is less than half as strong as the latter. Stainless steel is composed of steel and another metal aimed at improving the corrosion resistance and strength of the steel. Stainless steel presents good durability and strength. However, its high density presents a big drawback for constructing the UAV, since requirement **[OP-5]** limits the maximum weight of the UAV to 20kg.

[4]https://www.census.gov/econ/isp/sampler.php?naicscode=333&naicslevel=3 [Accessed on 2 June 2017]

[5]https://metalspecialist.continentalsteel.com/blog/bid/71587/The-Top-Lightweight-Metals-for-Aerospace [Accessed on 2 May 2017]

For the parts produced by means of AM, a new powder metal alloy called ScalmAlloy® is available for production applications[6]. Scalmalloy® is Airbus Group's second-generation alloy made of Scandium, Aluminium and Magnesium (Scalm). This alloy has been specially developed for additive manufacturing and presents exceptional high-fatigue properties. Scalmalloy® presents a high specific strength and exceptional high corrosion resistance compared to any other Aluminium alloy. This material can create an extremely light part while presenting the tensile strength of Titanium [7]. It shows excellent weldability for laser beam and friction stir welding and the welded joints have excellent properties. However, due to its recent appearance in the market, the lack of information on the cost of the material and its mechanical properties, more conventional alloys have been chosen.

By evaluating the material options stated above, the selected alloys for manufacturing most of the structural components of the UAV are made of Aluminium and Titanium. More details about the assigned material for each structural component can be found in Appendix B.

For manufacturing the propeller blades, carbon fiber has been chosen because of its high performance. Graphite composites have exceptional mechanical properties being strong, stiff, and lightweight. This is the material of choice for applications where superior performance and a lightweight structure is required. [8]

15.3. Production Methods & Cost Estimation per Component

This section presents the production method used for every component which will be manufactured. All the components except for the rotation mechanism frame will be produced by conventional manufacturing. The rotation mechanism frame will be produced by AM. A cost estimation of *off the shelf* or manufactured acquisition is determined followed by a more detailed explanation on the AM technology used and its costs.

15.3.1. Component production analysis

All structural and the main functional components are listed in Appendix B. All parts have been categorised by their acquisition, which can be *off the shelf* or *manufactured* by the company. For example the gears will be manufactured by the company being the production method simple casting and extensive machining. On the contrary, motors and batteries among other components will be obtained off the shelf. The rotation mechanism frame will be manufactured by means of AM, more specifically by Direct Metal Laser Sintering due to its high geometrical complexity. Because the propellers required for the UAV are not available in the market, they will have to be manufactured by the company. The propeller blades will be produced by conventional manufacturing, since the accuracy provided by AM is not sufficient for these parts. Note that heat treatments will be required for the parts that are welded together, such as the the arms and the frame, since welding locally weakens the material.

The table with production costs illustrated in Appendix B includes the off the shelf cost of the parts which will be bought. It also includes the cost breakdown of the components that will be manufactured such as the raw material cost per part and the cost deriving from manufacturing this part. The estimated waste material for the parts that are produced by conventional and additive manufacturing is 30% and 10% respectively of their final volume. A more detailed explanation of the estimated manufacturing cost including machine and operator for the parts produced by AM can be found in Section 15.3.2.

15.3.2. Additive Manufacturing of Complex Components

Additive manufacturing will be used to produce the complex geometry of the rotation mechanism frame. In addition to its complex geometry, the presence of several cutouts in the structure make AM the best available production method in the market. The rotation mechanism frame is made of Titanium 64, which can be obtained in the form of metal powder for AM. To determine which machine will be used to produce this part, the outer dimensions are first evaluated. The leading outer dimensions, volume and weight can be seen in Table 15.1. These dimensions limit the available machines which can be used given their building envelope size.

Table 15.1: Dimensions and weight of additive manufacturing component

Part	Units	Outer dimensions	Material	Weight p/piece	Volume p/piece
Rotation mechanism frame	2	270x190x190mm	Titanium 64	1.62kg	367cm^3

The rotation mechanism frame requires a building envelope of 270x190x190mm. Given this constraint, the machine which has been selected to produce this part is EOS M290, since it can 3D print very high quality metal parts and its building envelop allows to manufacture both the rotation mechanism frame and the landing gear. The EOS M290 uses

[6] http://www.technology-licensing.com/etl/int/en/What-we-offer/Technologies-for-licensing/Metallics-and-related-manufacturing-technologies/Scalmalloy.html

[7] http://www.zare-prototyping.eu/en/scalmalloy-exceptional-aluminium-alloy-now-available [Accessed on 2 June 2017]

[8] http://www.performancecomposites.com/about-composites-technical-info/124-designing-with-carbon-fiber.html[Accessed on 2 June 2017]

Direct Metal Laser Sintering technology, employing a fibre laser to melt and fuse metal powder. The specifications of the EOS M290 are the following [9]:

- Building envelope: 250 x 250 x 325mm
- Laser type: Yb-fiber laser, 400W
- Focus diameter: 100μm
- Power consumption: typical 3.2kW
- CAD interface: STL format. Optional, converter for all standard formats

Moreover, EOS M290 allows fast, flexible and cost-effective production of metal parts directly from the designed component parts in CAD data. The EOS M290 can process a variety of materials ranging from steels to super alloys and has an inert nitrogen or argon atmosphere [10]. It produces homogeneous part properties and the thinnest layer height of material it can print is 0.1mm.

The cost of this machine is 620.500€ including delivery, installation, training and a one-year service contract [10]. The estimated operation time of this machine for producing each rotation mechanism frame is six days. They will be machined in parallel with two separate machines, such that production time can be kept to a minimum for building the UAV. The total building volume of both rotation mechanism frames is 734cm^3. Assuming eight years of operation of the ESO M290, twenty hours per day operating and one hour of down time for cleaning and maintenance purposes of the machine, the cost of the machine is 10.6€/h. As a result, machine operating costs for twelve days plus the technician salary (estimated to be 30€/h for designing the support structure and setting up the machine) sum up to 3230€.

15.4. Manufacturing, Assembly & Integration Plan

The Manufacturing, Assembly and Integration plan determines the time sequence of the actions to be performed to build the UAV from all its individual components. Figure 15.2 illustrates the production plan starting from the raw material and manufacturing of the individual elements. Subsequently, the assembly process combines all manufactured individual parts and elements obtained off the shelf such as the batteries or propeller blades. Note that the diagram portrays the plan for the UAV, nonetheless, the ground station will require further integration with the finished UAV model.

Additionally, with the objective of eliminating waste and simplifying the workload, just in time (JIT) manufacturing philosophy will be implemented in the production plan. JIT manufacturing is defined as "a philosophy of manufacturing based on planned elimination of all waste and on continuous improvement of productivity"[11] and it can be easily incorporate in the engineering process by using Additive manufacturing technologies, allowing for adjusting production to the demand of the product.

[9] https://www.eos.info/eos-m290 [Accessed 19 June 2017.]

[10] http://www.engineering.com/DesignerEdge/DesignerEdgeArticles/ArticleID/7829/Metal-Sintering-Meets-Industrial-Needs-with-the-EOS-M-290.aspx [Accessed 19 June 2017]

[11] https://acc.dau.mil/communitybrowser.aspx?id=520801 [Accessed on 3 May 2017]

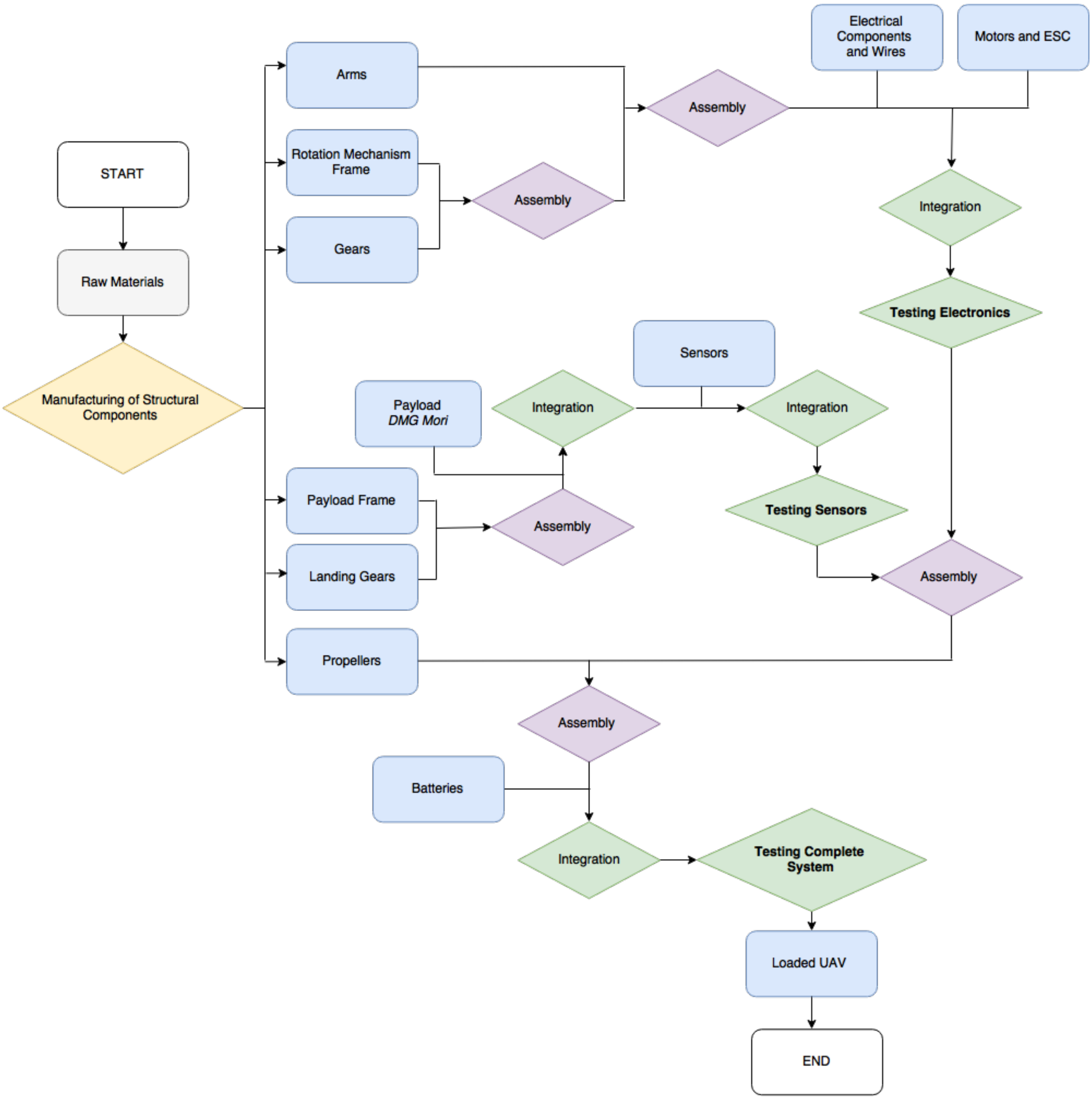

Figure 15.2: Manufacturing, assembly and integration plan of the UAV

16
Financial Analysis

This chapter discusses the financial aspects of the design. Firstly, the costs are established in Section 16.1 and with the costs three different business models are compared with each other and the RoI is determined to decide which business model is going to be used in Section 16.2. Lastly, in this chapter the market share is discussed in Section 16.3

16.1. Costs

This section presents an overview of all elements that add expense to the project. The cost breakdown structure contains all these elements and is shown in Figure 16.1. Followed by the different costs, which are divided in three different subgroups, the development costs that are presented in Section 16.1.1, the production costs in Section 16.1.2 and other costs with the maintenance and operational costs in Section 16.1.3. Since different business model will be compared in order to determine which model will be the best, a period of five years will be analysed for costs and profits.

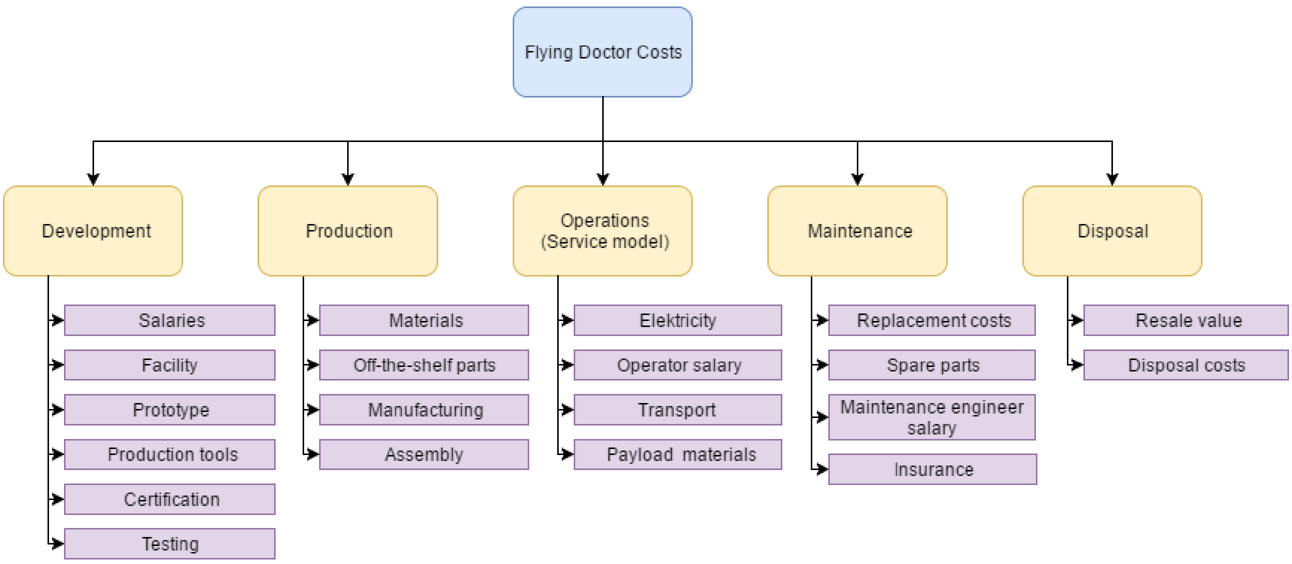

Figure 16.1: Cost breakdown structure

16.1.1. Development Costs

In the starting years of the project the development costs are the main costs. Salaries have to be paid, the location where the company is facilitated to work on the design and prototype needs to be rented. Some production tools, certifications and tests have to be considered as well. For predicting the developments costs as good as possible, it is assumed that a group of nine engineers are working full time on the design of the UAV for €50,000 a year and a facility to work on the design and prototype is rented for €6,500 a month. Furthermore, a rough estimation for the costs of the prototype, the production tools and the certification and testing is made. Table 16.1 gives an overview of the development costs for the first five years. The salaries and facility are shown for a period of five years, but they are monthly costs. The other development costs are assumed to be initial costs.

16.1.2. Production Costs

The production costs are based on the production and manufacturing of the UAV and can be divided for each subsytem in component costs. The component costs are derived from each subsystem design and are determined by selecting off-the-shelf products or material costs. The overall cost estimation for the production of one UAV including all the manufacturing costs is shown in Appendix B. In this appendix, the costs of the raw material are based on the volume that is required to make the parts. Material losses can occur in various ways, it may take the form of waste, scrap, defectives and spoilage. Since it is not possible to process the material such that no material losses will occur, an additional 10% of volume is

Table 16.1: Development costs

Type of costs	Costs [€]
Salaries	2,250,000
Facility	390,000
Prototype	150,000
Production tools	150,000
Certification and testing	100,000
Total	**3,040,000**

added for the material costs for additive manufacturing and 30% for conventional manufacturing. A smaller overview of the cost estimation for the production of one UAV is shown in Table 16.2.

Table 16.2: Production costs per UAV

Subsystem	Part	Costs [€]
Propulsion	Propeller (CFRP)	2848.00
	Motor [1]	4280
	ESC [2]	904
Rotation mechanism	Gear box	72.59
	Frame (Titanium 64)	3801.65
	Stepper driver [3]	40
	Stepper motor [4]	91.56
	Bearings [5]	77.96
Perching	Bar 1 (80 cm, Titanium 64)	97.51
	Bar 2 (40 cm + side bar, Titanium 64)	73.86
	Suction cup	160
	Detachment/Orientation servo[6]	70.12
	Sensor	26.20
Landing gear	Landing gear (Aluminium 7075)	73.64
	Rubber for on the landing gear	0.80
Ground station	Storage box	233
	Wheels	17.60
	Batteries	1441.80
	Battery charger	800
Navigation	Proximity sensors	128.16
	3D depth cameras	530.44
	Sonar Range Finders	60.00
Arms	Arms (Aluminium 6061-T6)	178.60
Payload frame	Frame (Aluminium 6061-T6)	131.20
Others	Wiring	20
Total		**16098.69**

16.1.3. Maintenance & Operational Costs

Lastly, the costs for maintenance on the UAV and the operational costs have to be taken into account. The maintenance and other costs are costs for the company, but within the sell and lease model the owning company of the UAV will have a contract for maintenance. Table 16.3 gives a rough overview for the different maintenance and other costs that every delivery of five UAVs will add to the costs. The costs are assumed to be invested when a delivery of UAVs is ready to be used.

Direct operational costs When the company is the owner of the UAVs and a service model is the business model to be used, other costs have to be taken into account. For every UAV that is stationary at an airport, two operators are needed to

[1]https://www.kdedirect.com/collections/uas-multi-rotor-brushless-motors/products/kde8218xf-120","KDE8218XF-120[Accessed on the 20 June 2017]
[2]https://www.kdedirect.com/collections/uas-multi-rotor-electronics/products/kde-uas125uvc","KDE-UAS125UVC[Accessed on the 20 June 2017]
[3]http://www.robotshop.com/en/big-easy-driver.html[Accessed on the 20 June 2017]
[4]http://www.omc-stepperonline.com/gear-ratio-641-planetary-gearbox-with-nema-8-stepper-motor-8hs150604spg64-p-310.html[Accessed on the 20 June 2017]
[5]http://www.skf.com/group/products/bearings-units-housings/ball-bearings/deep-groove-ball-bearings/deep-groove-ball-bearings/index.html?designation=61812&unit=metricUnit[Accessed on the 20 June 2017]
[6]http://www.active-robots.com/3205-0-towerpro-mg90-micro-servo[Accessed on the 20 June 2017]

Table 16.3: Maintenance and other costs

Type of costs	Costs [€]
Replacement costs & spare parts	50,000
Maintenance	10,000
Insurance	1,000
Total	**61,000**

be available for repairs 24 hours a day, a month salary of €2,700 is assumed for the operators. Besides the operator also transport, electricity and payload materials are taken into account. An overview is given in Table 16.4.

Table 16.4: Direct operational costs single UAV

Type of costs	Costs [€]
Operators salary	5,400
Transport and electricity	500
Payload materials	100
Total	**6,000**

16.2. Business Models & Return on Investment

The RoI is an efficiency measure of the investment. In order to determine the RoI Equation 16.1 is used. Using the equation the RoI can be determined at any moment. In this section the RoI is determined for the three different business models: the sell model, the lease model and the service model. As already mentioned a period of five years will be analysed for costs and profits. To make the RoI more precise, the present value (PV) is taken into account for the different costs and profits. It is assumed to use a discount rate of 5% to calculate the PV of the cash flows.

$$\text{Return on Investment} = \frac{\text{Gain from investment} - \text{total cost}}{\text{Total cost}} \tag{16.1}$$

16.2.1. Sell Model

When the UAV is going to be sold, the airliners will pay an amount of money to own the UAV. Since it is required to have a positive RoI from selling ten repair UAVs, it is assumed that after one and a half years the first five UAVs are ready to be sold and after that every half year another five UAVs will be sold. For determining the RoI within the sell model the market price for the product has to be established. Based on the price of reference manned or unmanned UAVs and the need to assure a margin on the RoI the estimation for the sell price of the UAV is €250,000. The production costs are based on the assumption that the first five UAVs are ordered after one year and the another five after every half year after that. It is assumed that the UAVs are delivered within a half year after the order is done. Furthermore, it is assumed that for an order there will be a deposit of 25% of the sell price at the moment of ordering and the other 75% is paid at the moment of delivery.

In Figure 16.2 the first five years are analysed for the sell model, as can be seen the revenue is increasing step-by-step and the positive RoI is reached after 24 months, so exactly when the first ten UAVs are delivered. The RoI at that moment is already around 34%. After every delivery the RoI is boosted but decreases a little bit until the next delivery, which is the typical trend of this business model. After five years the RoI is around 1.0.

16.2.2. Lease Model

The UAV can also be leased, in this case there is a contractual arrangement for possibly multiple years between the company and the airliner. The airliner obtains the right to use the UAV in return for monthly payments. The primary advantage for the company is the constant cash flow in contrast to the sell model when there is only during the order and the delivery of the UAV cash flow. There is also an advantage for the airliners, in stead of having the entire sell price once on their balance every month a respectively small amount of money has to be paid for the lease contract. For this model it is again assumed that after one and a half year every half year five UAVs are delivered and ready to be leased. For determining the RoI within the lease model a monthly price for leasing the product has to be established. It is again required to have a positive RoI after 10 UAVs. For determining the monthly lease price, it is aimed to have a positve RoI after one year of leasing for the second delivery of UAVs.

Figure 16.3 shows the costs and revenues for the leasing model for the first five years. With the aim to have a positive RoI after the leasing of 10 UAVs for at least a year, the RoI should be positive after 36 months. As can be seen this is reached, but the monthly lease price needed is €16,000. This seems quite high since with 15 months leasing the airliner

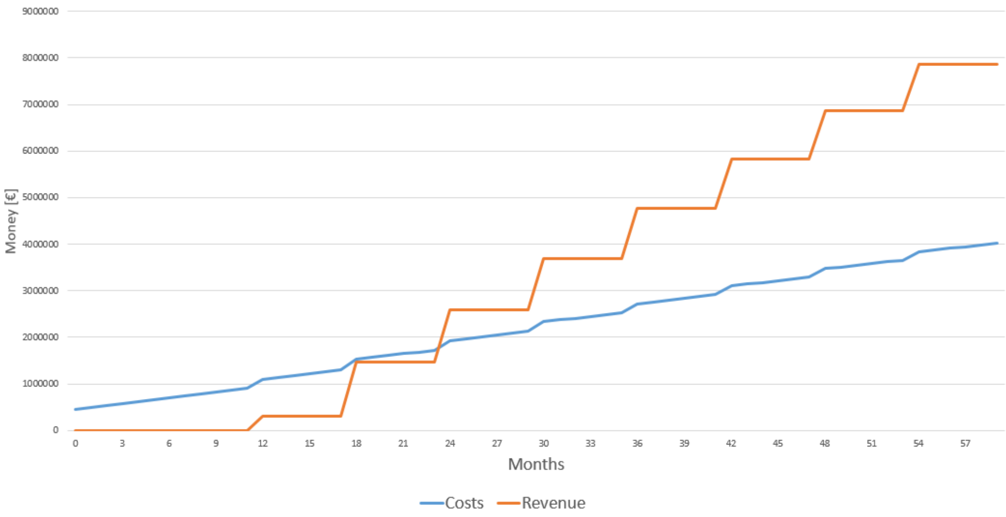

Figure 16.2: Revenues vs. costs sell model

could have bought the UAV. From the company perspective, the lease model has a late positive RoI compared to the sell model but after achieving this the revenues grow fast and the RoI after five years is around 1.8.

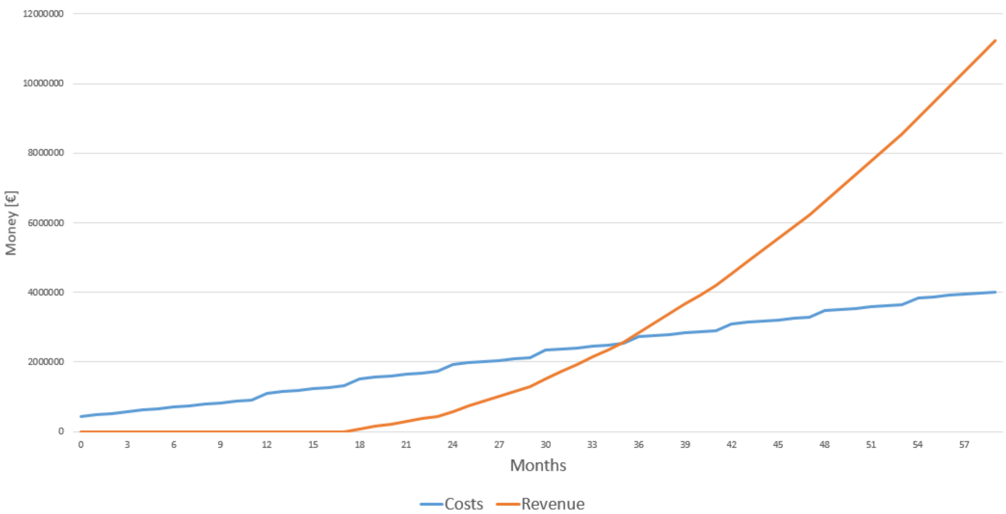

Figure 16.3: Revenues vs. costs lease model

16.2.3. Service Model

For the service model the airliners buy the UAV as a service rather than buying the UAV itself. The primary advantage for the company is that the service model provides recurring income. After the design and development phase revenues increase over time when the demand for inspection and repairs increases. The main advantage for airliners is that they do not have to buy/lease the UAV and do not have to employ and train specialised operators. The proposed concept will be that the airline receives repair and inspection services on demand. The company will be based near airports and will perform NDT inspections and repairs on the apron as well as in hangars. Airlines will then pay the company on a monthly basis, depending on the amount of repairs and inspections performed. The company can have greater profits since the UAV can be used for different airliners instead of selling or leasing a single UAV to an airliner.

In order to compare the service model with the other models it is required to determine the RoI of the service model. The additional costs for the company to perform repairs with the UAV had to be determined and the expected revenue has to be estimated. Regarding the costs, these will be similar to the previous business models. However, the company has considered the fact that it needs to be mobile to provide services at the airport and the company now has to train and employ operators to guarantee 24/7 service. As already discussed in Section 16.1.3, the operational costs are taken into account for this business model. Regarding the revenue, an estimate has to be made how much each inspection/repair operation will cost for the airline. Based on the case study in Chapter 4, the price an airliner has to pay for an inspection and repair is €602.

Figure 16.4 shows the costs for the service model versus the revenues for two different cases. The aim for the service model is to perform three repairs per day when stationary at an airport. In this case the positive RoI is achieved after 26 months, after this the revenues are extremely growing and in five years it has a RoI of 3.6. Since it is realised that the demand of repairs could be lower, it is also considered that on average only two repairs are done every day. In this case the RoI is achieved after 29 months and the RoI after five years is around 2.0.

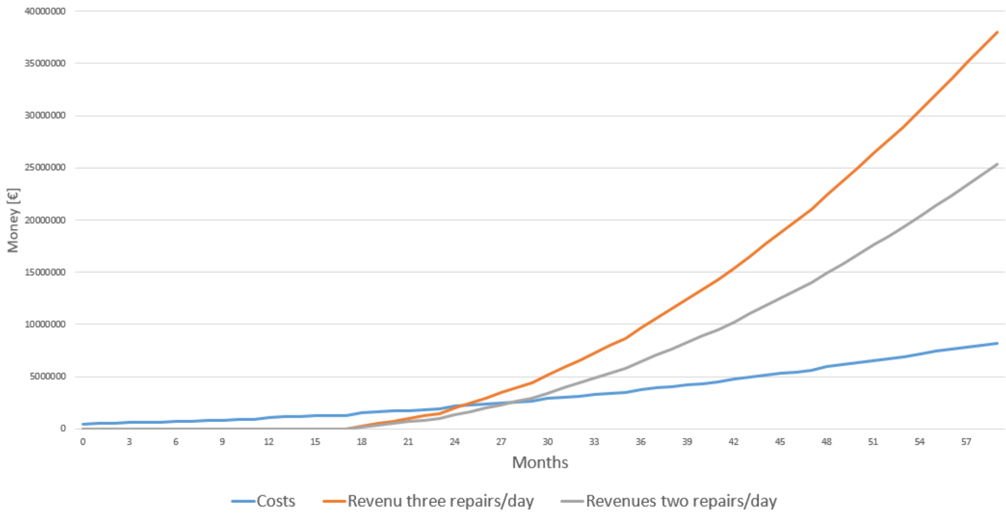

Figure 16.4: Revenues vs. costs service model

16.2.4. Conclusion on Business Models

To make an adequate decision on the different business models, the RoI of the different business models are compared at any moment in the first five years. Figure 16.5 shows the RoI for the sell model, the lease model and the service model for the two and three repairs per day. It is observed that the RoI of the sell model grows fastly within the first two years, but after that it is stagnating. The lease and the service model has no income for the first one and a half year but after that they have recurring income. For the lease model the RoI grows slowly, but it the slope increases during the five years. The service model is the winner in this comparison, fast and high profits can be made when choosing this model. It is decided to use the service model for providing services with the UAV.

Besides the beneficial RoI for the service model, from the airliners and company perspective the service model would bring a lot of advantages for both parties. As is discussed in the case study for the service model the airliner can have great benefits from the UAV with having fast repairs. For the company the service model also works like a protection of the design.

Figure 16.5: Return on Investment on different business models

16.3. Market Share

This section goes into detail about the estimated future market share. For this, the market price of the product and volume of the product are analysed. Furthermore, the most optimal business model has to be determined in order to determine the market share of the Flying Doctor UAV. Section 16.2 describes the chosen business model, which is determined to be the service model since this will yield the highest RoI. Furthermore, the recurring income will be the most profitable long term strategy.

16.3.1. Market Share Definition & Revenue Streams

The market share is defined as the value of the sales of a company as percentage of the total size of the target market. In order to determine the market share of the UAV, one has to analyse the amount of sales made in a well defined target market. Furthermore, the market size of this target market has to be determined, which is analysed in detail in Section 16.3.2. Finally, it should be noted that with the service model no UAVs are being sold. For this business model the revenue is coming from the airlines which are paying for the service. The costs are coming from the development, production and maintenance of the UAVs.

In this analysis it is assumed that the airlines pay per repair to the Flying Doctor operator company. The first production round will consist of five UAVs, each stationed at a different airport. Furthermore, it is assumed that at every airport three repairs/inspections are required per day. Now in order to determine the revenue streams, the price per repair is used as defined in Case Study 1 (See Section 4.2) and is equal to €602 for an average repair procedure. It is assumed that the first five UAVs are produced by 2019. Then every half year, five new UAVs are ready for operations at different airports. In order to determine revenue streams the following is assumed: three repairs/day/UAV. In the first half year, when five UAVs are available, this will yield fifteen repair/inspection procedures on an average day. For six months a total of $6 \cdot 30 \cdot 15 = 2700$ procedures are performed. Assuming the average price/repair of €602 the total revenue on the first half year is determined to be 2700· €602 = €1,625,400, which is equal to \$1.8 million.

16.3.2. Target Market

The main target market for the Flying Doctor are maintenance departments of airlines. This market is referred to as MRO and had an approximate global market size of \$62.1 billion in 2014 and is expected to reach a market size of \$90 billion by 2024[7].

This market analysis focuses on the main capabilities of the UAV which are NDT inspection and repair of small damages caused by air or ground incidents. These maintenance operations can be grouped in the "line maintenance" category (scheduled and unscheduled minor maintenance) which encompasses around 22% of the total MRO market as can be seen in Figure 16.6. This yields a target market size of \$13.7 billion in 2014.

[7] https://www.iata.org/whatwedo/workgroups/Documents/MCTF/AMC-Exec-Comment-FY14.pdf/ [Accessed on 3 May 2017]

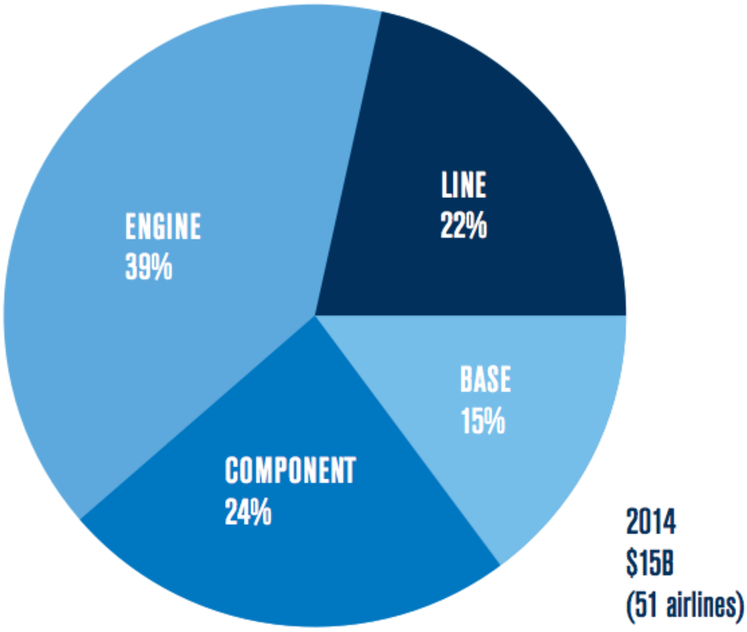

Figure 16.6: Share of line maintenance in total maintenance, repair and overhaul market[8]

Outsourced Line Maintenance

However, since the service model has been chosen, a more detailed target market can be defined, namely the "Outsourced Line Maintenance" (OLM) market. Depending on the type of airline a certain percentage of the MRO is being outsourced. Generally, four types of airlines can be defined as depicted in Section 16.3.2.

Table 16.5: Percentage of maintenance, repair and overhaul operations outsourced per airline type[9]

Type of airline	Percentage of MRO outsourced (estimated value)
Large fleet size & extensive route structure (Flag carriers)	0-5%
Limited amount of fleet types	20-25%
Limited amount of fleet types. "Critical need" philosophy	70-75%
Low cost carriers	100%

The above estimates differ greatly per airline, depending on various factors such as in-house expertise, budgets available and fluctuating MRO demands. For example, there are flag carriers which do outsource a large percentage of their maintenance. In order to get a better picture of the percentage of outsourced MRO, data from a diverse set (e.g. low cost, medium size and flag carriers) of US airlines is used in Table 16.6. This table indicates the percentage of outsourced MRO per airline between 2005 and 2007[10].

[8] https://www.iata.org/whatwedo/workgroups/Documents/MCTF/AMC-Exec-Comment-FY14.pdf

[9] https://www.researchgate.net/publication/254639079$_{G}lobal_{O}utsourcing_{o}f_{A}ircraft_{M}aintenance$

[10] https://docs.lib.purdue.edu/cgi/viewcontent.cgi?article=1039&context=jate [Accessed on 23 June 2017]

Table 16.6: Percentage of maintenance, repair and overhaul outsourced for US airlines between 2005-2007[11]

Airline	2005	2006	2007 (through Q3)
Alaska	92%	80%	81%
Hawaiian	80%	86%	89%
US Airways[a]	77%	81%	80%
Northwest	76%	83%	81%
America West[b]	76%	91%	91%
Continental	69%	68%	70%
JetBlue	68%	64%	65%
Southwest	68%	81%	85%
AirTran	66%	93%	94%
Frontier	65%	79%	80%
United	63%	66%	67%
Delta	48%	73%	72%
American	46%	49%	51%
ATA[c]	18%	85%	87%

From this dataset it can be concluded that on average the airlines spend 81.7% of their MRO expenses on outsourcing. However, it should be noted that these outsourcing percentages are for all elements involving MRO, not only the line maintenance category. The tables do however give insight in the fact that airlines are outsourcing a significant amount of the maintenance. This is another argument to validate the choice for the service model, which falls under the outsourced maintenance category.

However, to get insight in the final size of the OLM market (and not the outsourced maintenance market in general) more research is required. However, airlines generally keep data about specific maintenance spendings classified. Hence, no actual numbers are made public and only estimates are available. Table 16.7 presents the results of the level of outsourcing per maintenance category.

Table 16.7: Percentage of line maintenance outsourced (2008)[12]

Maintenance activity	*Percentage of outsourcing by cost (2008)*
Line maintenance	16
Base maintenance	53
Engine maintenance	75
Spares and rotables	77

The percentages will fluctuate over time, however for this analysis it is assumed the percentage of 16% is still valid in 2014. With this the final size of the OLM market is determined. Referring to the beginning of this section it was found that the line maintenance market is worth \$13.7 billion in 2014. From Table 16.6 it can now be determined that the OLM market size is equal to $0.16 \cdot \$13.7\text{billion} = \$2.19\text{billion}$.

16.3.3. Estimated Market Share

Now both the revenue as well as the target market size are present to determine the future market share. However, the target market size is based on the year 2014 and the sales are made in the year 2019. In order to make a correct market share estimate the market size by 2019 has to be determined. As outlined earlier in Section 16.3.2 the total MRO market will increase in value from \$62.1 billion in 2014 to \$90 billion in 2024. This yields a ten-year growth of 44.9%. Assuming this growth is equal every year one can determine the annual growth rate to be 3.8%, which yields a five-year growth rate of 20.4%. Hence the MRO market will have a market size of \$74.8 billion by 2019. Assuming the line maintenance will have an equal share (22%) in 2019 as in 2014, the line maintenance market size will be worth \$16.5 billion in 2019. Now the OLM market will be equal to 16% of this market, yielding a final target market size of \$2.64 billion. The 2019 market share *for the first half year* can now be determined making use of Equation 16.2.

[11] https://docs.lib.purdue.edu/cgi/viewcontent.cgi?article=1039&context=jate [Accessed on June 20 2017]

[12] http://www.aviationweek.com.ezproxy.libproxy.db.erau.edu/publication/om/loggedin/AvnowStoryDisplay.do?fromChannel5om&pubKey5om&channel5om&issueDat 08-01&story5xml/om_xml/2009/08/01/OM_08_01_2009_p44-151365.xml&headline5Whats+Next+For+The+Office%3F [Accessed on June 20 2017]

$$\text{Market share (2019)} = \frac{\text{sales value (2019)}}{\text{market size (2019)}} \cdot 100\% = \frac{\$1.8\text{million}}{\$2.64\text{billion}} \cdot 100\% = 0.068\% \tag{16.2}$$

Since every half year five new UAVs are added to the fleet which can operate worldwide, the market share will increase over time. Using the same calculation method as in Equation (16.2) the development of the market share until the first half year of 2022 is visualised in Figure 16.7.

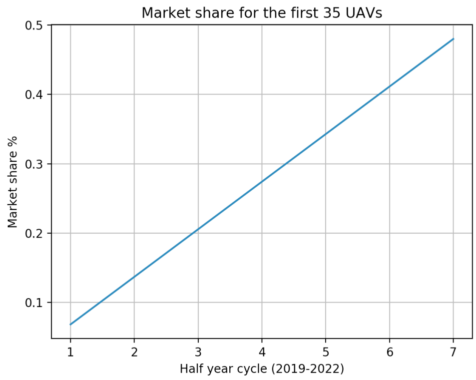

Figure 16.7: Market share 2019 to 2022

17 Design Analysis

17.1. Compliance Matrix & Feasibility

This purpose of this section is to check whether the design meets all the requirements that have been set. If a requirement is not met or some comments are needed to justify why the requirement is met a supporting text is given. Table 17.1 and 17.2 give the requirements that have to be met and their compliance.

[OP-1.5]

Assuming that the 20kg requirement is regarding the dry weight of the UAV the requirement has been fulfilled, although the entire weight of the UAV is not below the 20kg. Besides having the payload of 85kg, the payload miscellaneous parts and the batteries are not included for this requirement. The dry weight of the UAV is determined to be driving for this requirement and that is why the requirement is met.

[OP-4.1]

For this requirement it is hard to verify whether the UAV can be 80 % of the time available for outdoor operations. The problem that rainfall and other critical conditions are not simulated yet. Based on the percentage that 93% of the time the weather is dry at the Netherlands[1], the required 80% for outdoor operations should be possible. More detail on the simulation with gusts are discussed in Chapter 12.

[OP-6]

This requirement can not entirely be fulfilled since the payload has already dimensions bigger than this requirement. Nevertheless, except from the payload frame the UAV can be disassembled and fit in a 1x1x1m cube. Besides not entirely meeting this requirements it should be noticed that the idea for this requirement is the UAV to be transportable. In Chapter 13 more attention is paid to this requirement and being transportable is no problem.

[GEN-1]

For the certifications for the UAV the design needs to be further in the development process. At the moment it is not possible since a sufficient degree of maturity for the design is not reach in the process until now.

[GEN-4]

It is decided to use the service model for the UAV. The requirement is regarded to the sell or lease model. To determine if this requirement is met, the time needed for reaching a positive RoI is analysed for the different models. As is seen in Section 16.2, the positive RoI for the service model with three repairs a day is achieved at the same time as the positive RoI for the sell model. For the case only two repairs are needed on average each day, the RoI is still achieved earlier than the positive RoI for the lease model. Since the profits will also be much higher after five years, the service model meets the requirement as well.

[FD-CTRL-2]

The requirement that the system shall be handled by qualified persons is not met yet. Within the design process, also a training for operators will be developed to assure that the UAV is handled in the right way and problems can be observed directly so that critical situations are avoided. The requirement will be met in the future.

[FD-PL-3]

For the painting of one square meter area, it is not assured that the paint is included in the the UAV. Other solutions have been researched. On top of that, tape covering for the patch can be included but the mechanism to place the tape has not been decided upon, more on this in Section 6.5.

[1] http://www.buienalarm.nl/weer-feiten/hoeveel-procent-van-de-tijd-valt-er-neerslag-nederland

Table 17.1: Compliance of user requirements

Requirement	Description	Compliance
[OP-1]	The UAV shall be able to carry and place the payload.	✓
[OP-1.1]	The UAV shall be able to place the payload on any surface with a curvature of more than 2m.	✓
[OP-1.2]	The UAV shall be able to place the payload within 50x50mm of the target.	✓
[OP-1.3A]	The UAV shall securely fix to the aircraft structure during repair.	✓
[OP-1.3B]	The UAV shall not scratch or in other ways damage the aircraft surfaces.	✓
[OP-1.4]	The UAV shall be able to carry 85kg of payload.	✓
[OP-1.5]	The UAV shall be able to carry a payload of 1.3m x 1.3m x 1m.	✓
[OP-2]	The UAV shall operate autonomously after receiving operator commands.	✓
[OP-2.1]	The UAV shall allow the operator to define the repair target.	✓
[OP-2.2]	The UAV shall autonomously navigate to the target and place the payload on the target.	✓
[OP-2.3]	The UAV shall autonomously avoid collisions.	✓
[OP-2.4]	The UAV shall have a flight speed no greater than 5km/h at all times.	✓
[OP-2.5]	The flight envelope shall be at least 50x50x50m from the base station.	✓
[OP-3]	The UAV shall have a flight time of at least 30 minutes.	✓
[OP-4A]	Each UAV shall be available for outdoor operation at least 80% of the time (Schiphol airport).	-
[OP-4B]	Each UAV shall be available for indoor (hangar) operation at least 95% of the time (Schiphol airport).	✓
[OP-5]	The UAV shall have a maximum weight of at most 20kg.	✓
[OP-6]	The UAV shall fit in a 1x1x1m cube.	-
[GEN-1]	The system shall be certified for EASA and MSG-3 regulations.	-
[GEN-2]	The system shall be electrically powered.	✓
[GEN-3]	The system shall be at least 95% recyclable.	✓
[GEN-4]	There shall be a positive return on investment after at most 10 systems sold or leased to aircraft operators.	✓

17.2. Performance Sensitivity Analysis

For the design of the UAV two compromisable statements have been made. The first being the specific energy of the batteries which is described in Section 17.2.1, and the second being the coefficient of friction of the suction cups which is described in Section 17.2.2.

17.2.1. Batteries

With the contingency mass of 4.5kg in mind, the specific energy can decrease to 417Wh/kg in order to still meet the mass requirement. This is still an energy capacity which only can be obtained by Li-S batteries. It is now considered that when Li-Po batteries are taken instead of the chosen Li-S ones, till what extent the flight time needs to be reduced. With a maximum energy density of 265Wh/kg[2] and a maximum total battery mass of 25.65kg, the flight time is reduced to 1564s. This is not meeting the requirement of 30 minutes flight time. The 500Wh/kg specific energy is according to OXIS and Peter-Paul Harks definitely possible to reach, but already 400Wh/kg Li-S batteries are made. The batteries can fall back on this specific energy.

If the safety factor of 1.1 is not taken into account and the DoD is not fixed, then it is checked what amount of energy can be delivered by a commercially available Li-S battery having the mass of 22.65kg. A commercially available Li-S battery has, as already stated earlier a specific, a specific energy of 350Wh/kg. Then the energy provided will be 7928Wh. The flight time then will be reduced to 1730s with a DoD of 0%. This drastically reduces the life time of the battery. 1730s are almost 30 minutes, so practically the requirement of 30 minutes hover time is met.

17.2.2. Perching

One of the main assumptions that was made with the perching mechanism is that the coefficient of friction is equal to 0.5. This is reasonable in dry conditions between rubber and many other surfaces that aircraft are made off. However this can be decreased to 0.25 for wet surfaces[3]. This means that the required suction force will increase. Looking at the left side of Figure 9.8 for reference, Figure 17.1 visualised the new required suction force for combinations of θ and ϕ. In this figure roughly 58% of combinations of angles are still supported by the suction cup.

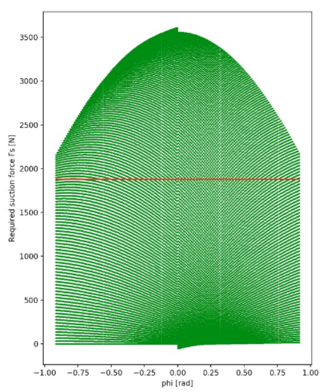

Figure 17.1: Required suction force for the suction cup with a friction coefficient of 0.25

[2] https://en.wikipedia.org/wiki/Lithium_polymer_battery [Accessed on 21 June 2017]

[3] https://www.festo.com/wiki/en/Holding_and_break-away_forces_on_suction_cups [Accessed on 21 June 2017]

Table 17.2: Compliance of mission and system requirements

Requirement	Description	Compliance
[FD-INIT-1]	Pre-flight check-up shall be done automatically.	✓
[FD-INIT-2]	The setup of the system shall be done within 10 minutes.	✓
[FD-INIT-3]	The system shall be activated by a remote.	✓
[FD-CTRL-1]	The inspection location shall be able to be manually defined by the operator at any point during operation.	✓
[FD-CTRL-2]	The system shall be handled by qualified persons (with a VCA).	-
[FD-CTRL-3]	The system shall receive and transmit instructions remotely.	✓
[FD-CTRL-3.1]	If the targeted inspection location does not lie within the flight envelope, the system shall ignore it.	✓
[FD-CTRL-3.2]	The system shall have a maximum response time of 0.5 seconds.	✓
[FD-CTRL-4]	The system shall be aware of its capabilities and limit the user to them.	✓
[FD-CTRL-5]	The system shall be remotely controllable by the operator.	✓
[FD-CTRL-6]	The system shall have a wireless communication link in both directions.	✓
[FD-CTRL-6.1]	The system shall have a communications link with a range of at least 100m.	✓
[FD-PERF-1]	The propulsion shall be redundant.	✓
[FD-PERF-2]	The propulsion system shall provide thrust to lift twice the weight of the system.	✓
[FD-PERF-4]	The system shall reach the inspection location in maximum of 15 minutes.	✓
[FD-PERF-5]	The UAV shall have position control accuracy of at least 20mm along all axes.	✓
[FD-PERF-6]	The UAV shall have a approach velocity of at least 0.5 m/s.	✓
[FD-PERF-7]	The system shall have an operational life of at least 500 flight hours.	✓
[FD-SAFE-1]	The payload shall not be damaged by the system.	✓
[FD-SAFE-2]	The system shall have warning lights.	✓
[FD-SAFE-3]	The system shall have an emergency fail button.	✓
[FD-SAFE-4]	The flight controller (FC) shall limit the UAV flight speed to 5km/h or less.	✓
[FD-NAV-1]	The system shall be able to scan the nearby surroundings in 3D for navigation.	✓
[FD-NAV-2]	The system shall be able to detect imminent collisions.	✓
[FD-NAV-3]	The system shall be able to find and track a location in 3D space.	✓
[FD-NAV-4]	The system shall be able to keep tracking the target through obstructions.	✓
[FD-NAV-5]	The system shall provide the UAV with position knowledge of within 10mm along all axes.	✓
[FD-PL-1]	The payload mount shall support its weight.	✓
[FD-PL-2]	The vibrations transferred to the payload shall be damped.	✓
[FD-PL-3]	The UAV shall carry enough paint to paint a one square meter area.	-
[FD-ATTACH-1]	The system shall attach itself to the aircraft firmly such that the accuracy of the milling machine does not become less than 1mm.	✓
[FD-DEV-1]	The system shall be designed by a team of nine engineering students.	✓
[FD-DEV-2]	The system shall be designed over the course of eleven weeks.	✓
[FD-DEV-3]	The system shall be designed with a budget of 62.50 euros for printing.	✓

18 Reliability, Availability, Maintainability and Safety Analysis

In this chapter, the reliability is firstly analysed in Section 18.1. Then the Availability of the UAV is considered in Section 18.2. Afterwards, the maintainability is discussed in Section 18.3. Finally, in Sections 18.4 and 18.5 safety measures will be discussed by means of a risk assessment.

18.1. Reliability

The reliability of the UAV determines when the system fails and whether the system is performing its operations in a correct way. Reliability determines the brand image, customer satisfaction and market position. A good reliability determines whether the company and design can sustain in the market.

Failure is primarily expected on the motors, batteries, battery connectors and suction cups. As discussed in Chapter 4 the desired lifetime should be five years. The motor is chosen to be a brushless DC motor, these motors have a life expectancy of over 10,000 hours[1]. The hover time per use is 30 minutes, this means that an airliner can use the UAV more than 10 times per day. As is described in Section 18.2, spare batteries will be delivered with the system. A Li-S battery can in the nearby future be charged and discharged approximately 2,500 times, as discussed in Section 17.2.1. Then for three uses per day for five years, three batteries need to be provided. This is the same amount for battery charging on 1C, required for the availability of the UAV. Battery connectors will deteriorate through extensive use. Replacing the batteries with a lot of attention and less power will help increasing the lifetime.

The battery connector is not expected to fail first. Suction cups will degrade or warp when they are exposed to heat and environmental factors[2]. Exposure to this should be avoided as much as possible. It is advised to protect the cups from these external forces and put the system in the storage box. Also, the suction cups and the area on the aircraft on which the suction cup is going to stick should be properly cleaned before use to prevent the decrease of the friction coefficient. When a rotor fails hazardous situations will be avoidable. If one rotor fails, the UAV stays in the air, but depending which rotor fails, the UAV will be or will not be controllable. Sometimes even two rotors can fail, but here also: it depends on which rotor will fail. The flight controller has redundant co-processors.

Also, the reliability is increased by analysing the fatigue life, performing a vibrational analysis and applying safety factors for the structural parts. Moreover, the power rail is slightly overdesigned, a few thermal considerations have been made and navigation has considered redundancy of its sensors. The flight controller has redundant co-processors, meaning that it is damage tolerant.

18.2. Availability

The availability of the UAV depends mostly on the weather conditions and the charging time of the batteries. In The Netherlands it rains 7% of the time[3]. The average wind speed on Schiphol is 21.3 km/h[4]. In February the average wind speed is 24.1km/h, which is the maximum and average wind speed and the wind speed used for the simulation of controls. The UAV can fly with these wind speeds and it can even fly in gusty winds with a maximum speed of 40km/h. This is in order to meet requirement **[OP-4A]** regarding the availability of the UAV during 80% of the weather conditions.

Charging batteries takes time. When the UAV should be deployed while the battery is still charging, the UAV is not available unless there is a spare battery. Therefore there will be three batteries provided at delivery. Then there will always be a battery charged.

For this project, one service model does not include a second UAV, unless the airline is buying more, since the expenses of a single UAV are quite high. Therefore maintenance should be performed in a short time. More on this can be found in Section 18.3.

Then for availability of the aircraft it should be noted that the paint should dry for eight hours, meaning that the aircraft should be grounded for at least this amount of time. This is completely unfeasible. Still a logistics choice should be made

[1] http://www.nmbtc.com/brushless-dc-motors/engineering/brushless_dc_motors_engineering/ [Accessed on 23 May 2017]
[2] https://www.hunker.com/12004055/the-best-way-to-make-suction-cups-stick-to-a-window [Accessed on 23 May 2017]
[3] http://www.buienalarm.nl/weer-feiten/hoeveel-procent-van-de-tijd-valt-er-neerslag-nederland [Accessed on 23 May 2017]
[4] https://nl.windfinder.com/windstatistics/amsterdam-schiphol [Accessed on 23 May 2017]

regarding this.

18.3. Maintainability

The maintainability is divided into big and small maintenance, which is preferably done at extreme weather conditions when the UAV is not able to fly. The big maintenance is basically repairing structural failures, motor replacement and more difficult operations. It is done by the company. Small maintenance consists of amongst others replacing propellers and tightening screws and it is done by the airliner itself. For maintenance the company has to make sure that the equipment needed is available. Therefore a sufficient supply of the UAV's spare parts should always be in stock. The company is responsible for this.

In order to make maintenance fast, the UAV is designed so that everything (except for the payload and its frame) is modular. This will make all the structural parts, subsystems and components interchangeable. A maintenance check is only performed after a certain amount of cycles, if there is a need for big maintenance an engineer from the company will come. This to reduce the costs and increase the availability of the UAV. After replacement the parts can be either reused or recycled.

The ground station needs to be maintained as well. Especially the software is a point of attention. It needs to be up-to-date to ensure optimal performance of the system. Software updates will be easily performed by pressing the update button. The company will notify the customer when new updates will be released.

The system will have some self diagnosis logistics. There is a redundancy of sensors, therefore, when sensors are giving incorrect information, they can be found easily and they can be replaced. For the gearing some lubricant is needed and it needs to be applied once in a while.

18.4. Technical Risk Assessment

This section gives an overview of all the technical risks that may occur in the development of the UAV. It addresses risk in three stages, pre-flight, mid-flight and post-flight. Section 18.4.1 focuses on the assessment of the risks that could potentially occur. These risks are presented in a risk map in terms of impact and probability in Section 18.4.2. Finally the risk mitigations are addressed to reduce the severity of the risks and will be presented in a new risk map in Section 18.4.3.

18.4.1. Operational Risk Assessment

The risk assessment is the identification of risks that might be present throughout the operation from the moment the UAV is handled by the maintenance engineer to the UAV completing its post inspection status. In addition the scope of this risk assessment includes the purpose of risk assessment is to identify the responsible subsystems behind the failure event and consequently dedicating more resources to mitigate the risk.

Pre-flight Risk

Inside the operating sphere, the user is an intimate part of the system. Due to this, risk due to human error will be taken into account. Pre-operation risks (PRE) refers to the risks involved during the time interval from the maintenance engineer picking up the UAV till the UAV finishes its pre-flight inspection.

PRE1 **Subassembly parts damaged** - The UAV is preconceived to be packaged inside a storage box for safe storage and portability. Some of the components will not be pre-assembled and have to be assembled by the maintenance engineer before operation. For example the arms need to be attached for the operations. The risk is present if the maintenance engineer has handled the assembling parts incorrectly. This will detrimentally affect the wear rate of the components.

PRE2 **Pre-inspection check fails** - The pre-flight check will be performed by the UAV as part of initialisation. The programmed inspection includes checks on transmitter, motor/engine, stabilisation mode, radio transmitter and voltage setting. The status of the pre-flight check is determined by the control board, which means the maintenance engineer is putting his decision to fly solely on the control board information. This poses a risk if the control board gives false positive error. Based on the specific system that gives a false positive error, the consequences of the failure can range from marginal to critical.

Mid-flight Risk

The operation focused in this subsection is in regards to taking off with the payload, performing the attachment and finally return to the ground station. This is called mid-flight and its risks involved mid-flight risks (MID).

MID1 **Propeller and power failure** - An aerial vehicle must maintain its source of power and propulsion to keep flying. The coupling between propeller and power makes both the most critical failure to the subsystems. When the payload and drone are attached to the fuselage already, the consequences can range from a required removal team to a total system failure creating highly hazardous conditions.

MID2 **Sensors failure** - In the case of sensor failure, it will cripple the UAV as 'blind', rendering it incapable of navigation. Without means of measuring its relative position, UAV will not be able to function as intended. It will also mean

Table 18.1: Technical risk map

<table>
<tr><td rowspan="4">Likelihood</td><td>Very Likely</td><td></td><td></td><td rowspan="2"></td><td rowspan="2">MID3</td></tr>
<tr><td>Likely</td><td></td><td>POS1, POS3</td></tr>
<tr><td>Unlikely</td><td></td><td>MID4, MID5
PRE1</td><td>PRE2
POS2</td><td>MID1, MID2, MID7, MID8, MID9</td></tr>
<tr><td>Very unlikely</td><td></td><td></td><td></td><td>MID6</td></tr>
<tr><td></td><td></td><td>Negligible</td><td>Marginal</td><td>Critical</td><td>Catastrophic</td></tr>
<tr><td></td><td></td><td colspan="4">Impact</td></tr>
</table>

that returning to the ground station or to the ground in general will be a challenge especially when there is an obstruction below the UAV.

MID3 **Collision** - During flight, a collision with an obstacle may occur, possibly leading to massive damage to the UAV, payload, aircraft or surroundings.

MID4 **Scratching paint** - If the attachment process is performed more roughly than acceptable, the attachment device can cause damage which results in surface scratches to the fuselage.

MID5 **Unsuccessful attachment** - The attachment process can be hard when the target location is located at a hard to reach surface (e.g. bottom/side of the fuselage). This attachment may require manoeuvres that are not in line with the required accuracy of placement. This results in unsuccessful attempts at attachment which result in a retry or a mission failure.

MID6 **Attachment device failing** - The payload can support its own weight through the use of an attachment device which is done through the use of vacuum cups[5]. These vacuum cups are sustained by a cable decreasing pressure, if this mechanism fails, the UAV attachment will have to take the entire load and may not be able to sustain it. This will proceed to a free fall possibly damaging the aircraft and creating a hazard underneath it.

MID7 **False pre-inspection update** - The UAV needs to navigate autonomously from the starting location to the prescribed location. The UAV then needs to attach to this location with an accuracy displayed by requirement **[OP-1.2]**. If this attachment position is significantly off, the payload will analyse an incorrect area, and may give false negative.

MID8 **On-board fire** - Both electrical components and engines are prone to catching fire. If not handled correctly this can result into damage and a possible crash of the UAV, possibly resulting in (significant) damage of the aircraft and/or injuring the operators.

MID9 **Orientation mechanism malfunction** - As depicted in Chapter 9, three of the four design concept requires an orientation mechanism in order to reach all surfaces. It is important to distinguish between the various orientation mechanisms. In the case that orientation mechanism A fails, the reach decreases. However, if orientation mechanisms B or C fails the UAV and potentially the aircraft can be damaged. Mechanism B can fail in case the flight controller malfunctions. Regarding mechanism C, there is the possibility of the suction cups not attaching properly to the aircraft due to wet surfaces.

Post-flight risk

The post-flight risks (POS) are the risks involved in the phase from the moment from which the UAV has landed after the final inspection until the moment the UAV is ready for the next inspection and repair cycle.

POS1 **Payload disassembly** - After landing the payload and UAV have to be separated manually, as well as the rotor arms of the UAV. This process can damage both payload and UAV if not performed correctly. Especially vulnerable components might be damaged.

POS2 **Improper UAV maintenance** - The UAV itself will need maintenance and possible repairs after flight. Maintenance will be performed correctly to ensure safe operation of the UAV for the next flight. Depending on the component which has not been repaired properly the impact can vary.

POS3 **UAV transport and storage** - During transport of the UAV to various maintenance locations, damage to the UAV may occur if not protected. Again, vulnerable components are prone to be damaged. As these types of damages are visible most of the time, they create no hazardous environment or potential danger.

18.4.2. Risk Map

Table 18.1 visualizes both the probability and the impact of the risks identified in Section 18.4.1. All red-coloured elements require risk mitigation. The impact-axis is divided into four levels defined as follows:

- **Negligible** - The impact of events in this level will only result in inconvenience and will not have a negative effect on the operations.
- **Marginal** - Small effect on technical performance possibly resulting in the need to repeat certain sub-tasks of the mission.
- **Critical** - A significant reduction in technical performance requiring significant portion of the mission to be repeated. Repair is required due to self-imposed damage.

[5] http://en.dmgmori.com/blob/172070/5439d5778a35de4a332cd668a5ddb973/pu0uk15-ultrasonic-composite-pdf-data.pdf [Accessed 21 May 2017]

- **Catastrophic** - Failure of the mission resulting in significant damage to at least the UAV, the aircraft, the operator or the other individuals.

18.4.3. Risk Mitigation

From Table 18.1 it can be seen there are four events which require risk mitigation. In the following text every event is listed along with measures to mitigate the risk along with the updated risk map after mitigation.

- **MID1** - In order to ensure constant power (fuel) to the engines it is advisable to include an auxiliary power source. This can be in the form of a backup battery pack and/or backup power or a combination of both. In case one of the power supplies fails there will always be a backup. For failure of the rotors, the propulsion system has to be redundant enough to allow full control for single rotor failure.
- **MID2** - In the case of sensor failure the UAV will not be able to position itself. This risk can be mitigated in two ways. The first way is to add backup sensors. This option is justified since typical sensors are very lightweight. The second way is to include a "trace flight path" function, which enables the UAV to trace its flight path back towards the ground station when all sensors failed.
- **MID3** - Collision can occur in two different ways. Either the UAV collides with an object due to the fact it loses navigational capabilities or a foreign object can collide with the UAV which operates normally. The latter is especially a risk when operating outside (eg. impact of birds). In order to mitigate this risk one can equip the UAV with additional sensors especially in place for avoiding collisions with other objects and automatically divert the UAV.
- **MID7** - In order to ensure the UAV delivers the payload at the predefined location use can be made of a camera module with which the maintenance engineer can check real-time if the repair is conducted at the right location. Adding a high resolution camera will increase the weight, however due to the importance of this procedure it is required.
- **MID8** - On-board fires can be detected early by making use of temperature sensors on board of the UAV in critical areas such as the battery pack and engines. In case the temperatures reaches a predetermined critical level the UAV will have to return back to its base autonomously. In this way the fire can be extinguished on the ground away from the aircraft and greatly reducing the probability of the UAV crashing due to fire damage.
- **MID9** - Reducing the risk of orientation mechanism B failing can be achieved by using back-up flight controllers in the case one malfunctions. This will reduce the probability of mechanism B malfunctioning. Furthermore, in order to reduce the risk of orientation mechanism C failing, it is advised to only operate this system when the skin of the aircraft has been dried. This will reduce the probability of mechanism C malfunctioning.

After mitigating the risks a new risk map can be setup and is visualised in Table 18.2. As can be seen the above risks have been mitigated primarily by reducing the likelihood of occurrence. Regarding MID2 both the impact as well as the likelihood have been reduced. Finally, although POS1 and POS3 do not have a significant impact their risk can be easily mitigated by establishing well defined procedures for handling the UAV. Furthermore, increased experience and routine levels of maintenance engineers will reduce the probability of occurrence of these risks.

Table 18.2: Technical risk map after mitigation

Likelihood	Very Likely				
	Likely				
	Unlikely		PRE1 MID4, MID5 POS1, POS3	PRE2 POS2	
	Very unlikely			MID8	MID1, MID2, MID3, MID6, MID7, MID9
		Negligible	Marginal	Critical	Catastrophic
		Impact			

18.5. Development, Legal & Financial Risk Assessment

This section discusses the risks for the development of the UAV and the corresponding impacts of these risks are addressed. Furthermore the risks regarding legal issues are discussed. Finally, the economical & marketing aspects are analysed. The section concludes with two risk maps and mitigation measures.

DLF1 **Battery TRL** - One of the important drivers of the project is the use of Lithium-Sulphur (Li-S). Although there are already commercially available Li-S batteries, they are only commercialised by several companies and therefore still not widely available. Currently, the Li-S batteries are still under development. The main issues with the use of these batteries are as follows:

- Li-S battery faces difficulty to safely operate at high temperatures
- Low Technology Readiness Level (TRL)

The main risk in the low TRL of the Li-S batteries lies in the fact that there is the possibility that less powerful batteries might have to be used. This will affect the performance of the UAV and might cause the UAV not to meet the set performance requirements.

DLF2 **UAV operations at airports** - Currently, regulations prevent the Flying Doctor UAV operating within the CTR (Controlled Traffic Region) of airports. This poses a problem for the on-apron repair/inspection concerning outdoor operations. The main risk is that when the UAV is ready to be deployed for operations around aircraft on the apron by 2019, legislation will prevent this. Regarding indoor operations the UAV is already complying with regulations, since this is not restricted by law. However, airline policy might restrict UAV operations near aircraft.

DLF3 **Product Demand** - For the market analysis it is assumed that at least three repairs/inspection are performed everyday per UAV. However, especially in the early stages after the product launch airlines might be reluctant to make use of the UAV service. This poses a significant risk, as the servicing business model requires a base of costumers to ensure the revenue streams as predicted. The probability of this risk occurring is high at the beginning, in the "early adopters" phase of the product.

DLF4 **Protection of intellectual property and design** - As it has been highlighted by the market analysis in Chapter 4, there are no current competitors in the MRO industry which provide automated repair solution. Being the pioneer in the industry, steps must be taken to safeguard the trade secrets to ensure sustainability of the business.

DLF5 **Liability Risk** - When operating the UAV using the service model, liability issues may arise. For example, when operating the UAV near an aircraft and damage is caused because of an unexpected wind gust. The question which then arises is: which party is reliable for the damage and which external factors are covered by insurance? In case the UAV crashes and damages the aircraft due to a malfunction in the software, the Flying Doctor company will be liable.

18.5.1. Risk Map

The following risk map in Table 18.3 visualises the probability and impact of each of the above described risks. The impact scales are not the same as defined as before, since the risks in this section are of a different category with different impact effects. Risks indicated in red require mitigation similar to Section 18.4.2. The impact scales for this analysis are defined as follows:

- **Negligible** - Impact of these risks are small and will not harm the business in the long term. Only short term consequences might occur.
- **Moderate** - The business might be harmed in such a way that the profit margins will become lower than projected. Temporary closure of the business might be required and significant revenue is lost.
- **Severe** - Events will cause the business to cease operation due to structural loss of revenue.

Table 18.3: Development, Legal and Financial risk map

<table>
<tr><td rowspan="4">Likelihood</td><td>Very likely</td><td></td><td rowspan="2">DLF1</td><td rowspan="3">DLF2
DLF3, DLF4, DLF5</td></tr>
<tr><td>Likely</td><td></td></tr>
<tr><td>Unlikely</td><td></td><td></td></tr>
<tr><td>Very unlikely</td><td></td><td></td><td></td></tr>
<tr><td></td><td></td><td>Negligible</td><td>Moderate</td><td>Severe</td></tr>
<tr><td></td><td colspan="4">Impact</td></tr>
</table>

18.5.2. Mitigation

The following section addresses the mitigation measures to take in order to mitigate the risks which are in the red zones of the risk map. As before, risk mitigation is primarily focused on reducing the probability of certain events happening.

- **DLF1** The development of the battery technology is beyond the scope of the team, and therefore has to be monitored closely. Post-DSE activity includes attracting investors to fund the project, but also ensuring close collaboration with the battery technology partners (Sion Power and OXIS Energy), to get hold of the latest technology. Sion Power in particular has a dedicated battery designed for UAVs and is therefore the best guideline regarding updates of the battery TRL level. This way the impact of reduced battery performance can be take into account well in advance such that measures can be taken.
- **DLF2** The way to handle this risk is to take into account the fact that in the beginning only indoor operations are allowed. This can be done by assuming lower revenue streams in the beginning of the product launch. This will reduce the impact of this risk. Furthermore, while in the design phase, efforts should already be made to legalise the on apron operations. An option could be to file a request for an exemption for the Flying Doctor UAV in particular. This will reduce the probability of this risk occurring.
- **DLF3** In order to handle the product demand risk, potential clients have to be approached well in advance. In order to reduce the probability of this risk it is valuable to already have service contracts before starting the design of the UAV. This way the revenue is guaranteed, even in the first stages of the product launch.
- **DLF4** The chosen service model allows to control the exposure of technology to consumers and potential competitors. in house engineers do have access to the technology used and this should be addressed with caution.

The following measures are set to mitigate the risk of intellectual property from being leaked resulting in a lower probability of this particular risk.
  - Background check all staff with access to protected technology
  - Setup non disclosure agreement for all staff
  - Patent special features, for example the perching mechanism
- **DLF5** The liability risk can be mitigated by having a insurance policy covering for events caused both by *external* as *internal* factors. In this way even an unnoticed flaw in the design will not cause the company to be liable. Furthermore, the business form should be carefully considered, taking into account personal liability. Having the insurance policy correctly setup, the impact of these events is reduced to be negligible.

After these mitigation measures, the new risk map for the Development, Legal and Financial risks can be setup and is visualised in Table 18.4.

Table 18.4: Development, Legal and Financial risk map after mitigation

Likelihood	Very likely			
	Likely	DLF1		
	Unlikely	DLF5	DLF2	
	Very unlikely			DLF3, DLF4
		Negligible	Moderate	Severe
		Impact		

19 Sustainability

In this chapter the sustainability of the design and its process is discussed. First, the sustainability fields are discussed and briefly analysed in Section 19.1. Then, the power generation is discussed in Section 19.2. And finally in Section 19.3 the recyclability plan is shown.

19.1. Sustainability Fields

As discussed in the Mid-Term Report, sustainability can be divided in three fields listed below.

- **Design** - The design sustainability can be split up in two different parts:
  - **UAV** - The sustainability of the UAV is mostly dependent on the following factors: material, power, noise emission and life time. The lifetime of the UAV is not dependent on the battery and the motors, since they can be replaced. It is expected that if the system fails, it will be on the structure. When overdesigning with a safety factor higher than 1, the life time can be increased. All the structural parts are designed with a safety factor higher than 1.2. The part with the lowest safety factor is the perching arm. If it fails, it will fail during gusty winds. The power consumption is described in Section 19.2.
  - **Ground station** - The ground station sustainability is dependent on power generation and the waste of resources. The latter should be reduced to a minimum by means of, for example, lean manufacturing. For this, refer to Chapter 15. The use and generation of power is discussed in Section 19.2.
- **End-of-life** - After a material exceeds its life time, it loses its usefulness and has to be disposed. End-of-life disposability leans on four pillars: reduce, reuse, recycle and recover[1]. The UAV is designed in such a way that parts can be easily replaced in order to increase the lifetime. Then at disposal, the different materials can be segregated without significant effort in order to increase the recyclability. More on recyclability can be found in Section 19.3
- **Design process** - During the design process the use of resources was limited. This also includes the waste of energy and material for prototypes, for example.

19.2. Power

The power used by the UAV is brought to a minimum by choosing an energy efficient design. Also, the power should preferably be generated from renewable resources such as solar, wind or hydro energy. It is obvious that a hydro energy generator can not be used. Also, a wind turbine placed on the UAV is unfeasible, since there is a dimensional constraint, which can be found in requirement **[OP-6]**.

In the Mid-Term Report solar arrays were considered, but the use of solar arrays is constrained by the size requirement. Since there is not much room in the mass budget, it is expected that the mass requirement is just met. Therefore the energy capacity per weight for solar arrays is considered. Solar arrays with a high efficiency mostly have a high weight. One efficient and lightweight array is found[19]; it has a power density of 2067W/kg and 283W/m^2 in optimal conditions. With a required power of 16.5kW, 8kg and 58.2m^2 of solar arrays is necessary to replace the battery fully. Although, it is performing well on weight (excluding frames and electronics), the area needed is too big to fly.

Only wind energy generators and solar arrays at the ground station are considered. Wind turbines are not mobile and unhandy on an airport, so they are unfeasible. Finally, solar arrays are considered. In order to charge the battery (with a total capacity of 8237Wh) fully in one hour in optimal weather circumstances (thus a solar flux of 240W/m^2) and a 100% efficiency for the charging process, with high efficiency solar arrays of 50%[2], a solar array area of 68.6m^2 is needed. This is too large to fly witly with. Therefore not a full replacement of the electrical battery chargers are recommended and charging with three phase power is chosen.

19.3. Recyclability Plan

Requirement **[GEN-3]** states that 95% of the UAV should be recyclable. It needs to be defined what this 95% requirement means. Therefore it is defined that 95% of all the UAV parts should be recyclable. Then, at end-of-life, all the parts need

[1] http://www.greenhome.com/blog/what-is-downcycling [Accessed on 4 May 2017]

[2] http://www.theecoexperts.co.uk/which-solar-panels-are-most-efficient [Accessed on 17 May 2017]

Part	Target
Gearbox	Reuse or shred, remelt and remanufacture
Housing	Reuse or shred, remelt and remanufacture
Bearings	Reuse
Stepper driver	Reuse
Stepper motor	Reuse
Propeller	Reuse or mold, seperate, recover and reuse[4]
Motor	Reuse
Electronic speed controller	Reuse or recycle[5]
Perching arm 1	Reuse or shred, remelt and remanufacture
Perching arm 2	Reuse or shred, remelt and remanufacture
Suction cup	Downcycle[6]
Detachment/Orientation servo	Reuse or recycle
Sensor	Reuse
Landing gear	Reuse or shred, remelt and remanufacture
Landing gear rubber	Process to semi-manufactured product[7]
Storage box	Reuse
Batteries	Recycle rubber[7] and rest of recyclability still unknown
Storage box wheels	Reuse
Proximity sensor	Reuse[8]
3D depth camera	Reuse
Sonar range finder	Reuse
Arms	Reuse or shred, remelt and remanufacture
Frame	Reuse or shred, remelt and remanufacture
Wiring	Educational purposes or copper recycling[9]

Table 19.1: Recyclability UAV parts

to be checked on permanent failure, because some (structural) parts of the UAV have different life times. If the structure permanently fails, it means that, for example, the sensors can be used longer and therefore it can be used in a future UAV.

Starting with the capability to split the Flying Doctor in different parts. For recycling it is required that parts of the same material can be split with ease. When two different materials are attached to each other, this is done with an attachment which is easily removable. The parts which need to be recycled needs to stay intact in order to increase the possibilities in reusing, upcycling or downcycling[3].

It is expected that the structure and the battery fail the first. Therefore sensors and the full ground station can be reused a number of times. From Table 19.2, it can be seen that only the batteries and the rubber attached on the landing gear will not be fully recycable. Regarding the battery, this is because Li-S batteries are a new technology and the recyclability will still be determined in the future. For rubber only a semi-product will come out, more processes needs to be undertaken before getting a feasible material back. Since there are for some parts more parts present in the UAV, the 95% recyclability is met.

[3]http://www.wikihow.com/Recycle [Accessed on 21 July 2017]

[4]http://www.colorado.edu/today/2016/02/15/cu-boulder-researchers-recycle-carbon-fiber-composites-new-equally-strong-material [Accessed on 21 June 2017]

[5]http://www.rc-airplane-advisor.com/electronic-speed-controller.html [Accessed on 21 June 2017]

[6]http://www.world.org/reuse/suction.cups [Accessed on 21 June 2016]

[7]http://www.vsrubber.nl/productieproces/ [Accessed on 21 June 2016]

[8]http://blog.pepperl-fuchs.us/blog/bid/352679/Life-Expectancy-of-an-Inductive-Sensor [Accessed on 21 June 2017]

[9]https://www.cnet.com/how-to/the-best-places-to-recycle-old-cables-and-chargers/ [Accessed on 21 June 2017]

Part	Target
Gearbox	Reuse or shred, remelt and remanufacture
Housing	Reuse or shred, remelt and remanufacture
Bearings	Reuse
Stepper driver	Reuse
Stepper motor	Reuse
Propeller	Reuse or mold, seperate, recover and reuse
Motor	Reuse
Electronic speed controller	Reuse or recycle
Perching arm 1	Reuse or shred, remelt and remanufacture
Perching arm 2	Reuse or shred, remelt and remanufacture
Suction cup	Downcycle
Detachment/Orientation servo	Reuse or recycle
Sensor	Reuse
Landing gear	Reuse or shred, remelt and remanufacture
Landing gear rubber	Process to semi-manufactured product
Storage box	Reuse
Batteries	Recycle rubber and rest of recyclability still unknown
Storage box wheels	Reuse
Proximity sensor	Reuse
3D depth camera	Reuse
Sonar range finder	Reuse
Arms	Reuse or shred, remelt and remanufacture
Frame	Reuse or shred, remelt and remanufacture
Wiring	Educational purposes or copper recycling

Table 19.2: Recyclability UAV parts

20 Post-DSE

The aim of the DSE is to provide a design within requirements to fulfil a specified function. When this design is provided, further development is still possible. How this development is going to occur is discussed in Section 20.1. This is again visualised in Section 20.2. The second visualisation will be time bound through the use of a Gantt chart to get a better understanding of the schedule in the post-DSE phase.

20.1. Further Development

Time is limited during the design of the UAV. Not all details can be taken into account with the limited working hours that have been provided to the design of the Flying Doctor. This means that there is room for further development. The aim of the report is to provide a substantial basis for the feasibility of the design. The design itself can be further developed in greater detail and with more consideration in further stages through testing. The stages past the DSE are shown in Figure 20.1.

20.1.1. Funding process

Before starting the further development of the design, funding is required to create prototypes and provide a salary for the employees. This is done by searching for investors that are willing to provide this funding. To persuade the investors that the design can actually bring in a positive ROI, the market analysis and a marketing analysis is created and put into a presentation. The exact funding that is required for the further development stages can be found in Section 16.1.

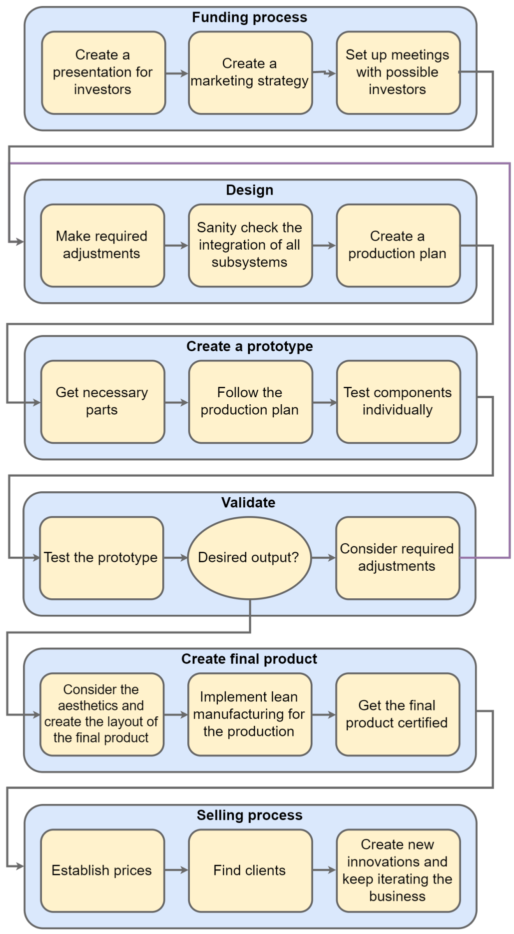

Figure 20.1: Development logic diagram of the post-DSE stages

20.1.2. Design

The design phase consists of readjusting design parameters to better fit outcomes of tests after validation has occurred. Before the validation it consists of providing a more in depth and more efficient design. More on this can be found in Section 22. The design process is aided by performing sanity checks on all subsystems during the design. When this results in a design that works on paper and is optimised, a prototype will be made. To help with this, a production plan is required to make the production of the prototype lean. Lean manufacturing is explained in Chapter 15.

20.1.3. Create a Prototype

When the design is verified to be working on paper, credibility is required through creating a prototype that will show a successful mission. To create this prototype the production plan needs to be followed. This is started by getting all of the required parts. When the prototype is created, parts that can be tested without destroying the entire prototype are to be tested individually. Then when the design seems to be functioning it needs to be validated.

20.1.4. Validate

As of now, no test for the system has been performed, meaning that claims of the UAV working properly, are not optimal. For the DSE period, no budget is available for constructing a prototype, disallowing a validation test. When the prototype is set up, its functionality needs to be tested. The requirements need to be validated and a meeting has to be set up with an actual aircraft to show that the mission can be performed accurately.

20.1.5. Create the Final Product

When the validation is successful and the prototype has been shown to have the ability to fulfil all specified functions in the functional flow, the design is to be finalised. This has to be done by firstly considering the aesthetics and final layout of the design. Furthermore an updated lean production plan had to be produced. When this is done, the final product has to be certified to get clearance from authorities to be used in actual manufacturing cases.

20.1.6. Selling Process

As the product is certified and ready to go, the UAV price should be finalised with potential clients. Most likely the clients will have overlap with the investors resulting in a reduced price for these people. When the design is finished, the product is ready, and revenue is being generated the next step is to start innovating again to allow for further progress within the sector.

20.2. Post-DSE Gantt Chart

Figure 20.2 visualises the project planning in the post-DSE phase. The planning is compliant with the deadline set for the first delivery of the five UAVs by the second half of 2019. A time buffer is included in order to account for unexpected events such as certification and legislation issues. The required time for these processes is hard to estimate due to the dependence on legislation.

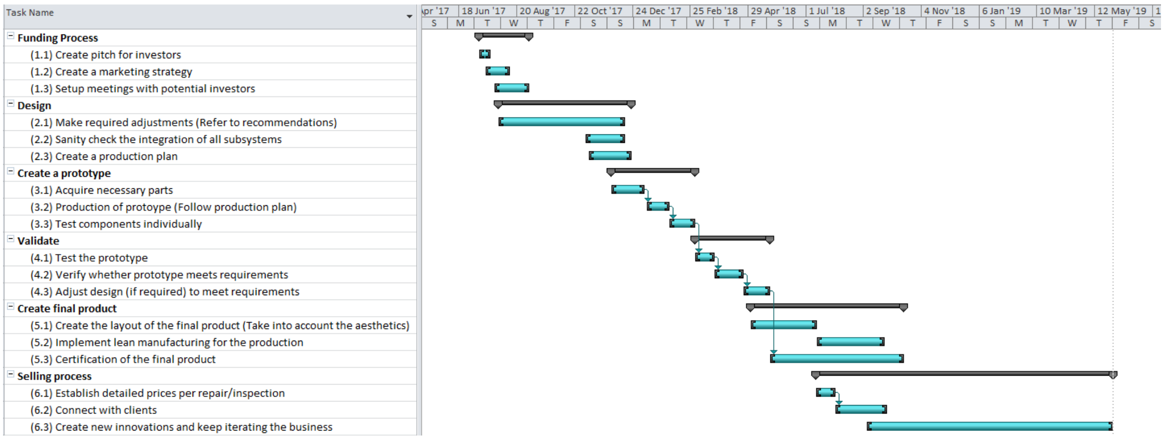

Figure 20.2: Post-DSE Gantt chart (2017-2019)

21 Conclusion

This report is the final step in the process of coming up with a detailed design for an UAV which inspects and repairs aircraft. The UAV is able to perform an autonomous operation after an operator selected the location where the inspection and repair is needed. Halfway through the process, multiple concepts were considered and a concept was chosen which was taken into the final detailed design process. The concept, which is unique due to the rotating arms which allow it to orientate the payload in all directions, is chosen based on its high performance on mass, reach, ergonomics, size and complexity in the trade-off.

The way the design is achieved consists of different approaches on multiple subsystems. The structural elements in the design are accomplished through the use of Autodesk Inventor, after which the entire UAV is assembled in this program. The Flying Doctor detailed design weight is 18.37kg, which is roughly 2kg lighter than the estimated dry weight for the concept. The propulsion system is designed to lift the entire UAV of 151kg including the payload, the batteries and the payload miscellaneous. The flying doctor is flying at 146.4kg which means an extra of 4.6kg can be reserved for other subsystems. One thing to note is that, the flying doctor's weight with the payload can be reduced by at least 3kg, by opting for one type of NDT, which will naturally reduce the inspection performance.
Some subsystems' specifications for the UAV to point out are as follows:

1. **Power:** Lithium-sulphur battery
2. **Propulsion:** Coaxial multirotor
3. **Structures:** Two 'T' shaped arms
4. **Landing gear:** four legs using topology optimisation
5. **Rotation mechanism:** Two stepper motors with gearing
6. **Perching mechanism:** Side arm aided rotation

Almost all of the requirements that were set in the early stages of the design process are met. In order to have a sustainable design the UAV is electrically powered and is more than 95% recyclable. The UAV can land easily on flat and the most curved surfaces and collisions are autonomously avoided. Some of the requirements need more attention and others can not be met at this moment in the design process. Despite not entirely meeting the requirement for the size, the UAV is still easily transportable.

The UAV is designed to make use of both off-the-shelf products and parts that have to be manufactured. For the manufacturing parts, additive manufacturing is used, on top of the conventional manufacturing methods. The production costs for a UAV amount to €16,099. A service model will be used to earn money with the UAV and with a price of €602 per repair and three repairs per UAV a day. Using this business model, it is possible to achieve a RoI between 2 and 4 within five years.

The flying doctor strives to revolutionise the MRO industry by reducing the airline downtime, which potentially could save hundreds of thousands of euros, and more importantly to perform less wasted maintenance practise for a cleaner future.

22 Recommendation

During the design of a product, the depth of the result is based on the time frame in which research can be done or more specifically man hours. For this specific design a time frame of 10 weeks has been provided. This has resulted in a relatively detailed design. However if time would have warranted it, further research and development could have been performed.

For the propulsion more investigation can be performed into motor modifications to help it better fit the design criteria. For the frame further structural layouts could have been considered. With a specific interest towards the micro structural sandwiches. For the rotational mechanism, more research could have been performed into the efficiency of gears to decrease its weight. The landing gear has a low resistance to torsional loads, it can be restructured to handle these loads better. The perching mechanism is overdesigned on many points and could have implemented a taper for this reason. Also a fatigue analysis can be performed on the mechanism itself to verify its life cycle as data that was found only considered thicker and bigger titanium beams. The NDT is not performed by the payload. Integration with the payload would benefit the simplicity of the data flow and would make the payload more efficient relative to its weight. Furthermore the chosen NDT method could use more support for its feasibility and a wider spectrum of possibilities could have been considered. The shell of the battery is not optimised yet, which can still be done. The full specifications for charging a battery can also be researched further. In order to make the design more sustainable, noise emisions can be researched, as well as some measures to reduce noise.

Bibliography

[1] M. Harrison. MRO Forecast and Market Trend. *JATA 12th Maintenance Cost Conference*, September 2016.

[2] C.C.A.Bekkers, S.K. Birjmohan, M.J.G.van der Drift, E. Hernandez Moore, D.H.P.L. Koppes, A.J.J.Meegdes, H.W.Njo, P.Scheenloop, and Z.Vinskas. *DSE Baseline Report*. TU Delft, 05 2017.

[3] C.C.A.Bekkers, S.K. Birjmohan, M.J.G.van der Drift, E. Hernandez Moore, D.H.P.L. Koppes, A.J.J.Meegdes, H.W.Njo, P.Scheenloop, and Z.Vinskas. *DSE Mid-Term Report*. TU Delft, 06 2017.

[4] Unknown. Mobile and stationary ULTRASONIC-machining of COMPOSITES for MRO and Production.

[5] R. Stoessel. Air-coupled ultrasound inspection as a new non-destructive testing tool for quality assurance. *Faculty of Design Engineering, Production Engineering, and Automotive Engineering, University of Stuttgart, Stuttgart, Germany,*, 2004.

[6] L. Cheng and G. Y. Tian. Surface crack detection for carbon fiber reinforced plastic (cfrp) materials using pulsed eddy current thermography. *IEEE Sensors Journal, vol. 11, no. 12*, 2011.

[7] N.P. Avdelidis*, T-H. Gan, C. Ibarra-Castanedo, X.P.V. Maldague. Infrared thermography as a non-destructive tool for materials characterisation and assessment. *Society of Photo-Optical Instrumentation Engineers*, 2011.

[8] K.Chatterjee, S.Tuli S.G.Pickering, D.P.Almond. Non-destructive testing of composite materials by means of active thermography-based tools. *Elsevier*, 2011.

[9] M.Lizaranzu, A.Lario, A.Chiminelli, I.Amenabar. Non-destructive testing of composite materials by means of active thermography-based tools. *Elsevier*, July 2015.

[10] N.P. Avdelidis, D.P. Almond, A. Dobbinson, B.C. Hawtin, C. Ibarra-Castanedo, X. Maldague. Aircraft composites assessment by means of transient thermal ndt. *Elsevier*, 2004.

[11] I. Jorge Aldave, P. Venegas Bosom, L. Vega González, I. López de Santiago, B. Vollheim, L. Krausz, M. Georges. Review of thermal imaging systems in composite defect detection. *Elsevier*, 2013.

[12] H.Fernandes, H.Zhang, A.Figueiredo, C.Ibarra-Castanedo, G. Guimarares, X. Maldague. Carbon fiber composites inspection and defect characterization using active infrared thermography: numerical simulations and experimental results. *OSA*, 2016.

[13] J.P.Ferreira, F.Lopez, V.Nicolau, A.Albertazzi, D.Willeman. Comparison of infrared thermography and shearography for nondestructive evaluation of composites materials by pulsed-heating excitation. *5th Pan American Conference for NDT*, 2011.

[14] P. Pounds, R. Mahony, J. Gresham. Towards dynamically-favourable quad-rotor aerial robots. 2014.

[15] B. Theys, G. Dimitriadis, P. Hendrick, J. De Schutter. Influence of propeller configuration on propulsion system efficiency of multi-rotor unmanned aerial vehicles. *2016 International Conference on Unmanned Aircraft Systems*, 2016.

[16] M. Brazinskas, S. D. Prior, J. P. Scanlan. An empirical study of overlapping rotor interference for a small unmanned aircraft propulsion system. *Aerospace*, July 2016.

[17] M.O. Tokhi et al. *Climbing and Walking Robots*. Spring, 2005.

[18] D. Wolters A. Stepek, X. Wang. Wind climatology of schiphol. May 2012.

[19] Daniel C. Law et al. Lightweight, flexible, high-efficiency iii-v multijunction cells. 2006.

A

Work Distribution

The task distribution can be found in Table A.1.

Table A.1: Work distribution

Person	**Worked on (Chapter/Section)**
C.C.A. Bekkers	i, 1, 2, 3.3, 9(.1, .2, .4), 10.3, 20.1, 22, A
S.K. Birjmohan	4, 9.3, 16(.3), 18(.4, .5) 20.2
M.J.G. van der Drift	xi, xiii, xv, xvii, xix, 8.4, 13(.1, .2), 14.3.4, 18(.1, .2, .3), 19
E. Hernandez Moore	6.5, 8.3, 15, B
D.H.P.L. Koppes	8.2, 12
A.J.J. Meegdes	8.3, 16(.1, .2), 17 , 21, B
H.W. Njo	iii,5.2, 6(.1, .2, .3, .4), 13.3, 14.3, 17, C
P. Scheenloop	3.2, 11
Ž. Vinskas	5(.1, .3), 7, 8(.1, .5), 10(.1, .2) ,14(.1, .2)

B
Component Production Cost

Table B.1: Production costs and manufacturing method per component

Subsystem	Name of part	Units	Acquisition	Cost per part[€]	Material	Raw material[€]	Manuf. technique	Manuf. cost[€]	Tot. Cost]€]
Rotation mechanism	Gear box	2	CM	-	Cast Iron	1.29	Casting and machining	70.00	72.59
	Rotational mechanism frame	2	AM	-	Ti-6Al-4V	142.91	Direct Metal Laser Sintering	3230.00	3,801.65
	Bearings	4	Off the shelf	19.49	-	-	-	-	77.96
	Stepper driver	2	Off the shelf	20.00	-	-	-	-	40.00
	Stepper motor	2	Off the shelf	45.78	-	-	-	-	91.56
Propulsion	Propeller	8	CM	-	CFRP + aluminium	356.00	Layup	311.50	2,848.00
	Motor	8	Off the shelf	535.00	-	-	-	-	4,280.00
	ESC	8	Off the shelf	113.00	-	-	-	-	904.00
Perching	Bar 1 (80cm)	2	CM	-	Ti-6Al-4V	3.76	Extrusion and cold forming	90.00	97.51
	Bar 2 (40cm+side bar)	2	CM	-	Titanium 64	1.93	Extrusion and cold forming	70.00	73.86
	Suction cup	2	Off the shelf	80.00	-	-	-	-	160.00
	Detach./Orient. servo	4	Off the shelf	17.53	-	-	-	-	70.12
	Sensor	2	Off the shelf	13.10	-	-	-	-	26.20
Landing gear	Landing gear	4	CM	-	Al-7075	0.91	Press forming and machining	70.00	73.64
	Rubber	4	Off the shelf	0.20	-	-	-	-	0.80
Ground station	Storage box	1	Off the shelf	233.00	-	-	-	-	233.00
	Batteries	3	Off the shelf	480.60	-	-	-	-	1,441.80
	Wheels	4	Off the shelf	4.40	-	-	-	-	17.60
	Battery charger	2	Off the shelf	400.00	-	-	-	-	800.00
Navigation	Proximity sensor	12	Off the shelf	10.68	-	-	-	-	128.16
	3D depth camera	4	Off the shelf	132.61	-	-	-	-	530.44
	Sonar Range Finder	2	Off the shelf	30.00	-	-	-	-	60.00
Arms	Arms	2	CM	-	Al 6061-T6	14.30	Extrusion and cold/press forming	150.00	178.60
Payload frame	Frame	1	CM	-	Al 6061-T6	31.20	Extrusion and roll forming	100.00	131.20
Wiring	Wires	-	Off the shelf	20.00	-	-	-	-	20.00
Total Cost									**16,098.69**

C
Wiring Gauge

Table C.1: Electrical wiring weight based with reference to AWG gauge

From	To	Distance [m]	AWG gauge [-]	Weight [kg/m]	Weight [kg]
60V rail					
Battery	Electronic speed controller	12	10	0.046	0.552
Electronic speed controller	Motor	0.8	10	0.046	0.0368
Battery	Inverter	0.5	12	0.0294	0.0147
Inverter	Ultrasonic milling	0.75	16	0.0116	0.0087
inverter	Shearography camera	0.5	24	0.00182	0.00091
24V rail					
Battery	Switching regulator	0.5	24	0.00182	0.00091
Switching regulator	IR camera	0.5	22	0.00289	0.001445
Switching regulator	Halogen lamps	1	22	0.00289	0.00289
12V rail					
Battery	Switching regulator	1	24	0.00182	0.00182
Switching regulator	Arm rotation motor	1	24	0.00182	0.00182
Switching regulator	Pressure sensor	3.4	24	0.00182	0.006188
5V rail					
Battery	Switching regulator	0.5	22	0.00289	0.001445
Switching regulator	Main control unit	0.1	24	0.00182	0.000182
Switching regulator	Flight controller	0.1	24	0.00182	0.000182
Switching regulator	3D camera	1	24	0.00182	0.00182
Switching regulator	Collision avoidance	12	24	0.00182	0.02184
Electrical line total [kg]					0.653652

Table C.2: Signal wiring weight based with reference to AWG gauge

From	To	Distance	AWG gauge	Weight [kg/m]	Weight [kg]
60V rail					
Main Control Unit	Electronic speed controller	12	22	0.00289	0.03468
Electronic speed controller	Motor	0.8	22	0.00289	0.002312
Main Control Unit	Inverter	0.5	20	0.0046	0.0023
Main Control Unit	Ultrasonic milling	0.75		0.19	0.1425
Main Control Unit	Shearography camera	0.5		0.19	0.095
24V rail					
Main control unit	IR camera	0.5		0.19	0.095
Main control unit	Halogen lamp	1	24	0.00182	0.00182
12V rail					
Flight controller	Arm rotation motor	1	22	0.00289	0.00289
Flight controller	Pressure sensor	3.4	24	0.00182	0.006188
5V rail					
Main Control Unit	3D camera	1	24	0.00182	0.00182
Flight Controller	Collision avoidance	12	24	0.00182	0.02184
Signal line total [kg]					0.40635